Technology Pathway Partnership
Final Scientific Report

Project Title: High Efficiency Concentrating Photovoltaic Power System
Reporting Period: June 2007 to December 2011
Date Submitted: 26 April 2012
Recipient: United States Department of Energy
Golden Field Office
Golden, Colorado
Award Number: DE-FC36-07G017052
Recipient Contacts:

Dr. John C. Hall	Ms. Sharyn Garnett
Program Manager	Contracts Administrator
Telephone: 562-797-1163	Telephone: 714 475 9626
E-mail: john.c.hall2@boeing.com	E-Mail: sharyn.p.garnett@boeing.com

DOE Project Team:

DOE Field Contracting Officer:	Michael Schledorn
DOE Field Project Officer:	Minh Le
Project Engineer:	Holly Thomas
Technical Monitor:	Kaitlyn VanSant

Acknowledgment

Too many people over too long a time participated in this effort to ever hope to accurately acknowledge the contributions made by all the team members. Their efforts were clearly critical to the successes achieved, however, I dare not risk that memory might fail and thereby wound by omission all those who built this program. That said special thanks are due to the two program mangers Russ Jones and Bob Burns who preceded me in this seat. I certainly do not deserve anything like the entire credit for all the successes of this program. All three of us would also like to acknowledge the leadership provided over the entire course of the program by Jeff Frericks under whose authority the program was executed

Special thanks also need to be extended two outstanding subcontractors that played critical roles in the success of this program. Comau Inc. designed, built, debugged, and operated the robotic assembly factory for the CPV panels. Their ability to respond quickly to demands of development program was outstanding and a real lesson that the productive capability of the United States has not atrophied.

Stanley Electric also merits special acknowledgement for their commitment to the success of the CPV effort. Their support and commitment to the program and to their products was outstanding.

John Hall
April 2012
Seal Beach, CA

Contents

List of Figures

List of Tables

Executive Summary

Project Summary

Boeing and its industry partners formed a Technology Pathway Partnership (TPP) to develop a new high performance, low cost concentrating photovoltaic (CPV) system in support of the DOE Solar Energy Technology Program (SETP). Significant progress was made on the multijunction solar cell development, performance, and production, as well as the development of the core CPV modules, 2D trackers, turnkey power plant system design, and other key components and elements of design. The Boeing approach utilized a high performance non-imaging optical architecture with a reflective primary and refractive secondary optical element as the foundation for the approach as it yielded best overall performance in terms of efficiency, solar acceptance angle, and cost. High efficiency multijunction solar cell technology was at the core of the design and, as a direct result of the DOE SETP program, significant progress on the maturation of the technology was made leading to 40% efficiency production cells being offered to industry today. For this effort, Boeing partnered with Spectrolab, PV Powered, LPI, COMAU, URS, PS&P, SCE, CSUN, and NREL.

The goal of the TPP program was to develop the pathway to 7–15 cents/kWh for utility scale deployments and foster industry participation in CPV production. We believe that the CPV technology developed under this program has the ability to meet and beat these ambitious goals with continued DOE and US Government investment and support for the CPV Industry. CPV has matured and should continue to mature as a technology market that can compete with PV and CSP solar power plant installations in high DNI locales.

Summary of project accomplishments (Goals and objectives)

Project Objective: The project sought to develop a new CPV system incorporating high efficiency multi-junction solar cells for the utility scale PV power market, and to foster availability of key components (cells and inverters) for the broad industry. This approach aims to achieve a $0.15/kWh LCOE by 2010 and $0.07/kWh by 2015.

Highlights from the Boeing and its industry partners SETP Program are as follows:

- Developed industry leading CPV cell, module and array technology
- Built and performed extensive testing on proof of design, manufacturing, and prototype modules and arrays
- Increased cell average production efficiency from 36.5% at inception to 40% with the C4MJ cell technology
- Achieved world record cell performance in 2008 with a 41.6% lattice-matched triple junction cell validated by NREL
- Developed and validated numerous improvements that increased solar cell manufacturing throughput, resulting in an increased MJ solar cell throughput per reactor by over 54%
- Achieved a CPV module conversion efficiency of 33.8% on a champion module and > 30% module efficiency consistently

- Developed innovative reflective-refractive (XR) optics that have the highest acceptance angle in the industry (± 1.8° at 800 suns)
- Developed a fully robotic, high volume, vertical manufacturing approach and built a pilot factory demonstrating key elements of this approach to demonstrate LCOE cost goal achievement.
- Validated overall approach to meet 15c/kWh (2010) and developed a pathway to 7c/kWh (2015) for an equivalent PPA for a Utility Scale power plant.
- Developed a technology roadmap including improvements in plastics and design that projects module pricing in the $1/W range.

Summary of Key Program Goals

Program Objective	Stage Gate Criteria	Program Highlights
Solar Cell Performance Improvements	Production Efficiency = 40%	40% mean production achieved 41.6% champion cell measured
Solar Cell production improvements	50% throughput improvement 300MW/y mean throughput rate capability	54% improvement achieved 175 MW/y capability installed (market-driven) by the end of 2012 with ability to expand to 250 MW/y
CPV System Design	Optical Architecture Selected Tracker Design Selected	Off-Axis XR non imaging optical architecture selected. 3.5kW Array, 24 Low cost 2D tracker utilizing COTS H/W selected.
Module Performance	Efficiency > 20% Min Accept Angle of 1 deg Max cell oper temp = 100degC	Efficiency Max = 33.8% Efficiency Avg > 30% Min Accept Angle of ±1.8° Max cell oper temp = 100degC
System Availability	99.9%	99.93% analytically demonstrated
Array qualification	Qualify per IEC-63108 STD	Testing program completed. Qualification per final product. Tracker built and tested.
Inverter Qualification	Demonstrate pilot production of inverter	260kW inverter demonstrated with 20 yr warranty offered.
POD Module Performance	POD output > 250W/m2	POD output > 300W/m2

Automated Mfg with Production Tooling Demonstrated	100kW produced for demonstration site.	33 arrays and 100kW produced, 2MW+ annual capacity demonstrated. Production tooling completed.
Volume Production	Projected capacity for all elements	LCOE =<0.15 cents/kWh validated with studies by Magna, APD, and Navigant.
Projected LCOE	$0.15 /kWh in 2010 <$0.15/kWh in 2015	$0.15 /kWh in 2010 validated <$0.07/kWh in 2015 projected
Commercialization	Identification of deployment plan	CM4J Solar Cell products now offered through Spectrolab System Elements in progress

Summary of Design

The CPV design chosen utilized a ground mounted, 24 module array on a 2D azimuth elevation tracker that can be mass produced and deployed easily in the field. A 6 optical pair module with off axis non imaging optics was chosen to provide a smooth, tightly packed, single surface to the sun to maximize aperture area as well as provide ease of cleaning.

Boeing High Efficiency Concentrated Photovoltaic Array

- **Power: 3.8 kW (Net-AC)/array**
- **Power: 158.4 W (DC)/module**
- **24 subpanel chassis per array**
- **6 Solar modules per subpanel chassis**
- **Single panel tracked array eliminates field alignment**
- **Auto-calibration tracker eliminate pointing errors**

Boeing High Efficiency Concentrated Photovoltaic Array System Developed under SETP TPP Program.

- Off-axis non imaging optics design
- 6 Mirror Reflectors
- 6 High Efficiency Solar Cells > 40%
- High Efficiency Module - >30%
- Negligible O&M
- Air cooled (No Water required)

Boeing's CPV Module demonstrated > 300W/m2 and >30% conversion efficiency.

This system of modules, panels and trackers were sized at 3.8kW with 40% CM4J solar cell efficiency with the intent of enabling ease of handling and low-cost tracking of the panels, and were specifically designed to have no field alignment or adjustment to reduce costs of installation. The system can be mass-produced and deployed in the field by experienced EPC contractors. No special education or training is required.

- 2- 5 MW / Yr solar panel mfg production facility demonstrated
- Highly automated factory with minimal production labor requirement
- Designed and built by World Class automotive and aerospace automated manufacturing experts
- Reproducible production line architecture
  - increase production by increasing capital
  - no or minor line redesign
    - Small square footage requirement– factory can be moved near deployment site to reduce shipping costs
    - Location in US…or Taiwan – high automation factors-out labor costs

The 2MW pilot production facility demonstrated robotic manufacturing of the modules and arrays with production tooling.

The solar cell portion of this Technology Pathway Partnership has made major strides in transforming multijunction CPV cell production from a small-scale, experimental operation to a major industrial endeavor. We have increased production capacity from less than 5 MW at inception to over 100 MW by the end of the program, and with firm plans to expand production in our Sylmar facility to 250 MW upon completion of the new 150mm wafer fab facility in 3Q2012. DOE funding has had a major impact on the industry by leveraging Boeing and its partners' funding to enable this progress. The DOE funding has been supplemented by our formal cost share, and also by $55M of capital investments directly supporting the objectives of the program but uncounted in the formal cost share. Capital investments have supported installation of upgraded MOVPE reactors for epitaxial wafer growth, automated welding, automated material handling, automated testing at both the wafer and bare cell level, and facilities upgrades to transition to 150mm wafer production.

Feature	Benefit	Design Factor
High Efficiency	High power with minimum fielded system	40% efficient solar cells in efficient optical system
High Concentration	Reduces cost of expensive semiconductors and overall system cost	825 suns concentration
Air cooled	No need for water in routine operations Resolves environmental issue for sitting	Passive cooling with heat pipes and radiators
Minimal Field installation time - low cost installation	Reduces cost for field installation	Ship completed & sealed unit Simple helical posts "Plug and play" installation
Wide acceptance angle	Reduces need for high precision tracker and tight optical alignment tolerances	Unique non-imaging optical systems design (XR)
No field calibration	Reduces time & effort in field installation Factory calibration ensures quality	Complete unit built in robotic assembly system
Negligible O&M	Reduces system operations cost Reflects high quality in design & qual	Strong reliability & Quality design process, including qual & test
Designed for low cost, robotic manufacture	Low cost to customer Simple scale up for volume production Minimal hand work for high quality repeats	Design to cost process Design for manufacture process
2D tracking with low cost tracker	Maximum power from panel throughout day maximizes revenue Low cost tracker allows for smaller, less costly units – scalability & affordability	Non-imaging optical systems design Design to cost tracker
Scalable design from ~ 1 MW to 100' s MW	Flexibility in sitting Allows location closer to transmission lines Lower, scalable project costs	250 kW system block design with off the shelf inverter

Key Features of the Boeing High Efficiency Concentrated Photovoltaic Array System.

New Higher Efficiency Epitaxial Device Structures

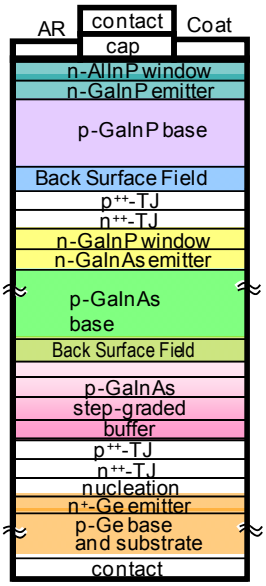

Improved Wafer Metallization Processes for Reduced Shadowing

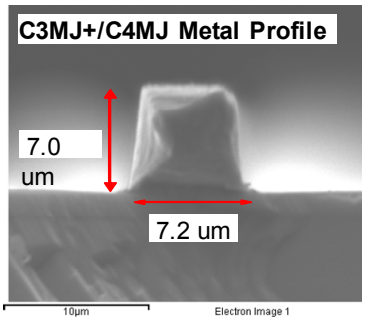

New World Record Solar Cell Performance

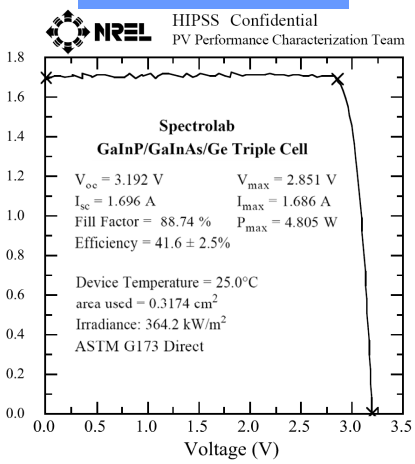

Extensive Qualification Testing of Five Product Generations

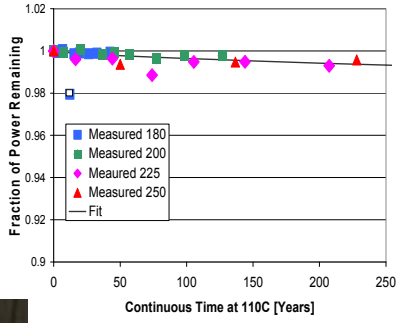

Cell Assembly Reference Design

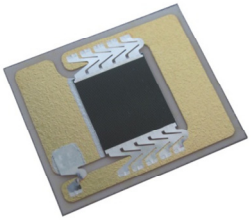

MOVPE Modernization

Factory Automation

US-based Germanium Supply chain Development

The TPP Program brought Multijunction cell technology from Space to Earth — delivering higher efficiency, lower cost, and increased manufacturing capacity

Design and Construction of New 150mm Wafer Fab Facility

Numerous solar cell design, performance, production flow and timing improvements implemented at Spectrolab in the course of the SETP TPP program

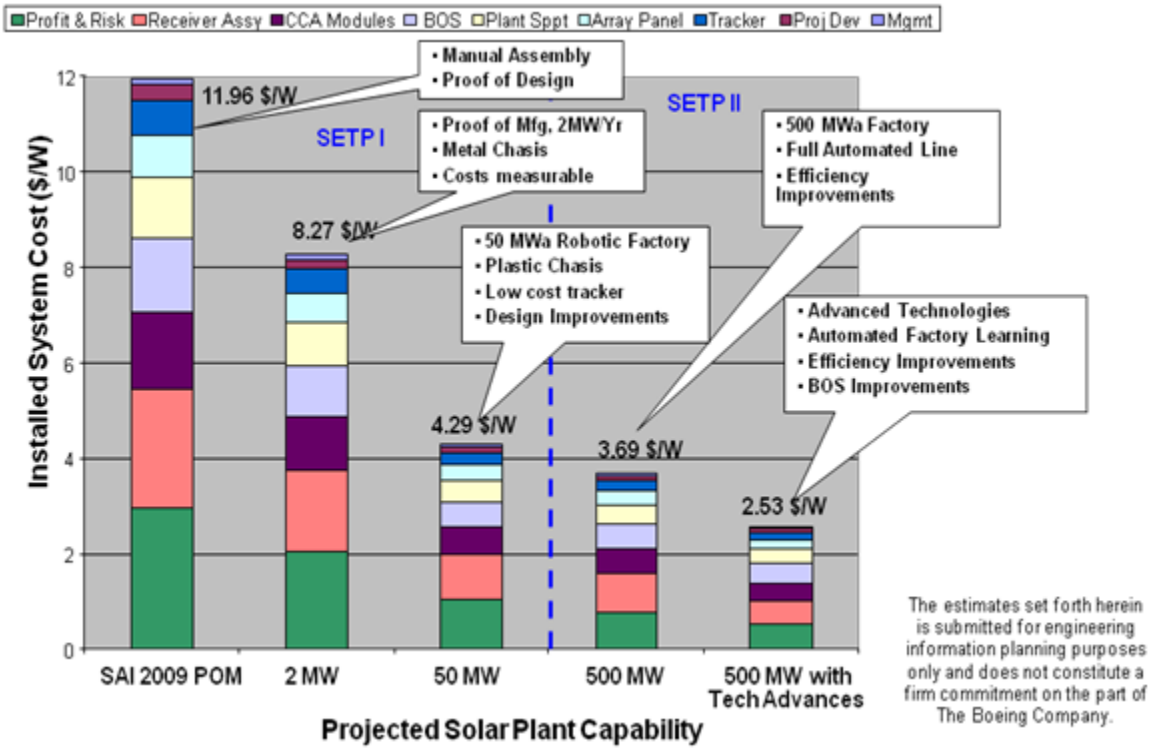

Project installed costs for CPV utility scale power plant.

The major areas of accomplishment for the cell technology portion of the TPP are highlighted on page 24. Spectrolab has introduced five generations of CPV cell technologies into volume production over the span of this program with the support of the DOE investment, taking the 36.9% average production efficiency of C1MJ technology at the program's inception to expected ≥39.2% average production efficiency of the C3MJ+ technology introduced into production in November 2010, and 40% efficiency C4MJ cells developed and partially qualified by the end of the program. Throughout the program, the Spectrolab cells maintained the highest available production cell efficiencies.

Summary of project activities over the entire period of funding

The project activities over the period of funding included developments and maturation of the solar cell, module, array, tracker and balance of system elements of a utility scale solar power plant. The activities were based on the hypothesis that an affordable solar power generating device utilizing high efficiency solar cells could be realized if efficient and low cost optics (mirrors) could be used to offset the higher cost of the semiconductor material. The approaches considered ranged from a minimum of 500 suns concentration to as high as 2000 suns.

Our approach for demonstrating a commercially competitive system entailed

- Improvements in high performance multijunction photovoltaic technology
- Implementation of non-imaging dual element optics which offer advantages with respect to achievable concentration (higher is cheaper), uniformity of semicon-

ductor illumination (improved semiconductor life and performance) and acceptance angle (inversely proportional to the precision and cost of support hardware)

The problems and challenges encountered in this effort included managing the waste heat as a result of highly concentrated solar energy, development of an environmentally tolerant design implementation to avoid undue aging both electronics and optics, development of efficient optical design to realize the full potential of the system, low cost tracking required to by the concentrating optics and demonstration of automated production capability required to realize the potential cost savings. All of these problems and challenges were discovered and overcome in the course of the program.

Throughout the course of the program no material deviations from our original planned methodology occurred. All of the stage gate milestones were achieved.

How the research adds to the understanding of the area investigated

The Boeing CPV system improves the state of the art for CPV and specifically improves the design, the performance, the manufacturing production capability, and balance of plant layout of CPV in order to reduce installation costs and overall LCOE for solar installations.

The design of the Boeing system utilizes a new approach to the optical architecture with a reflective/refractive free form optic designed to improve the acceptance angle over other approaches to maximize solar collection performance over the entire array.

The performance of CPV improved over the program taking it from an initial 23% module efficiency to over 30% module conversion efficiency with the addition of the new optical approach and module design. Other design improvements included materials and manufacturing approaches to reduce costs and provide environmental protection from humidity, heat, and UV exposure.

The C4MJ technology for the first time introduced a metamorphic epitaxial solar cell into high volume production, a real milestone for the industry. The C4MJ product qualification was completed in February 2011 and began production in March 2011. Spectrolab conducted its most extensive qualification tests to date for the introduction of this new technology, including a six-month field trial in collaboration with Amonix, with no evidence of any reliability limitations or performance degradation different from the extremely low degradation rates demonstrated with lattice-matched cells.

Spectrolab transitioned epitaxial wafer production to a new generation of MOVPE reactors with many design enhancements that open new avenues of process control, enabling the C4MJ technology (not feasible with the prior reactors) as well as a wide palette of potential future architectures for even greater efficiency. A significant portion of the efficiency improvements during the program have resulted from advances in wafer metallization processes, and those capabilities continue to advance with the C3MJ+/C4MJ technology. DOE investment through our TPP has also enabled production of quality epi-ready germanium wafers from a US source (Sylarus) for the first time, and Sylarus is now a qualified supplier for Spectrolab CPV products. The program has resulted in major cost reductions for CPV cells. Automation of the welding process reduced labor content in cells with interconnects by 82%, and installation of automated dicing saws

and pick & place capability from the dicing tape, in addition to automated test that replaced previous manual test, reduced cost of bare cells by 60% by the end of 2010,. Further cost reductions will result from the transition to 150mm wafer fabrication in 2012 as graphically summarized on page 25.

Manufacturing methodologies were developed that maximized the throughput capacity of a fully functioning production factory for both the solar cell process and the module and array production process. These technologies primarily included automation robotics but also included Spectrolab's 150mm fab line and reactor improvements.

Finally, dense packing approaches were developed for deploying CPV in large Utility scale power plants that increased energy collection densities considerably higher than flat panel or thin film power plant equivalents, thereby identifying a significant competitive advantage of CPV at the power plant level.

Overall Conclusions and How This Effort benefits the public

Based on the results achieved under this program, Boeing has achieved the stage gate criteria as required. From our view point, the TPP program has achieved the following benefits.

- The CPV technology and its impact on the solar market has matured significantly as a direct result of the SETP program
- CPV has the highest efficiency of any technology developed to date
- CPV is a competitive technology to all forms of PV (c-Si and thin film) and CSP
- Free Form XR non-imaging optics provide significant improvements to CPV performance and have advantages over Fresnel approaches
- A vertical fully automated manufacturing approach is the preferred production method for building and assembling the CPV modules and Arrays.
- CPV can achieve a much higher energy density (Wha/acre) over flat panel fixed tilt installations. The CPV system developed under this program has the ability to collect an average of 625MWha/acre energy density as compared to a fixed tilt flat panel installation typically estimated at 480 M Wha/Acre further demonstrating the competitiveness of CPV.
- Costs approaching 6 - 7c/kWh are potentially achievable with CPV.

Finally

Boeing and its TPP partners wish to thank the DOE for its contribution and support of the CPV technology development project.

Introduction

Project Title:	High Efficiency Concentrating Photovoltaic Power System
Covering Period:	August 2007 – Dec 2011
Date of Report:	Mar 2012
Award Number:	DE-FC36-07GO17052
Recipient:	The Boeing Company
TPP Members	Boeing, Spectrolab, LPI, others
DOE Project Team:	Dr. John Hall, Program Manager and Chief Scientist

Project Description Overview

The project will develop a new concentrating photovoltaic CPV system incorporating high efficiency multi-junction solar cells for the utility scale PV power market. A novel optical design will be developed to take best advantage of the cells; and reliability and cost of the tracker and balance of system will be improved as well. This approach aims to achieve a %0.15/kWh LCOE by 2010 and $0.07/$kWh by 2015.

Budget Summary

The total budget period information is as follows:

- Total estimated cost of project, including DOE funds to FFRDC = $45,314,582
- Recipient share of total approved budget from the DOE = $20,240,193

Major Tasks and Objectives for the Boeing High Efficiency Concentrating Photovoltaic Power System

Task/Title	SOPO Ref.	Overall Task Objective
1. Solar Cell Efficiency Improvement, Qualification and Field Test	1.3, 2.3, 3.3, 1.4, 2.4, 3.4	Improvements in state of the art triple junction cell technology Demonstrate solar cell production readiness and field durability
2. Solar Cell and Receiver Manufacturing Maturation	1.5, 2.5, 3.5	Lower cell production cost through improved manufacturing processes
3. CPV System Design	1.6, 2.6, 3.6	Conduct trade studies and design tasks to develop and optimize the design of the CPV module, panel, array, and power plant
4. System Engineering	1.7, 2.7, 3.7	Perform system-level, end-to-end engineering for the CPV system including reliability,

		failure modes and effects, design to cost, and test/validation planning
5. CPV System Manufacturing Maturation	1.8, 2.8, 3.8	Develop design for manufacturing for the candidate designs and implement factory designs
6. Proof of Concept (POC) Fabrication	1.9, 2.9, 3.9	Build and test proof-of-concept modules
7. Proof of Design (POD) Fabrication	1.10, 2.10, 3.10	Build, integrate and test proof-of-design modules and array
8. Proof of Manufacturing (POM) Fabrication	1.11, 2.11, 3.11	Build, integrate and test proof-of-manufacturing demonstration system
9. System Testing	1.12, 2.12, 3.12	Conduct qualification tests of modules and arrays and other components
10. Deployment Facilitation	1.13, 2.13, 3.13	Identify commercial partner(s) for marketing and distribution

The Boeing lead Technology Pathway Partnership was a team effort over three plus years. The team responsible for execution of this program is graphically summarized below

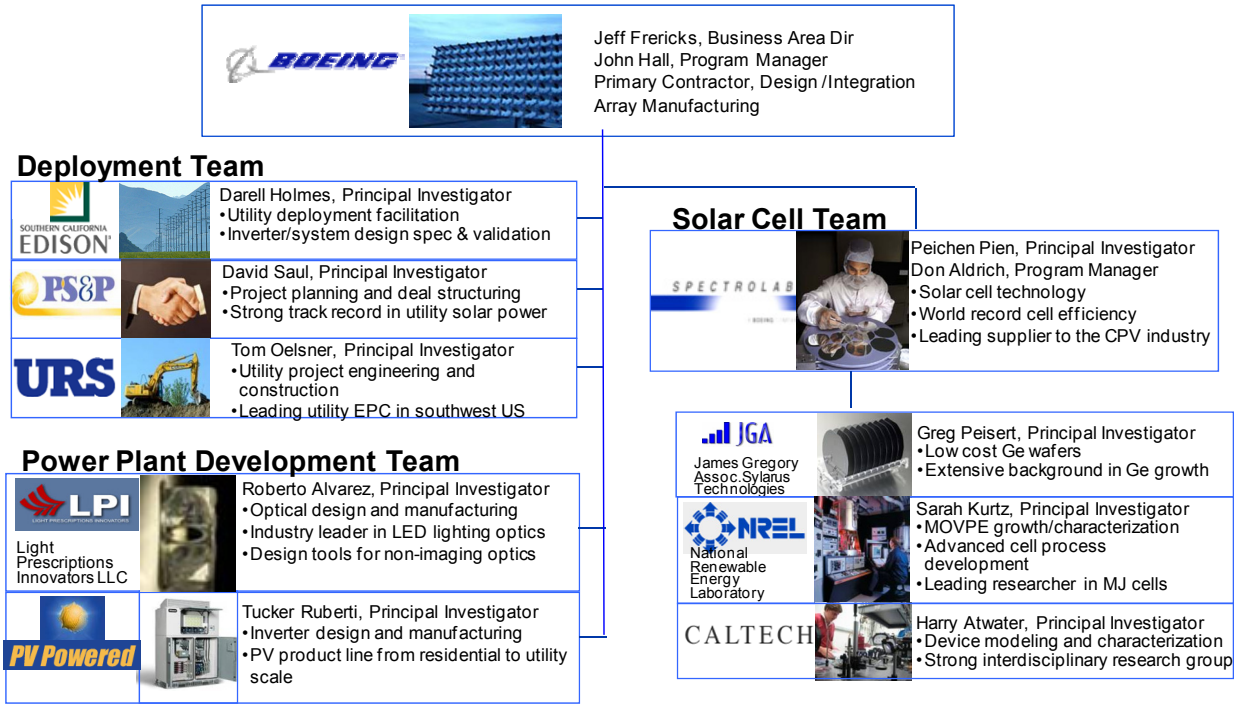

Boeing lead Technology Pathways Partmership Team

The program was managed by the DOE in gated manner which tracked performance versus milestones are enumerated below.

Gated Contract Management Summary

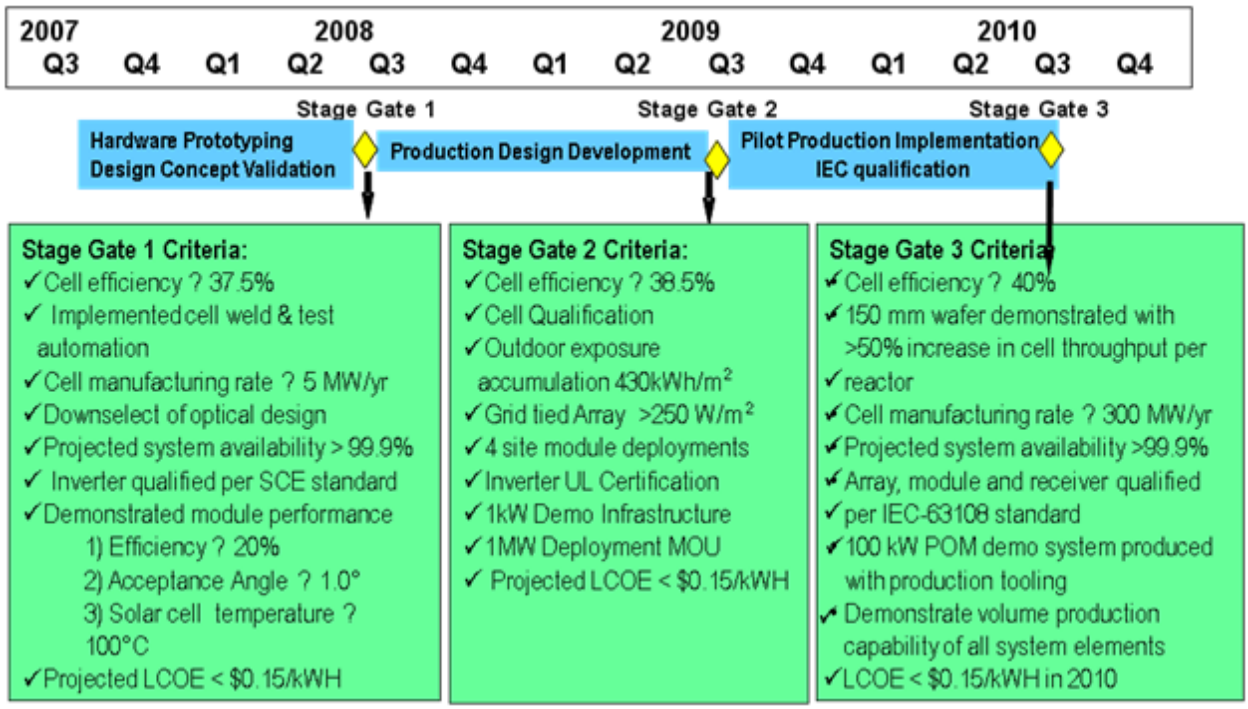

To report on such a diverse program in a clear and succinct fashion we have structured this report around the tasks described in the original contract for the three year planned program duration. Each major section of the report covers a group of contract tasks for the entire contract.

To further aid clarity we begin each section with the contract objective, and enumerate the major stage gate milestones associated with the task. This is supported by a bulleted list of major accomplishments. These summary sections are followed by detailed technical narrative the activities and results achieved for each task.

1 Solar Cell Efficiency Improvement, Qualification and Field Test - SOPO Tasks 1.3, 2.3, 3.3, 1.4, 2.4, 3.4

Task Objectives

The overall objective of this task is the improvement of cell efficiency and the qualifications of each improved generation of cells for terrestrial CPV applications. The more specific objectives for each level of improvements are,

- Conduct MOVPE cell growth experiments to improve concentrator cell voltage, current, efficiency. Develop metamorphic and lattice-matched multijunction cell, and novel cell architectures, for high efficiency. Perform modeling of concentrator solar cell efficiency and energy production.
- Conduct experiments to achieve narrower, lower resistance, metal gridlines with high reliability. Develop novel approaches to reduce series resistance and grid shadowing and improve cell isolation.
- Fabricate and characterize experimental cell builds.
- Conduct studies of receiver performance under more extreme conditions. Verify and improve long-term reliability of receiver materials and design.
- Develop receiver designs and materials for low-cost, high-throughput receiver assembly.
- Develop methodology and prototype equipment for testing new types of high-efficiency concentrator solar cells. Fabricate and calibrate solar cell test standards. Conduct studies to compare steady-state and transient test methods, and to compare cell measurements at independent solar cell test labs. Develop methodology and prototype equipment for outdoor testing of high-efficiency concentrator solar cells.

Highlights

- Qualified 5 generations of CPV cells over the course of the TPP program.
- Increased average production cell efficiency from 36.5% with C1MJ cells to 39.8% with C4MJ cells over the course of the program.
- Demonstrated a world record cell efficiency (at that time) of 41.6% for a lattice-matched, triple junction solar cell in 2008.
- Demonstrated cell reliability through qualification and field tests.

Table 1-1. Task 2, Cell Efficiency Improvement and Qualification Milestones

Period	Criterion	Results
1	1a-1. Production mean cell efficiency of 37.5%	Achieved 37.8% in volume in volume production of qualified commercial C2MJ cells developed in Phase I

Period	Criterion	Results
2	2a-1. Production mean cell efficiency of 38.5%	Achieved 38.7% in volume production of qualified commercial C3MJ cells developed in Phase II
3	3a-1. Production mean cell efficiency of 40%	Achieved 39.2% efficiency with C3MJ+ and 40% efficiency with C4MJ cells developed in Phase III. Both type are fully qualified and field deployed in commercial power plants

Technical Accomplishments

1.1 Advanced Cell Efficiency

Supported by TPP funding, Spectrolab successfully completed development of five generations of cell process technology and transitioned each to full production. At the inception of the program, Spectrolab had developed the C1MJ cell and put it into pilot production, but qualification was not yet completed. The qualification was completed in June 2007' By the end of Budget Period 3 in December 2010, when Spectrolab participation in the program ended, Spectrolab had successfully qualified the C3MJ+ technology and begun volume production, and much of the C4MJ development and qualification had been completed. Final qualification and release to production of the C4MJ technology was achieved in March 2011. Figure 1-2 shows the progression in production efficiency distribution for the C1MJ technology that existed at the outset of the program, the C2MJ and C3MJ technologies introduced in budget periods 1 (July 2007–June 2008) and 2 (July 2008–June 2009), respectively, and production C3MJ+ and C4MJ cells produced in 2011 (after the end of the Spectrolab TPP effort). The C3MJ+ was introduced into full production by Spectrolab as a direct result of the work under this program, by applying wafer process improvements developed for the C4MJ product to the lattice-matched C3MJ epitaxial structure. All of the C1MJ, C2MJ, C3MJ, C3MJ+ and C4MJ cells ("C" for "Concentrator," MJ" for "Multi-Junction," and the digit reflecting tech-

Figure 1-1. Spectrolab products introduced during the TPP program.

nology generation) were/are tested using the Spectrolab standard production test high concentration pulsed solar simulators, with calibration traceable to JPL balloon flight cells (such test standards are not yet available for C4MJ cells, as will be discussed further in Section 1.3).

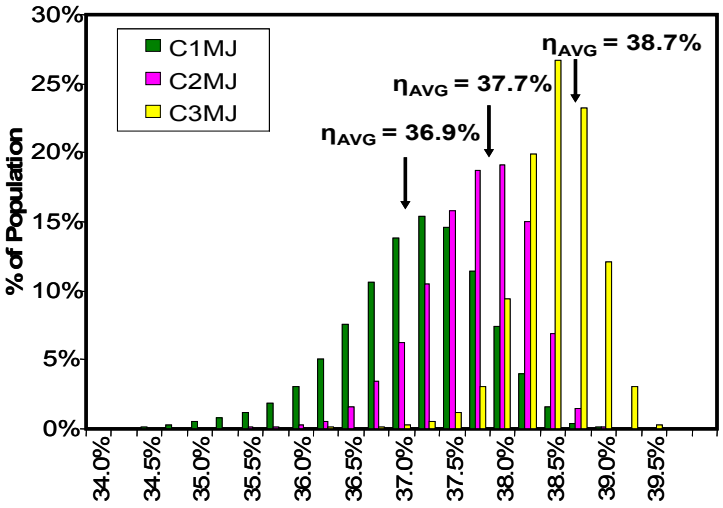

(a) C1MJ, C2MJ, C3MJ

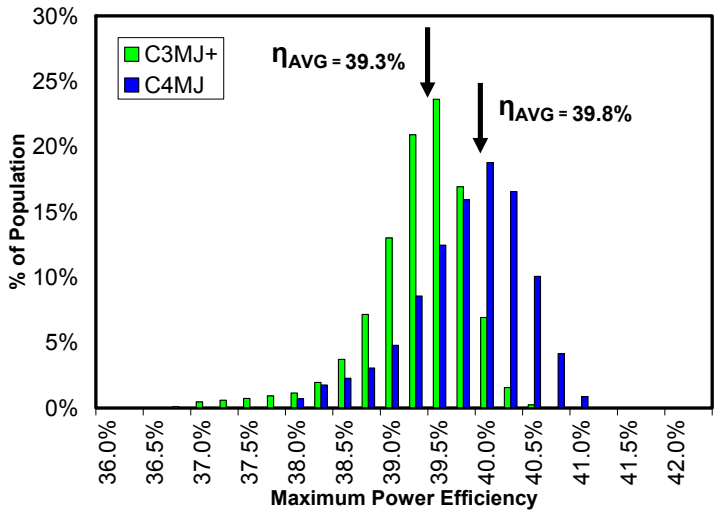

(b) C3MJ+ and C4MJ

Figure 1-2. Production Efficiency Histograms for Spectrolab CPV Cells (at 50 W/cm^2 illumination)

The differences between lattice-matched and metamorphic triple-junction cell structures are illustrated in Figure 1-3. C4MJ metamorphic cells transition the lattice constant of the top and middle cells from that of the growth substrate by means of a series of step-graded transparent buffer layers, designed to isolate the resulting crystal dislocations in inactive layers that are fully relaxed so that there is no built-in strain to propagate the defects to other layers. The introduction of our C4MJ technology represents a major departure from the prior state of the art using lattice-matched cells, and presents many manufacturing challenges for high rate production at high yield and acceptable cost. Overcoming these challenges was the primary device development activity of budget period 3 of the program (July 2009–Dec 2010).

The design improvements implemented for the C2MJ process in Budget Period 1 consisted of improvements in front metal patterning. It is well-known that shadowing of the semiconductor surface by the metal fingers that collect and conduct the photocurrent to the external circuit is an important loss mechanism. This is particularly true for cells designed for high concentration, since the current and hence metal density is correspondingly higher. Photoresist and metal deposition processes were modified to increase gridline aspect ratio (height / width). This allows grids to conduct equivalent or higher current while also admitting more light to the active layers. C2MJ uses the same epitaxial wafer as C1MJ, but generates extra current as a result of the reduced gridline shadowing. The modeled and

measured result was an average of 0.5% absolute efficiency improvement over C1MJ. Spectrolab began high volume production of C2MJ in May 2009.

The C3MJ design retained the same wafer metallization processes that were qualified in

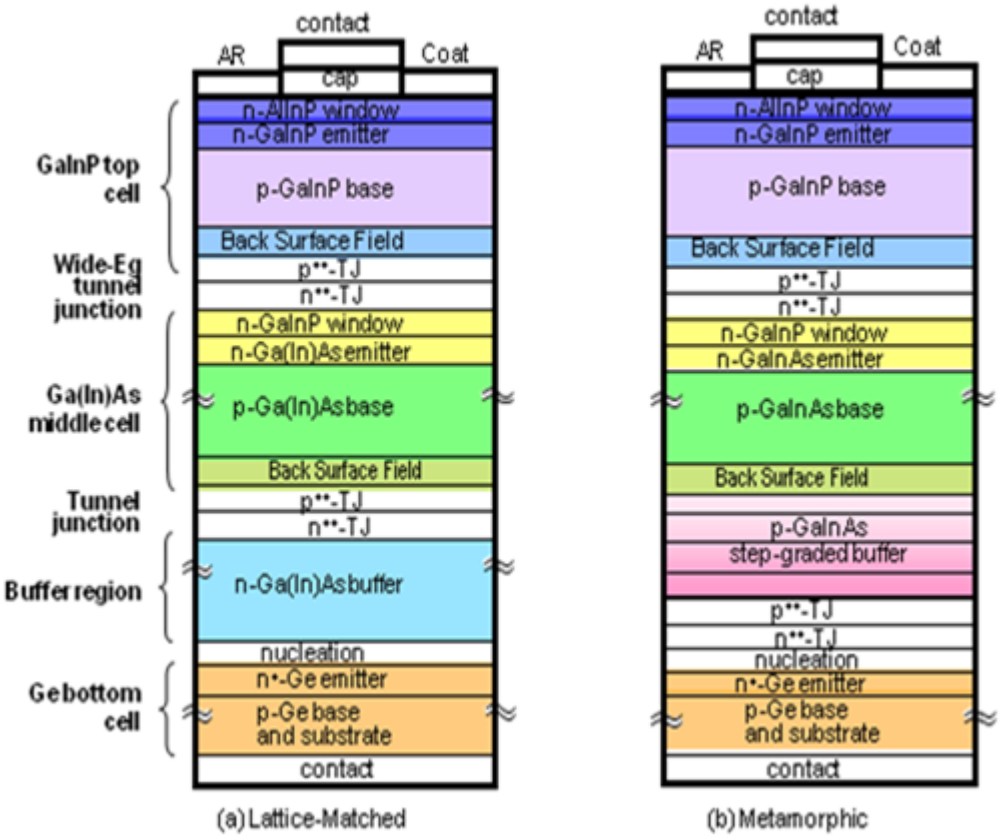

Figure 1-3. Lattice-matched and metamorphic cell epitaxial structures

the C2MJ process, but also incorporated an improved epitaxial design. The epitaxial process for C1MJ and C2MJ cells is common to both and is designated internally as CITJ; the C3MJ process uses a new epitaxial process designated internally as CUTJ. The CUTJ top cell band gap is higher than that of the CITJ process but the top cell is thicker, resulting in a more sharply defined absorption edge as shown in the spectral response comparison in Figure 1-4.

The C4MJ technology introduces both epitaxial structure improvements and wafer processing improvements. The metamorphic cell has a step-graded buffer layer between the bottom germanium cell and the middle cell to transition to a slightly larger lattice constant Ga(In)As middle cell, upon which is grown a lattice matched GaInP top cell; the middle and top cells more closely match the optimum bandgap combination for the solar spectrum, and higher efficiency cells in this configuration have been demonstrated. As illustrated in Figure 1-5, the combination of this lattice constant shift and control of the disordering in the (In, Ga) sublattice of the top cell, brings the metamorphic design closer to the optimum for a 3-junction cell with Ge as the bottom cell.

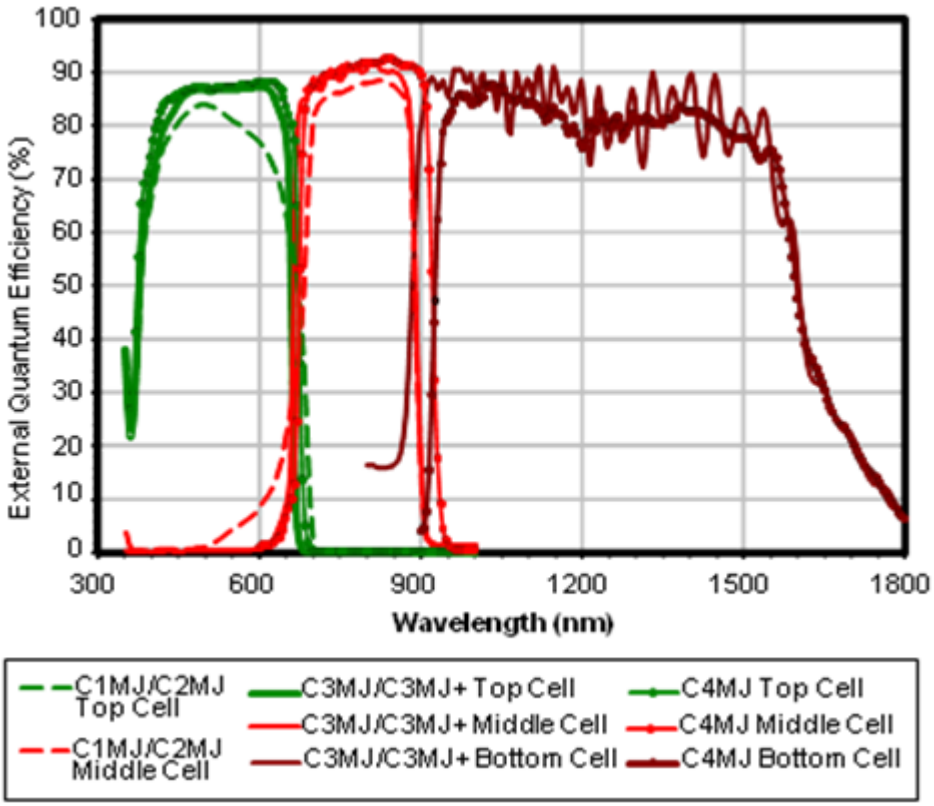

Figure 1-4. C1MJ/C2MJ, C3MJ/C3MJ+, and C4MJ Spectral Response

We have also carried forward continuing improvement of the lattice-matched cell, since it has also been demonstrated at 40% efficiency. Indeed, a lattice-matched cell fabricated at Spectrolab in February 2008 set a new world record for conversion efficiency as verified by NREL in August 2009 (see Figure 1-7). This cell performance surpassed the 41.1% record ostensibly held by Fraunhofer ISE (announced January 2009). This lattice-matched cell epitaxial structure was virtually identical to the C3MJ cell, with reduced grid shadowing as planned for C4MJ cell. Figure 1-8 compares the modeled device current-voltage curves for the three subcells for an upright metamorphic approach against a standard lattice-matched approach. The modeled 40% metamorphic cell has slightly higher I_{MP}, and lower V_{MP} compared to the lattice-matched design.

The C3MJ+ technology is a direct result of the work done during budget period 3 toward introduction of a metamorphic C4MJ technology, incorporating the wafer process improvements but retaining the proven C3MJ epitaxial structure. Because the C4MJ metamorphic technology constitutes higher risk both in manufacturing and in the field, it has been subjected to a much more rigorous qualification program than was needed for C3MJ (more on this topic in Section 1.3); introduction of C3MJ+ was by comparison lower risk, and a smaller set of tests was necessary to have full confidence in its manufacturability and field performance.

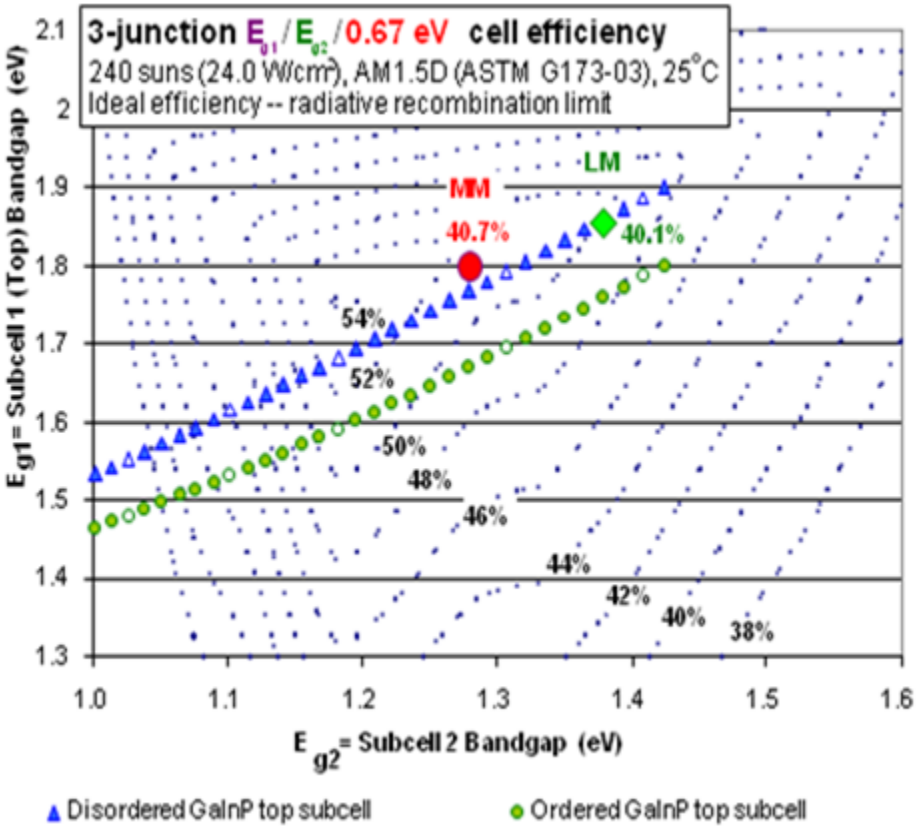

Figure 1-5. Efficiency contours for combinations of top and middle cell band gap (with constraint of Ge bottom cell).

.Over the medium to long term, we expect to introduce improvements to the fundamental epitaxial structures used in multi-junction devices, as illustrated in the device structure roadmap of Figure 1-6. All of our production cells prior to C4MJ have been lattice-matched. Lattice-matched cells have the obvious advantage of being a proven technology, and the ability to grow structures of very high crystal quality has been demonstrated. Further evolution of the lattice-matched approach is certainly possible, with promising candidate device architectures in 4, 5, and 6-junction configurations. We conducted research along several of these vectors in Budget Period 2 (July 2008–June 2009). We completed an extensive series of experiments and a major cell build in development of a new 4-junction cell design for terrestrial concentrator cells. Other achievements in the long-range research include our first demonstrations of 4-junction upright metamorphic terrestrial concentrator cells and 3-junction inverted metamorphic terrestrial concentrator cells. We also conducted research on the use and benefits of prismatic covers on concentrator cells to direct incoming light away from gridlines. Such an approach can permit a greater metal coverage on the front surface, reducing series resistance loss, without suffering additional shadowing loss, and can benefit performance of systems without a refractive secondary, by replacing the coverglass or other encapsulation with a prismatic microlens array. Figure 1-9 shows the gain in external quantum efficiency demonstrated for a cell with 20% metal coverage by grids.

1.2 Wafer Process Design

Wafer processing refers to the creation of completed solar cells, using the epitaxial wafers grown in the MOVPE tools. The wafer process includes deposition of anti-reflective coatings and metal grid structures on the front, and metal on the back to form the back contact. Improvements in the wafer process design account for much of the efficiency gains demonstrated in this program, progressing from the C1MJ process at inception of the program to the greatly improved process reduced to practice for C3MJ+ and C4MJ cells. During budget period 1 (July 2007–June 2008), we introduced the C2MJ process and this same wafer process was carried forward to the C3MJ design in budget period 2 (July 2008–June 2009), while we continued with numerous process initiatives to improve the wafer processing for both higher efficiency and cost reduction. Figure 1-10 illustrates the improvements to the front contact profile made over the course of the program, with consequent efficiency improvements (0.8% absolute from C1MJ to C2MJ, and 0.6% absolute from C3MJ to C3MJ+).

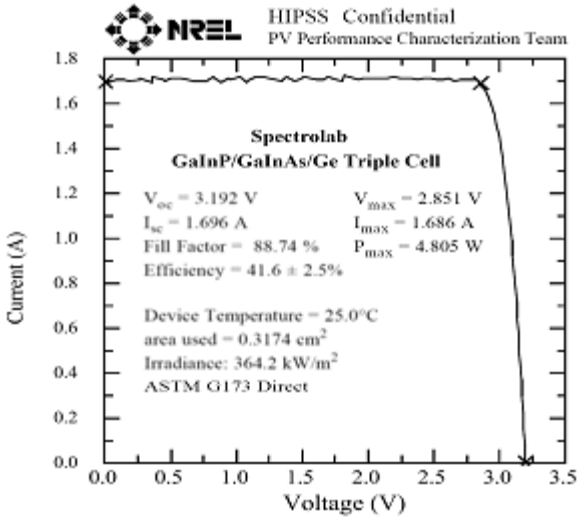

Figure 1-7. Spectrolab world-record efficiency cell, produced in 2008 and verified in August 2009.

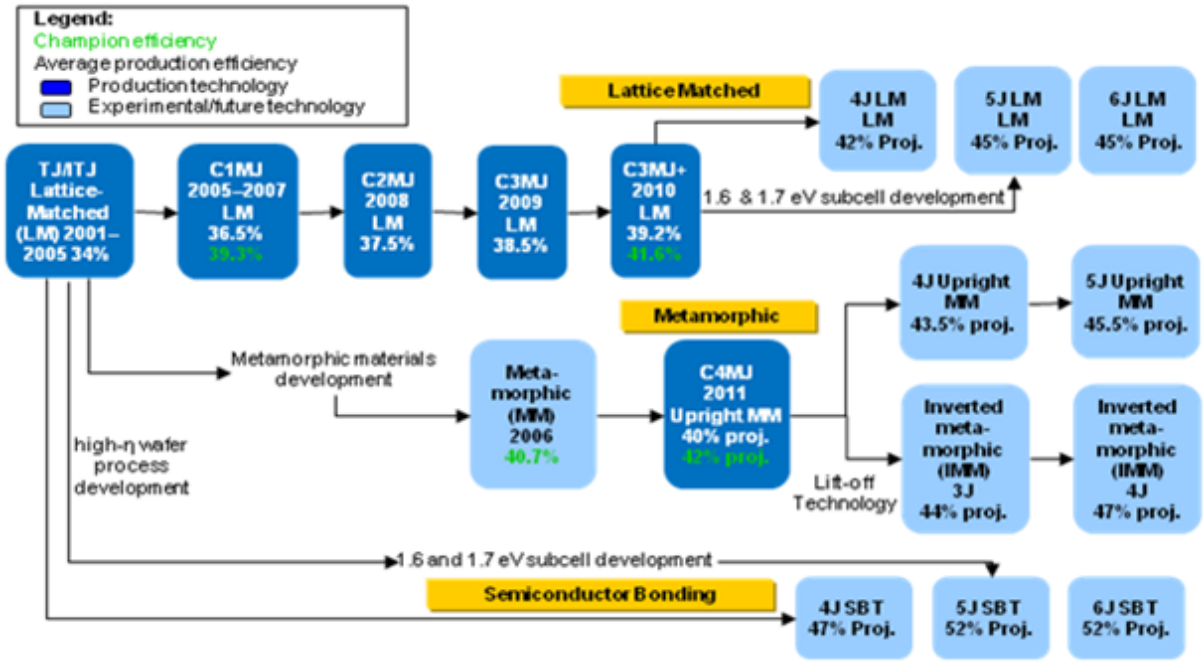

Figure 1-6. Cell epitaxial structure development roadmap

We modeled effects of gridline width, metal profile, and pitch on cell efficiency in 3-junction lattice-matched, 3-junction metamorphic, and 4-junction cells. The models developed were used to guide changes in gridline metallization for the C3MJ+/C4MJ proc-

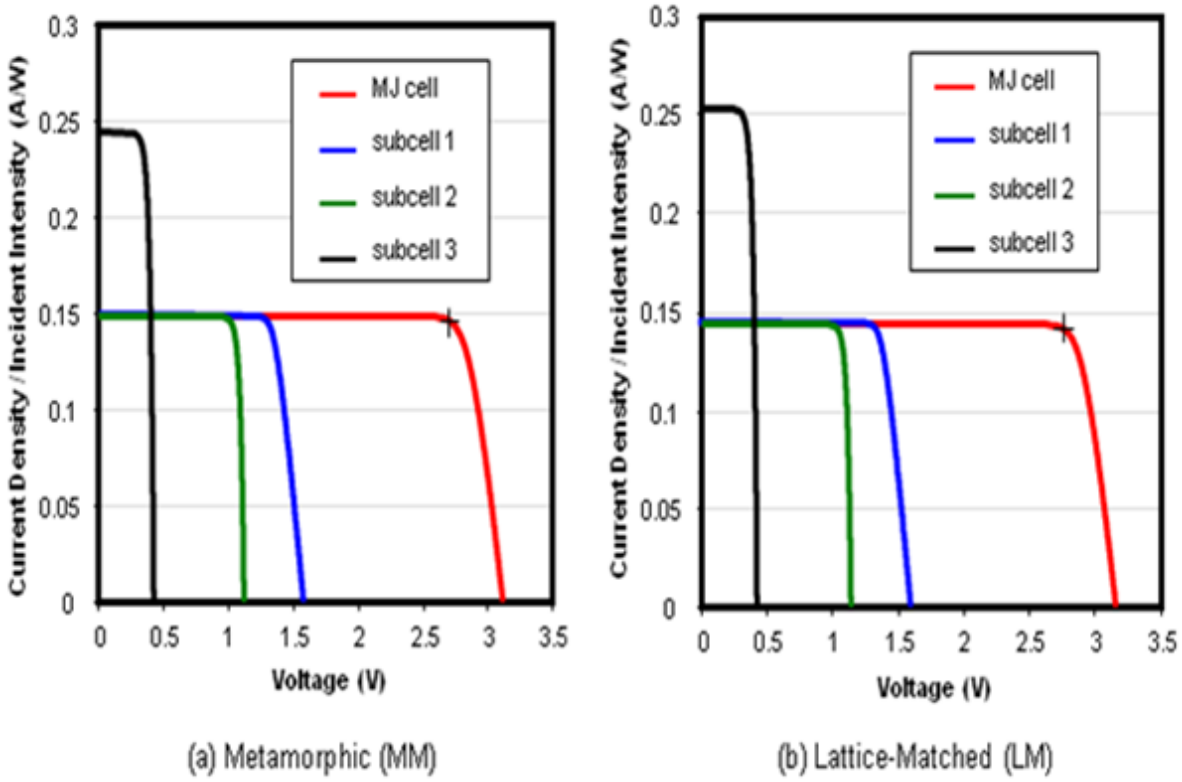

Figure 1-8. Target Current-Voltage Characteristics of 40% metamorphic and lattice-matched cells.

ess. Achievable grid finger width is limited by the photolithography process and by grid adhesion considerations. Figure 1-11 shows some key results from the gridline modeling. We showed that when both normal and off-axis illumination are considered, a grid finger aspect ratio close to unity is optimal. We also showed that little further gains are possible due to further reduction in gridline width for CDO-100 cells operating at 50 W/cm², but further gains are possible for smaller cells operating at higher intensity, with gridlines as small as ~3.5 μm.

Other process optimizations were aimed at further reduction of the shadowing associated with contacts. We pursued this through a series of experimental builds with standard epitaxial wafers and wafer process splits including:

- Optimized CAP etch / Self-Align process to reduce obscuration
- Grid profile/ new photoresist material for efficiency improvement and process cost reduction
- Evaporation process optimization to improve grid profile

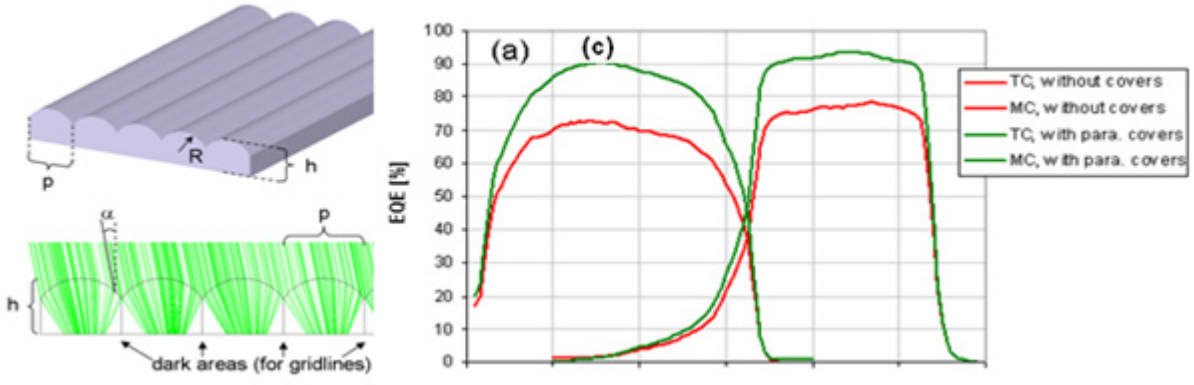

Figure 1-9. Demonstration of prismatic lens improvement on cell current.

(a) 3D rendering; (b) cross-section schematic with incident rays shown in green; (c) spectral response of 20%-metal-coverage cells with prism covers

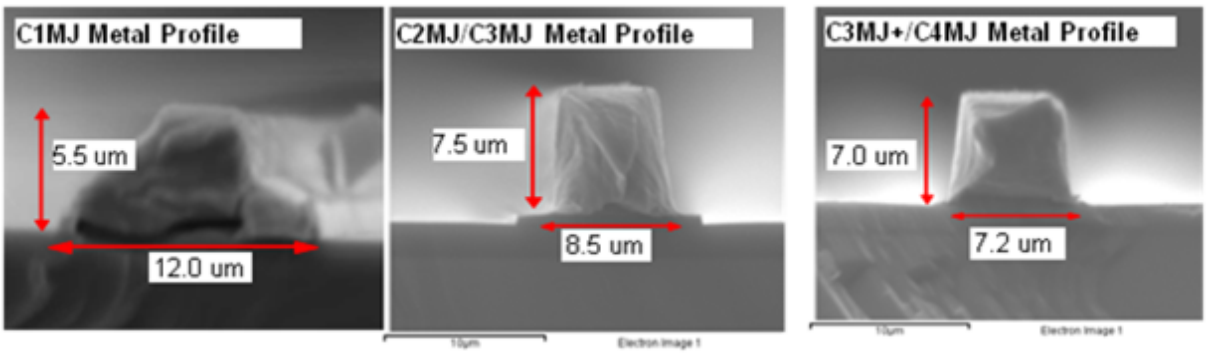

Figure 1-10. Progression of front contact design improvements.

In multijunction cell manufacturing, the front side of the epitaxial wafer has a cap layer that is the foundation of the ohmic interface to the semiconductor and is a narrower bandgap material than the top cell. In wafer processing, this cap layer is first etched away except where metals will be deposited, and then the wafer is coated with anti-reflective oxide layers; then the AR layers are etched away at the locations for metal grids and bus bars, and the entire wafer is then coated with the metals. Finally the metal is removed except where the deposition patterns were made in the AR coating. This final process is known as liftoff, and at the start of this program was essentially a manual process, with technicians intervening in the metal removal process to ensure complete removal of unwanted metal. In budget period 2 we completed development of a new automated metal lift-off process. We evaluated process equipment from two vendors and conducted trials on several different devices and with a variety of frontside processes. Based on these trials we formulated a baseline recipe that works for all device and process variations, device designs, and front metal stacks identified. Key criteria for development were process yield, materials consumption, and compatibility with all design and process variants. This capability will be implemented as part of the new 150mm wafer fab facility currently under construction.

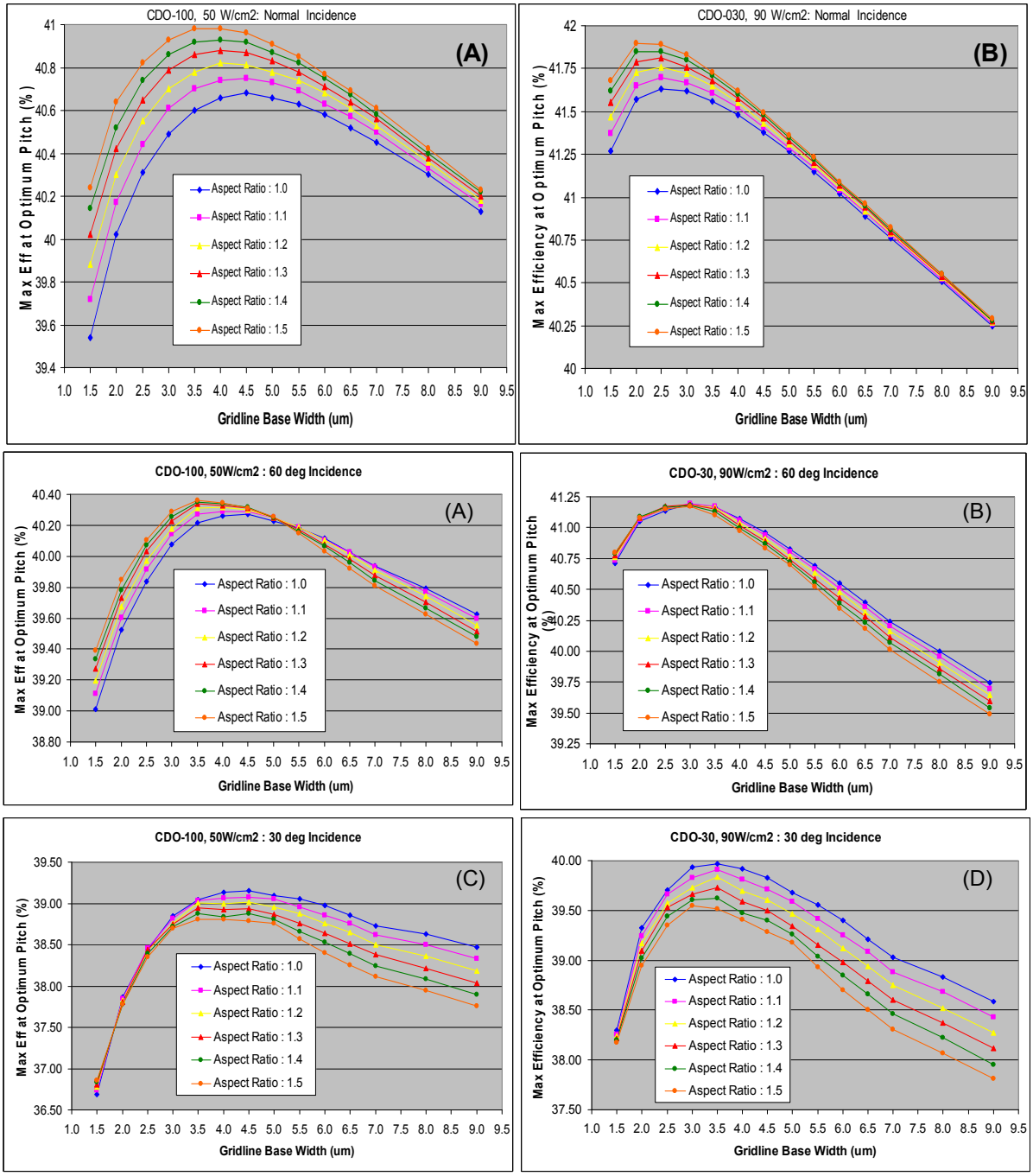

Figure 1-11. Gridline width and aspect ratio optimization modeling results.

We also developed a new wet mesa etch process for cell isolation targeted for very small devices (with active area smaller than 30 mm²) in budget period 2. A cross-section of a device fabricated with the improved process is shown in Figure 1-12. Previously, Spectrolab used a saw cut through the epitaxial layer to isolate the cell mesas from each other (a requirement for wafer-level testing) rather than etching. While the saw cut method was cost-effective for larger CPV cells and space cells, it was not well-

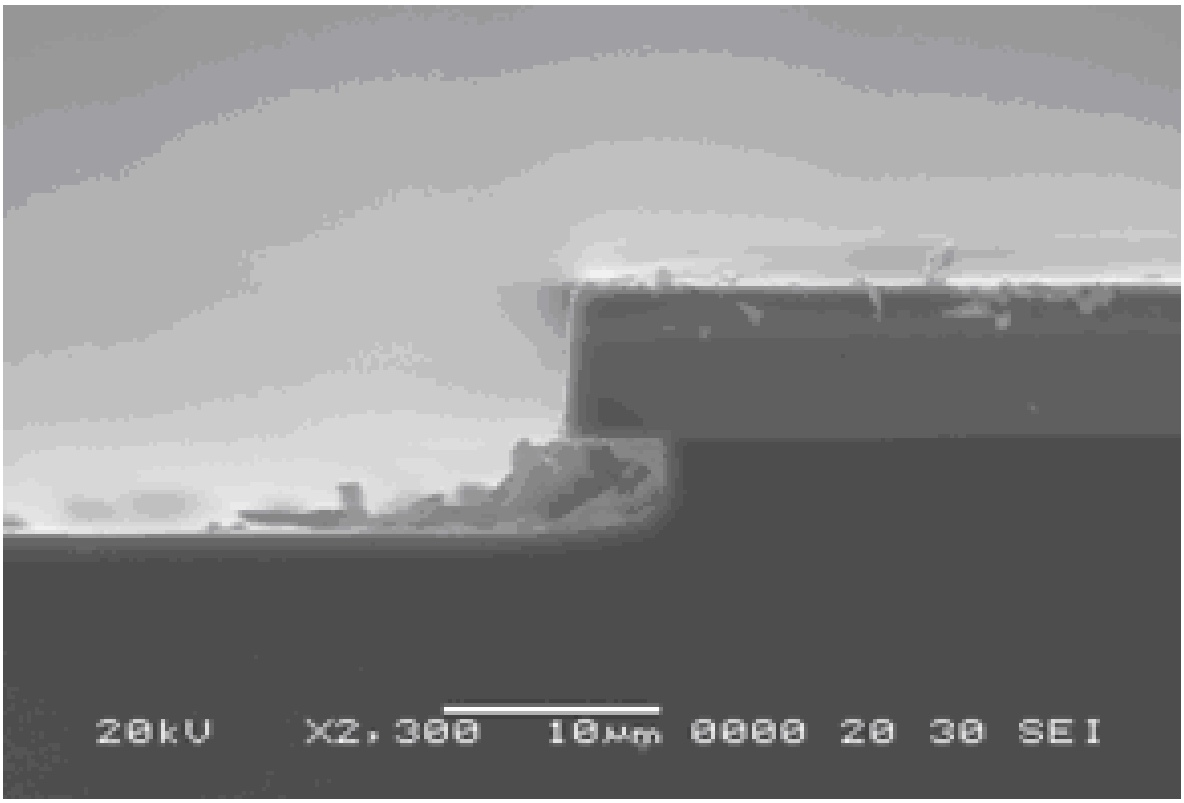

Figure 1-12. Mesa cross-section with new all-chemical process

suited for small cells for two reasons: (a) the number of saw cuts necessary increases as cell size decreases, and (b) edge defects resulted in poor performance of small cells, which have a greater ratio of perimeter to area. Analysis has shown that the wet mesa etch process is competitive for devices of all sizes and thus permits a single isolation process to be used in the new factory. Although full implementation in production awaits completion of the 150mm wafer fab facility, we have prototyping capability to replicate the process in small volume, and it has been successfully demonstrated on small cells with excellent performance (equal to that of larger cells) delivered to customers in mid-2010, and has been implemented for selected products in smaller volume, in advance of the completion of the 150mm facility.

C4MJ samples produced on the prototype 6” line have been on sun in a customer system since August 2010.

For the C3MJ+/C4MJ front metallization process, we added an optional gold cap layer. This layer was requested by some customers for improved wire bondability and improved visual appearance generally, but also adds cost. It has been made as a product option because many customers have been using the previous silver metallization effectively with both welding and wire bonding, so some customers may prefer to retain the silver surface for reduced cost. Overall, the work done during budget periods 2 and 3 has reduced process cycle time, and provided a strong foundation for the baseline process definition for the 150mm wafer process line.

1.3 Qualification Test

Test	Test Conditions	Qty	Requirement
Performance Tests			
LIV	50 W/cm2 under ASTM 173G	100%	Avg η_{mp}>38.5%; Min η_{mp} > 36.2%
Temp Intensity	50, 75 & 100 W/cm^2, ASTM 173G at 10°C, 25°C, 65°C, and 110°C	20	Characterization
Weld Degradation	LIV test before and after weld	100% of scribed parts	NP_{mp} > 0.98
Spectral Response			Characterization
Angle of incidence	X25 or SR illumination source	10	Characterization
Solar Absorptance	Measure reflectance	10	Characterization
Accelerated Life Tests			
Damp Heat	85C, 85% RH for 2000 hours	30	NP_{mp} > 0.9
Thermal Cycle	IEEE 1513 (500 cycles –40°C to +110°C)	25	NP_{mp} > 0.9
High Temp Soak in Nitrogen	unbiased soak at 200°C and 250°C in Nitrogen	15 at each T	NP_{mp} > 0.95 after 25 yrs

Figure 1-14. C3MJ Qualification Summary

The space heritage of this technology has mitigated many reliability risks for CPV customers due to the extensive qualification testing, flight performance history, and generally strong emphasis on reliability for Spectrolab PV products. However, there are significant differences between space and terrestrial environments, and Spectrolab has defined a qualification program addressing these environments and the IEC-62108 standard and subjected our concentrator cells to those tests. The original C1MJ technology was tested according to the Spectrolab-defined qualification test suite, and was subjected to and passed all tests prior to inception of the TPP program. Qualification of C2MJ and C3MJ was completed in mid-2008 and mid-2009, respectively, with some of the requirements met by similarity. **Error! Reference source not found.** summarizes the qualification test suite that was performed for the C3MJ technology. C3MJ+ technology uses the same epitaxial structure as C4MJ and the same wafer process as C4MJ, and was therefore qualified by similarity to both.

Test	Conditions	Requirement	Results
Performance	50 W/cm^2	Effmp > 37.6% target avg = 40.0%	Avg = 39.8%
Thermal Cycle	1500 cycles, -40°C to +110°C with 10 m dwell	unprotected cell < 2% degradation	NEff = 1.0
Unprotected Cell Damp Heat	1000 hrs, 85°C/85% RH	characterization	NEff > 0.98
High Temperature Soak	Unbiased soak at 180° C, 200°C, 225°C and 250°C	< 0.5% degradation after 25 year lifetime	NEff = 1.0
Outdoor Field Trial	> 10 kW on sun for 6 months	characterization	> 10 kW total
High Temperature Reverse Bias	-0.8V and -1.6V @ 140° C until failure	characterization	Complete
HTOL	1 A & 4 A dark forward bias at 160°C	characterization	NEff > 0.99
ESD	HBM 4000 V, CDM 2000 V	characterization	NEff = 1.0

Figure 1-13. C4MJ Qualification Summary.

Throughout budget period 3, focus was on completing a more extensive qualification test of the metamorphic C4MJ technology, with no tests omitted for similarity, and with some additional testing included, so that C4MJ cells entered into production with a high degree of confidence in their robustness in field deployment. Figure 1-14 summarizes the C4MJ qualification results. The C4MJ qualification testing showed that the meta-

morphic cells have comparable performance to the lattice-matched cells in all respects. For example, Figure 1-15 shows the equivalent degradation rate for C4MJ cells at 110°C (maximum warranted temperature) calculated from temperature soak data at four temperatures using an Arrhenius relationship, and indicates >200 years to 1% degradation.

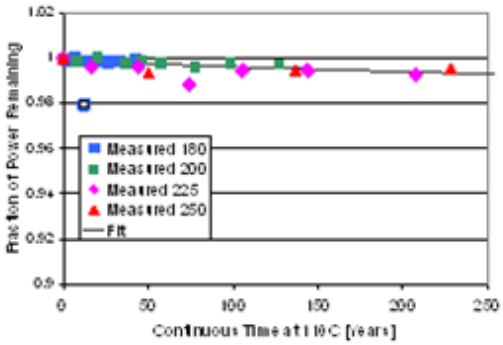

Figure 1-15. C4MJ Equivalent degradation rate at 110°C, based on thermal soak data.

Finally, C4MJ cells were subjected to a formal field trial in collaboration with Amonix as part of our self-imposed qualification requirement. A full MegaModule (1080 cells) was exposed for 6 months prior to release of the C4MJ product to production (and these same cells have remained on sun since August 2010). The cells thus endured 4.7 million cell-hours in the field environment, and >2 million on-sun cell-hours, as part of the qualification.

In budget period 1, Spectrolab developed a new high intensity light source, now offered as an illumination systems product as the XT-30, as shown in Figure 1-17. The XT-30 is designed for other types of performance testing beyond light I-V, such as thermal and combined effects testing. It is capable of illuminating a 1×1 cm aperture with 1000 suns continuously, spectrally corrected for AM1.5 (or other spectral distributions as desired).

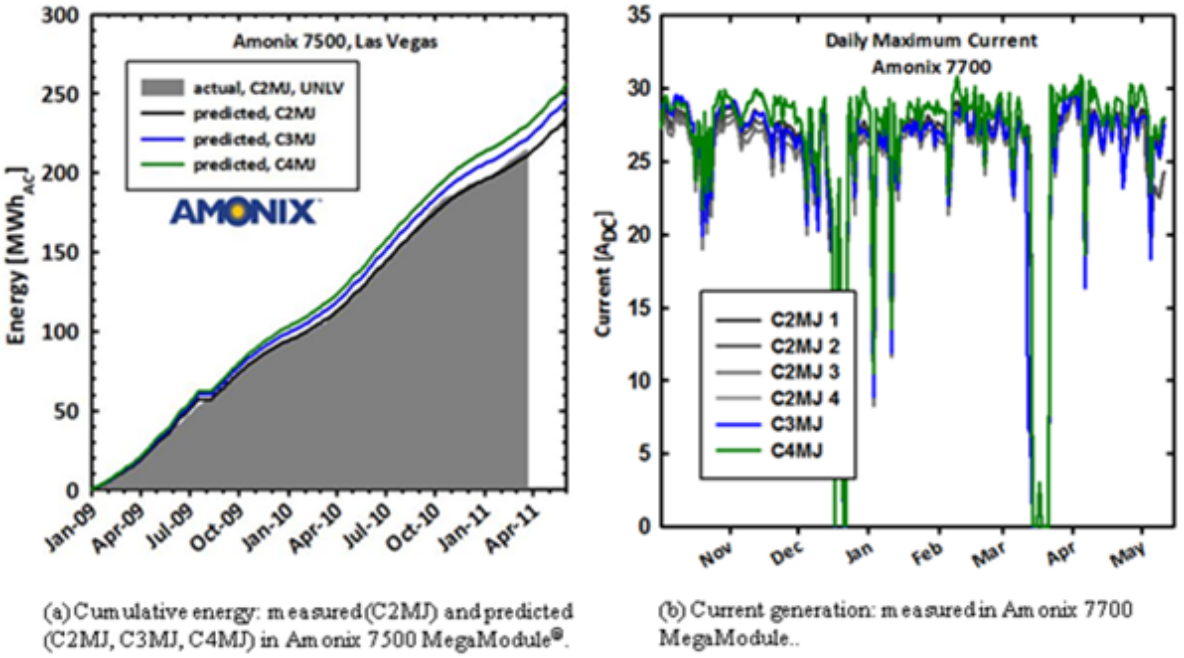

(a) Cumulative energy: measured (C2MJ) and predicted (C2MJ, C3MJ, C4MJ) in Amonix 7500 MegaModule®.

(b) Current generation: measured in Amonix 7700 MegaModule..

Figure 1-16. C4MJ Field Trial Results (in collaboration with Amonix).

Spectrolab has continued to improve overall qualification test capability, and in budget period 2 developed an illuminated thermal cycling test system, using the XT-30 as the

light source. This equipment will be used for "combined effects" testing of multiple generations of Spectrolab CPV cells, and is the first such test capability in the world.

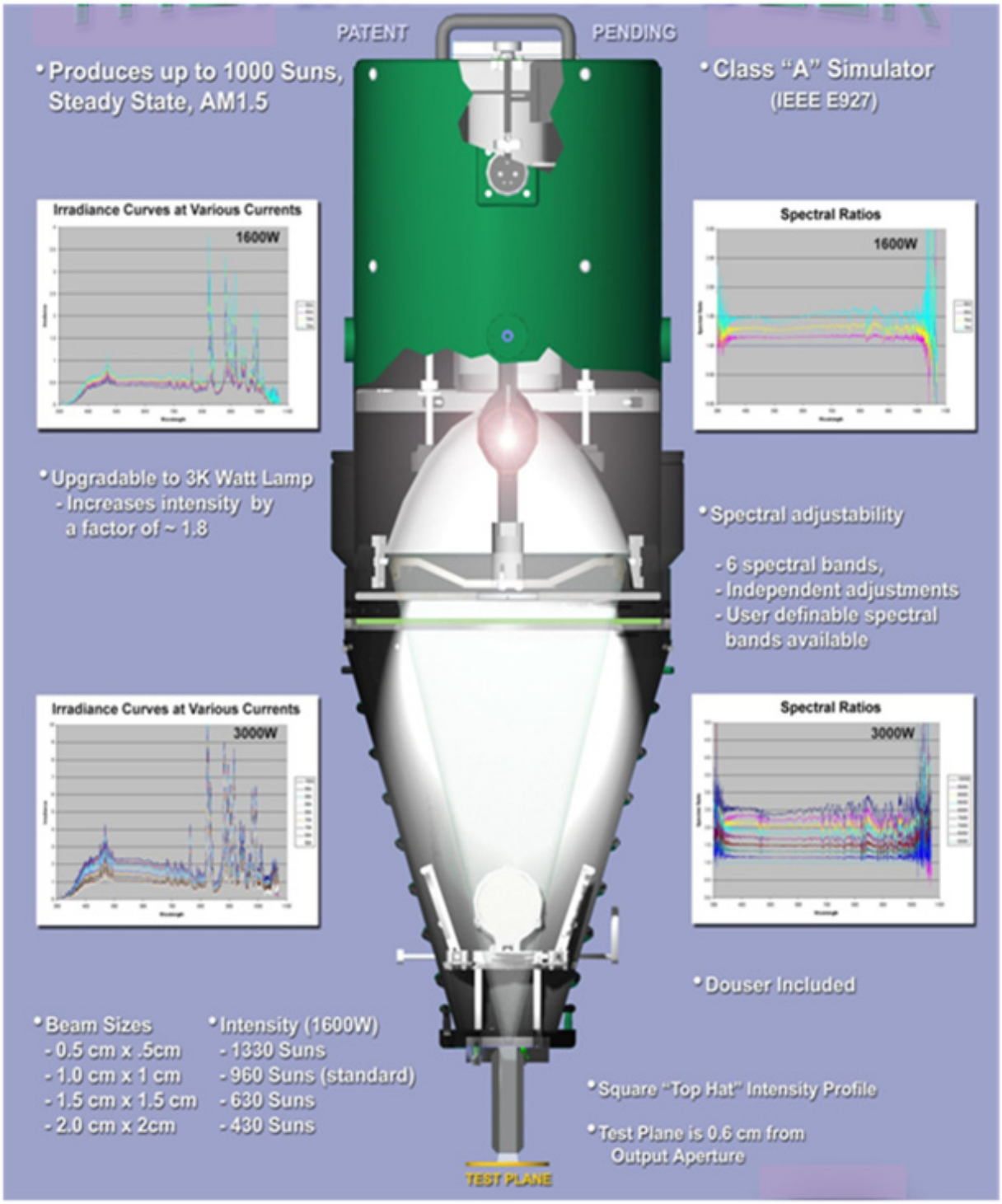

Figure 1-17. XT-30 Continuous high intensity light source for illuminated thermal cycle testing.

2 Solar Cell and Receiver Manufacturing Maturation - SOPO Tasks 1.5, 2.5, 3.5

Task Objectives

The objectives of this task were

- Develop automated device processing systems and implementation/ramp-up plans.
- Optimize receiver design and production process and reduce assembly and material cost.
- Upgrade wafer process technology and optimize process flow.
- Optimize material utilization, ingot growth, wafer sawing and polishing processes to reduce cost.

Highlights

- Transitioned CPV cell manufacturing to new, more capable and more automated MOVPE tool (Veeco K475)
- Demonstrated improved throughput and yield using K475 tools
- Developed Sylarus as a US source of germanium substrates for CPV production
- Supported by additional capital investments made by Spectrolab over and above the TPP cost share, inserted automated saw dice, cell pick & place, and both wafer-level and bare cell-level testing.
- Developed the process for 150mm epitaxial wafer manufacturing for C4MJ cell technology
- Designed and validated the wafer process for Spectrolab's new 150mm wafer fab facility, funded by capital investments over and above the TPP cost share and scheduled for completion in 3Q2011
- Developed and made available a reference design for concentrator cell assemblies (CCAs) with demonstrated processes for reliable soldered die attach

Table 2-1. Task 2, Manufacturing Maturation Milestones

Period	Criterion	Results
1	1b-1) Implemented cell weld & test automation that reduces touch labor by >60%	Touch labor was reduced from 4.2 minutes per cell to 0.78 minutes per cell (81% reduction)
	1b-2) Demonstrated cell manufacturing mean throughput rate of 5 MW/yr	15MW actual capacity for solar cell assemblies was demonstrated by actual cell production volume

Period	Criterion	Results
2	2b-1) Implementation of improved cell sectioning and cell handling processes that reduce touch labor by >20%	Installation of automated dicing saws result in a labor improvement of 7 minutes per wafer (53% reduction) and a mechanical yield improvement of 0.5%.
	2b-2) Demonstrated cell manufacturing mean throughput rate of 10 MW/yr	Based on product mix at stage gate 2 (69% bare cells or cells with interconnects, 4% Processed wafers, 27% epitaxial wafers), aggregate capacity shown to be 107 MW
3	3b-1) Wafer growth for larger, 150 mm wafer demonstrated with >50% increase in cell throughput per reactor	54% higher throughput achieved as a result of larger growth chamber, larger wafer and continuous operating mode
	3b-2) Demonstrated cell manufacturing throughput capability corresponding to 300 MW/yr	Factory expansion timed to match market opportunity, with planned completion in 3Q2011

Technical Accomplishments

2.1 MOVPE Production Development

Spectrolab has undertaken a major capital improvement program to address the needs for higher throughput and lower cost of terrestrial solar cells. As illustrated in Figure 2-1, this factory improvement includes upgrade of our epitaxial growth capabilities with new MOVPE reactors offering larger capacity per run, more automated operation, and much finer control of process variables for reduced performance variability.

A key component in Spectrolab's efforts to improve efficiency and reduce cell cost is the adoption of a next generation MOVPE reactor platform, the Veeco K475 reactor. Spectrolab is currently (as of February 2012) operating 4 of the new reactors with plans to transition all epitaxial operations to this platform (including space cells) by YE2014. These next generation MOVPE tools are optimized for a 150mm (6 inches) wafer size, but already offer a 40% higher capacity per tool, shorter cycle time, and reduced material costs on our current 100mm (4 inches) germanium substrates.

Key advancements of these next generation tools include a series of advanced in-situ process diagnostics including real-time emissivity-corrected pyrometers, a deflectometer for measuring wafer bow in real-time, and binary gas concentration monitors. Together, these diagnostic instruments provide improved process visibility and control for reduced performance variability.

Epitaxial wafer growth recipes supporting C1MJ, C2MJ, and C3MJ CPV product generations were rapidly adapted to the new tool platform, and with these adapted recipes we successfully completed a series of delta qualification tests. The next generation tool

has also been the exclusive platform for process development for the 40% C4MJ, to take full advantage of all the tool capabilities. In fact, the more complex C4MJ device structure requires these capabilities for reasonable yield, and cannot be manufactured using the older E400 MOVPE tools.

Figure 2-1. New Factory Automation Equipment at Spectrolab.

We first implemented the K475 reactor by establishing the C2MJ recipe as the first multijunction solar cell epitaxial recipe on this tool, and then built on this to develop the process for C3MJ on K475 reactor exceeding 38.5% efficiency. We then commenced to implement these same processes on the second and third K475 reactors. However, we encountered intermittent problems in achieving consistent tool operation. Resolution of these problems required a significant unplanned effort in close coordination with the tool manufacturer to address maintenance and control issues, and a disciplined improvement campaign with continuous production. As illustrated in Figure 2-2, a carefully managed cycle of variability analysis and improvement while keeping the tools in continuous production was employed to drive the production issues to closure, with both

average device efficiency and target availability being met by the end of the campaign. Since successful resolution of these issues, more than two million C3MJ cells have been produced on the K475 tools.

The K475 tools are capable of delivering a 54% increase in production throughput per reactor as compared to the older Veeco E series tools they replace. The key reactor design improvements are:

- A physically larger growth chamber
- optimization of the growth platter for 150mm wafers
- Continuous operating mode

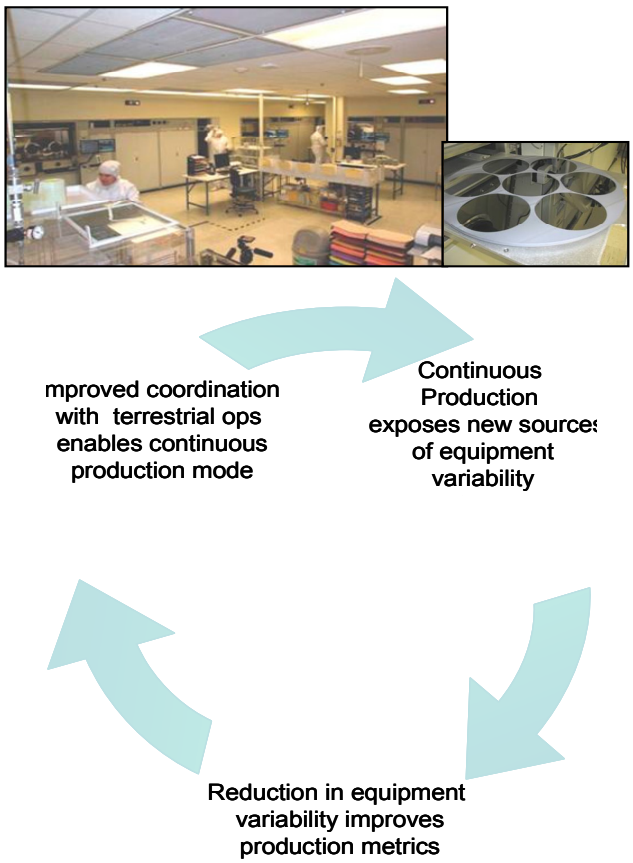

Figure 2-2. Production variability issues resolved through a disciplined campaign of continuous production.

2.2 Germanium Wafer Development

As part of the Spectrolab effort under this TPP, we engaged with Sylarus Technologies to achieve increased manufacturing capacity goals for epitaxial-ready (epi-ready) germanium (Ge) substrates and to reduce substrate price while maintaining quality standards. The motivation for this effort was to help develop the U.S. industrial base to meet expected market demand for CPV cells, since Sylarus is the only US-based manufacturer of Ge wafers, and more generally to diversify the list of qualified substrate suppliers.

As of this writing, the global 100mm Ge wafer capacity stands at about 500,000 wafers/year, and the space market consumes between 300,000 and 350,000 100mm substrates/year with an anticipated growth worldwide of 4 to 5 percent per annum. Therefore additional capacity is required to make terrestrial CPV viable.

CAPACITY GOALS	100 mm wafers/mo & wafers/wk	150 mm wafers/mo & wafers/wk
Jun 2008	10,000/mo = 2500/wk	1,000/mo = 250/wk
Jun 2009	20,000/mo = 5000/wk	5,000/mo = 1250/wk
Jun 2010	30,000/mo = 7500/wk	15,000/mo = 3750/wk

Figure 2-3. TPP Capacity Goals for Sylarus.

Spectrolab defined stage gate targets for the Sylarus effort consistent with the higher level DOE-established targets for the overall program. The stage gate targets for this effort addressed production capacity and target prices for both 100mm and 150mm Ge wafers. The capacity goals were as shown in Figure 2-3.

Sylarus demonstrated that scale-up to the stage-gate capacities is now feasible by adding equipment and trained operators. It does not require additional process development or capability. This program accelerated the scale-up capacity potential by three to five years because it resulted in a stable baseline wafer fabrication process with sufficient volume to establish a stable production flow supported by statistical process control (SPC). Figure 2-4 depicts some processing steps in the production of Sylarus wafers.

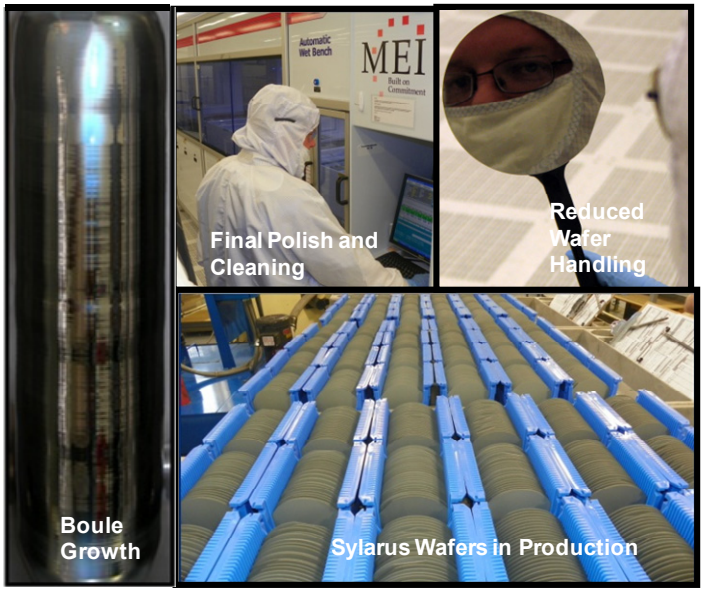

Figure 2-4. Sylarus process capability

Prior to the SETP program and Sylarus' entry into the market, the price for epi-ready 100mm Ge wafers was headed toward $80/wafer and higher. The effect of Sylarus' market entry as a competitor was to reduce the cost of substrates for the space and CPV markets from other Ge suppliers. It also motivated Sylarus to invest aggressively to take the cost out of wafer fabrication in order to ensure a viable business. The SETP/TTP program played an important role in that process. The program enabled Sylarus to accelerate convergence to a robust, repeatable process that required the company surmount numerous, unanticipated technical hurdles, and accelerated Sylarus' ability to achieve ISO9000 certification and to move to a qualified product with numerous customers.

In summary, the SETP/TPP program dramatically accelerated Sylarus' entry into the market with a high-quality, qualified, price-competitive product that meets the fundamental program goals and which can be produced in the desired quantities given a CapEx investment commensurate with market demand. During the course of this effort, Sylarus Technologies emerged as a viable, qualified vendor for 100mm germanium substrates for advanced multi-junction photovoltaics and is on track to become a qualified vendor for 150mm substrates. The company succeeded in developing a robust wafer fabrication process and collaborated with Boeing Spectrolab to ensure integration with Spectrolab's production line.

Sylarus market entry has already resulted in significant downward price pressure on Ge substrates. In addition to securing a U.S. domestic supply for these substrates, Sylarus is providing multijunction photovoltaic manufacturers with a qualified second source, rapidly expanding annual capacity, and expanded market choices.

2.3 Wafer Processing Factory Improvement

Spectrolab continues to make substantial capital investments in addition to our cost share commitment on the TPP program. The capital investments being made are additional commitments by Spectrolab and The Boeing Company toward the overall goal of making CPV a significant contributor to the US photovoltaic industry as envisioned by the TPP program. These capital investments directly impact the overall objectives of the TPP, and have taken our total factory capacity to just over 100 MW/year (calculated as DC power per cell at 50 W/cm^2 illumination, 25°C), up from a capacity at the beginning of the program of less than 5 MW/year. This capacity figure also has expected space production demands accounted for, i.e., this capacity is actually available for CPV production. The capacity figure will rise to ~250MW in 2012 as the new 150mm wafer fab facility comes into full production.

We have made numerous capital improvements as reflected in Figure 2-1. Figure 2.5-1 shows the saw dice and pick & place automation installed at the end of 2009 Replacement of our existing saws with improved automated saws resulted in a reduction in cycle time by more than 40% and an overall cost reduction by 40%. We have also installed an automated pick and place machine for removal of cells from the dicing tape and placement in trays for testing or other processing. This machine replaced a manual pick and place operation and elimination of the ergonomic stress of the manual process. This machine also adds important new flexibility to our factory process flow. It has the ability to accept wafers pre-tested at the wafer level, and pick and place parts into trays based on performance bins.

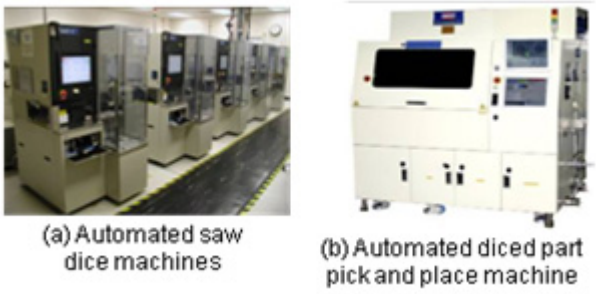

Figure 2-5. Saw Dice Area Upgrades

At the inception of the TPP program, Spectrolab planned to develop and install a new, highly automated wafer fab facility capable of processing 150mm epitaxial wafers, a key step in the evolution of the CPV cell technology to lower cost. As a result of the global financial crisis of late 2008 and resulting sharp decline in demand for our cells throughout 2009, a decision was made to postpone the investment in this expanded facility, and the completion of the new facility is now planned in 3Q2012.

Throughout budget year 2 (July 2008–June 2009) we researched the appropriate 150mm wafer processing equipment selection spanning the breadth of wafer processes with more automated capability. Upgrade of the fab line from 100mm to 150mm is the largest cost impact in our cost reduction roadmap, because it increases the quantity of parts per wafer by a factor of 2.36 (for the CDO-100). To manage this equipment selection process adeptly, and to be able to quickly analyze cost, footprint, and performance issues associated with the processing options before us, we have developed a tool to aid in sizing the factory requirements for a given throughput and process baseline. This tool enabled us to move forward with confidence when the final process was frozen and capital approved. This information was translated to capital funding requests for the construction and furnishing of the new 150 mm fab facility.

The facility modifications to build the 150 mm fab in the existing factory are under way. Figure 2-6 shows the floor plan of the new facility, highlighting the areas used for the 150mm wafer processing, the advanced technology processing (ATP), and space by-pass diode fabrication.

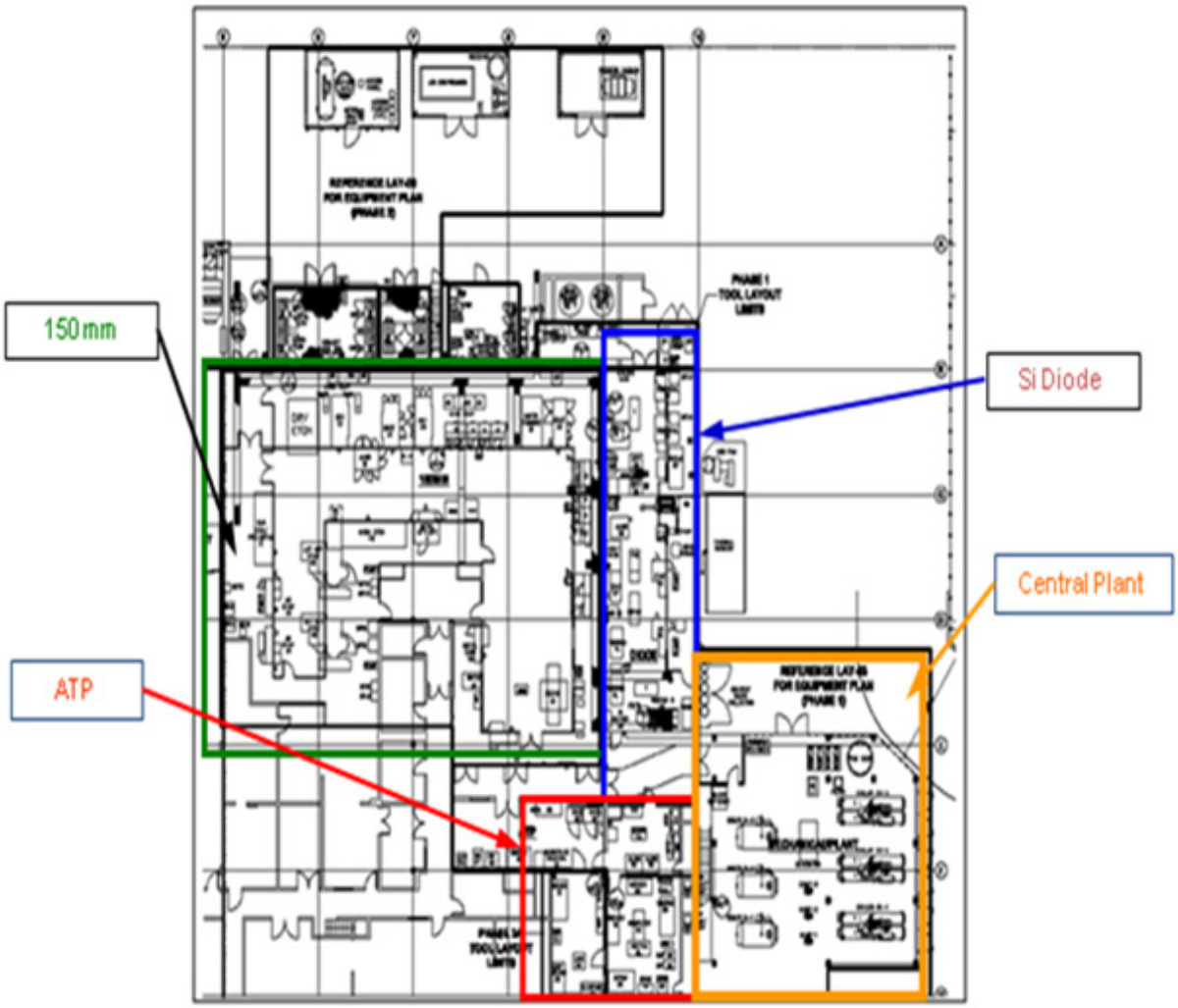

Figure 2-6. 150mm Wafer Facility Floor Plan

Figure 2-7 shows the overall timeline for construction of the 150mm wafer fab and associated facility modifications. Constructing this new facility has had particular challenges, in that it was required to take place with minimal disruption to existing production facilities and operations. To accomplish this, the work was divided into two phases. In the first phase, the old silicon diode area (used to manufacture space-qualified by-pass diodes) was shut down. We manufactured an adequate supply of the space diodes to meet production needs through the construction period. We then constructed the central plant, aided by a MOVPE shutdown for 2 weeks in September 2010 for safety system upgrades and a plant-wide shutdown for 3 weeks of the year-end holiday period in December 2010 for utility upgrades (the only times our manufacturing operations were taken off-line by the factory expansion activities).

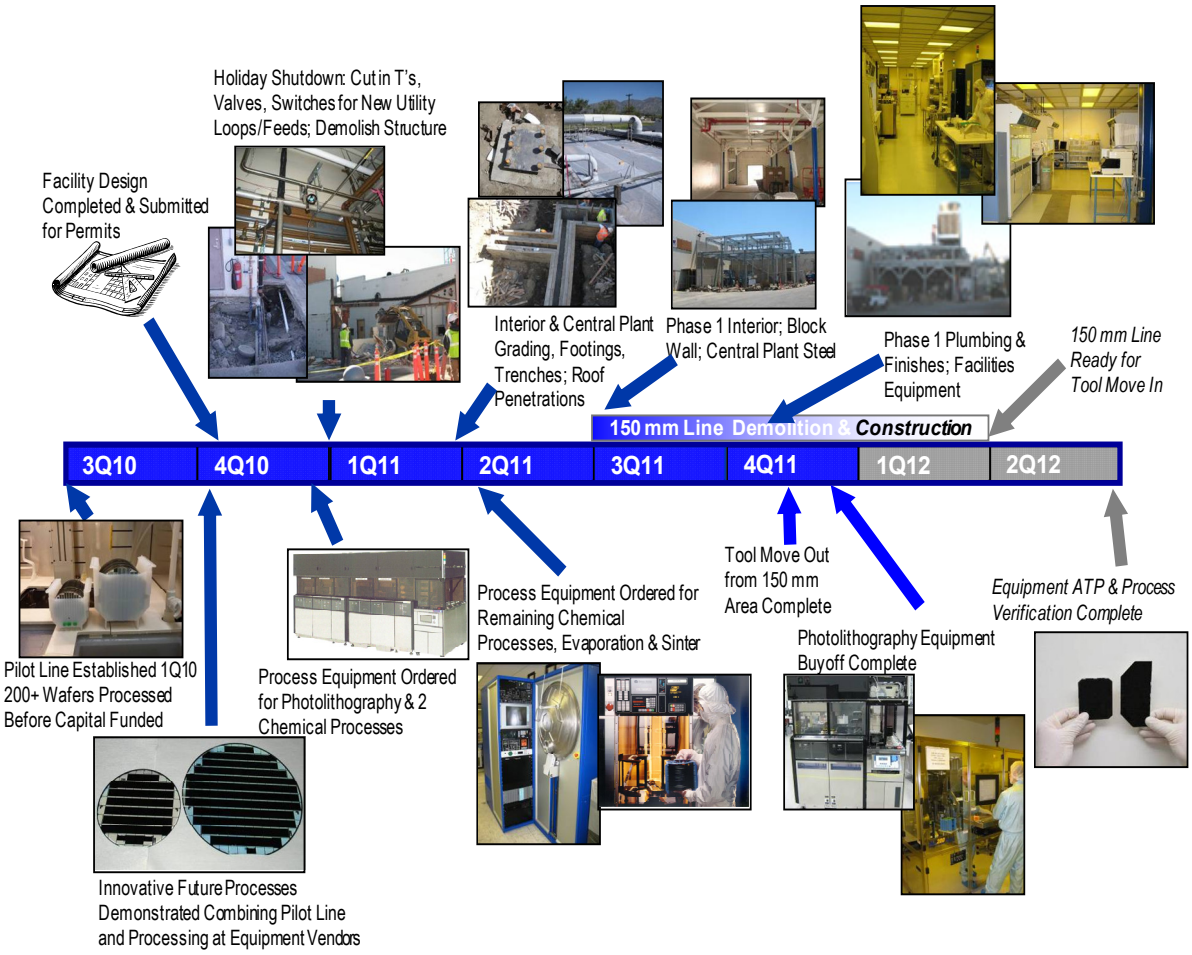

Figure 2-7. Spectrolab Factory Upgrade Timeline.

At the time of this writing (February 2012), phase 1 has been completed, and production work has commenced in the diode fab area and advanced technology products laboratories. Remaining activities for completion of phase 2 and commencement of CPV wafer manufacturing are on schedule for a production start in August 2012. All process equipment has been ordered.

During budget period 2 we refurbished some existing equipment to be able to run pilot runs of 150 mm wafers. This required hardware upgrades from evaporators to wet bench equipment modifications. This allowed us to continue process development to a final process freeze with high confidence in the results, and has also facilitated simultaneous development of the C4MJ epitaxial process on both 100mm and 150mm wafers. Figure 2-9 shows developmental results for C4MJ 150mm wafers, with efficiency distribution equivalent to that of the 100mm wafers.

Throughout the program, we have continued to work with Sylarus to develop them as a viable second source. Spectrolab is working with multiple Ge vendors to develop their 150mm Ge capability and qualify them as Ge suppliers for our 150mm line.

Figure 2-8. Progress toward Completion of the Spectrolab Factory Upgrade

2.4 CPV Assembly and Test

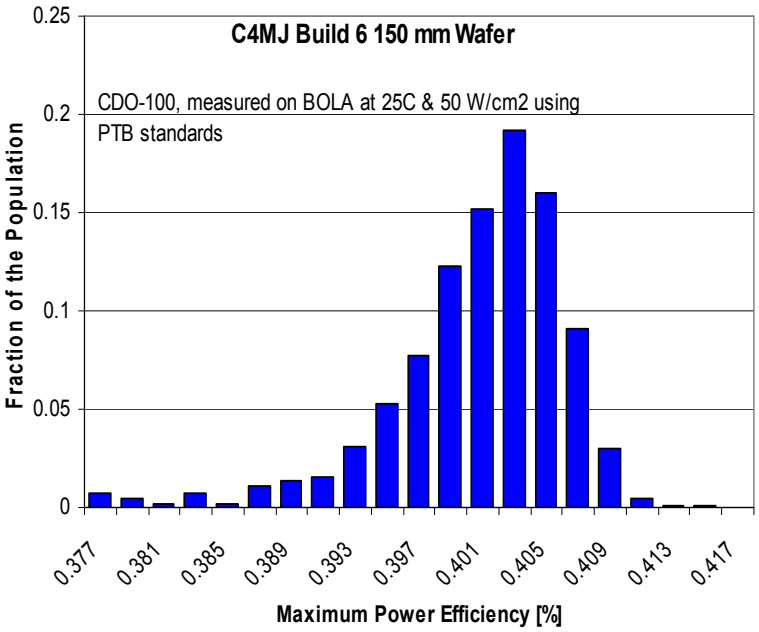

Figure 2-9. C4MJ Cell Performance Distribution Comparison between 100mm and 150mm Wafers.

The initial phase of automation for two key manufacturing steps, interconnect welding and illuminated I-V performance testing, was successfully completed in 2007 through mid-2008. The automatic tester also automatically sorts cells into closely matched performance bins so that customers can use matched cells to minimize performance losses in series strings (last picture in Figure 2-1). The CPV community has not yet determined the most effective method of screening parts for reliability, therefore the automated tester was designed for flexibility and improved screening over high throughput. The tester is capable of performing dark IV, electroluminescence, reverse bias and LIV. We introduced the second generation of automation cell tester with much higher throughput (> 5 times) during the second year of the program; we began production operations initially at the automation supplier's facility in October 2009 and in our own facility in January 2010; this equipment has demonstrated ≥110,000 cells (2.2 MW) per week capacity with three-shift operations. In 2011 we began shipping cells with sample testing that was proven to be highly effective at finding most defective cells while testing only 20% on an aggregate level (by selectively testing cells from known lower yield locations on the wafer). With this scheme, the automated bare cell tester is able to support a factory throughput of over 500,000 cells per week.

In the latter half of 2008 and early 2009 we successfully implemented automated testing at the wafer level (4th photo of Figure 2-1). This provides a flexible test capability for cells of any size, again with cells sorted into matched performance bins, via an electronic map delivered with the wafer. We also have upgraded our wafer dicing parts handling system to be able to make use of plastic dicing rings in place of the expensive metal rings previously used (see Figure 2.6-1). These plastic rings can be used to supply diced wafers on tape for customers who do not yet have production dicing saws in place. Wafer probe testing, combined with wire bonding, enable reduction of bus bar dimensions. This significantly increases active area per wafer, leading to 5~10% cost reductions. For example, we reduced the bus bar dimensions for 30mm² active area cells, from 300 μm to 180 μm, and thereby increased the number of cells per wafer by 9%.

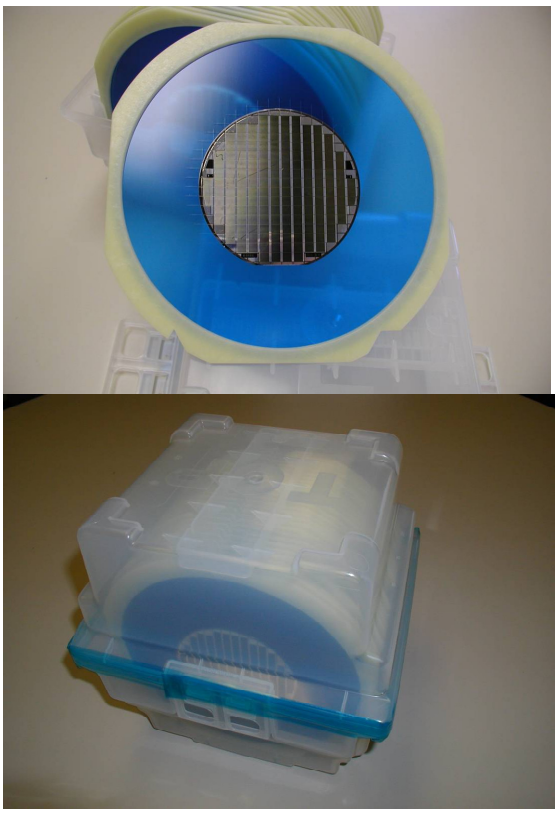

Figure 2-10. Wafers on Tape in Plastic Dice Rings.

2.5 Concentrator Cell Assembly (CCA)

Spectrolab began the TPP program with a very limited, prototype hand assembly process for CCAs and ambitions to grow that nascent capability into a full production line. As the program and the industry developed, we recognized that there are other companies interested in the CPV industry and with established business models and capabilities to manufacture CCAs. By mid-2008 we adjusted our business strategy to focus our own effort and capital investment in the semiconductor product, and to work as an industry enabler in CCA production by developing a reference design and working with capable large-volume contract manufacturers and also directly with our customers to ensure volume supply capability of a reliable CCA product for the market.

We worked with two major manufacturing companies to assist development of their CCA manufacturing capability. Several other contract manufacturers were also considered. Spectrolab also takes an active role in transferring the CCA assembly process we developed to our customers; for example, we successfully taught one customer to cost-effectively implement and scale up the Spectrolab vacuum soldering process, with excellent results.

Figure 2-11. CCA Pilot Assembly Line.

During budget periods 1 and 2 we moved the CCA from a prototype design with hand assembly to a more mature design, being manufactured on a prototype production line, and initiated engineering confidence tests. We designed and implemented an optimized DBC ceramic carrier design for cost reduction from a world leading volume supplier and are now receiving these components to support POM CCA production. We developed an interconnect design that can be punched for lower cost through use of automated interconnect punch equipment. This design features a “loop” that is designed to prevent shorting of the cell and provides strain relief for increased reliability. We also implemented lower profile, low cost packaged diode.

We implemented at Spectrolab a vacuum CCA reflow process for near void free die attach, pictured in Figure 2-11. This process completes the soldering step of the assembly of the CCA in a single reflow operation using fixtures designed to position the components accurately with solder performs to accomplish the reflow. Most importantly this is a "pilot" process scalable to high volume production with the addition of higher capacity equipment, either at Spectrolab or at an outsource supplier facility, and Spectrolab has now made about 40,000 CCAs (>650 kW) using this line, including all of the CCAs used in the Boeing CPV arrays for the TPP. During budget period 2 we also implemented the prototype of the test suite needed for testing the CCA in a fully automated, high volume line. The test suite, pictured in Figure 2-12, includes a 4-up CCA illuminated I-V test fixture being used for higher throughput in our manual HIPSS tester.

We have improved the CCA design from the original "Gen 1" configuration designed at the beginning of the program to the improved "Gen 1a" configuration shown in Figure 2-13. At the start of budget period 3 we completed the first set of engineering confidence tests, and the thermal cycling results (500 cycles from –40°C to +110°C) uncov-

Figure 2-12. CCA Test Suite

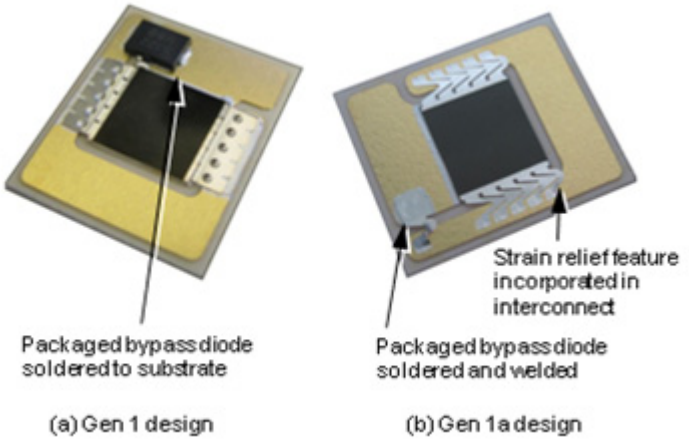

Figure 2-13. Spectrolab Gen 1 and Gen 1a CCA Configurations

ered several design flaws inhibiting the long-term reliability of the Gen 1 CCA. The design changes made in Gen 1a addressed those issues, and also reduced cost and made the overall profile lower (improving compatibility with some optical designs) by moving to a bare bypass diode. As shown in Figure 2.7-5, these changes resulted in

thermal cycling without observed failures after 1500 thermal cycles, which was calculated by NREL to be equivalent to worst case lifetime for CPV applications ("Quantifying the Thermal Fatigue of CPV Modules," CPV-6, Freiburg Germany, April 2010).

With successful demonstration of these changes, our reference design using welded interconnects is complete; engineering attention has now shifted to wire bonded assemblies, since this approach is much more common in the industry today, and to working with contract manufacturers for qualification of production designs.

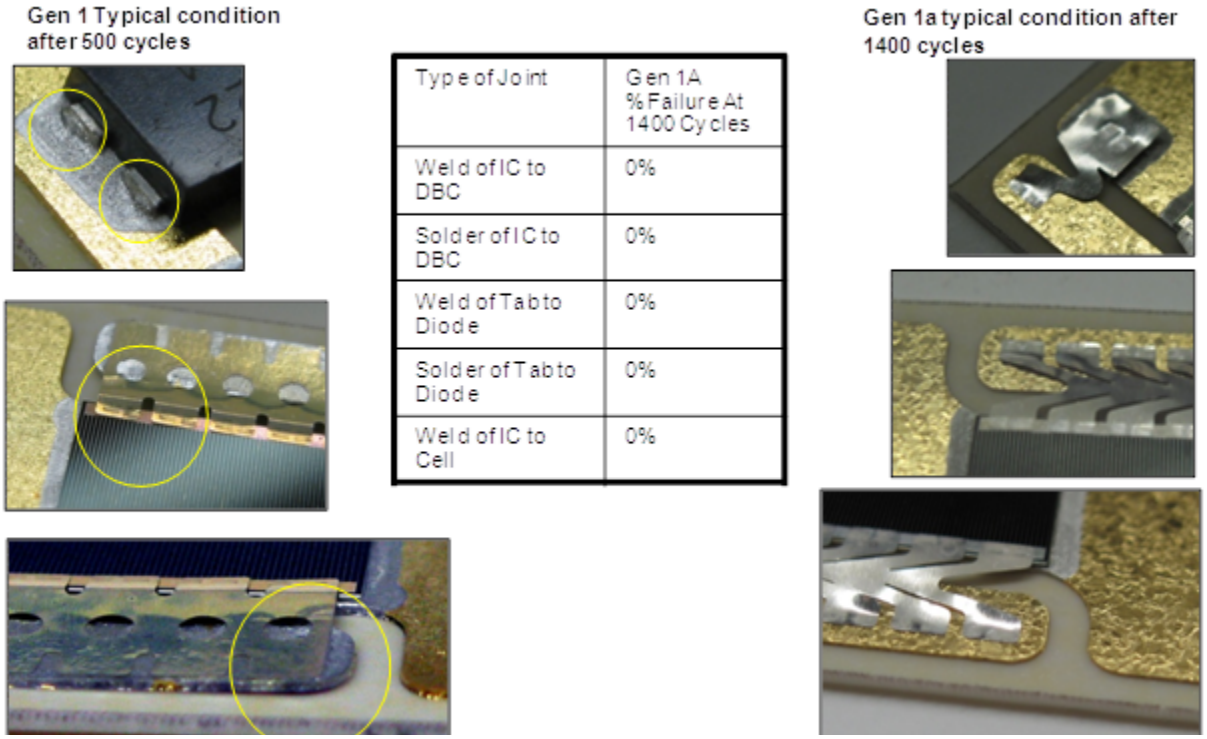

Type of Joint	Gen 1A % Failure At 1400 Cycles
Weld of IC to DBC	0%
Solder of IC to DBC	0%
Weld of Tab to Diode	0%
Solder of Tab to Diode	0%
Weld of IC to Cell	0%

Figure 2-14. Thermal Cycling Reliability Improvement of Gen 1a CCA Configuration

3 CPV System Design – SOPO Tasks 1.6, 2.6, 3.6

Task Objectives

The objectives of this task were

- Perform overall design of the solar power plant, including module, panel, array, and power plant block.
- Conduct trade studies to evaluate different concentrator module design options, considering cost, efficiency, life and weight. Develop a cost effective optical module design based on allocated Design to Cost (DTC) targets. Build and test prototype optical modules.
- Develop receiver design specific to the Boeing module design. Conduct packaging analysis (performance, life & environmental) and build and test prototypes.
- Perform overall design optimization of the panel and array. Evaluate optimum size of the panel and array to support shipping, assembly, shadowing, installation (weight) and tracker size. Evaluate material compatibility with cost goals and design life. Design panel/array structure to support anticipated load conditions. Design the optimum method of electrically interconnecting the modules in the array.
- Conduct trade studies to establish best overall tracker design for the selected solar array. Perform tracker design/development for the solar array within constraints of DTC targets. Study cost reduction for the tracker electronics.
- Perform overall design of the inverter. Evaluate optimal Inverter requirements (input voltage, power rating, efficiency, and integration of BIT/Diagnostic functions). Study feasibility and costs associated with various cooling approaches for the inverter. Perform Inverter development to support reliability and DTC targets.
- Perform overall design of a nominal power plant. Perform trade studies to evaluate overall system performance and BIT monitoring. Perform overall design of the utility sub-system including system interfaces, controls and utility tie in.

Highlights

- Selected off-axis non imaging optics for the solar concentrator design based on maximum acceptance angle ($\pm 1.75^\circ$) and optical module efficiency (>23%).
- Improved module efficiency from 23% to >33% through a combination of accurate spectral modeling and improved component optical performance.
- Developed a low cost (<$0.15 per W) high reliability (>99.8%) heat pipe based heat sink.
- Developed a robotically manufacturable module design based on a metallic chassis to enclose and align individual receivers.
- Developed a unique receiver wall which combined the cell/CCA, heat sink, secondary optics and inter-receiver for six receivers into a single assembly amenable to robotic manufacturing.

- Developed truckable panel design amenable to automated factory assembly which could be delivered ready for mounting to the power plant site.
- Developed a tracker design with an automatic alignment system based on peak panel power at a projected volume cost of > $0.15/watt.

Table 3-1. Task 3, CPV System Design

Period	Criterion	Results
1	1c-1) Down select of XR optical design that achieves concentration, pointing acceptance angle, and uniformity to meet POC cost targets	Off axis XR optics base lined based on trade studies which indicated a 10% higher aperture area and improved packing factor with an acceptance angle of ±1.75°.
	1e-2) Demonstrated Proof of Design tracker	Developed, demonstrated and deployed a COTS tracker with a self aligning sun tracking system based on peak panel power and projected volume cost of> $0.15/watt.

Technical Accomplishments

3.1 CPV Architecture

During the proposal phase of the program the decision was made to pursue a non-imaging concentrating optic for the CPV system. This decision was largely based on the much wider acceptance angle offered by this approach when compared with the alternatives.

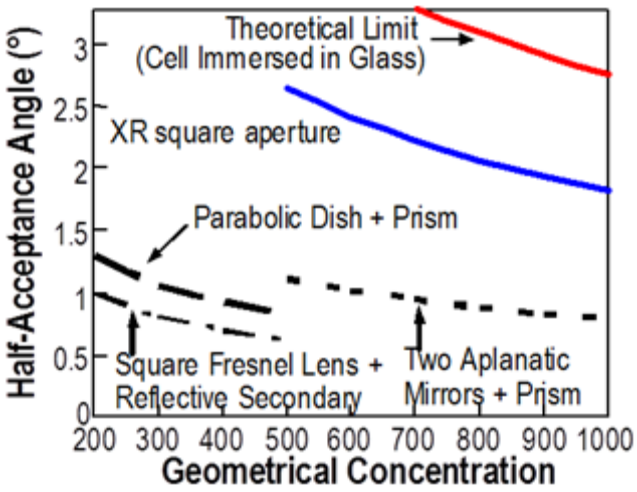

Figure 3-1. Comparison of acceptance angles for CPV optical approaches

The data in Figure 3-1 demonstrate the doubling of acceptance angle likely to be achieved with non-imaging optics. This was viewed at the start of the program as having very positive consequences with respect to tolerances required for the equipment used to align the concentrator with the sun. “XR” is a short-hand notation used by optics designers to denote that the design has two elements, the first being reflective (“X”) and the second being refractive (“R”).

Once the non-imaging approach was selected the program faced two options: an on-axis approach in which the receiver assembly is centered with respect to the primary concentrating optical element, or an off-axis approach wherein light is reflected to the side of the primary concentrating mirror. The deciding factors in the trade were

- The receiver assembly blocks approximately 10% of the light main input solar aperture in the on-axis case.
- It is clearly easier to clean a window without a central heat sink protrusion.

3.1.1 Off-Axis Non-Imaging Optics

In summary, analysis and projected performance of the optical system formed by a SMS XR concentrator + mixing rod demonstrated that the XR concentrator leads to a very high acceptance angle with highly uniform cell irradiance.

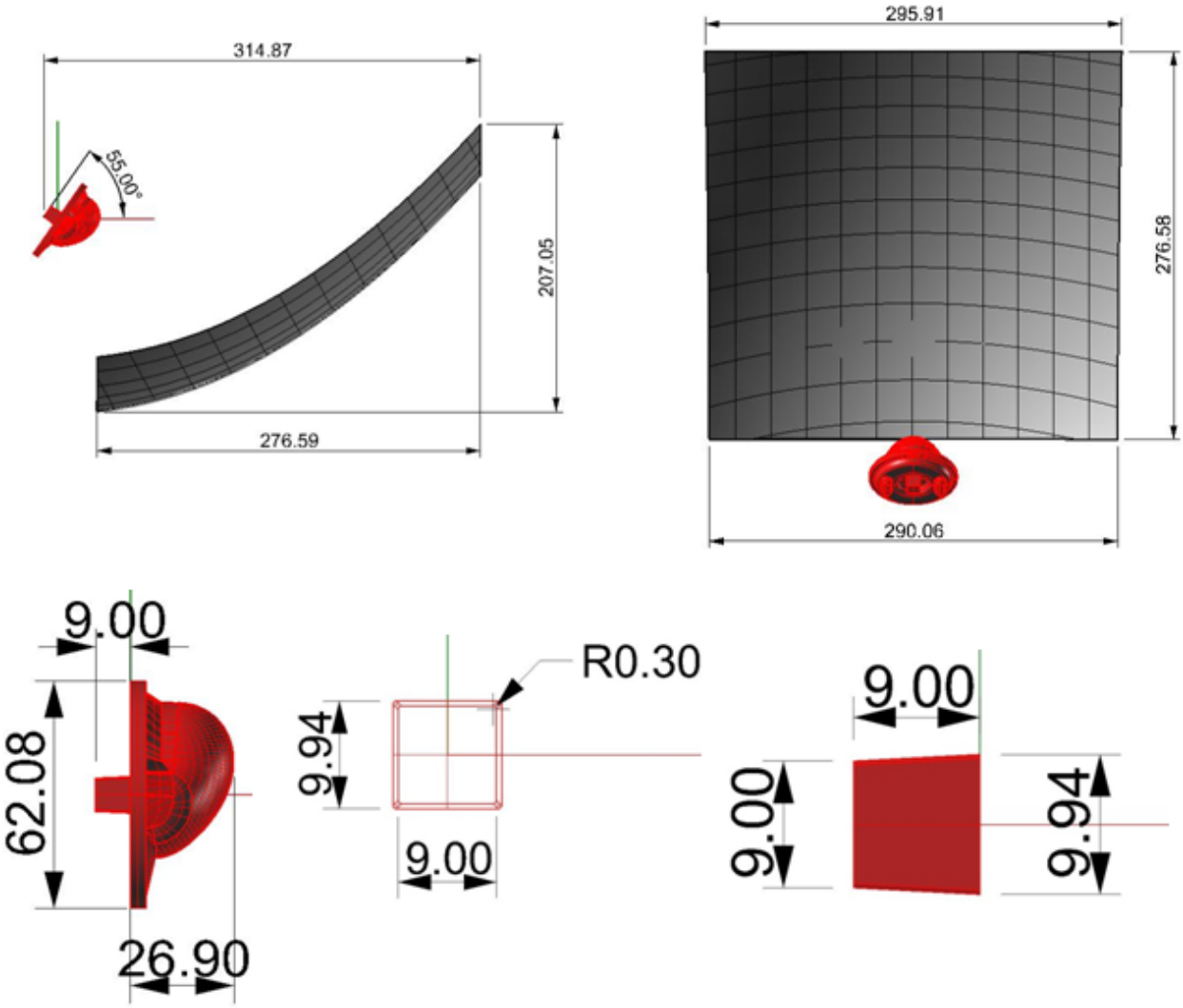

Figure 3-2. Dimensions of XR and SOE dimensions for the off axis (all dimensions are in mm)

Analyses of the described concentrator were performed by ray tracing with the objective to determine the angular transmission, optical efficiency and irradiance distribution on the concentrator exit aperture. Additionally, the tolerances of the system have been analyzed, i.e. the effect of the misalignment of the system on the optical efficiency, ac-

ceptance angle, and irradiance distribution on the cell. In order to have an idea how the prototype would behave, a spectral analysis was done.

3.1.1.1 Transmission Curves and Irradiance Distribution on the Solar Cell:

One of the characteristics needed for the evaluation of the concentrator optical performance is the angular transmission of the concentrator. The angular transmission is defined for a given incident beam of parallel rays as the power reaching the cell surface over the power incident on the concentrator aperture (i.e. the optical efficiency as function of the angle of incidence of the parallel beam). For this calculation it is assumed that all the rays are in the parallel beam with the same radiance. The solar direct radiation can be modelled as a set of parallel beams (with the same radiance) whose directions point inside the solar disk. The angular radius of the solar disk is 0.26°.

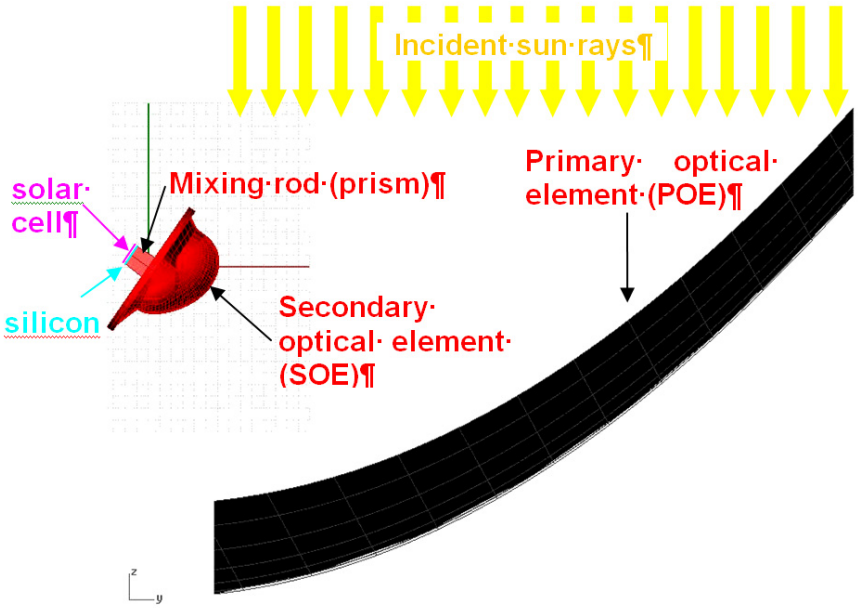

Figure 3-3. SMS3D XR concentrator (side view)

Two important merit parameters of the concentrator are derived from the angular transmission curve: the optical efficiency (η_{opt}) and the acceptance angle (α).

- The optical efficiency of the concentrator is the maximum value of the angular transmission when the angle of incidence is equal to zero (normal incidence). Notice that the power reaching the cell is not necessarily the power incident on the cell geometric surface because the cell coating may reflect part of the radiation and the grid will block some light. The definition that is used here is that power on the cell surface (not inside the cell) over the power of a parallel beam reaching the entry aperture.
- The acceptance angle is the angle between the direction at which the angular transmission peaks and the direction at which the optical efficiency falls down to a 90% of the maximum.

The angular transmission is usually represented in normalized form called relative angular transmission. The relative angular transmission is the angular transmission normalized to its maximum value, so, the maximum value of the relative angular transmission is always 1. The angular transmission (not relative) can be obtained by multiplying the relative angular transmission times the optical efficiency. Henceforth in this document transmission curve will mean relative angular transmission.

The transmission function T gives for any incident beam of parallel rays the percent of power that reaches the cell surface, assuming that any ray of a parallel beam has the same radiance. The direction of the incident parallel beam can be determined with 2 direction cosines (p,q). Thus, in general T is a function T(p,q). The transmission curve in the x-section is the function T(0,q) and the transmission curve in the y-section is T(p,0). Figure 3-4 explains both sections. In practice, instead of representing T(0,q) or T(p,0) T(a) is represented where a is either arcos(p) or arcos(q), depending on the type of section. The Figure 3-5 gives the transmission curves for both sections.

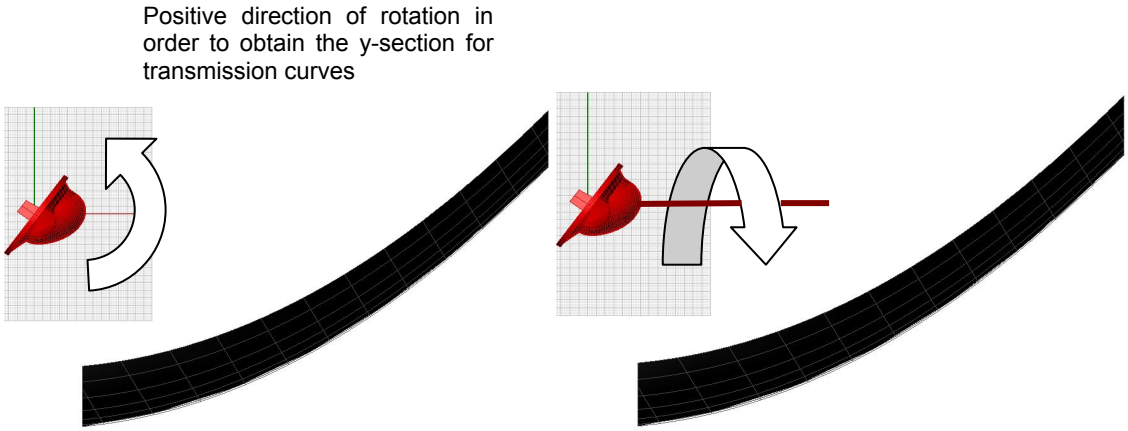

Figure 3-4. Definition of x and y sections used for transmission curves

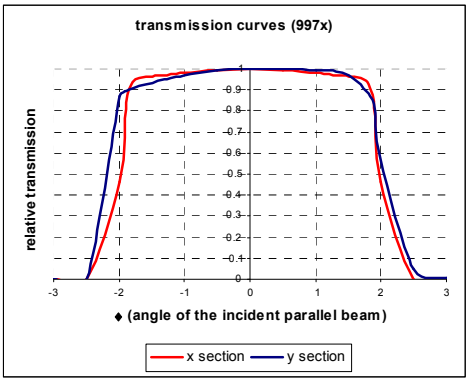

Figure 3-5. Transmission curves at nominal position considering angular radius of the solar disk 0º and no rounding of lateral edges of mixing rod (acceptance angle ±1.81º)

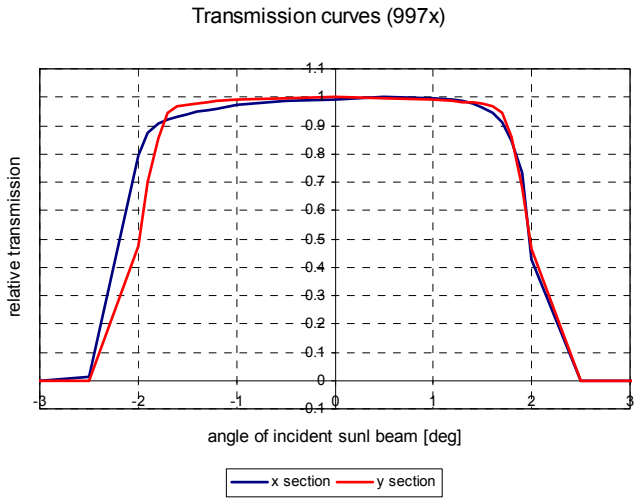

Figure 3-6 Transmission curve at nominal position considering angular radius of the solar disk 0.26º (acceptance angle ±1.76º); included rounding of lateral edges of mixing rod (radio 0.3mm)

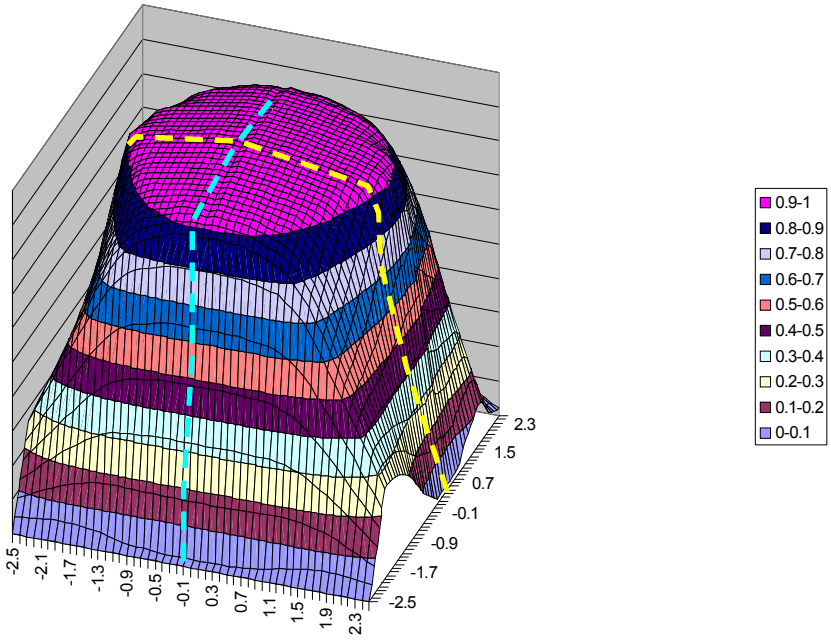

Figure 3-7 Relative angular transmission in 3D (T(p,q)) the cross sections (yellow and blue lines), are the x and y sections

Sometimes the relative angular transmission is calculated taking into account the angular size of the sun instead of using a beam of parallel rays. This is a straight forward way to show the concentrator angular performance under more realistic conditions. In this case the resulting relative angular transmission is a convolution of the sun size with the relative angular transmission calculated using a parallels ray beam. Figure 3-6 and Figure 3-7 show the relative angular transmission calculated taking into account the sun size.

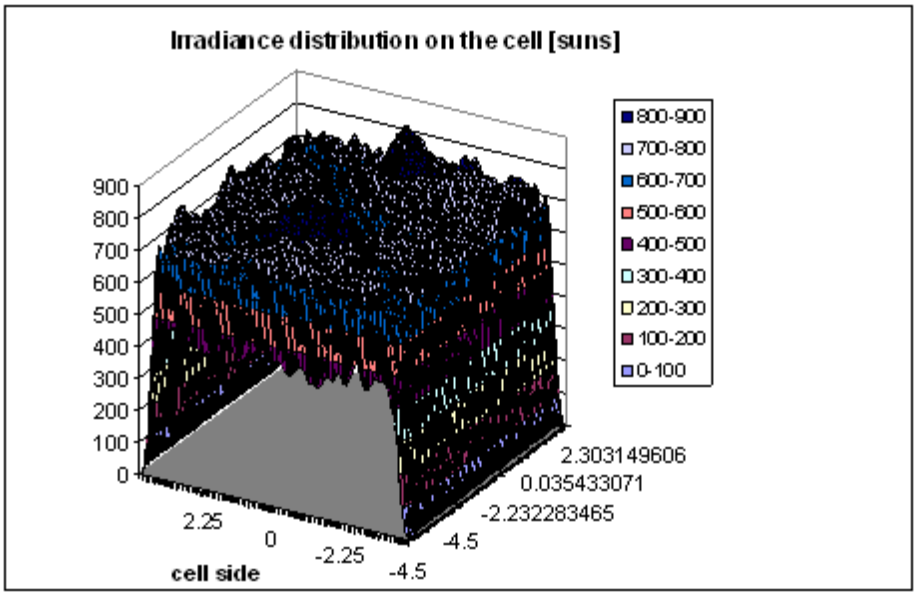

Figure 3-8 Irradiance distribution on the cell. Centered sun

Additionally, an analysis of the irradiance distribution on the solar cell was performed. The results for the centered sun and assumed input irradiance of 900 W/m2 are shown in Figure 3-8. In Figure 3-9 is shown the irradiance distribution in the case of tracking error of 1.5º in the y direction, what is the worst case (the peak irradiance in the rest of directions is smaller)

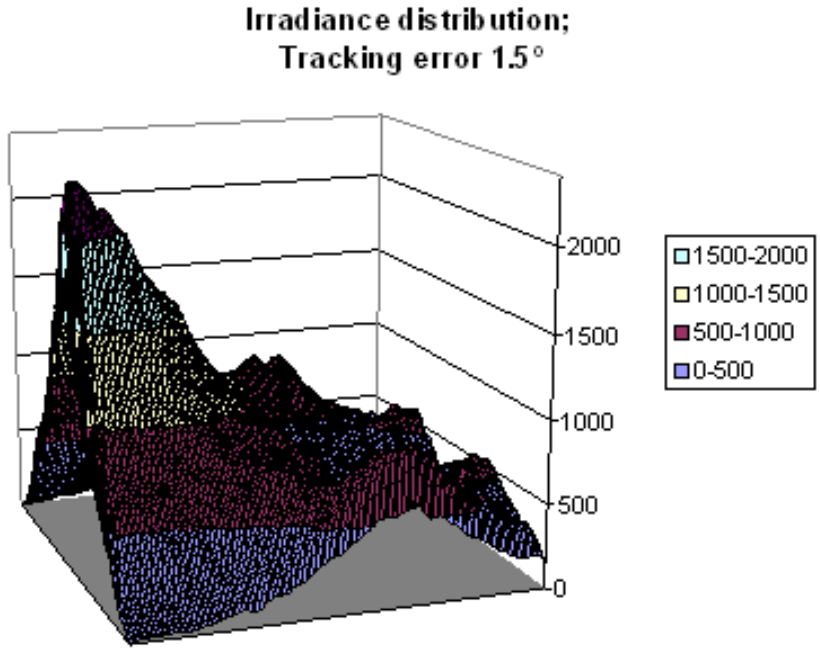

Figure 3-9 Irradiance distribution on the cell off axis +1.5º y-direction (worst case). Peak irradiance is 2304 suns (DNI 900W/m^2)

The summary of simulated optical losses (relative and absolute) can be found in the next Table 3-2. Their graphical representation can be seen in Figure 3-10.

Table 3-2. Numeric summary of optical losses.

Optical losses	Relative	Absolute
		100.0%
Transmission after SOE shading	100.0%	100.0%
Cover transmission (no AR coated)	91.0%	91.0%
Mirror fill factor	100.0%	91.0%
Mirror reflectivity	95.0%	86.45%
SOE transmission (no AR coated)	94.99%	82.12%
Mixing rod rounding	98.68%	**81.04%**

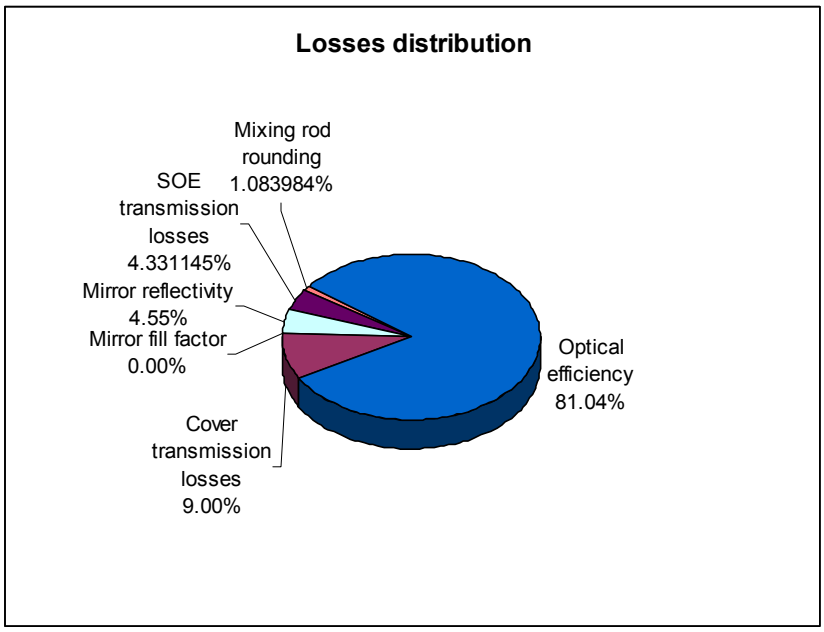

Figure 3-10. Graphical summary of optical losses.

The behaviour of the XR concentrator can be summarized as follows:

1. Concentration ratio C_g=997.97x ($C_g=A_{entry\ aperture}/A_{exit\ aperture}$; exit aperture area=mixing rod aperture area)
2. Optical efficiency η_{opt} (includes Fresnel losses, transmission of the cover and mirror reflectivity): 81%;
3. Acceptance angle (the nominal transmission curves are shown in Figure 3-6)
    - x section ±1.75°
    - y section ±1.77°
    - Peak irradiance on the cell 883x (for perfect tracking).

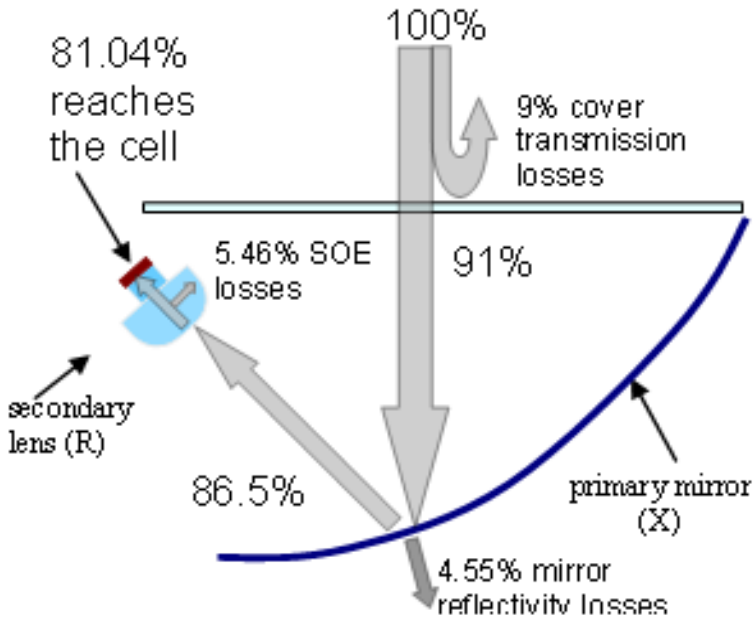

Figure 3-11 Distribution of the losses through the system

3.1.1.2 Spectral Analysis:

Tthe spectral optical efficiency of the whole system was simulated. For these calculations, the following parameters were used:

Cell active area (cm²)	0.81
Concentrator aperture area (cm²)	807.872675
Geometric concentration	997.4

The following sources of optical losses were considered:

1. Heat-sink fins shading	Calculated, 0% for off axis
2. Cover transmission	Supplied by manufacturer
3. Mirror reflectivity	Supplied by manufacturer
4. Secondary transmission	Calculated + absorption supplied by manufacturer

Rounding of the mixing rod lateral edges has been included additionally with an estimated loss of 2%. Values of generated photocurrent in each subcell for different production materials can be found in Table 3-3: the ideal case (without optical losses), the worst case (where no anti-reflective coatings are used on cover nor on SOE) and the best possible real solution (with all AR coatings included). In Table 3-3 below, optical efficiency for different wavelengths can be seen for both cases shown in the table (with and without anti-reflective coatings).

Table 3-3. Component optical efficiency as a function of wavelength

Short circuit current (Isc)	Top cell (A)	Middle cell (A)	Bottom cell (A)	Total (A)	Opt. eff.,	Optical conc. (suns)
No optical losses	9.64	9.91	16.68	9.64	100%	899
With simulated losses: Cover: Pilkington Mirror EMF (on PC)	7.69	7.94	13.14	7.69	80%	717
With simulated losses: Cover: Porous SiO2, Schott Mirror: EMF (on PC) SOE: BBAR	8.56	9.22	15.16	8.56	89%	798

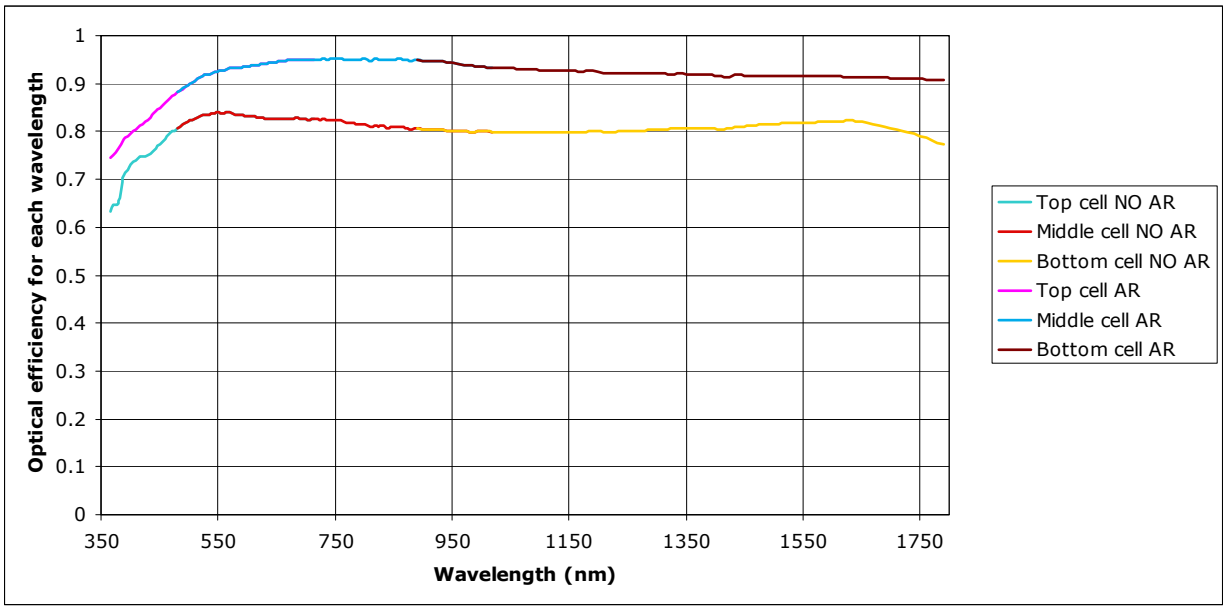

Figure 3-12 Optical efficiency for different wavelengths

3.1.1.3 Comparison of the Effect of Difference Detected in Spectral Reflectivity:

In this section we have considered influence of the different spectral reflectivity of the possible applied mirrors for the POEs. In Figure 3-13 are shown spectral reflectivities for EMF mirror made on PC and PMMA and in the Table 3-3 the photocurrents for the same mirrors (the rest of the parts are without antireflective coatings).

In the same figure there are also data labelled as “EMF(PMMA)*coefPOE6/POE2” (green curve). These data are rescaled from the EMF(PMMA) mirror by the measured coefficient. The coefficient has been taken from spectral measurements of two samples of the POE (labelled as POE2 and POE6) where one had a yellowish look. The “good” one (the one with normal appearance) was simulated as the EMF (PMMA) mirror.

3.1.1.4 Comparison Between First and Second Surface Mirror

This section discusses the spectral optical efficiency for the silver coated mirror. Two cases have been studied. The first one is an ideal first surface mirror (Ag coated), and the second one is an ideal second surface mirror, where the first surface is glass (nglass=1.52). Both cases are summarized in Figure 3-14. In Figure 3-15 a graphical

comparison is provided for the spectral reflectivity of the two cases. Table 3-4 provides numeric values of generated photocurrent when these two types of mirrors are implemented in a system where the glass cover and secondary optical element have no anti-reflective coatings.

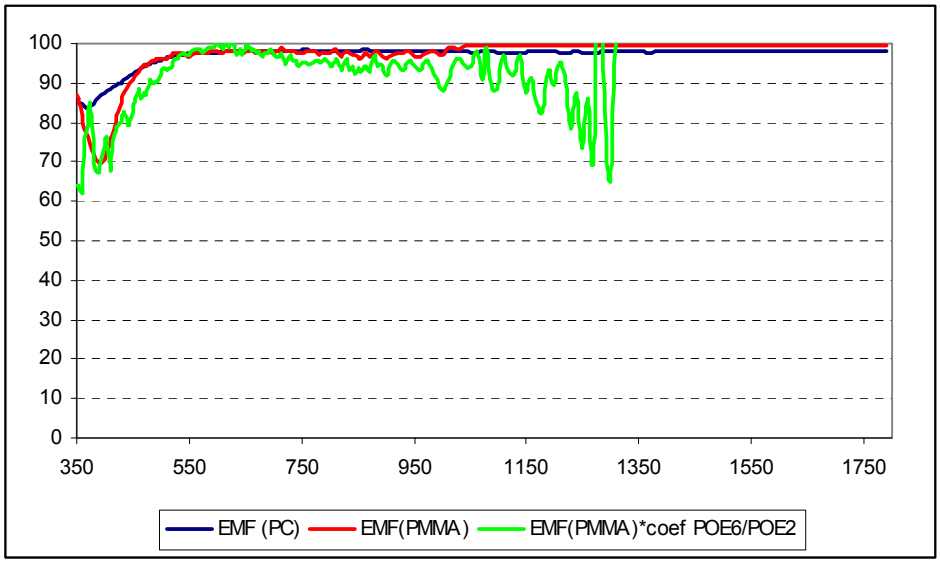

Figure 3-13. Spectral reflectance of EMF mirrors; blue curve is metallization on PC and the red one on PMMA; green curve is from measured data

Table 3-4. Numerical Estimates of Isc various optical designs

Short circuit current (Isc)	Top cell (A)	Middle cell (A)	Bottom cell (A)	Total (A)	Optical efficiency	Optical concentration (suns)
No optical losses	**9.64**	**9.91**	**16.68**	**9.64**	**100%**	**899**
With simulated losses: **-Cover: Pilkington** **-Mirror: EMF(PC)**	**7.69**	**7.94**	**13.14**	**7.69**	**80%**	**717**
With simulated losses: **-Cover: Pilkington** **-Mirror: EMF(PMMA)**	**7.60**	**7.90**	**13.26**	**7.60**	**79%**	**709**
With simulated losses: **-Cover: Pilkington** **-Mirror: EMF(PMMA)*measured coefficient**	**7.49**	**7.74**	**13.45**	**7.49**	**78%**	698

Values of reflectance are calculated which include absorption in the glass. Change of refractive index with wavelength is not included (data weren't provided).

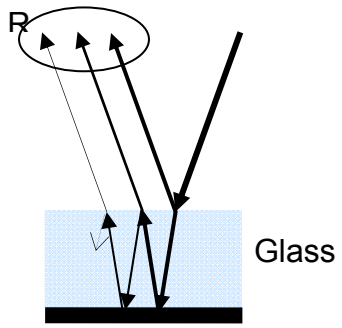

Figure 3-14 Considerations for reflectivity calculations of the silver second surface mirror

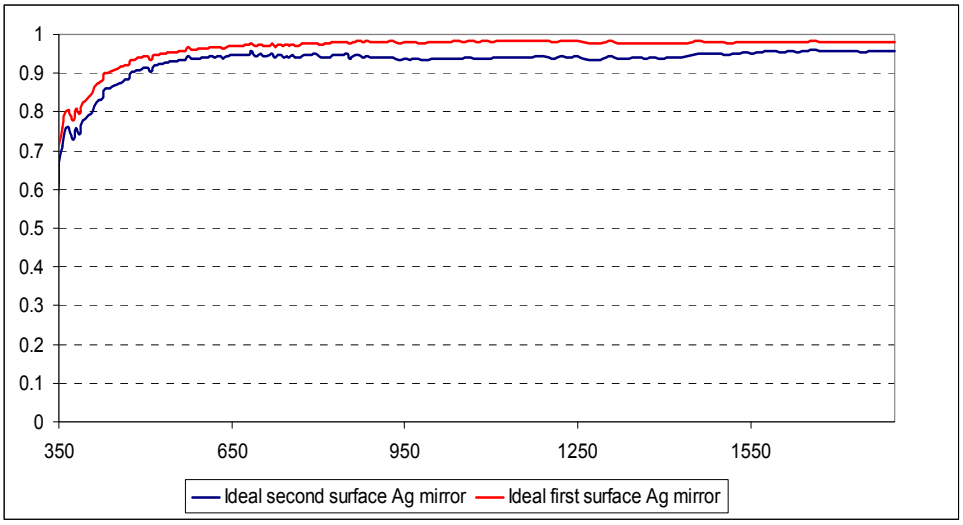

Figure 3-15 Spectral reflectance of Ag protected mirror

Table 3-5. Numerical estimates of Isc various optical designs

Short circuit current (Isc)	Top cell (A)	Middle cell (A)	Bottom cell (A)	Total (A)	Optical efficiency	Optical concentration (suns)
No optical losses	9.64	9.91	16.68	9.64	100%	899
With simulated losses: -Cover: Pilkington -Mirror: ideal Ag coated first surface mirror	7.55	7.89	13.15	7.55	78%	704
With simulated losses: -Cover: Pilkington -Mirror: ideal Ag coated second surface mirror	7.32	7.64	12.62	7.32	76%	683

NOTE: The efficiencies shown in this table are less than the real one should be (even lower than the one obtained with EMF mirror without silver coating). That is due to low reflectance of pure Ag in the UV part of the spectrum. In the real case there is another metal layer underneath the silver, so the reflectivity in the UV is higher. Due to lack of data, calculations were carried out with pure silver.

Tolerance study: This part summaries the analysis of the assembly tolerance of the optical system, which is formed by a XR concentrator + mixing rod.

Variables whose tolerance is analyzed are:

1. Optical efficiency.
2. Acceptance angle (half angle) [degrees].

To calculate maximum irradiance at the cell active surface an extended light has been used with the same angular spread as the sun.

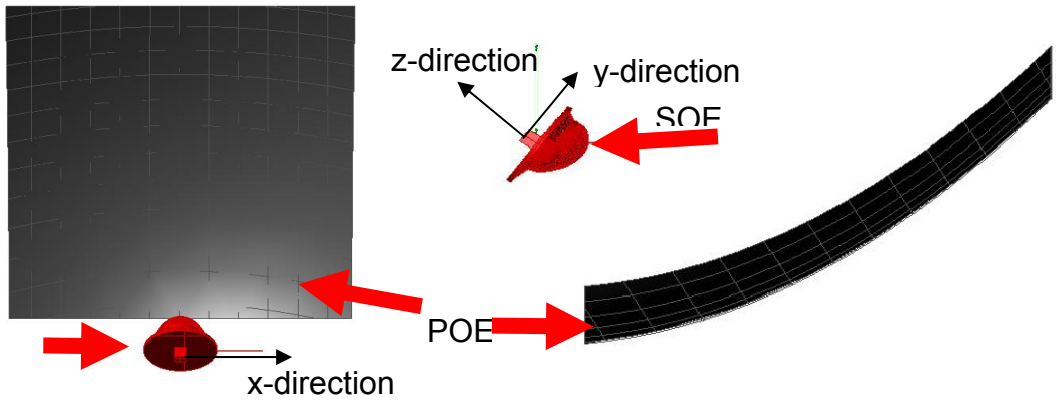

Figure 3-16 Directions of variation of relative position between the elements of XR; top (left) and side (right) view of the system

Table 3-6. Ray-trace input parameters

Mirror reflectivity	95%	
Dielectric parts:		
Refractive index	1.52	
Fresnel losses	**YES**	
Absorption	JUST FOR λ=546nm	(default wavelength in TracePro)
Solar cell area	10x10mm^2	
Mixing rod		
Length	9mm	
Area	9x9mm^2	
Rounding of lateral edges	**NO**	
Silicon rubber	**NO**	
Refractive index		
Absorption		
Thickness		
Cover transmission	91%	
Input irradiance	900W/m^2	
NOTE: The raytrace analysis of acceptance angle have been done considering angular radius of the solar disk 0º, while the efficiency and irradiance analysis have been done considering angular radius of the solar disk 0.26º. Rounding of homogenizing prism walls, and the influence of the silicone rubber were neglected. The rest of the parameters were the same as in the previous section.		

In Table 3-7 can be found the results summary of the preceding analysis. The values shown are the ones that had the maximum deviation from nominal values, for displacement from -2 to 2mm and for twist of -2 to 2 degrees.

Table 3-7. Summary of tolerance study results.

SOE+cell							
		Displacement			Twist		
	Nominal value	x direction	y direction	z direction	x	y	z
Acceptance angle							
x section	1.84º	1.65º	1.63º	1.518º	1.816º	1.804º	1.82º
y section	1.81º	1.76º	1.705º	1.636º	1.857º	1.86º	1.83º
Peak irradiance	855x	1480x	1259x	1172x	1090x	1145x	957x
Efficiency	82.12%	81.9%	81.7%	81.38%	81.56%	82.04%	81.98%
Cell							
x section	1.84º	1.11º	1.83º	-	-	-	-
y section	1.81º	1.81º	1.14º	-	-	-	-
Peak irradiance	883x	931x	921x	-	-	-	-
Efficiency	82.12%	59.7%	59.8%	-	-	-	-

It can be seen that for the acceptance angle the most critical is simultaneous displacement of the SOE and cell in the z direction, since the average value drops from 1.84º to 1.518º for x section and to 1.63º for y for the 2mm displacement error. Also the fall of the acceptance angle is to be accepted in the case of removing cell from the assembly in both analyzed directions; in this case the acceptance angle decreases to the 1.11 degrees for 2mm displacement.

In the case of peak irradiance on the cell, it can be kept below the maximum value for the multi-junction solar cells (about 1500 suns), for all analyzed positioning errors, thus the displacement of the SOE + cell 2mm in the x direction increases the peak irradiance on the cell to the 1480 x (Figure 3-17).

The optical efficiency is only slightly impacted by consolidated variation of position of SOE and cell. However, if the cell is displaced relative to the SOE then the receiving area is reduced and there is a proportional drop in efficiency. For example, in Figure 3-17 an optical efficiency drop of efficiency of 22% approximately (from nominal value of 82% to 59.8%) is demonstrated by cell displace relative to the SOE

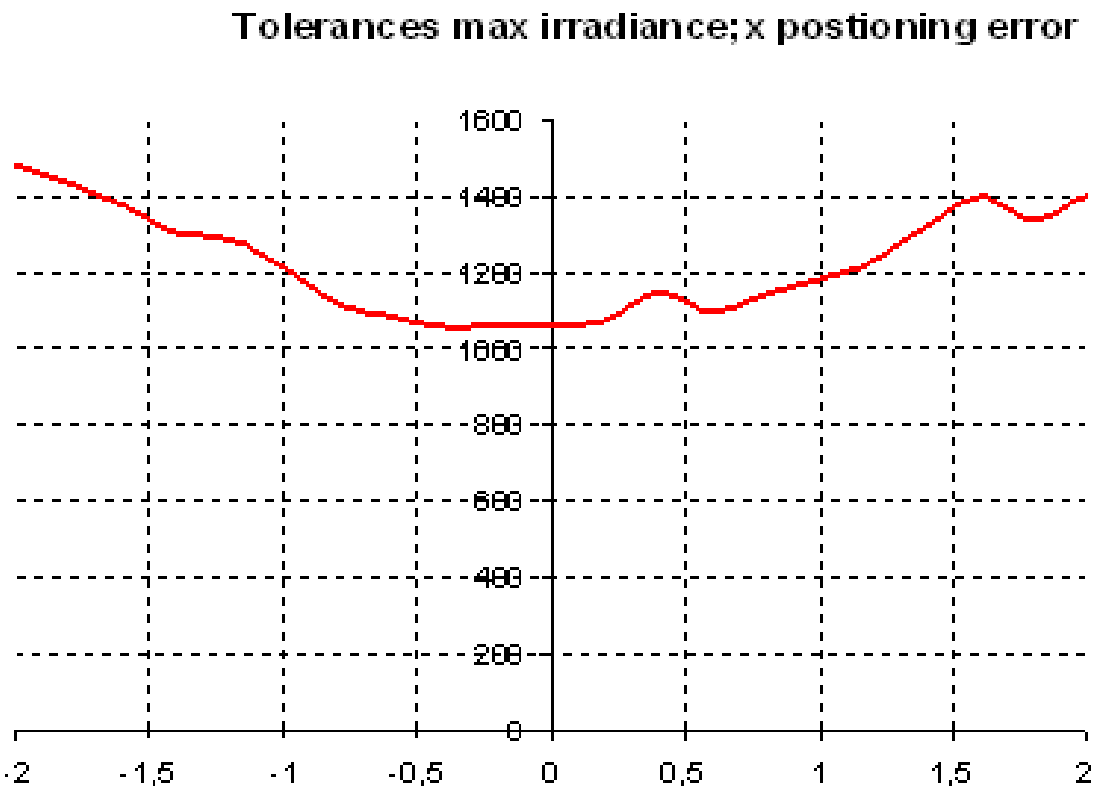

Figure 3-17. Maximum irradiance vs. x displacement of SOE and cell.

3.1.1.5 Optical Efficiency as Function of Silicone Refractive Index

This section is focused the optical efficiency (defined as power on the cell active surface/power on the concentrator aperture) dependence on the refractive index of the silicone adhesive used in a XR optical system to glue the solar cell to the secondary optical element (SOE).

The input parameters used for the ray-tracing are:

1. Mirror reflectivity: 95% (assuming perfect mirror coating)
2. Dielectric parts: n=1.52 (glass), includes Fresnel losses
3. Active solar cell area 9x9 mm
4. Mixing rod length 9 mm
5. Cover transmission 91%
6. Radius at the lateral edges of the prism: 0.3 mm
7. Silicone thickness: 50 microns (500 microns shows similar result, Figure 3-19).

Figure 3-18 shows the optical efficiency dependence on the silicone index of refraction used for encapsulating the solar cell (in red). In the figure, the black curve is a regression curve for the traced values. This regression curve is only valid for the range between 1.40 and 1.54.

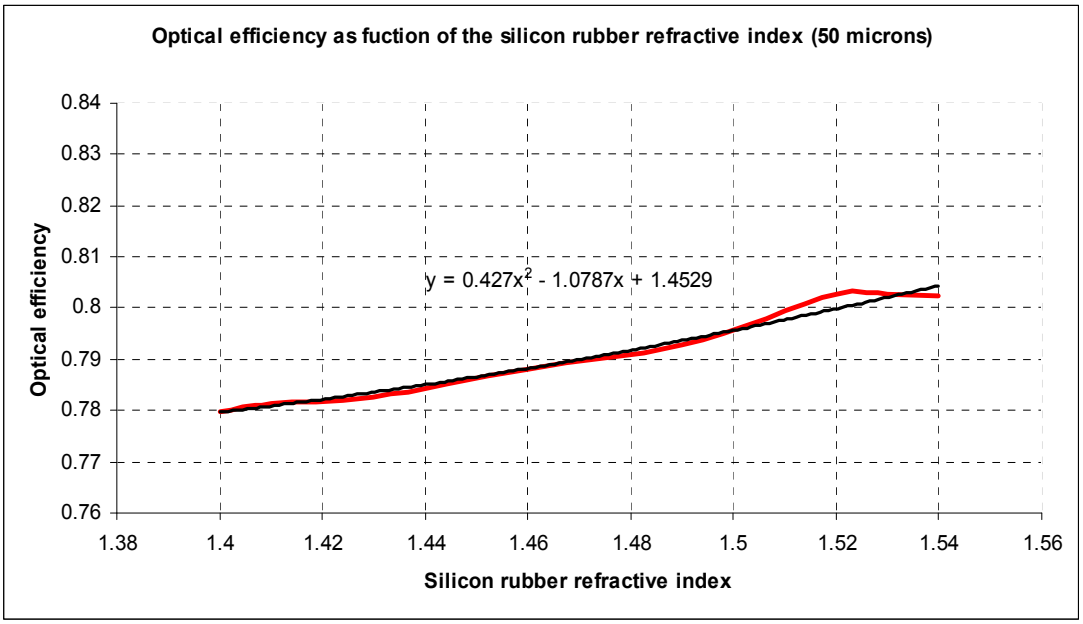

Figure 3-18 Optical efficiency as function of the silicon rubber refractive index.

Figure 3-19 assesses the impact of optical bond thickness and index of refraction on optical efficiency. For reference the design base lined a 100 μ optical bond. Figure 3-20 assesses differences between the original off-axis design (prototype B) and the prototype C design base lined for full scale engineering.

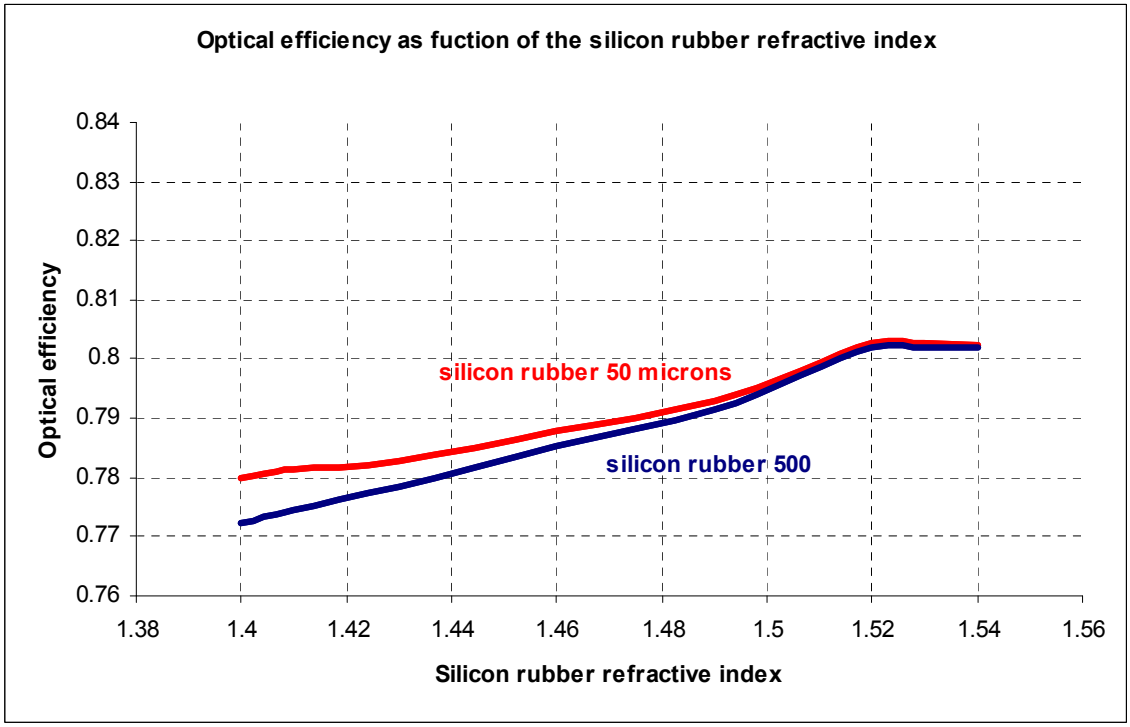

Figure 3-19 Comparison of the prototype B optical efficiency for different thickness of the silicon rubber.

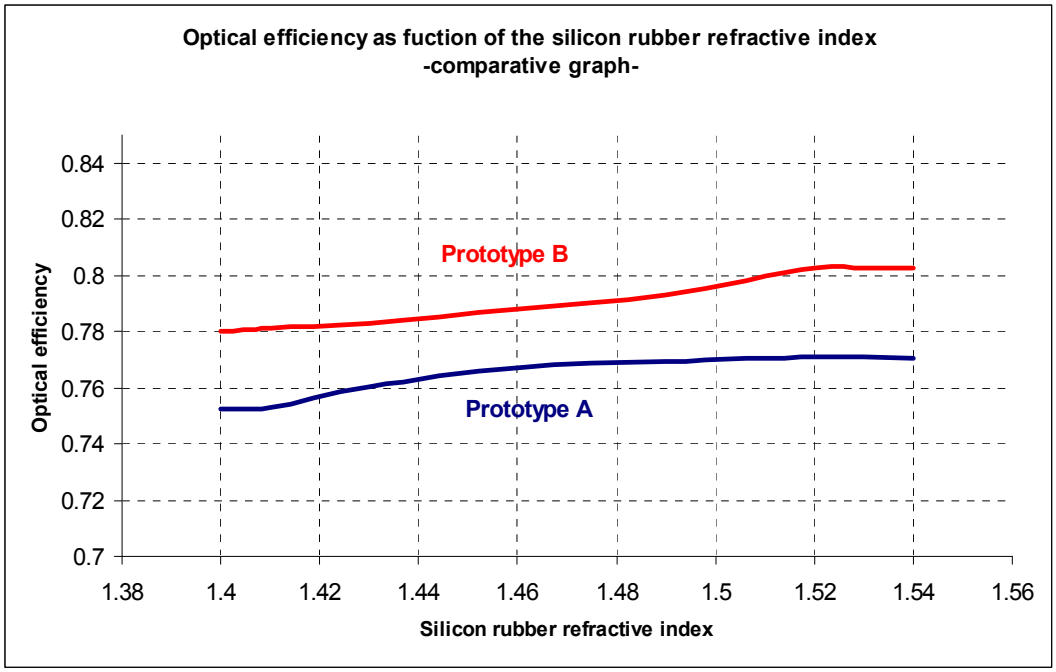

Figure 3-20 Comparison of optical efficiency with silicon rubber of 50 microns for prototype A and prototype B.

3.1.1.6 Differences Between Prototype B and C:

The off axis design has been implemented in two different physical manifestations. Prototype B was a single receiver plastic module employed for initial trials. Full engineering development occurred with prototype C where six receivers are contained in series in a single enclosure (see Section 3.2).

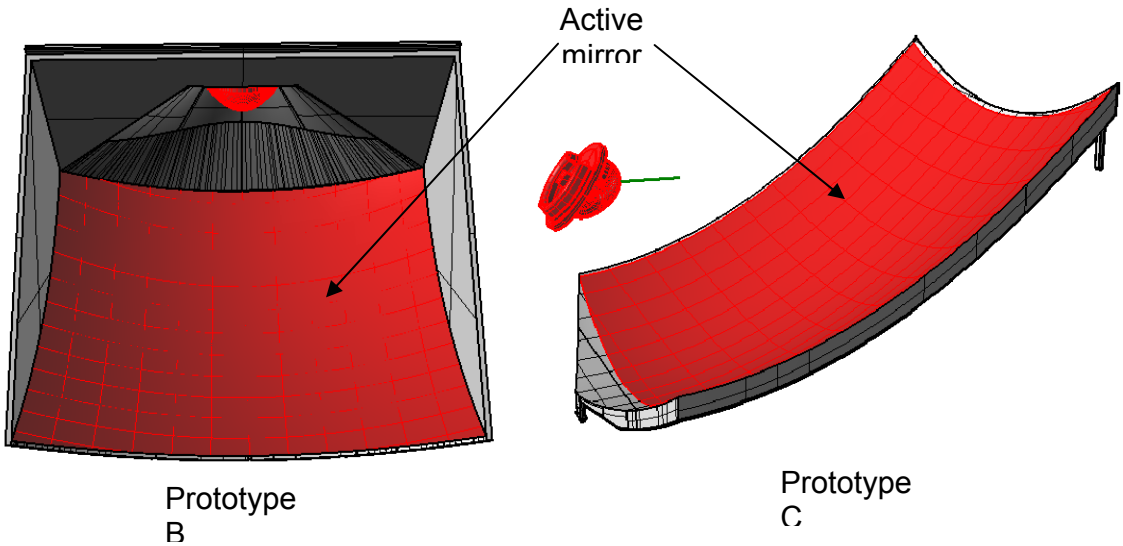

Figure 3-21 Prototype B and C modules with marked active mirror area.

In Figure 3-21 can be seen both prototypes B and C. The main difference from the optical point of view is active mirror area. Due to that the geometrical concentration is decreased (values are shown in Table 3-8).

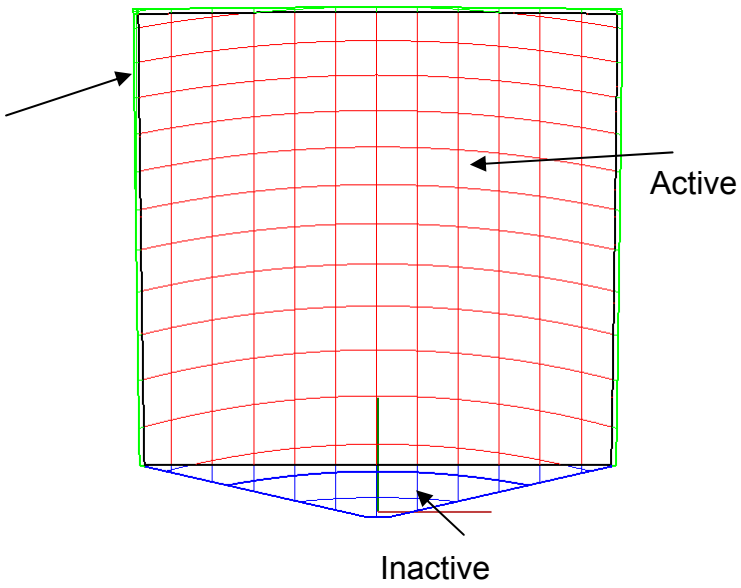

Figure 3-22 Prototype C POE, top view.

Table 3-8 Geometric Properties of Prototypes B and C.

	Prototype B	**Prototype C (designed: red + green area in Figure 20)**	**Prototype C (produced: red area in Figure 20)**
Active mirror area (mm^2)	80787.267	82582.0576	80076.037
Geometrical concentration	997x	1019x	988x

Figure 3-22 shows a top view of the prototype C POE, where the red area is active mirror area, the green is the area that is not working properly due to deformation during the molding process, and the blue area is the area that is used just as a structural part.

From the values in Table 3-8 it can be seen that the active mirror area from prototype B to C is decreased for 0.9%, while total area losses in prototype C are 3%.

3.1.2 Optical Development

3.1.2.1 Quantum Model

The development test data reported in Section 6.3 demonstrates a substantial disparity with the performance predictions in Section 3.1.1. In part the disparity turned out to be the result of mechanical issues which are described in Section 3.2. However, in addition to the mechanical issues it was apparent that the performance could also be substantially improved by optimization of performance of the optical components relative to overall transmission and tailoring to the characteristics of the multijunction cell.

One step in this process was development of a quantum model for comparison of predicted optical performance based on the actual spectrum of the solar excitation energy after optical concentration with the measured output of the triple junction solar cell. The spreadsheet quantum model developed for this purpose employs as input

- The wavelength-dependent optical reflectivity and transmissivity of the module optical components (window, primary optical element, secondary optical element) for 90° incident radiation and for the SOE as a function of incidence angle.
- The time- and date-dependent measured solar spectrum at Seal Beach, CA where performance measurements were performed.
- The quantum efficiency of the triple junction solar cell.

The function of the model was to identify areas for possible improvement and deficiencies in performance between as designed and as built.

3.1.2.2 Primary Optical Element

At the inception of the program the decision was made to pursue front surface injection molded silver coated plastic mirrors for the primary optical element based on cost and performance. The chief barrier to this solution is the need to assure that the mirrors meet the design life with 30 years of deployment. This in turn led to two mirror requirements

- The mirror must demonstrate stable reflectivity after prolonged UV testing.
- While it is possible to protect the mirror from weathering (e.g., rain) it is not practical to deploy the mirror in a fully inert environment. Thus a silver mirror must incorporate a protective coating on its upper surface. For example, this could be a vacuum deposited layer of SiO_2 on the upper surface

While mirrors samples from numerous suppliers were evaluated, after screening only mirrors provided by EMF and Stanley Electric were operationally tested. High intensity UV stability test results for the EMF mirror are provided in Figure 3-23.

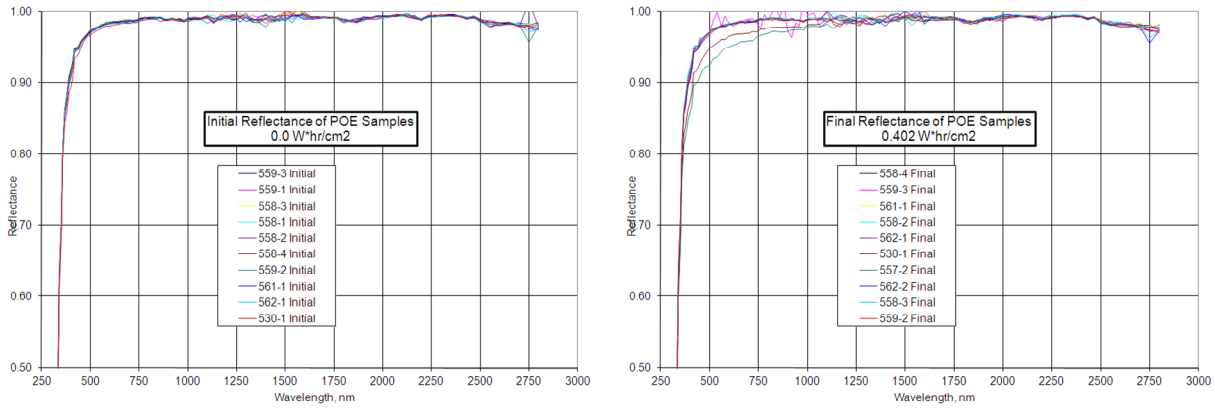

Figure 3-23. Pre and post test reflectivity of EMF mirror samples.

As can be seen in Figure 3-23 the reflectance of the EMF mirror was essentially unchanged after UV exposure. Similar tests have been carried out on test coupons of the original Stanley mirror configuration. Post-test exposure data are provided in Figure

3-24. The data compare very well with the post test exposure data for the EMF mirror. Based on these component evaluation results the EMF coating was qualified for POD and the Stanley coating for POM.

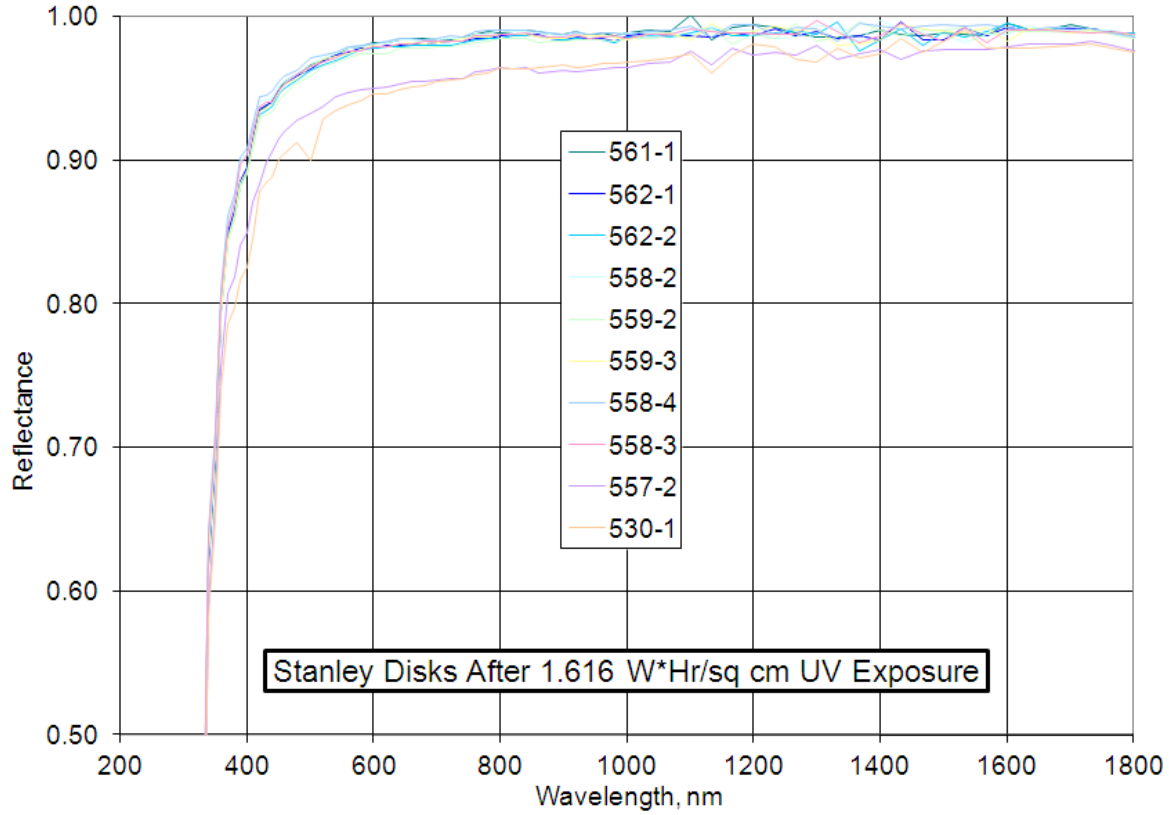

Figure 3-24. Stanley disks after 1.616 W*Hr/sq cm UV exposure, no pre exposure data provided.

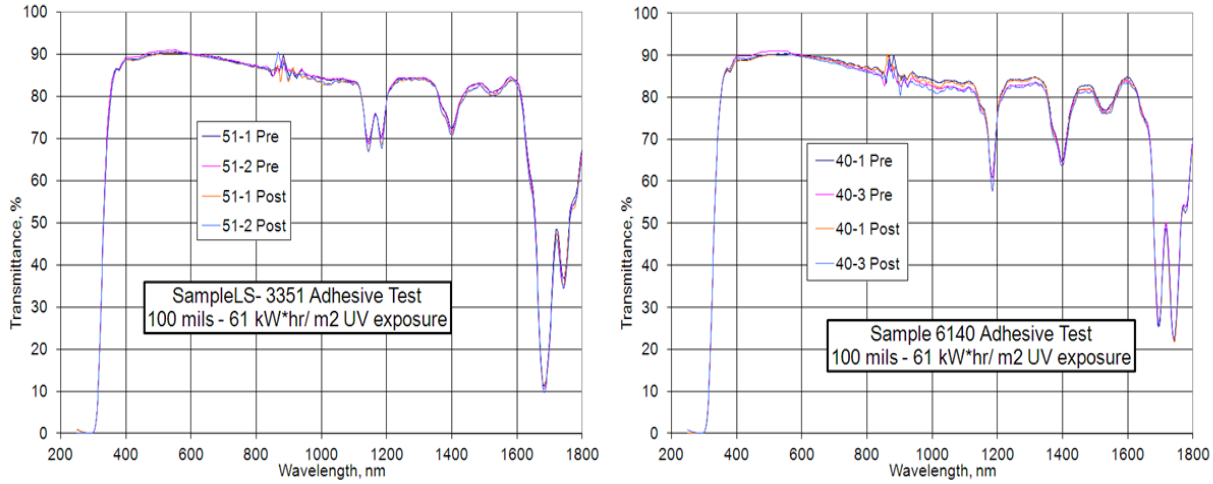

Figure 3-25. Accelerated UV stability data for methyl (LS6140) and phenyl substituted (LS 3351)optical adhesives.

3.1.2.3 SOE to Cell Optical Bond

The identified environmental issue for the optical bond is UV degradation of the silicone polymer bond material under the very intense radiation (>700 suns) dosage. Both methyl (LS 6140) and phenyl (LS 3351) substituted materials from Nusil Corporation were evaluated for UV stability. A high intensity Phoeson LED lamp was employed with a peak intensity at 370 nm, more than 10X that available for a typical mercury lamp. To further accelerate the test, sample thickness was 2.5 mm, 25 X the thickness of the of the optical bond. All of this yielded a total acceleration factor of approximately 750 before accounting for UV intensity reduction on passage through the glass window and SOE (~2X).

Life test data for the two candidate adhesives are presented in Figure 3-25. As can be seen the data are nearly indistinguishable and both adhesives appear to be fully stable in the UV environment. Nusil offers the methyl substituted adhesive for solar energy applications and the general opinion in the solar community is that methyl adhesives demonstrate greater stability that phenyl adhesives. However, as was discussed in Section 3.1.1, index-matched adhesives do provide superior performance. This motivated the attempt to qualify the LS3351 and eventually, based on both the Figure 3-25 laboratory results and module test data (described in Section 6.4), the material was deemed qualified for POM. However at the time of POD this was not the case and the lower performance LS6140 was employed.

3.1.2.4 AR Coating

Examination of Figure 3-11 shows that the unoptimized design loses 9% of the incoming light through reflection at a 90% incident angle. Serious reflective losses also occur at the SOE. In order to maximize performance (and thereby minimize LCOE) AR coating on both surfaces were investigated, optimized and implemented.

Three different AR coating supplied by Xerocoat, Schott and Centro Solar have been used for the module window. All three appear to be of inorganic silica-based high surface area materials bonded to glass in a fashion that leads to a tempering effect. Environmental testing by the suppliers and actual field experience demonstrate that all the coatings have the requisite durability.

With the Spectrolab C3MJ and C4MJ cells the critical feature is the transmissivity of light through the optics between 350 nm and $\approx$ 1000 nm as either the short wave length top junction or the middle wavelength middle junction limit output current. As shown Figure 3-26 all the coatings offer significant enhancement to the transmissivity in this region. Schott was employed for POD; however, they ceased to manufacture the product leading to the use of Centrosolar for POM.

Selection of the AR coating material for the SOE is more complicated. Reflectivity depends on both incident angle and wavelength. The distribution of light with incident angle has been analytically modeled by LPI and these data are provided in Figure 3-27 for the intensity at the SOE surface and at the surface of the cell. The conclusion from these data is that reflectivity needs to be minimized for an incident angle that is centered about 20° off normal.

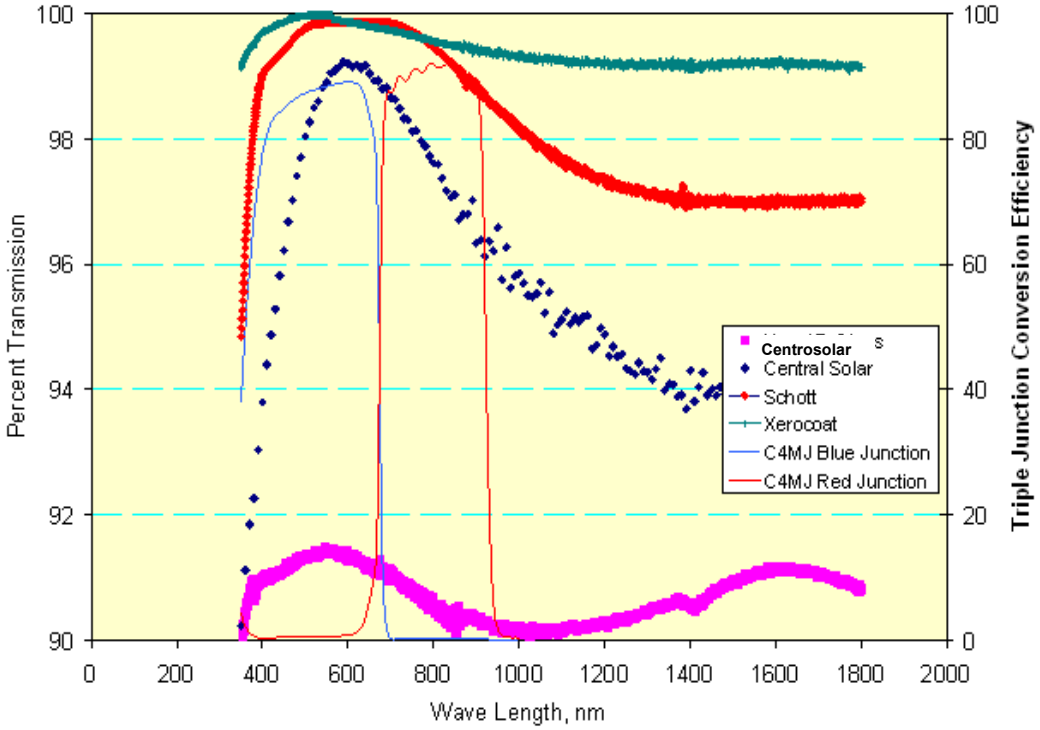

Figure 3-26. Window transmissivity data and C4MJ spectral quantum efficiency for different AR-coated glass based window materials.

It was also discovered that the first SOE AR coating employed was not optimized over the range of frequencies for the two top cell junctions. These data are provided in Figure 3-28. Based on these data Auer was contracted to optimize their coating for different incident angles and these data are also provided in Figure 3-28. The baseline AR coating was employed in POD, however, the improved coating was implemented in the POM design and at the power plant. The results of these improvements are described in Section 6.4.

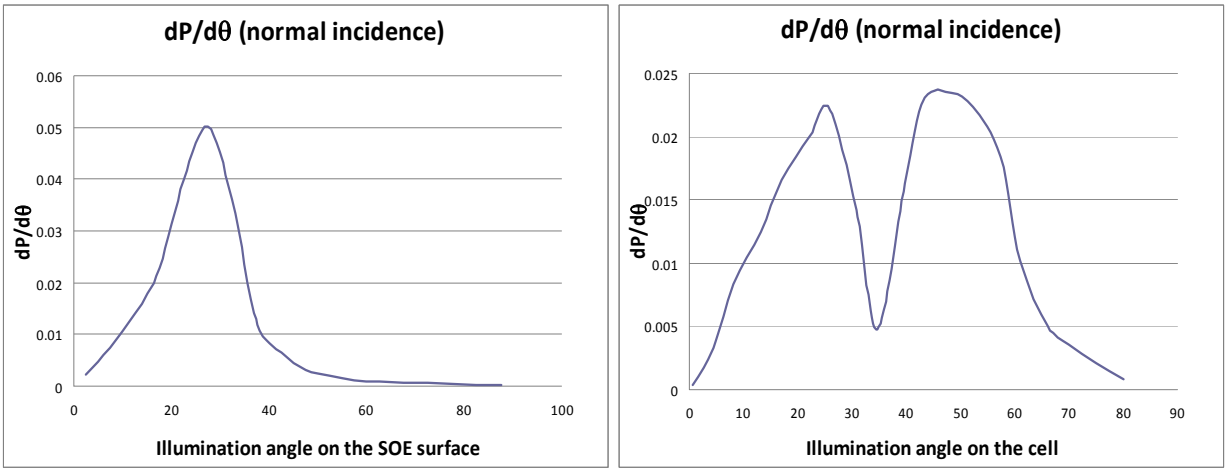

Figure 3-27. Relative angular distribution at the SOE.

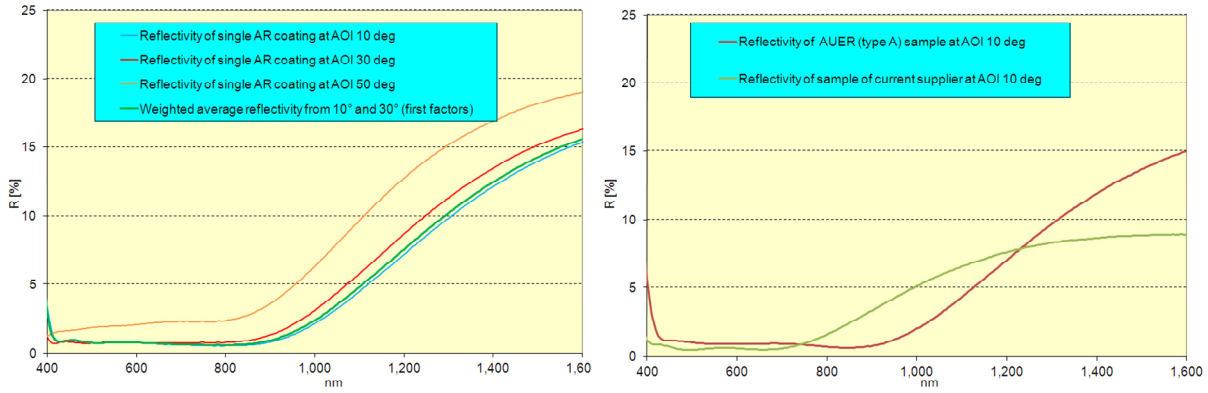

Figure 3-28. Frequency dependency of the reflectivity for the original (POD) coating and an alternative supplied by Auer (right) and reflectivity of the optimized Auer coating versus wave length for three incident angles (left).

3.2 Module Design

3.2.1 Receiver and Heat Sink Design and Development

3.2.1.1 Conductive vs. Heat Pipe

Heat sink cost was viewed as one of the key challenges facing the program. Two possible solutions presented themselves,

- Implement a purely conductive solution based on extruded aluminum.
- Exercise the supply chain to determine if low cost heat pipe solutions were available from the personal computer business space.

The reason for pursuing a heat pipe was a material mass and cost analysis which demonstrated that for a specification complaint heat sink the mass of aluminum in a conductive heat sink cost more than the mass of copper and aluminum in a in a heat pipe based heat sink. Early in the program the thermal requirement established in conjunction with Spectrolab that that the maximum allowed cell temperature was 100°C assuming a 50°C ambient temperature and a 70 W thermal input (DNI = 1000 W/m^2, 800 cm^2 aperture area, 85% optical efficiency). This requirement was based on continuous no power extraction operation which is clearly an artificial condition for a commercial power plant and the requirement was revised to a 40W continuous load thermal requirement based on power extraction with a 40% cell. With this modified requirement analytical solutions were demonstrated that kept the worst case continuous operation cell temperature below 100°C. These solutions were based on both conductive and heat pipe based approaches.

Even with the modified requirement the mass of aluminum required for a technically compliant heat sink represented a substantial materials cost which in true volume production will dominate price, unlike the situation with space hardware. This observation is quantified by the data presented in Table 3-9. The bottom line (compare two highlighted rows) is that the complexity of a heat pipe is offset by a 50% materials cost reduction. This reduces the problem to discovering/developing a supply chain for large quantities of low cost heat pipes.

Table 3-9. Comparative materials and performance cost data for heat pipe design options. Temperature cost is based on system cost of $4 per watt and a performance factor of -0.1% per °C. Materials costs are based on $3.0 for copper and $1.25 for aluminum.

	Area	ΔT	Mass	Material	Mat. Cost	T Cost	Total Cost
Prototype B	1626	28.4	826	Cu	5.46	-0.32	5.14
Prototype B with 1.2mm Al Fins	1522	38.4	247	Al/Cu	0.88	1.15	2.02
Prototype B with 0.6mm Al Fins	1691	40.8	137	Al/Cu	0.58	1.50	2.08
Prototype B with 0.4mm Al Fins	1776	37.8	96	Al/Cu	0.46	1.06	1.52
Prototype B Conductive, 3mm Base	1890	43.8	429	Al	1.18	1.94	3.12
Prototype B Conductive, 6mm Base	1890	40.2	462	Al	1.27	1.41	2.68
Prototype C	2560	37.8	173	Al/Cu	0.87	1.06	1.93
Prototype C, Bent Heat Pipes	2560	33.6	173	Al/Cu	0.87	0.44	1.32

3.2.1.2 Low Cost Heat Pipe

Based on the observations above the decision was made to pursue full development of a heat pipe based heat sink. The overall design approach was

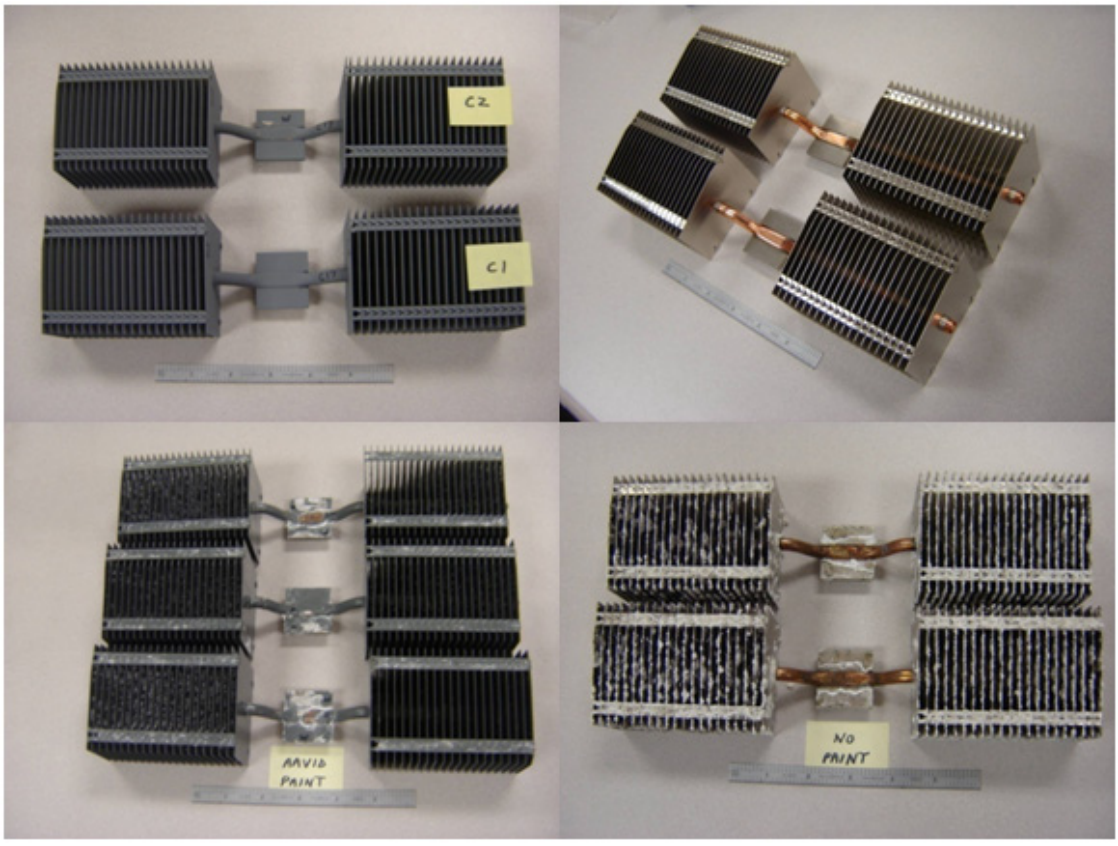

Figure 3-29. Painted (right) and unpainted (left) heat sinks before (top) and after (bottom) seven days of testing at 95°C and 95% RH.

- Use a pure copper heat pipe with water for the working fluid. The anaerobic water-copper system is thermodynamically stable. Thus after infant mortality there should be no issue with life.

- Thermally attach the heat pipe to the cell CCA via an aluminum coupling block. This block also serves to attach the resultant assembly to the chassis structure (see Section 3.2.1).
- Attach aluminum fins to the heat pipe to sink the heat to external quasi static air. Attachment has been affected by both soldering and adhesive bonding

The decision to couple aluminum and copper does create a potential for a corrosion cell. The decision was based on minimization of cost, as well as the realization that the system will mostly be deployed in desert-like environments, and that corrosion will occur on the aluminum rather than the copper and thus does not represent a catastrophic failure mode.

In fact the experience is that after 2 years no performance loss has been observed with unprotected aluminum and minimal corrosion is observed with painted aluminum on copper in the humid marine Seal Beach environment. In addition, laboratory salt fog testing has shown that painted aluminum is clearly superior to bare aluminum as the fin material in contact with copper. The final product employed on the POM hardware is shown with both approaches before and after qualification salt fog testing in Figure 3-29.

3.2.1.3 Thermal Bond

The second critical element of the design is the thermal bond between the heat sink block and the CCA. This bond should

- Be high a heat conductor;

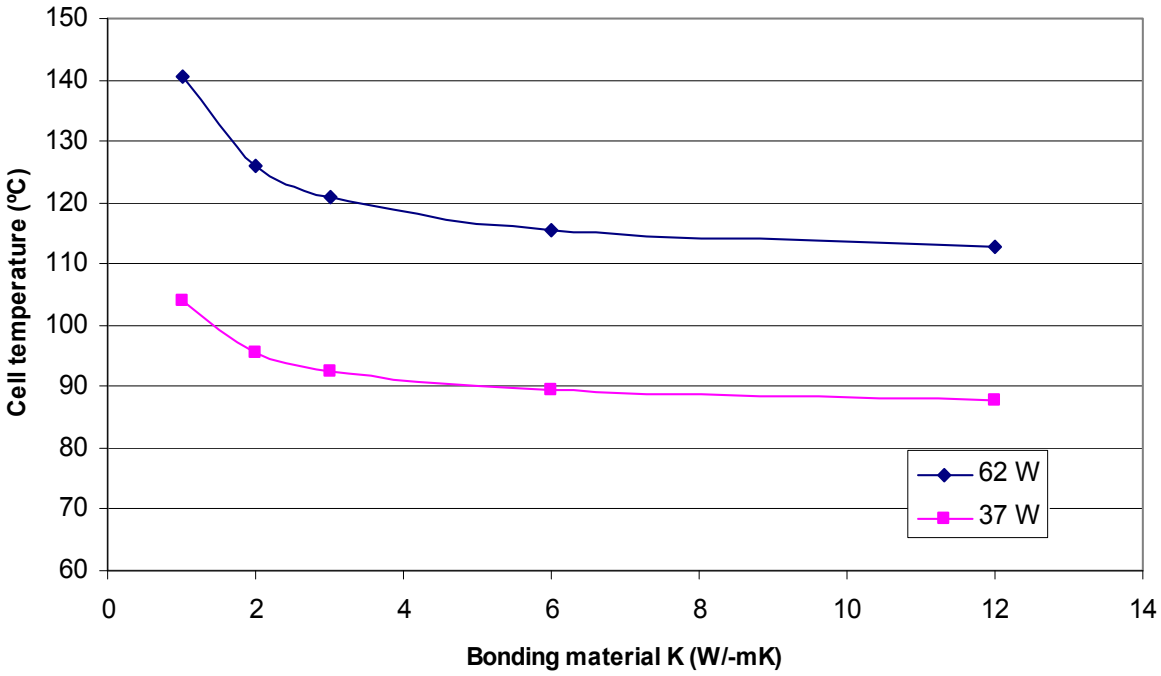

Figure 3-30. Performance of the thermal joint as a function of the bond material for both operational and non operational worst case thermal environments.

- Mechanically compliant and resilient through thousands of thermal cycles and the inducted stress between the CCA ceramic carrier and aluminum heat sink block;
- Be an electric insulator with a stand capability on the order of 2000 V above ground;
- Cure without appreciable shrinkage.

After numerous candidates were evaluated, two adhesives from Dow Corning, DC 4173 with a thermal conductivity of 1.5 $Wm°C^{-1}$ and DC 6534 with a thermal conductivity of 6 $Wm°C^{-1}$, were selected and qualified. While the more highly conductive material is clearly preferred based on analysis (see Figure 3-30) and test, note that the operational performance difference is only about 10°C. For practical reasons the DC4173 has been generally employed based on its greater availability, shorter curing time and lower cost.

3.2.1.4 Performance Validation

We have validated the performance of the heat sink/CCA subassembly both analytically and by test with a simulated deployed configuration (restricted air flow). The analytical results are summarized in Figure 3-30.

Figure 3-31 represents the heat sink in the restricted air flow environment which results when modules are mounted on a panel. The calculated temperatures of early heat sink designs provided a result in excess of the 100°C limit. This was addressed by a 20% fin area increase for the production configuration.

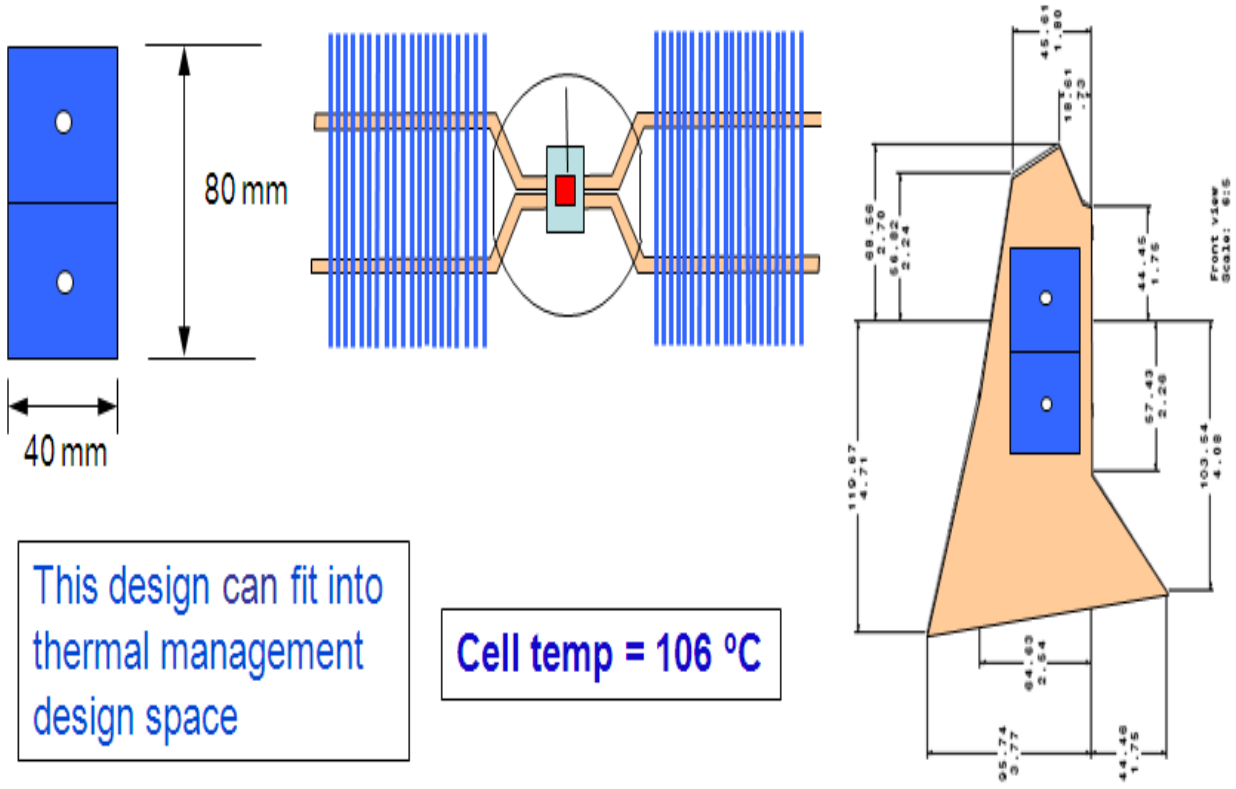

Figure 3-31. Thermal model environment and result for the operational system.

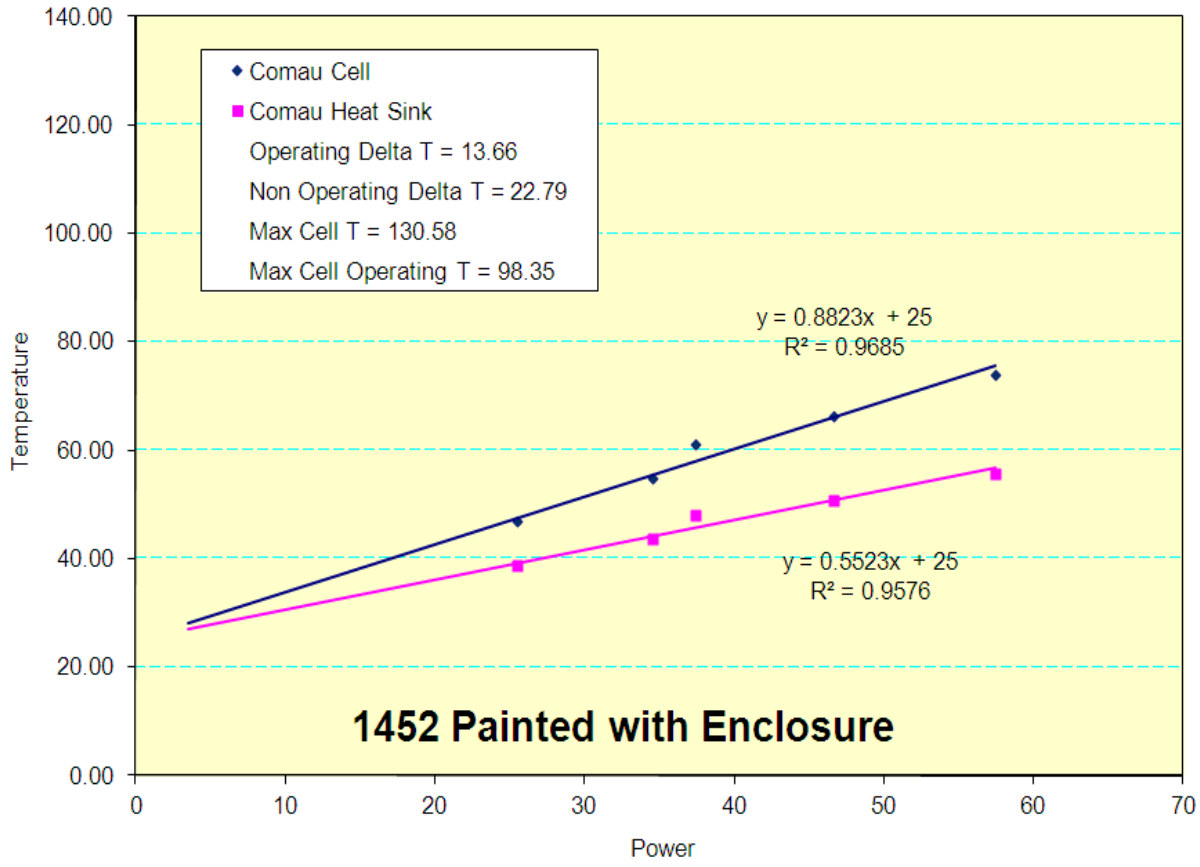

Figure 3-32. Thermal validation test result for the production heat sink design in the simulated heat sink enclosure with the DC6534 thermal adhesive.

Laboratory validation of the POM production design was carried out by operating the cell as a LED (assuring that emitted light was energy captured in the thermal system). Numerous tests were carried out with a simulated inter-module space between 0 and 40 watts of thermal power. Typical results with the DC6534 adhesive are provided in Figure 3-32 and show compliance of the design with worst case operational conditions.

3.2.2 The Module

For purposes of this discussion the module design is broken down into two major components, the receiver wall and the chassis assembly. This is both a design distinction and a manufacturing distinction that has been followed from hand built units all the way through robotic assembly.

An overview of the module design is provided in Figure 3-33. The building block for the module is the triple junction cell carried on the CCA. Six CCA/heat sink assemblies are mounted to a receiver wall and bused in series on the inside surface of the receiver wall. After busing the AR coated SOEs are bonded to the CCAs with the optical adhesive described in Section 3.1.2.3. The cups in the receiver wall are designed to fixture the SOEs in the correct optical alignment relative to the front surface silvered POE reflective optical elements. The receiver wall is mounted and sealed to a continuously welded steel chassis which contains the reflective POEs and provides accurate posi-

tioning between the POE and the SOE. The chassis is closed with an AR coated window which is sealed to the upper flange of the steel chassis. The window serves the critical mechanical function of rigidizing the chassis thereby guaranteeing that optical alignment is maintained. A critical lesson learned in the development of the design was the criticality of a stiff module structure to assure maintenance of optical alignment during assembly and in operation.

Greater detail on the design and assembly process is contained in the following subsections. These process were developed for manual assembly, but except as noted re-

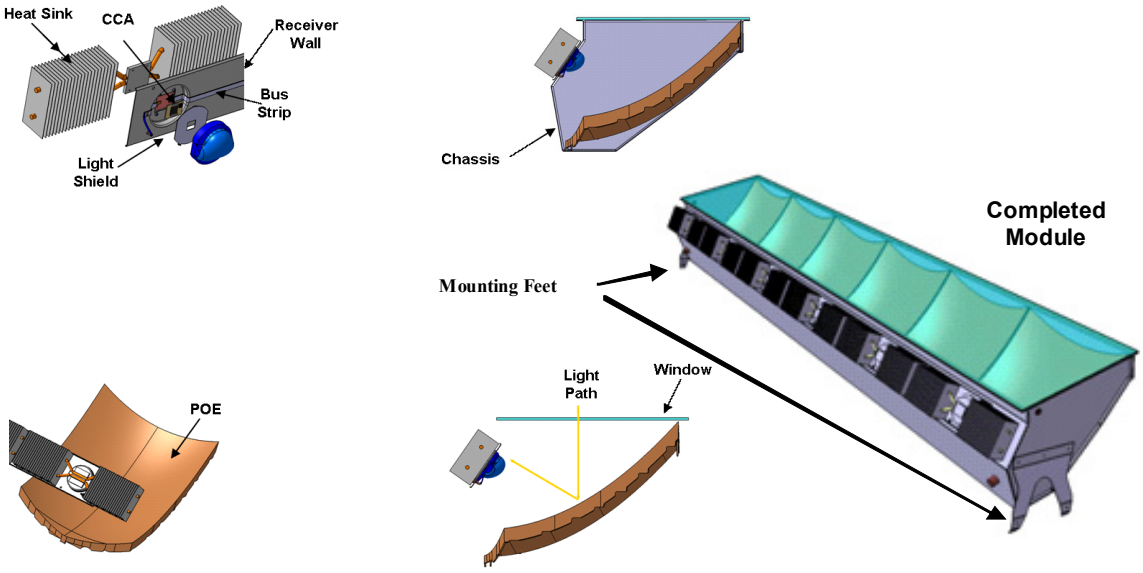

Figure 3-33. Overview of the Boeing CPV module design

mained the same during robotic assembly.

3.2.2.1 Chassis Assembly

The chassis assembly consists of various parts and subassemblies. The primary parts of the chassis assembly are (see Figure 3-34).

- The sheet metal chassis – Designed such that subsequent assembly requires a minimum of hard tooling to facilitate the assembly. As originally conceived this was a simple sheet metal box spot welded together. As requirements became clear it evolved to a seam welded sealed box with high precision mounting features. This affected cost and lead a future design evolution (see Section 4.4).
- The Primary Optical Elements (POEs) as described in Section 3.1.2.2.
- The cover glass as described in Section 0.
- The vent assembly – The vent assembly, consisting of and inner vent, outer vent, and a double washer, is installed wet with sealant thru the chassis wall. The vent is passive and requires no further operations.
- Purge assembly pass-thru – The purge assembly pass-thru is comprised of a Swagelok bulkhead fitting and two double washers, and is installed as is the

vent, wet with sealant. The Swagelok fitting contains a barrel nut and sleeve elements, which are preassembled into the fitting and shipped loose in place with the module assembly. A thread protecting sealing cap is removed from the fitting and discarded.

- Desiccant packages – Five desiccant packages are installed into the module by adhesive backed aluminum tape.

The secondary parts are the adhesives and fasteners used during the assembly of the chassis. Twenty-two Torx fasteners and associated spacer nuts are epoxy bonded into pre-drilled holes in the chassis to create the blind stud fasteners required for subsequent receiver wall installation.

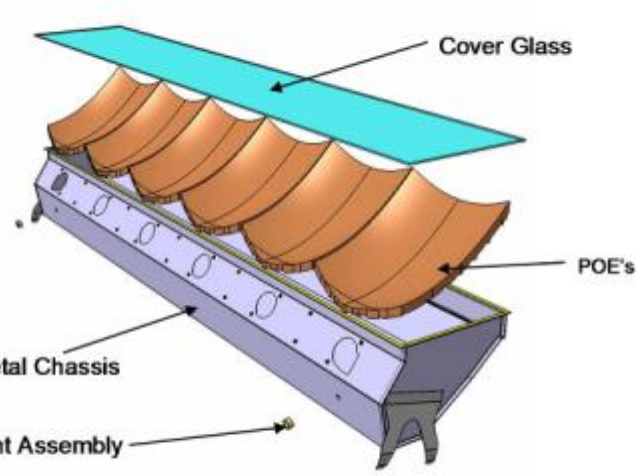

Figure 3-34 Chassis primary components.

Selected chassis' have been modified to accept a combined temperature/humidity sensor, which is installed through one of the sidewalls under the POEs. If a temperature/humidity sensor is required, it is installed by creating a ½" diameter hole in the selected sidewall with a chassis punch per the engineering location, and installing the probe from the inside of the chassis. Again, the sensor is installed wet with sealant, and has a back-to-back jam nut arrangement with both mounts and seals the penetration. The associated wire harness is attached, coiled and stowed to the adjacent chassis side wall with Kapton tape.

The next operation is to install the POEs. The sheet metal chassis is flexible prior to installation of the cover glass. In order to preserve the self-alignment features of the chassis, installations that have influence on alignment, like the POEs, are performed with the chassis in a restrained condition, on a granite surface plate. This allows the POEs to be installed in a "no load" condition, and reduces the probability of POE movement during subsequent installations. The POEs are designed with three chassis interface tabs; two aft tabs that control height and rotation, and one forward tab that controls location in three axis. The aft tabs are designed primarily to control rotation, and are simply constrained in the long, short, and short transverse axis of the chassis with chassis location features, but are not physically retained. The front tab, however, controls POE location in respect to its associated SOE, and is thus retained with a clip element in the chassis and molded-in detents in the forward tab. All three tabs are in-

stalled wet with fast setting epoxy and are manually snapped into place using finger pressure and features of the chassis to obtain alignment. (see Figure 3-35). The aft end of the POEs are restrained with simple clamps while the epoxy sets (nominally about 3 minutes).

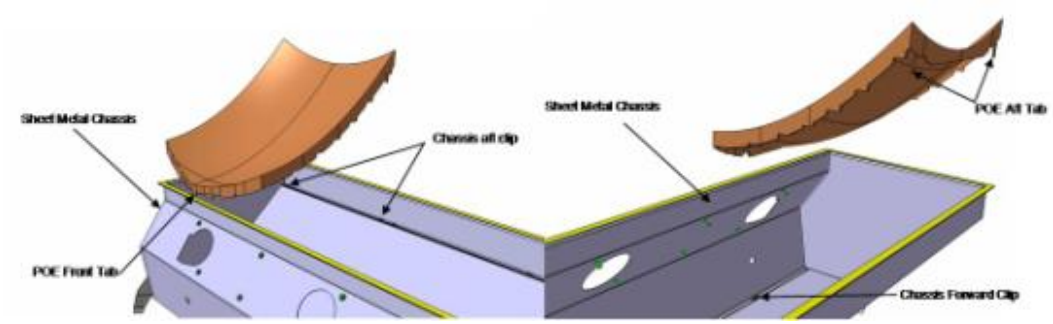

Figure 3-35. POE tabs and chassis clips

The chassis is now prepared for window bonding by performing an isopropyl wipe of the window interface surface. Primer is applied to the window, and is contained to the area of subsequent adhesive contact. A two-part acrylic adhesive, mixed via a static mixing tube attached to a pneumatic adhesive dispenser, is applied to the chassis interface surface and wiped with a notched trowel to form and locate the adhesive bead to a configuration that nets proper coverage with minimal squeeze-out. Spacers are manually equally distributed around the adhesive bead to develop the cured bond line thickness, and using three technicians for stability, the window manually located onto the chassis assembly. Clamps are applied over the spacers, and the chassis is left undisturbed for a minimum of two hours to allow the window adhesive to cure. Upon cure of the window adhesive, the chassis becomes a true torque box, exhibiting the stiffness required to ensure mirror retention and proper alignment (see Figure 3-36).

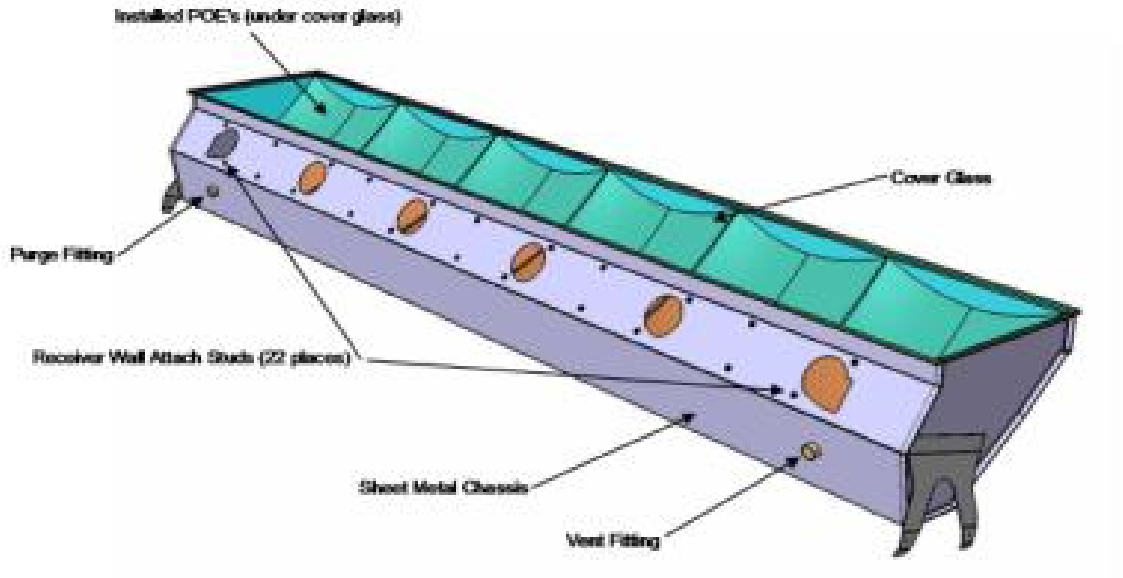

Figure 3-36. Completed chassis assembly.

1.1.1.1 Receiver Wall

The primary parts of the receiver wall are the sheet metal receiver wall plate, heat sink assemblies, concentrator cell assemblies (CCAs), light shields, short and long bus strips, SOEs and electrical pass-thru. The secondary parts are the fasteners, adhesives and tapes required of the assembly (see Figure 3-37).

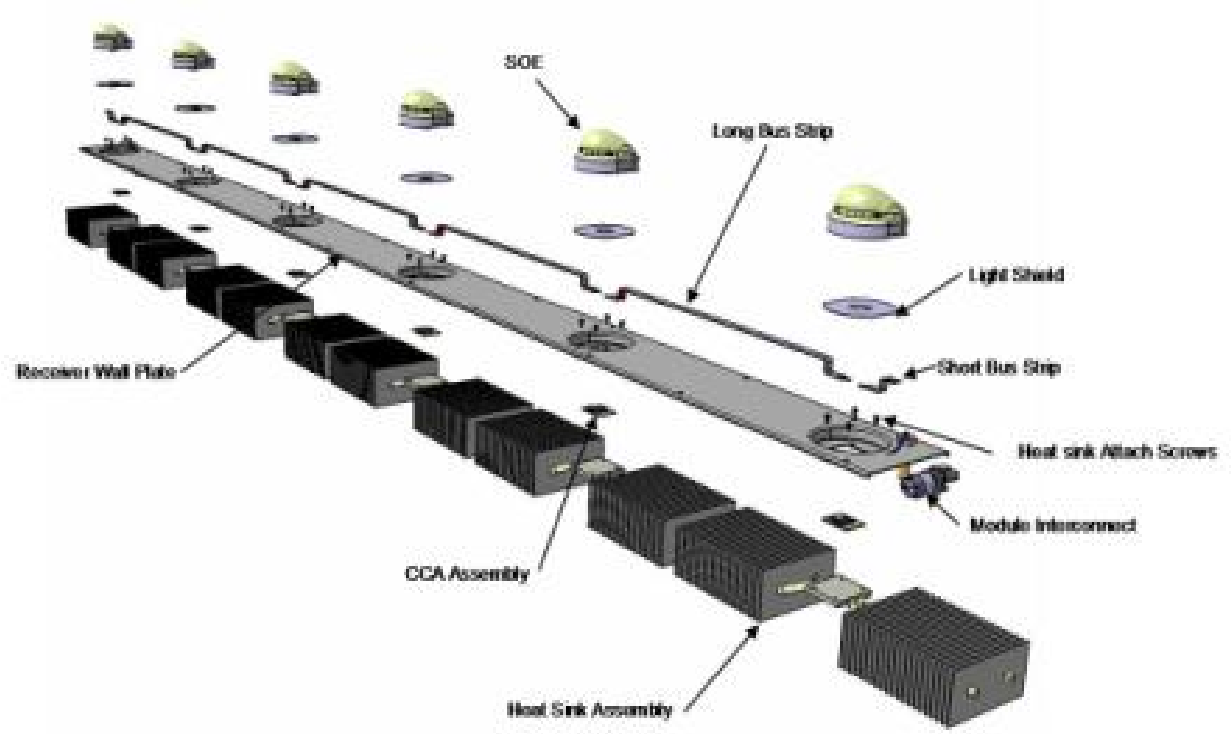

Figure 3-37. Receiver wall components

The receiver wall assembly is accomplished by developing a series of subassemblies which are assembled together at a final installation station. The assembly has a defined sequence and relies on features of the receiver wall plate to develop proper alignment and interface to the next assembly. The assembly of the receiver wall is accomplished using the following sequence:

The heat sink/CCA assembly, with the associated thermal bond, creates the first subassembly. The heat sinks interface surface is abraded and a bonding primer applied and the same is done to the back surface of the CCA. A for manual assembly layer of Kapton tape is applied to the heat sink surface, and using an indexing tool and razor knife the Kapton tape is trimmed to become a mask for the application of the thermal adhesive. Automatic dispensing is employed for robotic assembly. The thermal adhesive is applied to the masked heat sink surface and wiped across the surface using a flat bladed trowel. By using the thickness of the Kapton tape as a spacer, the remaining adhesive provides the necessary volume to develop the proper bond line thickness between the heat sink and the CCA. The Kapton masking is then removed and an indexing tool applied to the surface.

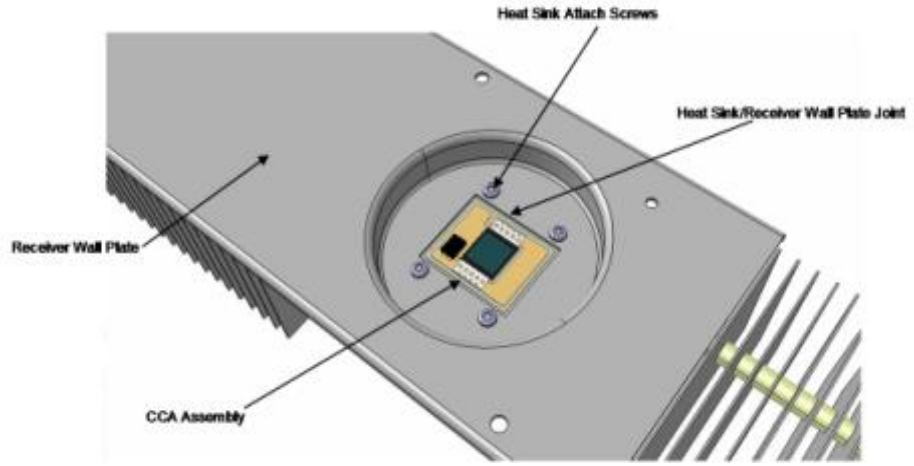

Figure 3-38. Installed heat sink-CCA assembly.

This tool locates the CCA in relation to the mounting holes in the heat sink, and provides an interface for a clamp block that is applied to the non-critical surfaces of the CCA. A back-up block is applied to the far side of the heat sink, and a spring clamp applied to the joint. This assembly is oven cured for an hour and left to cool prior to tool removal. Once cool, the tool is removed and for manual operations only a protective layer of Kapton tape applied to the solar cell surface. In manual assembly only a forward-bias test is performed on the CCA to validate survival thru the bonding process. The process documentation is completed and the heat sink/CCA subassembly put into stock to await subsequent installation.

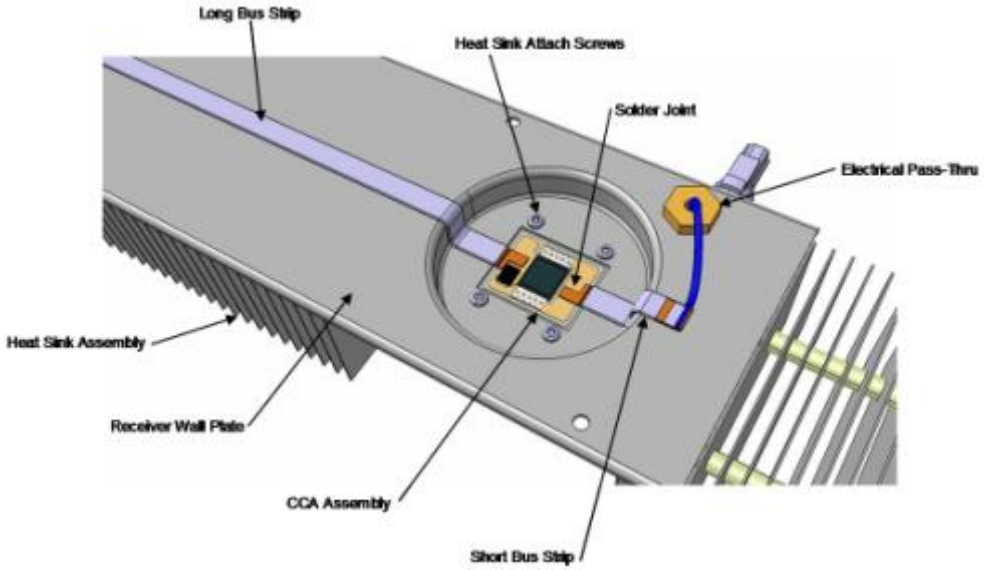

Figure 3-39. CCA installation details.

The receiver wall plate is prepared for assembly by installing layer of Kapton tape along the surface where the long and short bus strips are located, and two electrical pass-thru fittings, one at either end, are installed wet with sealant. A layer of sealant, containing

.010” diameter glass beads for bond line control, is applied to the faying surface of the heat sink/CCA assembly. The heat sink/CCA assembly is located onto its interface with the receiver wall plate and fastened with four thread-forming Torx screws (see Figure 3-38). The tolerances associated with the heat sink mounting holes and the mounting holes in the receive wall plate develop the manufacturing tolerance necessary to locate the CCA properly to enable subsequent installations. During this operation, the protective Kapton covering on the solar cell remains in place if the assembly is manual. The in-process receiver wall assembly is mounted onto a holding fixture to minimize flexing of the assembly and stressing the subsequent solder joints. The receiver wall assembly remains in this holding fixture until final installation into a chassis assembly.

Upon curing of the heat sink sealant, the copper traces on the CCA associated with the bus strip weld operation are cleaned of any residual adhesive or foreign contamination and readied for bus strip installation and soldering. The bus strips are primarily self-locating, interfacing the bore in the receiver wall plate and the copper trace on the CCA. The five long bus strips and the two short bus strips are placed into position and temporarily taped in place. The assembly is moved to a parallel gap soldering station, where each joint undergoes a computer-controlled application of heat and pressure that reflows the solder pre-soldered bus strip end and creates the series connection between the six receiver assemblies (Figure 3-39).

For manual assembly only a visual inspection and a pull test are performed on each joint, and a continuity test conducted end-to-end to verify a proper series connection has been developed. This accomplished, the terminating wires, one at each end, are hand soldered to the small bus strips, fed thru the electrical pass-thru fittings, ferrules and barrel nut on the fittings tightened, and the continuity test repeated. The receiver wall assembly is then subject to a hi-pot and continuity test and results documented. The receiver wall plate/receiver assembly is then readied for SOE bonding.

During manual assembly at this point in a controlled environment, the Kapton tape is removed from the solar cell surface and the cell surface inspected for any contamination. A forward bias test is performed on each CCA, and on the receiver wall series. Upon acceptance, the four Torx screw heads are prepared for bonding of the SOE light shield by wiping with solvent and allowing to air dry. An adequate amount of Room Temperature Vulcanizing (RTV) sealant is applied to each screw head and the light shield visually located and pressed into position. A nominal weight is applied to the light shield, and the RTV left to cure. Upon curing, the weight is removed and an optical adhesive, mixed with .003” diameter glass beads, is applied to the solar cell surface. The SOE, which has been prepared by an application of bonding primer to the cell interface surface, is placed onto the optical adhesive. Features of the SOE and receiver wall plate develop the proper alignment and rotation control of the SOE.

During manual assemble for the SOE is taped in place to retain location, and four small beads of fast setting epoxy applied to the joint between the receiver wall bore and the outside diameter of the SOE to hold it in place during curing of the optical adhesive. This step is modified for robotic assembly and the automatically dispensed UV cured adhesive is used for purpose. A subsequent bead of sealant is applied circumferentially around the outer diameter of the SOE to receiver wall joint to provide additional mechanical support, and the assembly left to cure overnight (Figure 3-40).

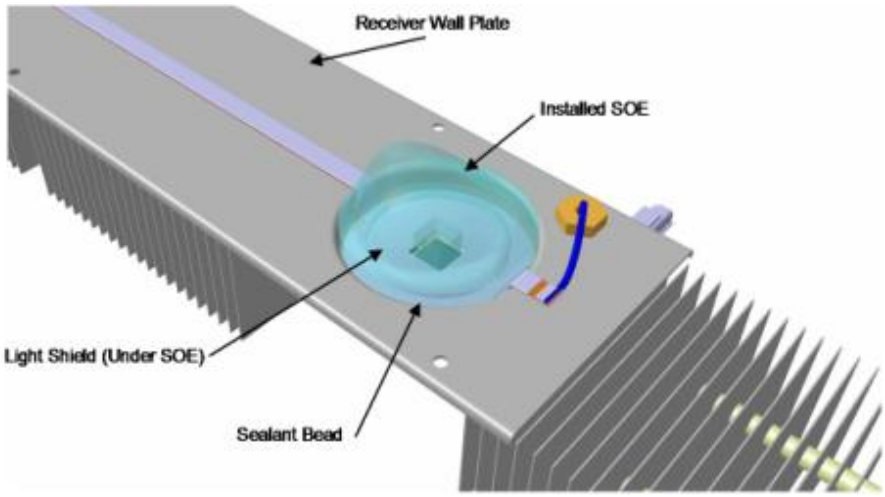

Figure 3-40. Installed SOE

Upon cure of the optical adhesive and the SOE sealant, each receiver is forward bias checked, as well as the entire series checked for both forward bias and continuity. In automatic assembly at this point a 2000 V high pot test is carried out to assure module electrical integrity. Upon acceptance, the receiver wall assembly is returned to the assembly environment, where a protective layer of aluminum tape is applied to the bus strips adjacent to the SOE, and the wires attached to the short bus strips to provide protection in the event of off-pointing during operation. The receiver wall receives a final continuity test and documentation, and upon acceptance is stocked to await subsequent installation into a chassis assembly (Figure 3-41).

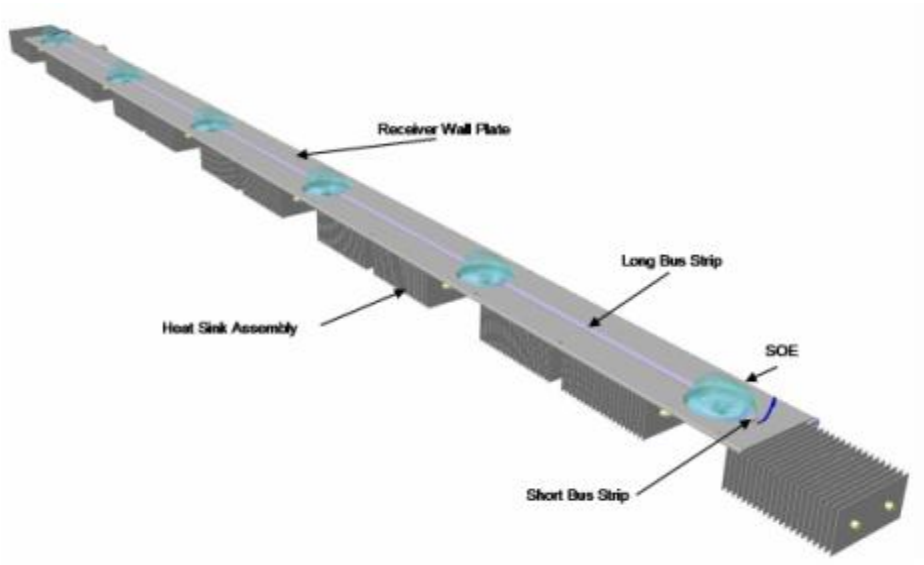

Figure 3-41. Completed receiver wall.

3.2.2.2 Module Assembly

The module assembly is comprised of two elements; the receiver wall assembly and the chassis assembly. Both the chassis assembly and the receiver wall assembly incorpo-

rate features that provide a determinant assembly environment, mitigating the requirement for tooling to develop alignment of the optical pairs (Figure 3-42).

The chassis is readied for receiver wall installation by jigging a holding fixture, and if the assembly is manual the protective tape over the receive wall penetrations is removed and the POE surfaces vacuumed. The receiver wall, still in its holding fixture, is check-fit onto the chassis assembly, and screw clearances for the twenty-two attachment fasteners verified. The receive wall assembly is removed, and the faying surfaces of both the chassis and receiver wall are prepared for sealant application by solvent wiping with isopropyl alcohol and air drying. The cleanliness of the SOEs and the surrounding area on the receiver wall then verified. A thin bead of sealant is applied to the receiver wall paying special attention to the ends of the receiver wall and screw penetrations. The receiver wall is immediately installed onto the chassis, pushed on until contact is made with all twenty-two spacers, and the receiver wall holding fixture removed. Washers and nuts are then installed onto the twenty-two chassis studs and torque applied to final specification. Excess sealant squeeze-out is removed from the receiver wall/chassis joint, and the assembly is left to cure for a minimum of 1 hour (see Figure 3-43). The module assembly receives an in-process continuity and isolation check, and is checked for an indication of voltage under the shop light environment

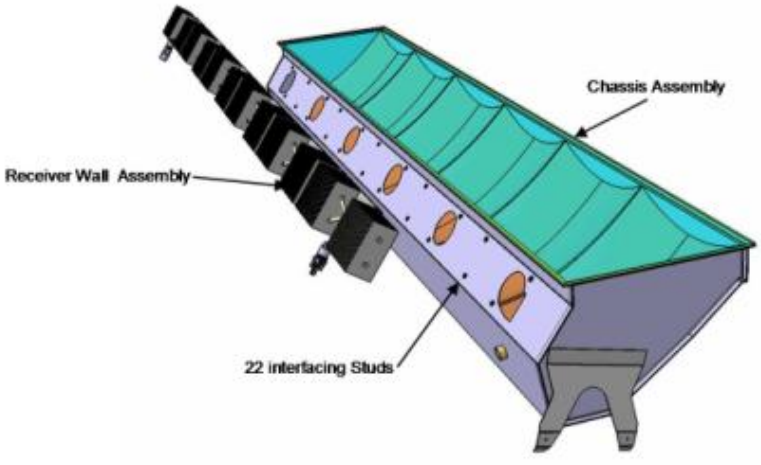

Figure 3-42. Module assembly components.

Figure 3-43. Completed Module assembly.

3.2.3 Environmental Control

3.2.3.1 Purging

The module is by design vented to the outside air (sealing would require expensive structures not compatible commercial cost requirements). Without intervention diurnal temperature changes will inevitably equilibrate atmospheric composition between the module and the environment. This will in turn lead to water condensation at night on a window surface radiatively coupled to deep space (3°K). Humidity equilibration can first be prevented by periodic module purging with dry air. A simple spreadsheet model demonstrates that a simple purging cycle will dry out a module after 4 or 5 cycles. This module will maintain its average relative humidity below 50% through a week of temperature driven exchanges with outside air even assuming a diurnal 30°C ΔT and 80% outside humidity. The reliability of dry air purging and its implementation at a plant level have been considered and are included in the capital and O&M cost models.

Auto regenerating desiccant has been employed along with purging on all POD modules. Thermodynamically a reversible desiccant should evolve water (dry out) whenever the activity of water in the desiccant is higher than the activity of water in the vapor phase. This may occur either though lowering vapor phase relative humidity or increasing the system temperature (see, for example Figure 3-44).

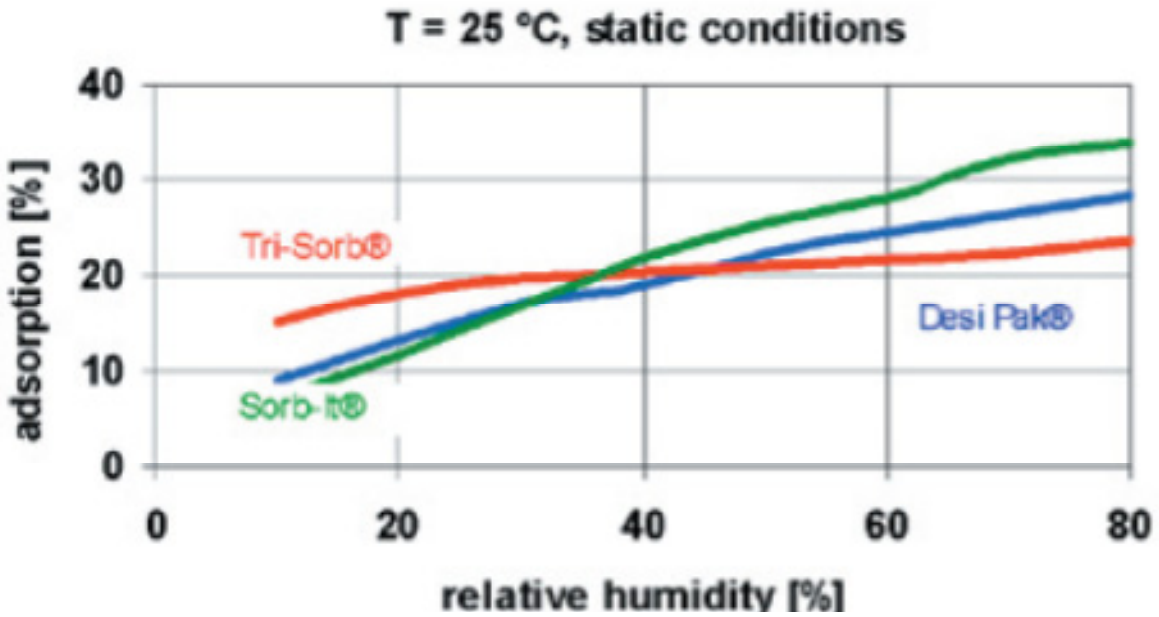

Figure 3-44. Operation of surface adsorption desiccants.

Broadly speaking desiccants function either through compound formation (e.g., hydration) or surface adsorption. Desiccation through compound formation will likely be accompanied by a significant negative free energy. Reactivation of such desiccants (when possible) requires a substantial thermal input to overcome the original energy released. Passive drying, if it occurs at all, will probably be too slow to be of value.

For our purposes surface adsorption is more likely to be passively reversible as we would expect little in the way of smaller free energy and the percent of water adsorption

would be a function of relative humidity. This effect is shown Figure 3 43. Of particular interest is the material labeled Desi Pak® which is a bentonite clay. The material operates by physical surface adsorption. The degree of adsorption is a function of relative humidity and as a natural product the material should completely stable.

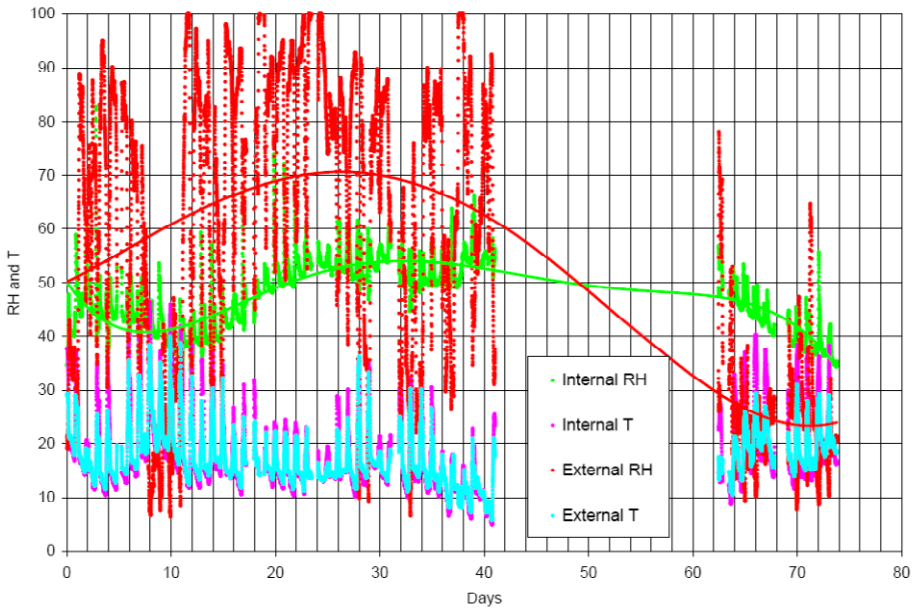

Figure 3-45. Temperature and relative humidity data for a Boeing CPV module built with self regenerating desiccant and operated without purging.

To demonstrate this desiccant we built a module with 5 packs of clay desiccant applied to the back wall of the chassis. The module is equipped with both internal humidity and temperature probes. It was mounted to a tracker and tested for two mounts through the late fall and early California winter (rainy season).

The telemetry from this module is provided in Figure 3-45. As can be seen the interior humidity of the module cycles on both an intra-day and inter-day basis as a result of diurnal temperature changes and outside weather changes. When the sun rises the RH falls as the temperature and vapor pressure of water rise. Air is expelled from the module and its water content falls. Note also that the temperature of the module during the day is usually greater than the ambient temperature which will lead to further drying. When the sun sets the internal RH does rise but typically is less than the rise in external ambient humidity.

Inter-day the internal and external humidity do track each other, however, the internal humidity is clearly buffered by the desiccant and never exceeds about 55% even during prolonged periods of high external RN (rain). No condensation of water was ever observed in this module whereas identical modules without desiccant beside it had their internal glass surfaces covered with condensed water.

3.2.3.2 Passive Desiccant

The above approach of active purging combined with internal auto regenerating desiccant has been successfully applied to the POD for more than two years of continuous

operation. However, concerns still remain with respect to the cost of the purging system (both capital and O&M). In addition, as will be discussed in Section 8.5.2 the environment control was at least partially responsible for the field deployment problem encountered in the 100 kW power plant.

As an alternative to purging, development of an environmentally self-regulating module has been carried out. The concept was to control the internal relative humidity of the module with a desiccant that self-regenerates based on diurnal temperature changes, which leads to a decrease in daylight relative humidity. The operation of such a system would involve the following principles.

- Nightly falling temperature leads to an increase in relative humidity.
- Falling temperature also leads to an increase in air density, causing an influx of air into a vented CPV module.
- By equipping the module with a desiccant, internal condensation is prevented.
- During daylight periods, rising temperature causes the desiccant to expel into the vapor phase, which, due to the natural temperature increase, is at a lower, non-condensing relative humidity.
- The moisture-laden air so formed is expelled from the module by the temperature-driven decrease in air density.

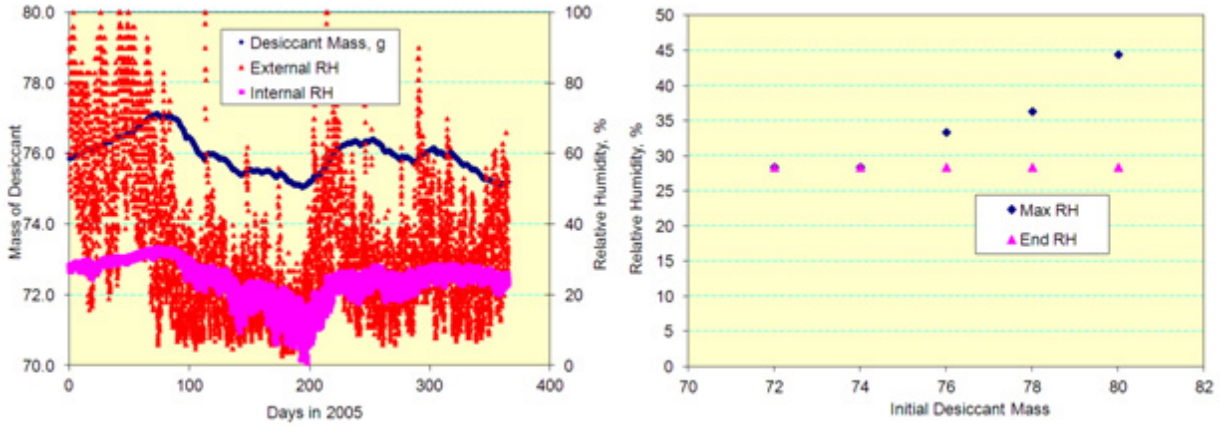

Figure 3-46. Modeling output for a passive desiccant system based on Phoenix deployment.

The concept has been subjected to a controlled engineering analysis. A model system was built using one year (2005) of Phoenix, Arizona, weather data and the critical dimensions of the POM module. The model assumed a starting dry desiccant mass of 70. All air-breathing by the model was assumed to be equilibrated with the desiccant. What this means in practice is that the module must, with the exception of the vent port, be air tight and that the vent must be coupled with a desiccant exchange column to assure intimate contact between and thus equilibration between the gas and solid phases.

Typical results for the model are provided in Figure 3-46. The left side of the figure provides a typical example assuming a starting desiccant mass of 76 g. On the right-hand side, data are presented for a range of initial desiccant masses (wetter or drier initial

desiccant). The most noteworthy feature of these data are that in all cases the final relative humidity reaches the same value, demonstrating that the system is working as expected.

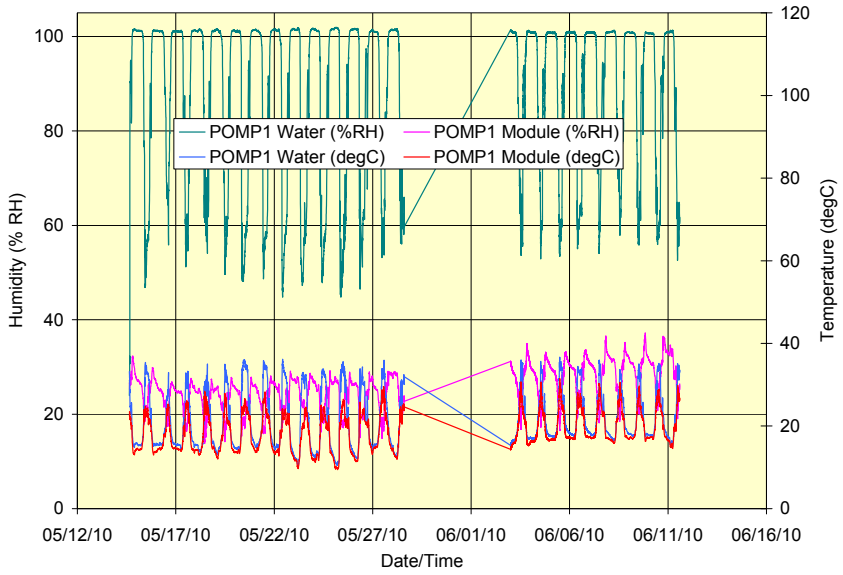

Figure 3-47. Environmentally Self-Regulating Module Demonstration.

As the final step the performance of a self-regulating module was demonstrated in a worst case test. In this demonstration, all incoming air (as a result of nighttime pressure equalization) was humidified to 100% relative humidity (RH). The desiccant drying bed was operated at ambient outside temperature, and the daytime module temperature was about 10°C above ambient temperature due to solar heating. Precision flow meters assured that the system was leak tight.

Test results shown in Figure 3-47 fully met expectations for the performance of a self-regulating module. Despite repeated injections of water-saturated air during nightly air influx, the module was able to maintain an internal relative humidity that even at night never exceeded 35% RH. It should be added that during the course of this test, the module continued to provide full electrical output.

A desiccant is selected which can reversibly exchange water with the gas phase based largely on the difference in relative humidity between the air in the module and the desiccant. Exchange may be assisted by a limited diurnal temperature differential.

The success of this worst case test led us to implement the solution of the corrective action modules described in Section 8.5.2. All modules were equipped with internal temperature and humidity probes. Data for a representative module is provided in Figure 3-48.

The module referenced in Figure 3-48 has consistently operated in the humid Seal Beach environment with a relative humidity between 20% and 40% RH. Furthermore the relative humidity of the module has consistently decreased over the 4 month period of the test. With respect to the long term life of the desiccant, it is a natural product (clay) and by design is regenerated daily in this application. Finally, it is implemented

as an external (and cheap) part of the module meaning that replacement as a matter of routine maintenance is conceivable.

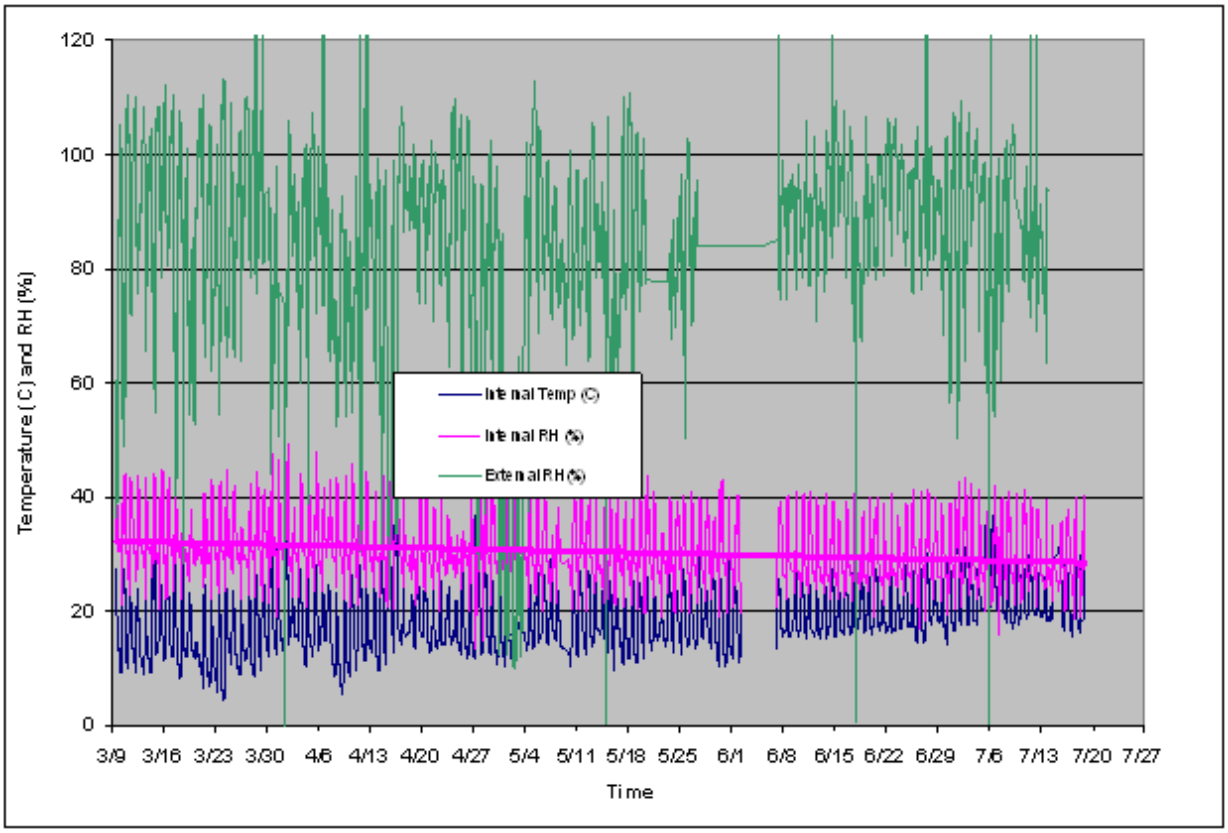

Figure 3-48. Data for module S with fully passive relative humidity control.

3.3 Array Design

3.3.1 Panel Design

The original concept for the production panel was that a completed panel would be sized such that it could be trucked from the factory to a power plant site as a completed unit and directly installed on the tracker. This led to a width limitation of 8 feet. The previous discussed 6 receiver module is dimensioned at 6 feet by 1 foot and lead to a basic panel configuration of a three module length (≈ 24 feet) and an eight module width (≈ 8 feet). Two such panels end to end cover the bed of an interstate legal truck.

The structure has been analyzed for static deflection in order to optimize the thickness of the torque tube. As shown in Figure 3-49 the basic structure exceeds our requirements for all reasonable tube thicknesses.

The thickness of the panel from the bottom of the torque tube to the top of the module is about 20”. It is thus conceivable that four to five panels could be stacked into tall Conax shipping contained and 8 to 10 transported per truck load. In fact this did not turn out to be the case for numerous detailed reasons and the most that could be shipped in the POM phase of the program were four per truck in individual shipping containers. Also it

turned out that that the shipping container width led to a wide load classification that further limited interstate transport.

Torque Tube Thickness (in)	Max. Torque Tube Defl. (in) Max. Defl. (in)		
0.087	(0.145 x 0.6)	0.175	0.229
0.116	(0.145 x 0.8)	0.151	0.201
0.145		0.137	0.185

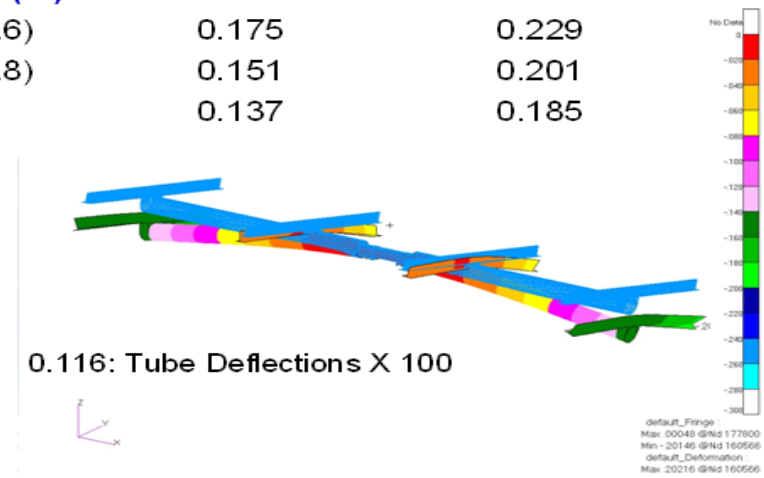

Figure 3-49. Typical structural analysis example for the static deflection of the Boeing CPV frame.

Once the modules were attached to the panel they were wired in series as shown in Figure 3-50. During the course of the contract all panels employed a purging strategy for environment control. The purging consisted of dry compressed air which, to assure uniform air flow, was ducted to the panel by equal length tubing.

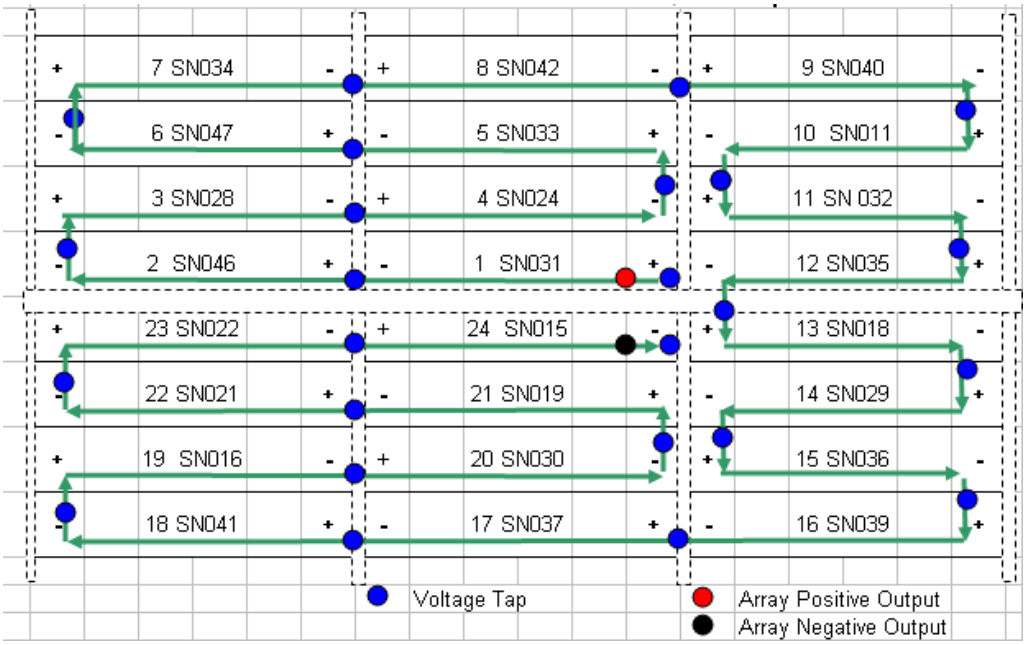

Figure 3-50. Panel wiring diagram.

3.3.2 Tracker and Software Controller Design

The initial approach taken for the tracker required for the array design was to rely on commercially available tracking systems. However, after several attempts to secure a

third party source were unsatisfactory it became apparent that there was no viable commercially available solution. Moreover, the cost and complexity of the available tracker offerings made it technically clear that a new approach was required.

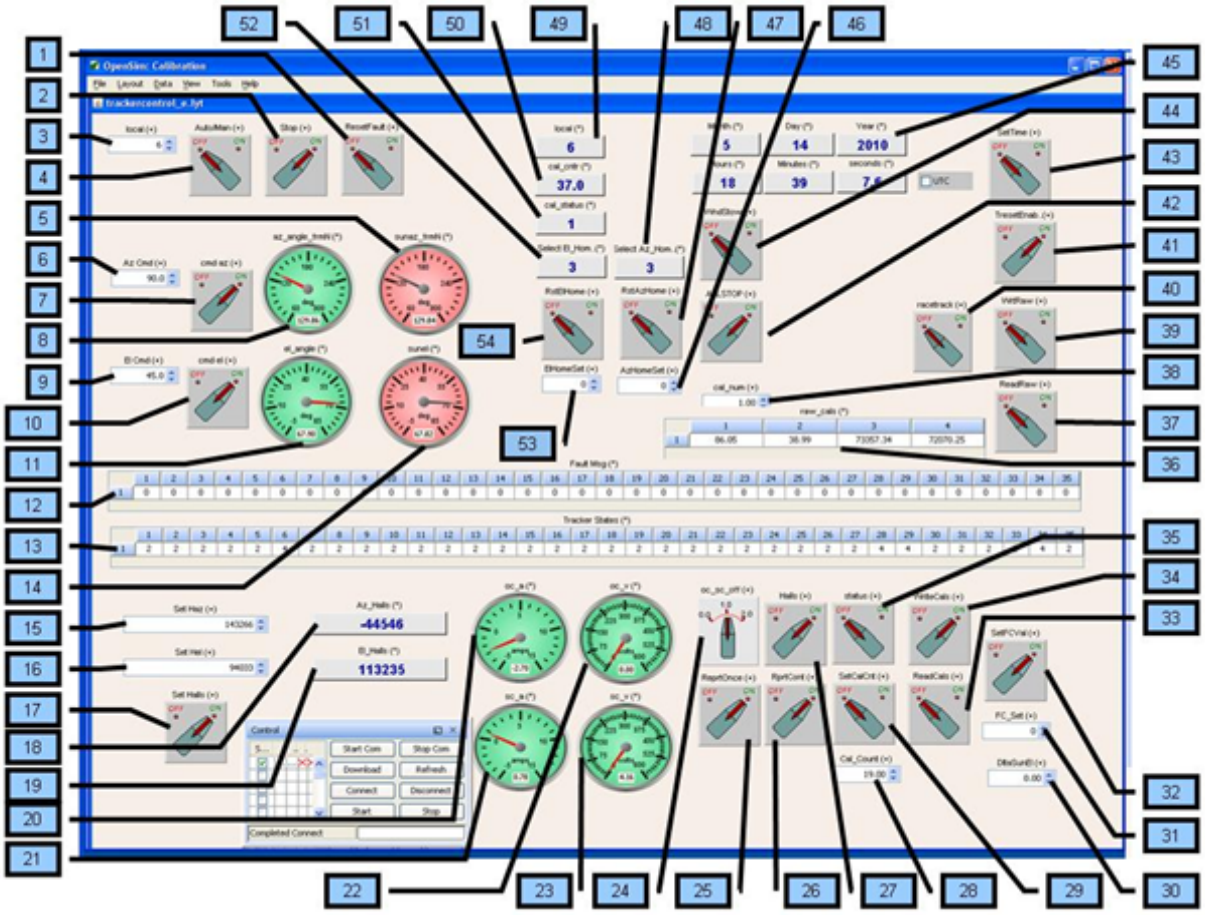

Figure 3-51. Graphic user interface screen.

Boeing augmented the team with experienced designers, controls experts, and software designers to address the tracker solution with a fresh approach.

The tracker development was one of the major success stories of the program. Prior to this point the CPV industry had been using trackers that cost between $1.25-$1.50/watt. When the price point for a commercial scale deployment is aimed at <$3.50/watt this leaves little margin for cost of modules, arrays, and balance of plant elements. Boeing felt that a design cost of less than $1.00/watt was achievable.

Boeing set out to design a tracker based on several key requirements:

1. Pointing accuracy must be less than 1°.
2. Cost must be less than $1000 based on the power output of one POD design array. This cost target was validated with our automation partner, Comau. Comau agreed that this cost target was sound based on their experience building assembly lines for Mid size truck transmissions.
3. Must be able to demonstrate life greater than 20 years.

4. Must be installed by 2 men in 30 minutes or less.
5. Control of the tracker should be as autonomous as is economical. Controller costs must be amortized over the number of tracker units controlled and added to the unit cost in item 2.

The tracker development effort was headed by a common IPT lead with assigned personnel from Design, Stress, Software, and controls. The same cost modeling tools applied to the system level costs were applied to the tracker to document the design to cost philosophy that dominated the whole program.

The tracker mechanical assembly focused on the development or identification of a slew drive component. Many unit suppliers were identified. The final selection was made with Kinematic Manufacturing Inc (KMI) being selected to provide the slew drive hardware.

The elevation drive is a linear actuator. Several design options were considered but none provided the combination of reliability and low cost of the Venture Manufacturing linear actuator.

The tracker controller system consists of a central computer which issues commands to a microcontroller located at each tracker in the field. The microcontroller responds to a set of simple commands. These include the following:

- Move tracker in azimuth.
- Move tracker in elevation.
- Report tracker status.
- Report tracker short circuit current and open voltage.
- Report tracker open circuit current and voltage.
- Report tracker position in azimuth and elevation.

These commands are used by the central computer to orchestrate the activities of tracking the sun, boresighting the arrays, and issuing manual commands desired by the operator. Boresighting an array consists of positioning the array at a point in time to maximize the short circuit current the array produces and save the estimated sun position at that time combined with the array azimuth and elevation positions at that time. Multiple boresights (>29) are then used to calibrate the array. Calibrating consists of fitting 5 parameters (representing pole tilt, azimuth offset, retracted length of the linear actuator, and angle offset of the modules) to minimize the mean error between bore sight data and a model of the tracker. Calibration needs to be performed on each tracker before it can accurately track the sun open loop as a function of time.

A graphical user interface (GUI) shown in Figure 3-51 runs on a pc that can connect to the central control computer. This GUI gives an operator the ability to easily control the entire field of solar trackers. A legend key for the GUI is provided in Table

Table 3-10. Key to GUI interface

1. Fault Reset: A switch used to reset a fault message (12) back to 0.
2. Stop: A switch to stop the current displayed tracker's motion.
3. Local: Input which tracker to show on current display.
4. Auto/Man Switch: Switches current displayed tracker from automatic mode to manual mode and vice/versa.
5. Solar Azimuth: Displays solar azimuth at current time (widget 45).
6. Azimuth Command: Inputs desired azimuth angle command. (90=east, 180=south, 270=west)
7. Azimuth Command Switch: Issues azimuth command identified in (6) to currently displayed array.
8. Azimuth Angle: Displays last reported azimuth position from current array.
9. Elevation Command: Inputs desired elevation angle command. (90=straight up, 0=point at horizon)
10. Elevation Command Switch: Issues elevation command identified in (9) to currently displayed tracker.
11. Elevation Angle Display: Displays last reported elevation angle position from current tracker.
12. Fault Message: Displays fault messages for trackers 1 through 35. See Table 1-1 for a description of fault messages.
13. Tracker States Display: Displays current states of trackers 1 through 35. See Appendix A for a description of tracker states.
14. Solar Elevation Display: Displays solar elevation angle at current time (widget 45).
15. Set Azimuth Hall: Sets Azimuth Hall count to be sent to current tracker.
16. Set Elevation Hall: Sets Elevation Hall count to be sent to current tracker.
17. Set Halls: Issues azimuth and elevation hall counts to the current tracker.

18. Azimuth Hall Value: Displays last reported azimuth hall count from the current tracker.

19. Elevation Hall Value: Displays the last reported elevation hall count from the current tracker.

20. Open circuit amps: Displays the last reported open circuit amperage of the current tracker's array.

21. Short circuit amps: Displays the last reported short circuit amperage of the current tracker's array.

22. Open circuit voltage: Displays the last reported open circuit voltage of the current tracker's array.

23. Short circuit voltage: Displays the last reported open circuit current of the current tracker's array.

24. Current/Voltage Report Switch: Chooses between reports returning open circuit (oc), closed circuit (sc) or no current voltage data.

25. Report Once Switch: Issue a request for a one-time report of current voltage and hall counts chosen by (24) and (27). Only active when tracker is in manual mode (tracker state 2).

26. Report Continuous Switch: Issue a request for continuous reporting of current/voltage/hall counts (as chosen by (24) and (27)). Only operative when tracker is in manual mode (tracker state 2).

27. Hall Count Switch: Choose whether hall counts are included in report once or report continuous commands (see (25) and (26)).

28. Cal Count Input: Chooses how many successful boresights to manually set the current tracker to. This value will replace whatever the current boresight counter is when the set cal count switch (29) is activated.

29. Set Cal Count Switch: When activated the current value in (28) replaces the boresight counter.

30. Delta Sun Elevation: Input that immediately adds to the current sun elevation as calculated by the solar ephemeris algorithm in the code (in degrees).

31. FC Value: Value to set the tracker Fully Calibrated flag to when the Set FC Value Switch(32) is activated. Should only be set to either 1 or 0.

32. Set FC Value Switch: Command to replace the Fully Calibrated flag of the current tracker with the value in FC Value (31).

33. Read Cals Switch: When activated the software will read the last written Calibration Data File for the current selected local tracker from the hard drive and replace the existing calibration data with the data in the Calibration Data File.

34. Write Cals Switch: When activated the software will write the existing calibration data for the current selected local tracker to a file on the central controller hard drive.

35. Status Switch: TBD.

36. Boresight Data: Data from a boresight number equal to the value in cal_num(38). The solar azimuth and elevation, and the raw azimuth and elevation hall counts calculated to point the array optimally to that solar az, el. Data is for the current selected tracker.

37. Read Raw Switch: When activated the central software will read the last written boresight data file for the current selected tracker. The data will overwrite any raw boresight data in the central software.

38. Cal Number Value: This value is used to choose which raw boresight data is displayed in (36).

39. Write Raw Switch: When activated the central software will write all the current boresights for the selected tracker to the central controller hard drive.

40. Racetrack Switch: When activated while the current selected tracker is in manual mode (tracker state 2) the tracker will track the mode with constantly changing offsets between -4 to +4 deg. The pattern will repeat every 2 hours.

41. Time Reset Enable: When off, the central controller will not update it's time every hour. When on, the central controller will reset it's time every hour using a GPS receiver.

42. All Stop Switch: When activated, this switch will stop all trackers' motion.

43. Set Time Switch: When activated (and Time Reset enable (41) is on), this switch will reset the central controller time.

44. Windstow Command: When this switch is on all trackers will windstow.

45. Time and Date Display: This displays the central controller time reference in UTC time.

46. Az Home Set: Value to set Azimuth Homed flag to when Reset Az Home (47) is activated. This value should no other value than 0,1,2 or 3. A 0 will force the tracker to not move in azimuth until the sun is detected. If set to 0, the fully calibrated value should be set to 0 also before setting the tracker to automatic mode.

47. Reset Az Home: Switch that, when activated, sets the Azimuth Homed flag to the value in Az Home Set (46).

48. Select Az Home: Display of current tracker's Azimuth Homed Flag value.

49. Local: Display of current tracker local id.

50. Cal Counter: Display of number of successful boresights the current selected tracker has.

51. Cal Status: Display of the Fully Calibrated Flag value for the current selected tracker.

52. Select El Home: Display of current tracker's Elevation Homed Flag value.

53. El Home Set: Value to set Elevation Homed flag to when Reset El Home (54) is activated. This value should only be set to 0, 1, 2, or 3. A 0 will force the tracker to perform an elevation homing maneuver. If set to 0, the fully calibrated value should be set to 0 before setting the tracker to automatic mode.

54. Reset El Home: Switch that sets the Elevation Homed Flag to the value in El Home Set (53).

The tracker and control software were both validated by loads tests and acceptance angle measurements. The first major validation occurred when POD array (see Section 7) was mounted on the KV tracker after approximately 6 months of testing an Inspira tracker. As demonstrated in Figure 3-52. There is no change in performance.

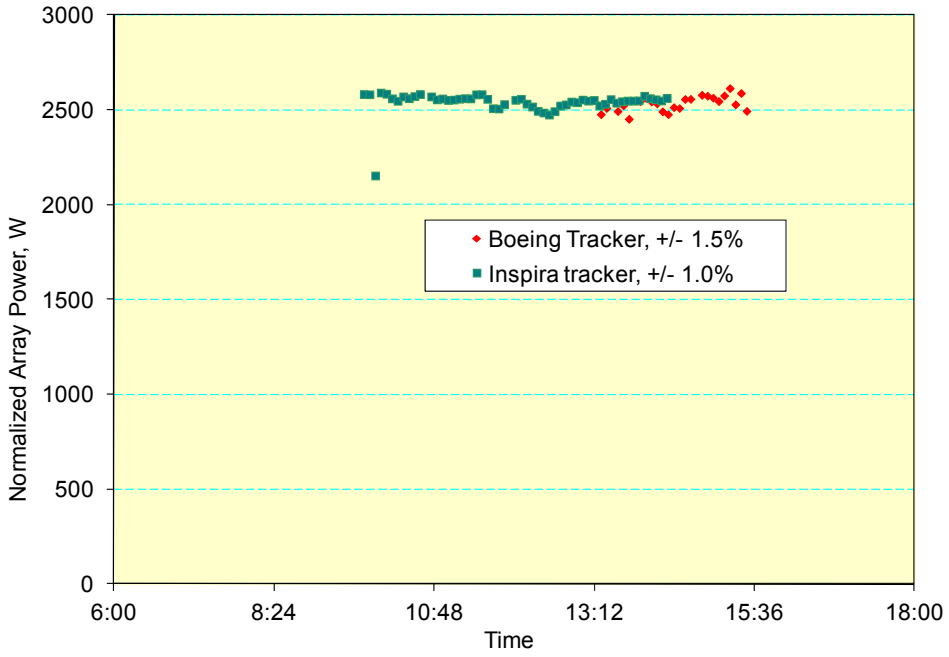

Figure 3-52. Performance of the POD array Inspira and KV trackers.

3.3.3 Lessons Learned - CPV Design

This section describes some important lessons learned in the course of the program.

Hardware Quality Control – This product relies on determinant assembly (self tooling) and any deviation in tolerance or configuration has an effect not only on the offending part but also on any subsequent assembly. Three components within the design exhibited conditions which are directly related to module performance: the sheet metal receiver wall plate, the sheet metal chassis assembly, and the SOE. The design relies on the sheet metal assemblies for sealing, alignment, and structural stability. The two sheet metal components received in support of this activity required rework to bring them to drawing specification, and in a few occurrences were accepted as-is and incorporated into the assembly. While the system was able to perform, some level of performance was lost to offending hardware. Lesson Learned: Source inspection of hardware and first article acceptance should be incorporated into the procurement process.

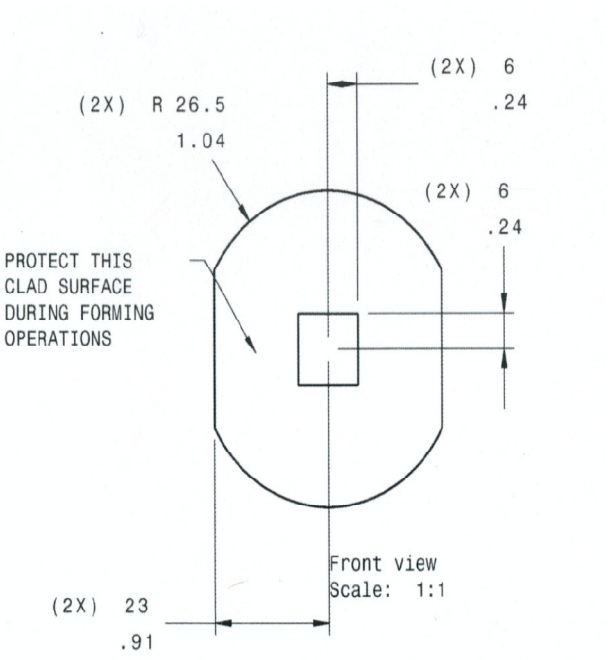

Figure 3-53. Light Shield for protecting the CCA during off-pointing

Light Shielding – The light shield is a thin aluminum disk with a central square hole shown in Figure 3-53 which was intended to render harmless and scattered concentrated sunlight. It was learned by early failures in the development of the module that concentrated sunlight during off-pointing can impact the CCA adjacent to the kaleidoscope, damage the CCA and contaminate the lower SOE surface leading to cracking of the SOE. The light shield deployed between the bottom surface of the SOE and the CCA has been 100% effective in stopping and is covered in a patent application.

Sealing – A second early development lesson was the need to rigorously exclude liquid water from the interior of the module. This is critical in the area of the CCA where the ~ 3V potential of cell can, in the presence of condensed water, lead to electrochemical processes between the cell and adjacent conductive surfaces and between the junctions of the cell. Conformal coating somewhat impedes this, but the front surface mirror even with a outer protective layer is also water sensitive. This module enclosure is leak tight except for vents were the moisture is controlled (see Section 3.2.3)

Material Handling – The current module design is very robust in its assembled configuration; however the subassemblies are not as robust. The receiver wall assembly, for example, is prone to flexing as a subassembly if not supported properly. This flexing can result in over-stressing of solder joints, degradation of optical bond lines, and deformation of the receiver wall sealing surfaces. These conditions presented themselves

early in the prototype manufacture and were mitigated largely through use of handling fixtures and proper training.

Assembly Alignment – The assemblies are much more robust and stiffer than the individual parts. As an example, the chassis assembly, containing the POE's, sheet metal chassis, and window, had to be restrained and planar during installation or misalignment of the POEs to their local reference datum would result. It was noted that prior to window installation the chassis/POE subassembly was dynamic, and if not held planar during window installation would retain an out-of-alignment condition.

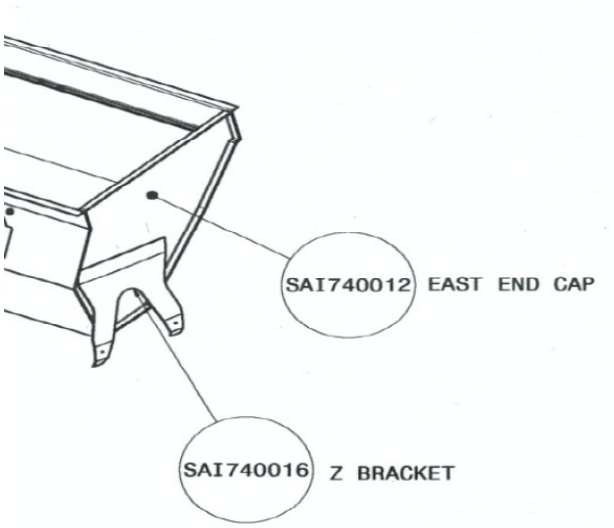

Figure 3-54. Z Bracket attached to the end of the chassis

Detail Retention – The design of the POE is such that of three tabs used for attachment to the sheet metal chassis only one is designed to be auto-retained. Injection mold release considerations and design necessity lead to this condition. In operation, the POEs were found to be moving within the assembly. We incorporated a fix by bonding all three tabs to the chassis with fast curing epoxy during installation. No further dynamic misalignment was observed.

Chassis Assembly Stiffness – The chassis assembly without the cover glass is an open box and inherently is not stiff in torsion along the long axis. Since the POEs are directly coupled to the chassis, any flexing of the chassis affects POE/SOE alignment. A major component of the stiffness of the module is the cover glass and the associated bonding adhesive. The cover glass has to be coupled to the chassis with as near a non-compliant adhesive (read high shore hardness) as can be practical to transmit shear loading efficiently through the cover glass to provide stability in torsion.

Solder Reflow – The series connection relies on a reflow solder joint at each end of each bus strip. The connection is made with a parallel gap soldering process, and is accomplished in-situ within the receiver wall assembly. During the early development stages, solder failures plagued nearly other module. By way of physical analysis it was determined that improper controls were levied on the soldering process and more development was in order. A stand-down of fabrication was conducted and a soldering development action was established. The main findings were improper surface preparation, improper tinning, inadequate heat during weld cycle, and inadequate weld cycle time. Further actions were taken with production of test articles and documentation of anomaly and failure conditions. The result of the process development was that surface preparation, tinning and electrode cleanliness were the suspects. Processes were developed for each, and consistent success in soldering was the result.

Process control to eliminate foreign substances as well as pre-solder cleaning must be employed, minimal tinning of the bus strips must be practiced, and welder electrodes must be cleaned periodically (after about every twelve joints) when used in an uncontrolled shop environment.

3.3.4 Panel

Trucking – As mentioned, the manufacturing strategy implemented in this program was to assemble a deployable panel in the automated factory environment. The non-imaging panel design, however, does not efficiently ship. Furthermore, advanced cost studies (see Section 0) show that larger panels have real cost advantages. This conclusion is at least inferentially confirmed for flat panel PV where panel assembly is carried out in the field.

Vibration – The Z Bracket which joins the chassis to the frame (see Figure 3-54) was intended to provide a compliant mount between a less determinant frame and a more determinant chassis. With this bracket, substantial tolerance relaxation can be allowed in the frame and compensated for by precise location of the chassis during the attachment (spot weld) of the chassis to the frame. However, we discovered during transportation that the Z Bracket can act as a turning fork and destructively vibrate. One panel, in fact arrived at the deployment site with loose modules. This problem was solved by use of vibration dampers during transportation.

Four Point Mount – The rationale for the four point mount is to assure alignment of the six receivers. However, with the rigid chassis the only degree of freedom in the chassis location is rotation about the long axis of the chassis. This could as well be solved with a three point mount which would facilitate mounting as it could do away with overlapping spot welds.

4 System Engineering – SOPO Tasks 1.7, 2.7, 3.7

Task Objectives

The objectives of this task were;

- Coordinate all engineering activities, including supplier interface;
- Manage trade study process to establish optimum system design;
- Conduct reliability analysis of the overall system, including each sub-element, d) identify low reliability components and work with design engineering to achieve reliability goals;
- Perform failure modes and effects analysis;
- Maintain detailed system cost model and establish and manage design to cost (DTC) targets;
- Plan POC/POD/POM installation and testing activities (including site surveys, facilities coordination, utility interfacing, etc.).

Highlights

- System availability projected at 99.93%, in excess of the 99.9% requirement.
- A reliability model has been developed to allow maintenance cost projections of the life of the power plant once individual equipment life estimates are available.
- LCOE projections at less than $0.15 per kWh for the 2010 POM design.
- Path to an LCOE ≈$0.07 per kWh developed for large scale deployments in the 2015 time frame.
- Performance and cost estimates indicate the projected LCOE is less than $0.15/kWh with high confidence for the current configuration with a realistic path to $0.070/kWh based on evolving technology and increasing production rates. This estimate has been independently validated by Navigant (the DOE auditor, See Appendix A), McKinzie Consulting and Magna.
- Enabling technology demonstrated for the 2015 objective based on injection molded plastic chassis combined with a modularized field replace receiver assembly manufactured with low cost automatic equipment.

Table 4-1. System Engineering Stage Gate Criteria

Period	Criterion	Results
	1d-1) Projected system availability > 99.9% in 2010	Requirement exceeded, ~99.93% analytically demonstrated.
	1f-1) Projected LCOE < $0.15/kWh in 2010. LCOE calculations will show POC demonstrated results for all targeted TIOS and particularly for stage-	1f-1) Projected LCOE < $0.15/kWh in 2010. LCOE calculations will show POC demonstrated results for all targeted TIOS and particularly for

Period	Criterion	Results
	gate #1 CSFs.	stage-gate #1 CSFs.
2	2d-1) Projected LCOE < $0.15/kWh in 2010. LCOE calculations will show POD demonstrated results for all targeted TIOS and particularly for stage-gate #2 CSFs	2d-1) Projected LCOE < $0.15/kWh in 2010. LCOE calculations will show POD demonstrated results for all targeted TIOS and particularly for stage-gate #2 CSFs.
3	3c-1) Projected system availability > 99.9% in 2010	Requirement exceeded, ~99.93% analytically demonstrated.
	3e-1) Projected LCOE < $0.15/kWh in 2010. LCOE calculations will show POM demonstrated results for all targeted TIOS and particularly for stage-gate #3 CSFs.	3e-1) Projected LCOE < $0.15/kWh in 2010. LCOE calculations will show POM demonstrated results for all targeted TIOS and particularly for stage-gate #3 CSFs.

Technical Accomplishments

4.1 System Availability

The TPP FOA listed "System Availability" as a Key Performance Parameter. Boeing's proposal offered "Proposed System Availability – A_O" of greater than 99.9% in 2010 and greater than 99.95% in 2015. The FOA provides the definition:

> "System availability is the time the system is available to produce kWhrs when the resource is available."

This definition is consistent with IEEE Std 762-2006, which provides standard definitions for use in reporting electric generating unit reliability, availability, and productivity. This standard provides the definition:

> "The available state is where a unit is capable of providing service, regardless of whether it is actually in service and regardless of the capacity level that can be provided."

We completed an analysis of system availability during Budget Period 1 demonstrating compliance with the requirement.

The solar power plant system will be unavailable with respect to producing any power when the sun is available, only when certain critical elements fail or when the output of the power plant is voluntarily curtailed by management.

The large number of solar arrays, inverters, and other supporting equipment connected in parallel makes the overall power plant essentially immune to failures of individual such equipment or even many simultaneous failures. Thus, most of the power plant does not contribute to unavailability. Any failures in the solar field will manifest themselves as a graceful degradation of power output, not a loss of availability. Similarly, the

system is not vulnerable to central control failures because each tracker normally operates in an autonomous tracking mode.

A single-point series failure occurs with:

- Loss of any part of the generation interconnect transmission line (gen-tie);
- Failure of the primary transmission interconnect transformer (the on-site substation high-voltage step-up transformer);
- Failure of various other components of the transmission interconnect substation;

Voluntary curtailment by plant operators (management) while insolation is available is also charged against availability. Significant events that would be expected to require such curtailment include:

- Placing the solar arrays into a safe state in anticipation of potentially hazardous environmental conditions (e.g., high wind or high temperature);
- When maintenance of a single-point series component occurs (e.g., the transmission interconnect transformer)

Note that rain would generally not result in voluntary curtailment. Since rain is not damaging, the system would continue to be operated until there is no DNI worth using. Since lack of the solar resource does not lead to loss of availability, the frequency of rain need not be analyzed.

4.1.1 Voluntary Curtailment

Specification SAI_SP130001A, the system requirements document, stipulates that the arrays must be fully operational up to 12 m/s and must be capable transitioning to a safe position at any wind speed up to 15 m/s. This latter requirement thus sets the lower bound for wind-induced curtailment. Wind-induced curtailment results in a hit to availability only during daylight hours.

Figure 4-1 shows the cumulative probability and probability density functions for daylight wind with Phoenix TMY2 data. The numerical value of the probability of daylight wind exceeding the 15 m/s threshold in any one-hour period is 0.04%. The maximum daylight wind speed in the Phoenix TMY2 data set is 16.5 m/s.

A similar analysis can be performed for ambient temperature. Figure 4-2 shows the cumulative probability and probability density functions for ambient temperature in Phoenix TMY2 data. Specification SAI_SP130001A stipulates that the arrays must be fully operational to at least +50°C. The maximum temperature in the Phoenix TMY2 data set is +46.1°C. Since the Phoenix TMY2 ambient temperature record never exceeds +50°C, voluntary curtailment to protect against thermal extremes never happens. The probability is 0.00%.

4.1.2 Forced Outages

The reliability of large power transformers is considered “poor” with a probability of failure of about ~1% per year. Assuming one week to perform emergency service on the transformer (or to bypass it with a temporary unit) requires a transformer service contract. The contribution of this failure mode is thus 1 week/event X 0.01 event/year or 0.02% per year.

For the purposes of this analysis, it was assumed that the project-owned gen-tie would be significantly more available than the interconnect transformer since wires, insulators, and poles are significantly more reliable than transformers and are faster to repair. The actual reliability will, of course, be a function of the length of the gen-tie – a parameter outside the scope of the power plant system design project. For the purposes of this analysis, the contribution of the gen-tie is taken to be probabilistic noise

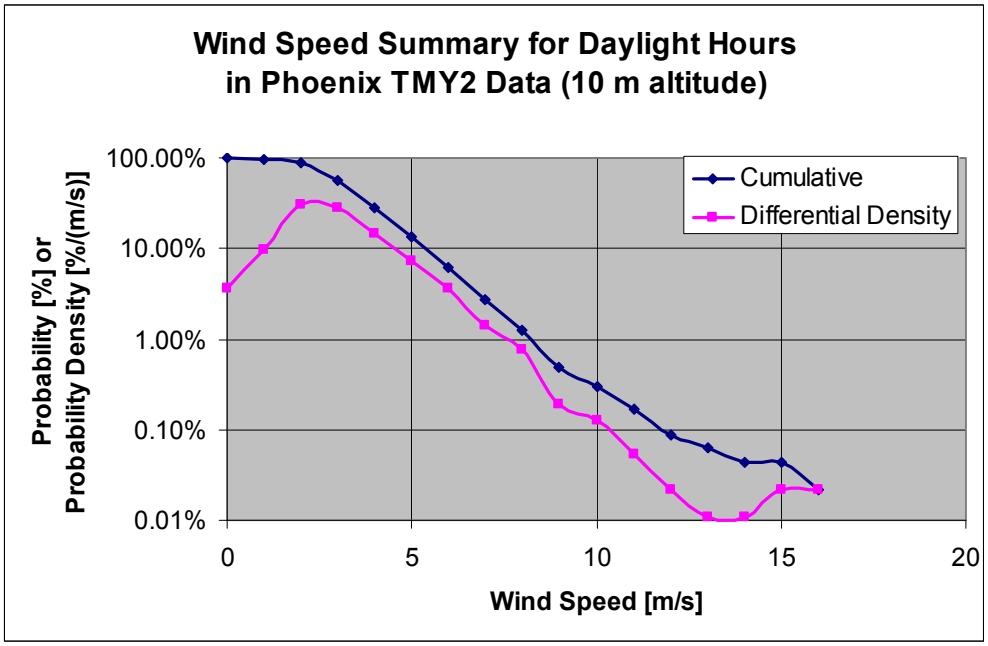

Figure 4-1. Wind Speed Summary for Phoenix TMY2 Daylight Hours.

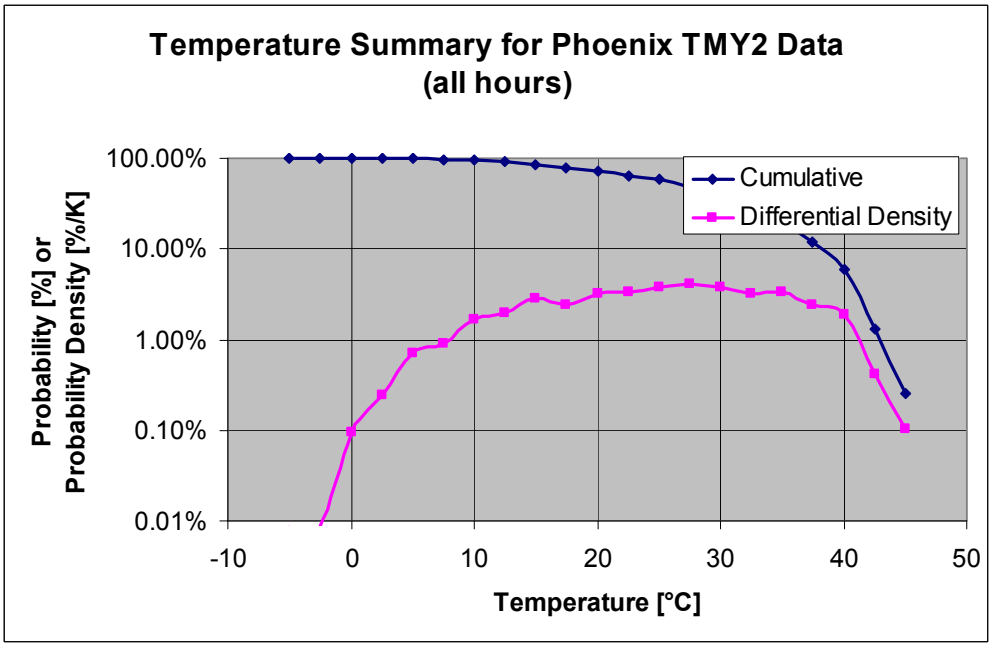

Figure 4-2. Ambient Temperature Summary for Phoenix TMY2 Daylight Hours.

4.1.3 Critical Maintenance

To avoid losing availability due to transmission interconnect substation maintenance, we have assumed that any required main transformer service would take two work-weeks plus the loss of generation during the intervening weekend. Clearly, any such preventive maintenance work would be scheduled during winter. The lost revenue from during such a period would be about $200k (20 MW, 5.5 hr/day typical average insolation Nov.-Feb., 12 days, $0.15/kWh base, 1.00 effective Time-of-Delivery allocation). To avoid this loss of revenue, a temporary bypass transformer is assumed during this time. As a result of this revenue loss avoidance, higher availability is obtained as a "free" by-product. This shows a solution based on improving LCOE, not driven by availability factor.

The reduction to availability associated with this operation is then the time required to deenergize the system to install the bypass transformer and reenergize, followed by reversing this action (after the service has been completed). This activity is expected to take about 1.5 hr for each step and this service would be performed once every 5 years. Thus, the contribution of this maintenance activity to unavailability is about 0.01%.

4.1.4 Availability Factor for Phoenix

Taking into account all the above factors, we have:

- 0.04% probability of voluntary curtailment for high winds
- 0.00% probability of voluntary curtailment for high ambient temperature
- 0.02% probability of grid-interconnect transformer failure
- 0.01% probability of voluntary curtailment for interconnect transformer maintenance activities

The net of these contributions is an Availability Factor of ~99.93%. This figures exceed the 2010 goal of 99.9%.

4.2 Reliability Model

4.2.1 Tools

The tools listed in Table 4-2 form the basis for RM&SH analyses for the TPP Program. These tools perform the mathematical or statistical assessment of the data. These form the basis for design requirements imposed on suppliers and/or for product managers on the program to use as a part of selection criteria.

Table 4-2. SAI Reliability and Maintainability Standard Tools.

Tool	Platform	Usage
RELEX™	PC	R&M Predictions, Reliability Block Diagrams, Failure Modes and Effects Analysis
EXCEL™	PC	Unique Modeling – Allocations
WEIBULL++™	PC	Field Data analysis
MILESTONES PRO 2006™	PC	Task and Schedule

The Boeing RM&SH analyses and assessments utilize the RELEX™ Reliability tool for general reliability assessments. This tool provides an integrated database for the following efforts:

- Reliability predictions;

- Maintainability predictions;
- Failure modes effects analysis (FMEA);
- Reliability block diagrams.

In addition, the tool has an import/export capability that, by using a common reporting status from suppliers, allows small firms to provide data in a predefined format that can be used to roll up the overall data at the system level from all of the primary sources.

4.2.2 Statistical Distributions

The analytical approach for reliability analyses starts with using appropriate statistical distributions to characterize the number of maintenance events expected each year (which are then translated to man-hours charged to the operations and maintenance cost lines). The following are examples illustrating the assumed distributions unless data or research suggest or dictate otherwise. All of the distributions share a common set of assumptions that are derived from general experience of failure distributions from a wide variety of products across many industries. These are:

- For electronic parts, a Weibull distribution is used, with a default of β=1 and γ =0 (β and γ defined below) except where field data or other data suggest otherwise.
- For mechanical parts, a normal distribution is used, with coefficient of variation (defined below) ranging from 0.01 for strength of metals to 0.2 for specific mechanisms.
- Failures are assumed to be memoryless (prior events do not affect future events)

Reliability analyses are an integrated and iterative element in the design process, beginning with concept definition, ensuring that reliability is an attribute of design, and that the reliability design requirements and O&M requirements are consistent with the predicted LCOE. The analyses principally use the two mathematical models described below.

4.2.2.1 Weibull Distribution

The Weibull form is generally applied to electronic parts (such as ICs, resistors and capacitors), circuit cards and assemblies that have relatively constant hazard rates. The Weibull distribution with variables characteristic life η (MTBF) and β (slope factor) provides a general characterization of the reliability of the device. For systems where there is no effort to identify the root cause of the failures or to modify the circuit to remove the source of the failure the Weibull can represent the exponential distribution with parameters of β=1 and γ=0. The default form of the distribution yields the probability distribution function (pdf):

$$f(t) = \frac{\beta}{\eta}\left(\frac{x-\gamma}{\eta}\right)^{\beta-1} e^{\left[-\left(\frac{x-\gamma}{\eta}\right)^{\beta}\right]}$$

where β is the slope characteristic of the population, x is the point of interest (time) for the assessment and γ is the characteristic life (mean) of the population. The cumulative distribution function (CDF) is:

$$F(t) = 1 - e^{\left[-\left(\frac{x}{\eta}\right)^{\beta}\right]} = 1 - R(x)$$

For most electronics, the β values range from 1 to 2. Assemblies are generally higher (3+) while items such as high stress equipment can range up to 5. A value of β=1 results in an exponential distribution.

4.2.2.2 Normal Distribution

All mechanical items such as relays, mechanical joints, solder joints, gears and motors are modeled as normally distributed. The general form of the PDF is

$$f(t) = \frac{1}{\sigma\sqrt{2\pi}} e^{\left(\frac{x-\mu}{2\sigma^2}\right)^2}$$

and the CDF is

$$F(t) = \frac{1}{\sigma\sqrt{2\pi}} \int_0^x e^{\left(\frac{x-\mu}{2\sigma^2}\right)^2} dx$$

The coefficient of variation is defined as the ratio (σ/μ). The following values of coefficient of variation are used unless supplier or field data provide otherwise:

- 0.01 – used on such items as structural elements or where metals are extensively used with consistent alloys across the system
- 0.05 – used on items with continuous use or that are subject to steady loads
- 0.1 to 0.2 – used on items with lower duty cycles or that are subject to wider variation of loads

4.2.3 Serial Maintenance

In a long life system such as the subject solar power plant, many units will be repaired or replaced over the life of the system. For equipment that is maintained so as to be approximately continuously in service, each nominal unit (e.g., the tracker at location #438) might experience a series of such repairs or replacements. We may call such a series of events “serial maintenance”.

The probability that a single unit out of a population of repairable or replaceable units will fail and need to be repaired or replaced depends on the installation history of that unit or unit’s function (e.g., the tracker at location #438 might be initially tracker S/N 1037 but be repaired in year 3 and then replaced by S/N 2285 in year 8). If the probability of each failure mode is described by a probability function that is not a constant-rate function (e.g., normal or Weibull), then a statistical approach must consider the probability that a subject unit might have failed and then been returned to nominal operation at any time since the power plant was initially placed into service.

This problem can be solved by a summation of conditional probabilities. The probability that a unit will fail depends on how long it has been in service and when it was placed into service – something only known probabilistically. For a given unit, it will not be known exactly how long it has been in service. The unit might have been in service since t_0 or replaced last year (t_{n-1}), or replaced sometime between t_0 and t_{n-1}. A unit

placed in service at t_x ($t_0 \leq t_x \leq t_{n-1}$) will have some probability that it survived until now and is thus the specific unit being evaluated. The summation of the probabilities that each candidate unit survived from its time of being placed into service as a unit occupying the place (role) of the unit in question is 1.0 – exactly one of the units that was placed in service for this unit's role is the one that is currently the Unit in question.

A unit placed into service at time t=n with in-service probability ps(n) will fail during the time interval of interest with the probability described by integrating the hazard function (either a normal or Weibull distribution) from t=x-1 (since the unit must have survived to the beginning of this time period to be of interest) to t=x (the end of the period of interest). The sum of all such probabilities (i.e., the sum over all possible in-service times) is the total probability of needing to replace a unit in the time period of interest.

This approach has been implemented in the Excel numerical model described in the next section.

4.2.4 Numerical Model and Results

The serial maintenance probability model described in the previous section was implemented as a Visual Basic macro in Excel. The parameters driving this model are captured in a spreadsheet organized according to a WBS that matches the cost modeling activity. An example of the reliability parameters section is shown in Table 4-3, specifically for the inverter. An example of the maintenance parameters section is shown in Table 4-4, again for the inverter. As can be seen in the inverter rollup, WBS 4.3 of Table 4-3, the expected operational lifetime for the given parameters is about 6 years, shorter and more conservative than the 10-year minimum warranty expected for the inverter. Table 4-3 also clearly indicates the use of different distributions for different subassemblies and components. Table 4-4 captures current best estimates of how much effort is required to perform each type of repair operation.

Table 4-3. Example Reliability Model Parameters (for Inverter).

System Configuration					Reliability Parameters													
					Failure Rate						Failure Probability Distribution			Operational Regime				
WBS	Repairable Assy (Repair Assy can be an R&R or RIP)	Qty/Assm	Parent Quantity	Total Quantity	Dominant Failure Mode	Mean Failure Rate, Elements	Mean Failure Rate, Rollup	Effective MTBF	Rollup MTBF, Nominal	Data Source	Distribution	σ (Normalized)	α	Nominal Annual Operation	Duty Cycle	Actual Annual Operation	Expected Operational Lifetime
					FMD 93/95	[event / Mhr]	[event / Mhr]	[hr]	[hr]					[hr/yr]		[hr/yr]	[yr]
4.3	Inverter	96	1	96			39.6		25253					4292	100%	4292	6
4.3.1	Equipment	1	96	96			39.6		25253					4292	100%	4292	6
4.3.1.1	Power	1	96	96			17.5		57143					4292	100%	4292	13
4.3.1.1.1	IGBT Drive Board	1	96	96	FTO	2.5		400000		EE	Norm	0.2		4292	100%	4292	93
4.3.1.1.2	IGBT	6	96	576	FTO	2		500000		EE	Weib		1.50	4292	100%	4292	116
4.3.1.1.3	Main Transformer	1	96	96	OC	1		1000000		EE	Norm	0.2		4292	100%	4292	233
4.3.1.1.4	Line Filter Inductor	3	96	288	OC	0.5		2000000		EE	Norm	0.2		4292	100%	4292	466
4.3.1.1.5	Main Contactor	1	96	96	OC/SC	0.5		2000000		EE	Norm	0.2		4292	100%	4292	466
4.3.1.2	Control	1	96	96			9.5		105263					4292	100%	4292	25
4.3.1.2.1	Main CCA	1	96	96	OC/SC	1.5		666667		EE	Weib		1.50	4292	100%	4292	155
4.3.1.2.2	cPCI 3U CPU Board	1	96	96	FTO	1.5		666667		EE	Weib		1.50	4292	100%	4292	155
4.3.1.2.3	cPCI 3U Power Board	1	96	96	FTO	2.5		400000		EE	Weib		1.50	4292	100%	4292	93
4.3.1.2.4	cPCI 3U Backplane	1	96	96	FTO	0.5		2000000		EE	Weib		1.50	4292	100%	4292	466
4.3.1.2.5	Front Panel Interface	1	96	96	FTO	1		1000000		EE	Weib		1.50	4292	100%	4292	233
4.3.1.2.6	Internal Control Power Supply	1	96	96	FTO	2.5		400000		EE	Weib		1.50	4292	100%	4292	93
4.3.1.3	Mechanical	1	96	96			12.6		79365					4292	100%	4292	18
4.3.1.3.1	Cooling Fan	2	96	192	No Output	5		200000		EE	Norm	0.2		4292	100%	4292	47
4.3.1.3.2	Fan Filter	1	96	96	Clogged	2		500000		EE	Norm	0.2		4292	100%	4292	116
4.3.1.3.3	Mech/Electrical	1	96	96	OC	0.5		2000000		EE	Norm	0.2		4292	100%	4292	466
4.3.1.3.4	Wire Harness	1	96	96	Frayed, Cut, degrad	0.1		10000000		EE	Norm	0.2		4292	100%	4292	2330

Figure 4-3 and Figure 4-4 show the primary outputs of the Excel-based model. Table 4-4 provides a summary of the time history of annual service events and required labor hours. To judge the real effects on LCOE, Figure 4-3 also shows the discounted rela-

tive cost of out-year maintenance by discounting (to the Year 1 time) the number of labor hours required annually. Figure 4-4 provides a Pareto chart that rank-orders the most significant contributors to maintenance. Note that it is maintenance cost (labor) that drives all these activities, not reliability *per se*. Using the two charts it is easy to see the effect of (un)reliability on maintenance events and labor requirements.

Table 4-4. Example Maintenance Model Parameters (for Inverter).

System Configuration					Repair Parameters								
							Crew Characteristics			Repair Time Characteristics			
WBS	Repairable Assy (Repair Assy can be an R&R or RIP)	Qty/Assm	Parent Quantity	Total Quantity	Criticality	Repairable	Basic Crew Size	Crew-Size Safety Adder	Total Crew Size	Equipment MTTR	Crew Overhead Time (ea. person)	Repair Overhead Time	Total Labor per Repair
							[man]	[man]	[man]	[man-hr / repair]	[man-hr / man]	[man-hr / repair]	[man-hr / repair]
4.3	Inverter	96	1	96									
4.3.1	Equipment	1	96	96									
4.3.1.1	Power	1	96	96									
4.3.1.1.1	IGBT Drive Board	1	96	96	2	TRUE	1		1	1.0	0.2	0.3	1.4
4.3.1.1.2	IGBT	6	96	576	2	TRUE	1		1	1.0	0.2	0.3	1.4
4.3.1.1.3	Main Transformer	1	96	96	2	TRUE	3		3	4.0	0.2	0.3	12.8
4.3.1.1.4	Line Filter Inductor	3	96	288	2	TRUE	3		3	4.0	0.2	0.3	12.8
4.3.1.1.5	Main Contactor	1	96	96	2	TRUE	2		2	0.5	0.2	0.3	1.6
4.3.1.2	Control	1	96	96									
4.3.1.2.1	Main CCA	1	96	96	2	TRUE	1		1	0.5	0.2	0.3	0.9
4.3.1.2.2	cPCI 3U CPU Board	1	96	96	2	TRUE	1		1	0.3	0.2	0.3	0.7
4.3.1.2.3	cPCI 3U Power Board	1	96	96	2	TRUE	1		1	0.3	0.2	0.3	0.7
4.3.1.2.4	cPCI 3U Backplane	1	96	96	2	TRUE	1		1	0.3	0.2	0.3	0.7
4.3.1.2.5	Front Panel Interface	1	96	96	2	TRUE	1		1	0.5	0.2	0.3	0.9
4.3.1.2.6	Internal Control Power Supply	1	96	96	2	TRUE	1		1	0.5	0.2	0.3	0.9
4.3.1.3	Mechanical	1	96	96									
4.3.1.3.1	Cooling Fan	2	96	192	2	TRUE	2		2	1.0	0.2	0.3	2.6
4.3.1.3.2	Fan Filter	1	96	96	2	TRUE	1		1	0.3	0.2	0.3	0.7
4.3.1.3.3	Mech/Electrical	1	96	96	2	TRUE	2		2	4.0	0.2	0.3	8.6
4.3.1.3.4	Wire Harness	1	96	96	2	TRUE	2		2	4.0	0.2	0.3	8.6

The maintenance requirements shown in Table 4-4 are representative of the results based on current estimates of reliability parameters.

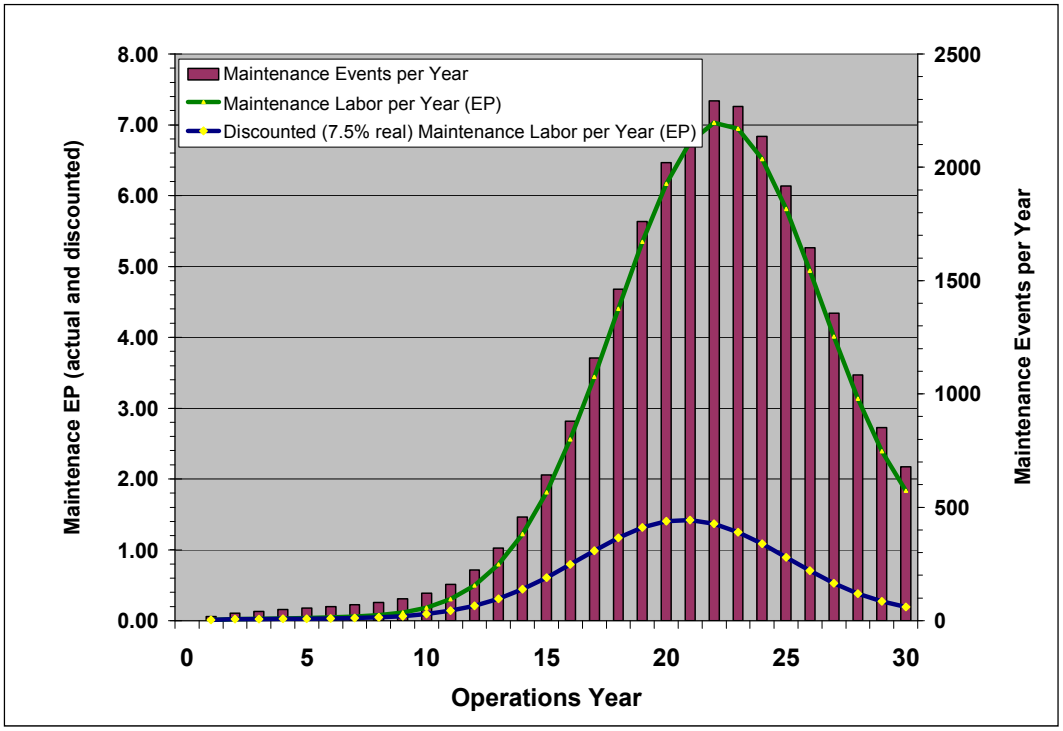

Figure 4-3. Power Plant System Maintenance Attributes.

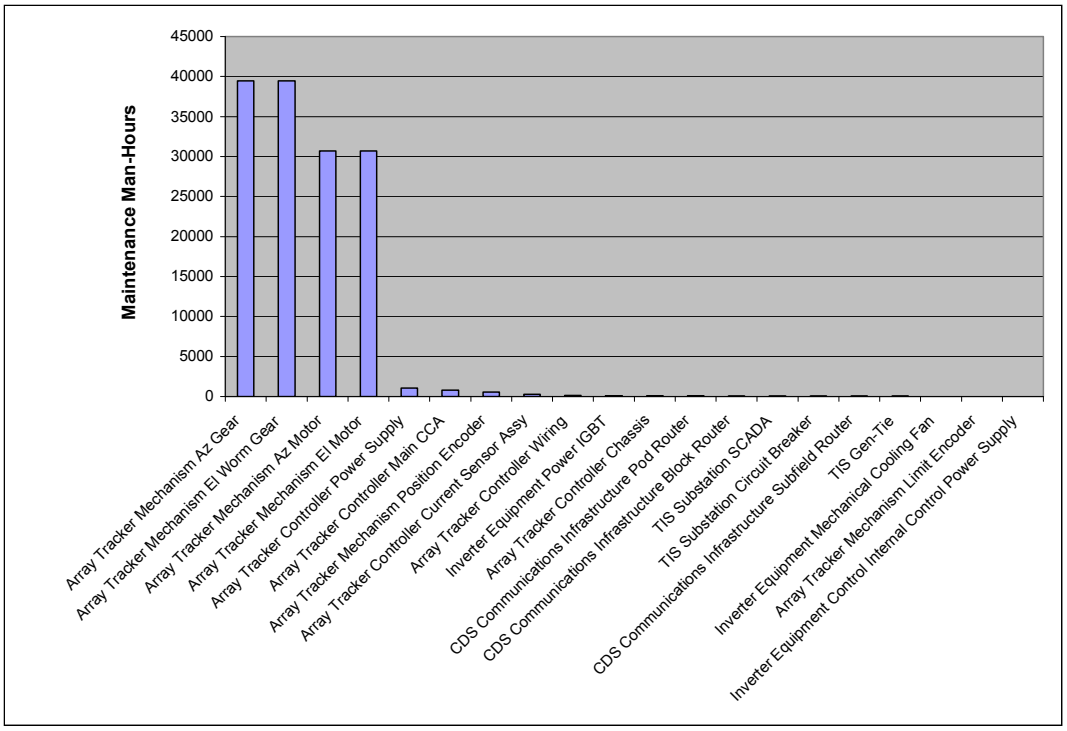

Figure 4-4. Ranking of Primary Maintenance Contributors.

4.3 Cost Model Methodology and Maturation

The program plan was to design a concentrated photovoltaic product technology that was capable of achieving $0.15/kWh LCOE with an improvement roadmap to $0.07/kWh. The Boeing program completed a CPV product and system design, performed component testing, executed the proof of design and proof of manufacturing projects, and performed extensive product maturity tasks supporting five key affordability findings:

1. The project demonstrated that all CPV components, materials, and assembly tolerances are suitable for fabrication and assembly with existing high volume automated production process technology as demonstrated at the Comau facility. Compatibility with automated assembly processes is necessary to meet full scale production rate and cost allocations.

2. There is a substantial industry base capable of providing CPV product components. Multiple suppliers were qualified per Boeing supplier management practices to build test components and arrays. Actual costs (small lot for test arrays) and rough production quotes received from suppliers support the high confidence in meeting the project cost allocations required to meet the goal LCOE of $15/kWh.

3. Independent cost assessments by outside companies confirmed with confidence that the CPV high volume production would meet the cost levels needed to support the $0.15/kWh LCOE objectives. The independent product assessment of cell efficiency increasing to 45% and configuration improvements were consistent with a feasible path to $0.07/kWh.

4. Increased cell efficiency to 45% per the technology roadmap with expected reduction in material and labor cost substantially increases the likelihood that the CPV technology will reach $0.070/kWh LCOE objectives. Forward looking technology roadmaps (see Figure 4-5) strongly indicate the required efficiency is achievable, with further investment, and increases in production volume will lower material costs to the point that the lower goal can be achieved.

5. The evolved module configuration results in a smaller footprint for the automation assembly cells and dramatically lowers the factory capital cost.

At Stage Gate 3 the LCOE for the Boeing CPV 20MW (name plate) power plant project is based on the installed cost and the operational costs for electricity produced over a thirty year operational period. The Boeing conceptual CPV power plant is maintained at 6,816 concentrator array units as the power collection devices on a 126 acre site. The 6,816 arrays deliver power to 96 inverters (a ratio of 71 arrays per inverter). Physical definition of the notional 20 MW power plant was maintained during the third phase to focus the available funds toward the construction of the 100kW demonstration pilot plant. Recent improvements in expected cell efficiency and changes in the module design will result in a power plant architecture with less arrays producing more energy.

The performance of the notional 20 MW power plant was analyzed using the conditions described byTMY2 data for Phoenix, Arizona. The module and panel assembly location for the pilot plant was Detroit, Michigan. The full scale automated production plant location was assumed to be Mesa, Arizona to be in closer proximity to most of the future CPV installation sites.

The Boeing approach continued to investigate the complete power plant system definition, which includes: arrays, logistics planning, electrical support distribution subsystem, site construction, power system, and operations. Design updates specifically have addressed module and array materials, labor, handling, and operational reliability. Increases in module performance have been resulting in projected installed cost improvements. Throughout the program,, high volume fabrication companies and consultants participated in cost assessment exercises and supported project design evolution as well as improving cost confidence.

At Stage Gate 2 the System Cost Analysis and LCOE Report was provided to the DOE that described the steps Boeing had taken, and the steps the team had planned to further reduce costs, as depicted in Figure 4-5. Cost confidence tasks were planned with coordination of the growing supplier list and design maturity. The report described how the Design to Cost process was applied on a part-by-part basis starting with the original proof of design modules. In the case of heat pipes and structural components there were factors of 10X and in some cases 100X improvement in part costs. The report and the update provided at Stage Gate 3 included the inputs used with SAM for calculating the LCOE. The SAM input file was released to NREL for evaluation purposes. Technical and cost information was provided, as transparently as possible, to the DOE auditor Navigant Consulting, Inc. (see the Navigant report to the DOE in Appendix A) within the constraints of supplier proprietary agreements.

The Stage Gate 2 roadmap described the expected evolution path. The current baseline design has incorporated the step wise configuration changes that lead to the in-

creased confidence in achieving the $0.07/kWh LCOE goal. A new configuration change, not originally included in the design, had the design goal of minimal fasteners and assembly from one side.

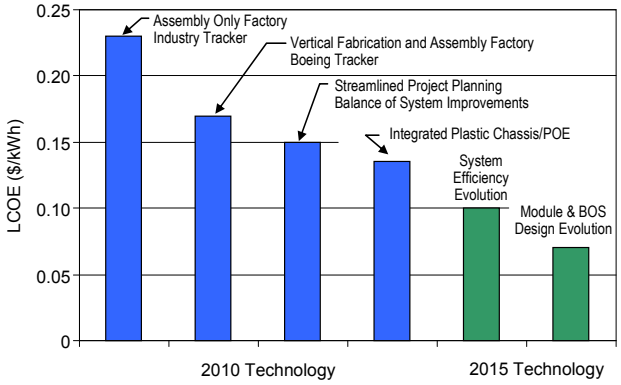

Figure 4-5. The Boeing CPV Cost Reduction Roadmap provides realistic steps toward 2010 and 2015 LCOE objectives.

The installed cost target, based on 2010 CPV technology, is $80.5M for a (CY2012 Installed Power Plant) for a targeted $0.150/kWh LCOE with 10% Investment Tax Credit (ITC). The Stage Gate 3 Boeing LCOE was $0.162/kWh at Phoenix based on 38.5% cell performance and on current cost estimates input into the Solar Advisor Model. The LCOE at a Daggett, CA located power plant was $0.145/kWh. The current predicted LCOE at Phoenix with current C4MJ production cells is below $0.150/kWh with margin. The Boeing concentrated photovoltaic system technology evolution roadmap provides a realistic track toward operational maturity and achieving 2015 $0.07/kWh LCOE.

From the beginning of the program, the Boeing team followed a Design-to-Cost process that guided the team toward defining module, array, and balance of system elements that lead to meeting the LCOE objectives. Cost targets were established, or allocated, at key WBS levels and reviewed against estimates as they were developed and refreshed, as depicted in Figure 4-6. As an element was identified to the top ten cost driver list and/or deviated significantly from the allocation, the team directed its focused attention to determine alternate approaches. This iterative process aided the team in progressing the design, manufacturing processes, and supplier list. Some costs were estimated, with supplier quotes, below the allocations and some costs predicted above the allocation resulting in a net result that met the LCOE objective.

Once the basic cost allocations were established a cost reduction roadmap plan was prepared to establish the longer term planning objectives. The roadmap plan, Figure 4-7, supports factory development and supplier sourcing communications by setting expectations as the production capacity grows. The corresponding targets are consistent with meeting the DOE 2015 financial objectives of achieving $0.07/kWh with 2015 CPV technology. Every aspect of power plant production costs is captured in the roadmap plan. The roadmap plan is used to evaluate the production capital investments required to achieve the installed plant objectives. By 2016 three 75MW/Yr capacity assembly fac-

tories with supporting material sourcing logistics are planned to be fully installed and operating to meet future expected product demand.

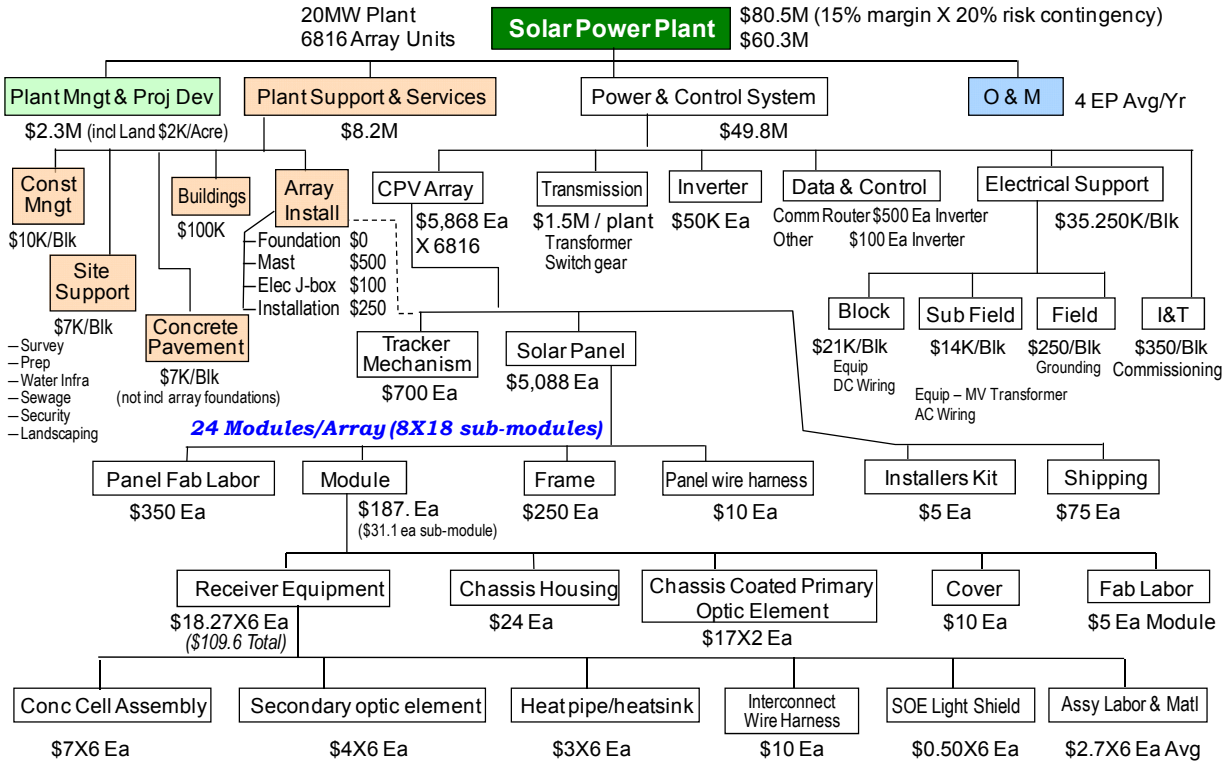

Figure 4-6. Cost allocations based on the high volume production configuration with plastic chassis developed to meet financial goals.

Supply chain infrastructure development requires further maturation towards entering full scale production of the CPV product. This is a priority activity ramping up between Boeing and the licensee partner. Various suppliers across the product component and assembly levels were sent Request for Quote (RFQ) packages to initiate the process of establishing the network on material, production, assembly, and logistics chains need to enter full scale production and meet the business financial objectives of all future participants.

Establishing ultimate cost confidence is a future commercialization activity that consists of producing parts and knowing the actual price paid for the parts, including logistics support, and assembly. High cost confidence sufficient for critical commercialization “go ahead” points was derived from supplier quote responses based on a rigorous request for quotation (RFQ) process. In 2010Q1 the SES CPV partner performed an independent industry survey to evaluate the likelihood of meeting the cost allocations provided by Boeing. Advanced Purchasing Dynamics, Comau Inc., Magna International Inc. (Exteriors & Interiors Division), and Tower International were four of the manufacturing companies that participated evaluating the cost credibility. More importantly, they were using the technical and cost information to decide if their companies would benefit from participating in the CPV business. The result was a very favorable response and each of the companies expressed strong participation interest. Additionally, Advanced Purchasing Dynamics was hired by the SES CPV team to perform an industry base and inde-

pendent cost assessment. Based on the positive response from each of independent assessments and various industry suppliers, SES established a supplier management team to proceed further. The SES CPV team partner issued RFQs, providing material and component suppliers with firm production quantity and delivery schedules as well as proposals for equipment capitalization requirements and agreements. Multiple qualified suppliers for each component and/or assembly are invited to participate in the supply chain development process and win a role to minimize the program's cost. The industry-standard RSMeans "Electrical Cost Data" handbook was used as a cost data source for many common construction elements of the CPV power plant. In general the cost data in the hand book is for small lot sizes and for moderate size projects. RSMeans costs data was cross checked with specific supplier data, publications, and internet pricing in the area conductors, conduit, transformers, concrete, and tracker device components. The direct use of RSMeans provided a conservative estimation method for starting points and used to establish cost confidence with supplier inputs. Results strongly indicated the ability of the product to be below $4/W in full initial production with a clear and likely path to $2.5/W based on configuration improvements, increased efficiency, and increasing production volume.

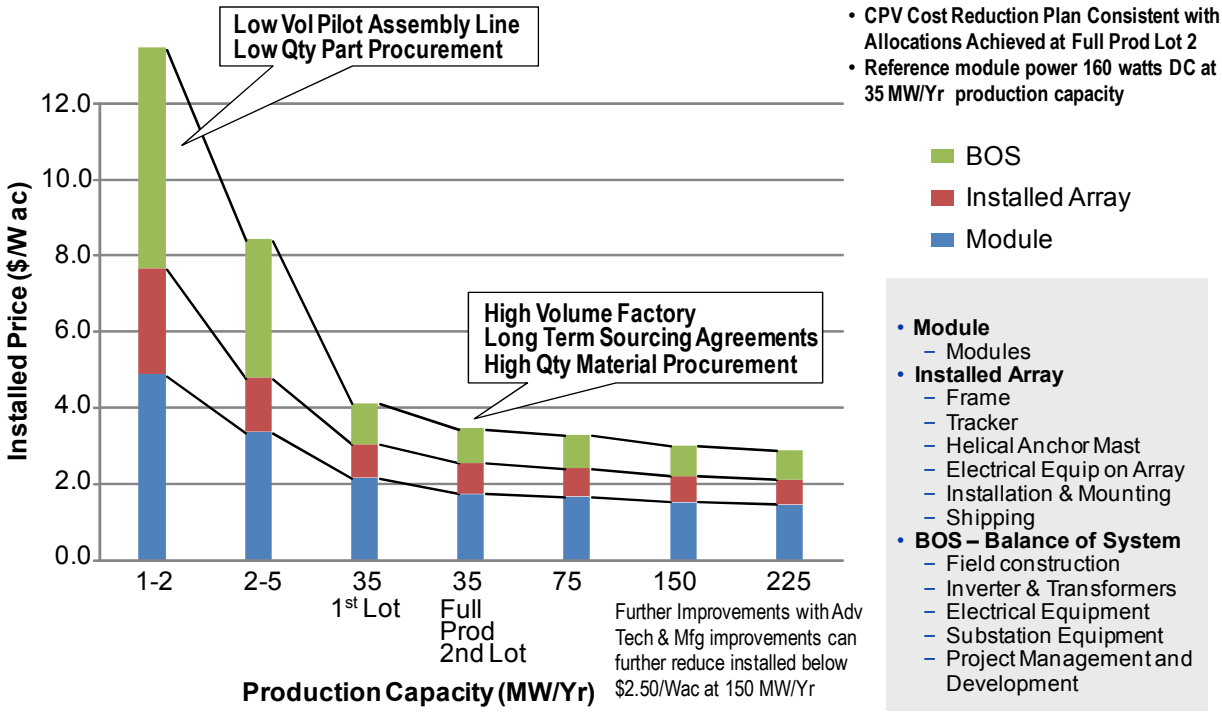

Figure 4-7. CPV Cost Reduction Roadmap Plan.

Other cost confidence approaches were investigated. The Boeing team performed an early RFQ process and received encouraging formal responses from suppliers. We performed learning curve analysis as well. Since all of the components of the POM were procured as developmental units, in low quantity, and with very low volume fabrication practices, the as-built costs benchmark conservative estimates for the theoretical first unit production costs. When cost reduction curve mathematics are applied (i.e. every doubling of quantity results in a 15% cost reduction) we find there are seven doublings

to the initial high volume production rates. This simple cross check indicates the allocations are achievable.

The Stage Gate 3 configuration was a set of components that required approximately 50 fasteners per module for attaching the receiver units to the module plus twelve electrical welds on the receiver wall. Existing automated fabrication and assembly technology was suitable to perform the operations. Special handling of the receiver wall was required for assembly onto the primary module housing. Since Stage Gate 3 the team worked with tooling and automation suppliers to evolve the configuration with the objective of defining a module with fewer parts, reduced fasteners, no welds, and supported a layered assembly process. The result was a module with "Twist Lock Bayonet" receiver units that require no fasteners. The electrical interface is a pressure contact method which was tested successfully. Material handling was improved with the receiver unit attached to the receiver wall after it was attached to the primary module housing. The expected result is better than 75% less assembly cost. Technical details of this approach are provided in Section 4.4.1.

The Stage Gate 3 design required a two side access method for attaching the receiver unit to the receiver wall. The Boeing Company has decades of experience with structural, electrical, and optical assembly methods that utilize both one side and two side part access for the assembly process, and has development experience with many processes on airplane structures with fasteners that installed with tight tolerance with access from only one side. This paradigm was applied to the CPV module with supplier collaboration. The new configuration with a one side attachment process was tested as described in other sections demonstrating feasibility that will result directly into lower cost and improved LCOE.

Independent cost estimates from three sources strongly indicate high confidence in achieving $0.15/kWh and that the roadmap to $0.070/kWh is reasonable.

4.4 Cost Reduction

4.4.1 Module Redesign for Cost Reduction

The single greatest cost in the POM design is the steel chassis. This enclosure is required to hold the POE mirrors in alignment relative to the receiver wall and form a leak-tight enclosure to protect the front surface mirror and the high voltage photovoltaic circuitry. While this is in principle inexpensive, issues with respect to alignment and sealing have prevented significant cost reduction.

The option of replacing the steel enclosure with an injection molded plastic chassis was conceived in late 2009. A plastic chassis promises a substantial cost reduction which can be further enhanced by merging the enclosure wall with the mirror substrate. A joint design study was initiated between Boeing and Delta Technologies in Detroit, MI. Delta optimized the plastic chassis mold design for plastic flow and warpage. Thermal analyses were also carried out to assure the thermal distortions and cte mismatch would not lead to operational mis-alignment. The net result was a high confidence design which offered a near term cost of $45 per chassis-mirror set and a road map to a $25 cost based on reducing the plastic wall thicknesses.

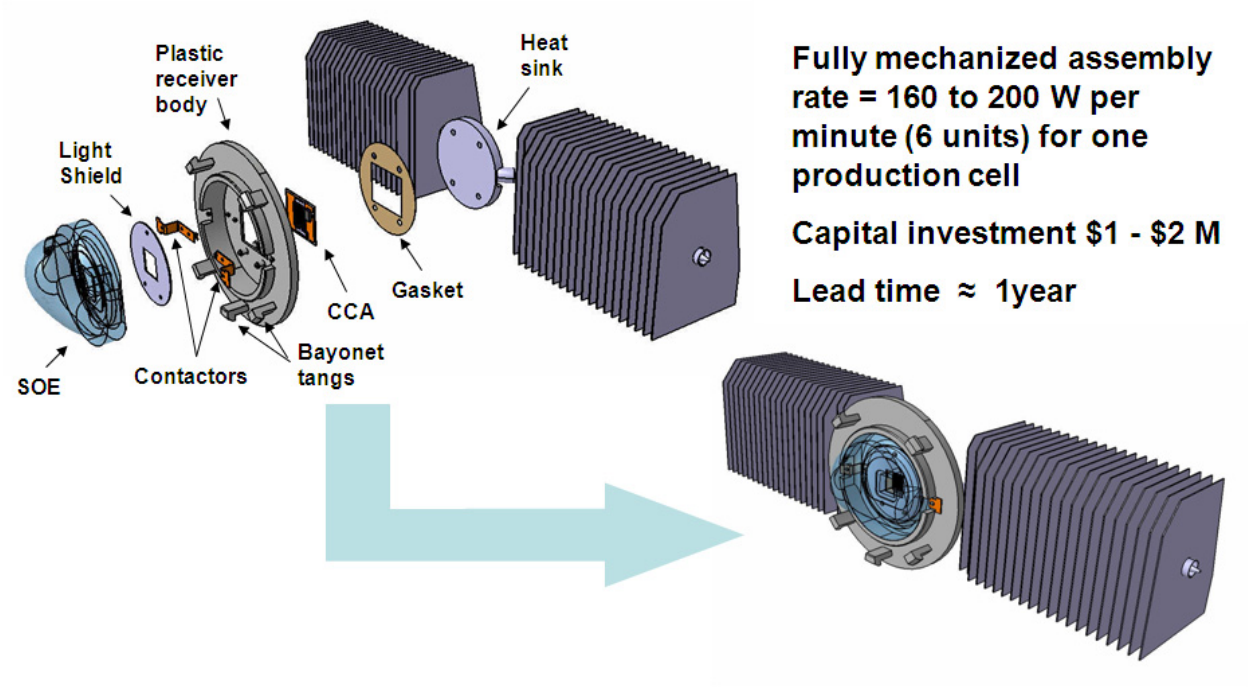

Figure 4-8. Receiver assembly concept.

In 2011 the concept was further refined by the inclusion of a receiver assembly which incorporates in a single assembly the functions of the CCA, CCA to circuit connections, the heat sink and the secondary optic. This concept (see Figure 4-8) incorporates approximately 75% of the parts cost and assembly complexity into one easily handled unit. Furthermore it allows field replacement of the unit either for purposes of maintenance or in the event of significant improvements in cell technology.

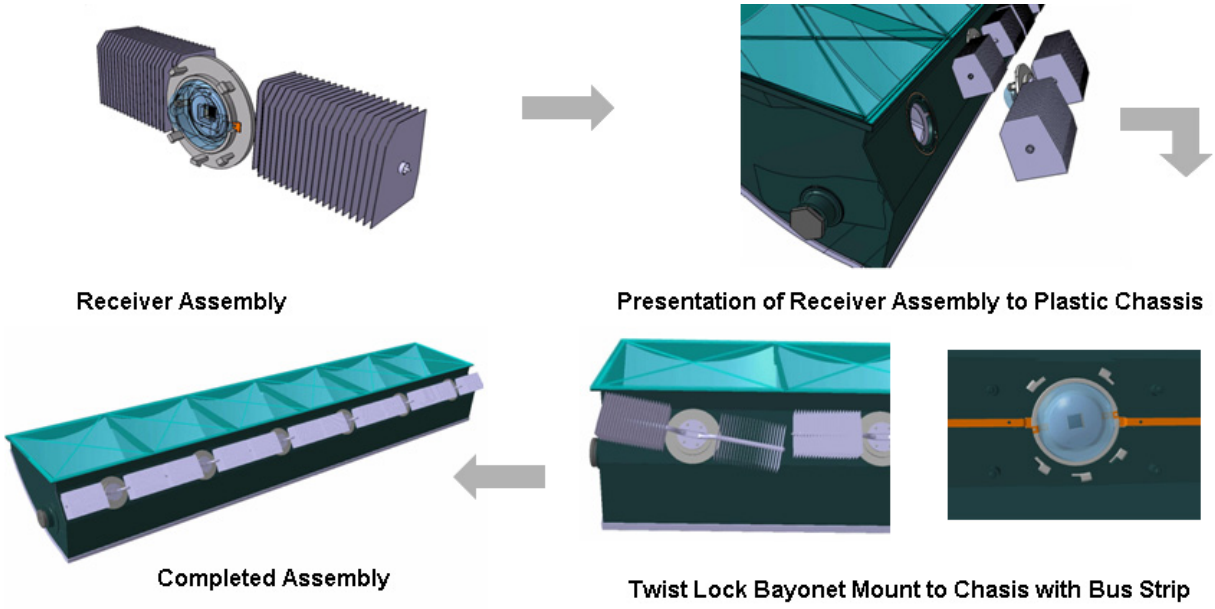

Figure 4-9. Receiver assembly combination with the injection molded plastic chassis.

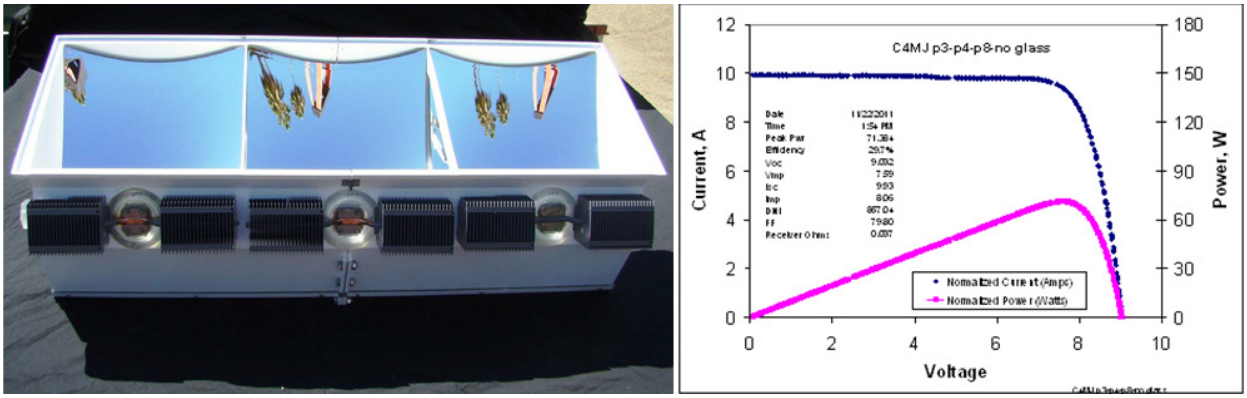

Figure 4-10. Rapid prototype demonstration of the receiver assembly – plastic chassis CPV approach.

The net result in conjunction with the plastic enclosure is a much simpler assembly process employing lower and more accurate parts (see Figure 4-9). The chassis-mirror enclosure is a simple light weight box. Functionally the result is identical to the much more complex steel chassis-separate plastic mirror-receiver wall design. Just one example makes this point, the number of screw fasteners has been reduced from 52 to 1.

This concept has been reduced to practice with stereo-lithographic rapid prototyping for the required plastic parts. The result is shown in Figure 4-10. As can be seen the demonstration could only be carried out in a three receiver chassis owing to size limitations of the stereo-lithographic manufacturing. Mirrors were obtained by removing back side mounting features from existing POM hardware. Despite these necessary compromises 30% conversion efficiency was achieved.

4.4.2 Array Cost Reduction

4.4.2.1 Lower Cost Panel Assembly

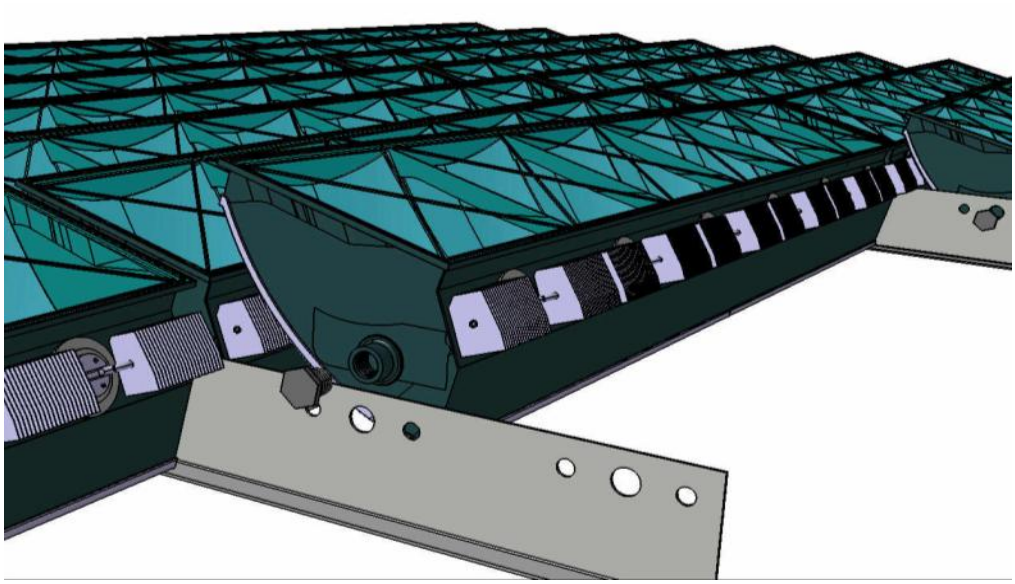

Figure 4-11. Module to frame field mounting for plastic chassis based design.

As discussed in Section 8 one of the finding of the POM exercise was that transportation issues outweighed cost reduction from factory assembly of a tracker ready panel. As part of the design development of the plastic chassis an assembly approach has been developed for the panel based on a one fastener three point mount of the module to its mating frame rails.

The plastic module is designed with two plain studs on one end and a single female threaded stud on the other end. As shown in Figure 4-11 the panel mounting rails are built with three in line holes. A module is then mounted by inserting the two smooth module studs into the two small diameter out board holes. The opposite end female threaded stud is then mounted to the adjacent rail via the central large hole with a mating shouldered plastic bolt. As individual modules weigh on the order of 25 pounds assembly is easily a one person job and should be at least as fast as in field flat panel assembly today.

4.4.2.2 Frame Design

After completion of the POM a new approach to the frame was developed based on a central deflection inhibiting "spider: shown in Figure 4-12. This design combined with the reduced mass of the plastic module relative to the POM design reduces the frame mass per square meter of illuminated area in half.

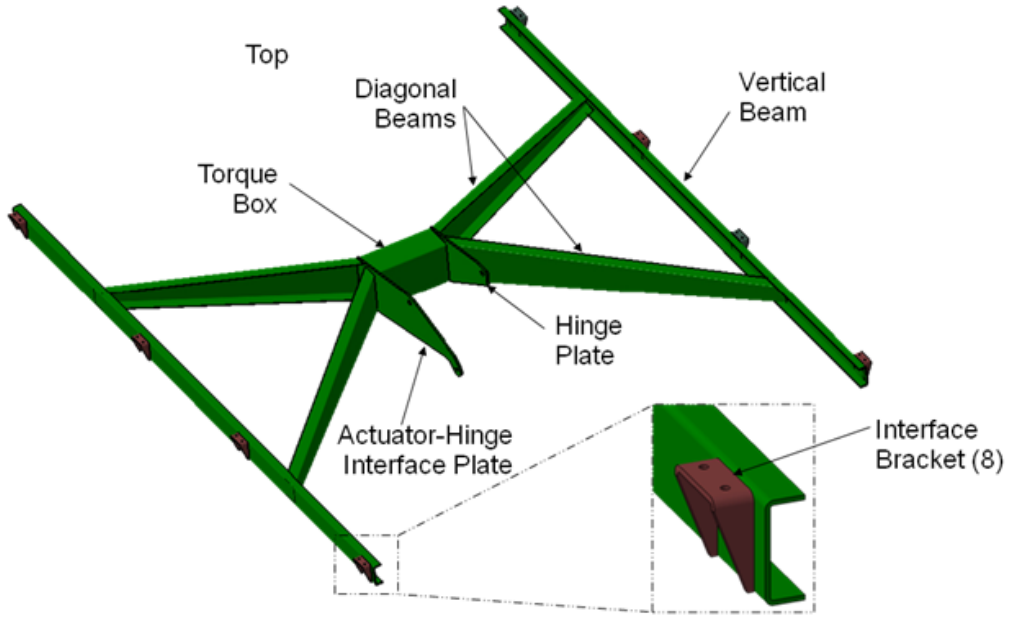

Figure 4-12. "Spider" distribution design for an advanced low mass frame.

4.4.3 Reduced Balance of Systems

Simultaneous with the SETP program Boeing Energy began developing business opportunities as a systems integrator in the renewable energy space. This led to an increased appreciation of the role of Balance of Systems in determining LCOE. Balance of Systems is an inverse function of the $Wh/m^2/yr$ produced by the plant. Items such as permitting, inter-array conductors, land cost etc will all contribute a smaller fraction to the LCOE as $Wh/m^2/yr$ increases.

It is also of course well understood that on a module and panel basis CPV areal specific power as compared with PV as result of the higher conversion efficient efficiency of a multijunction cell, its lower temperature coefficient and superior sun tracking. This, for example, is demonstrated in Figure 4-13 where the performance of 20 m^2 array of commercial multi-crystalline panels (15% STD module efficiency) is compared against the performance of a CPV module (~30% STD efficiency) normalized to the same array area.

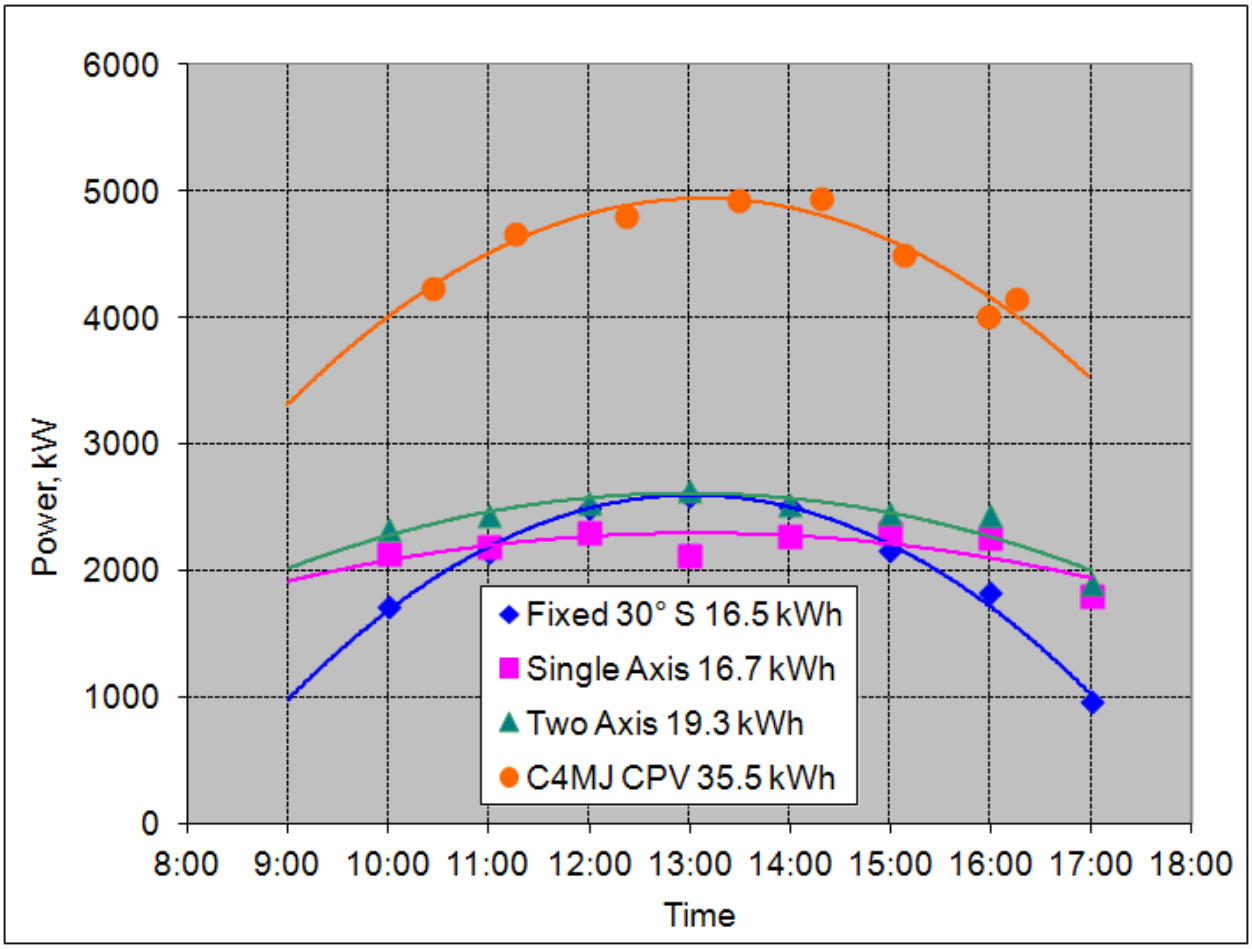

Figure 4-13. Performance comparison of a 20 m2 panel of multi-crystalline silicon PV modules with the area normalized performance of a CPV module. Data taken at Seal Beach, California March 20, 2011.

Considering all of this in 2011 we initiated an effort to model the effects of increasing array packing density on power plant output. As a standard of comparison Boeing at the time was carrying out a detailed assessment of a potential flat panel silicon PV power plant in the California Imperial Valley. The performance metric at that fixed tilt panel plant plant was 44 GWh/$10^6 m^2$/yr. The limit to packing density at the site was access space for panel cleaning equipment. This in fact represented a real potential advantage for CPV as the two axis tracking obviates the need for discrete access roads.

The CPY based model employed TMY2 data for the Imperial Valley. Shadowing is treated with the appropriate geometry and published sun elevation data for the Imperial

valley latitude. The results of the effort are provided in Figure 4-14. There are two conclusions from the data in Figure 4-14:

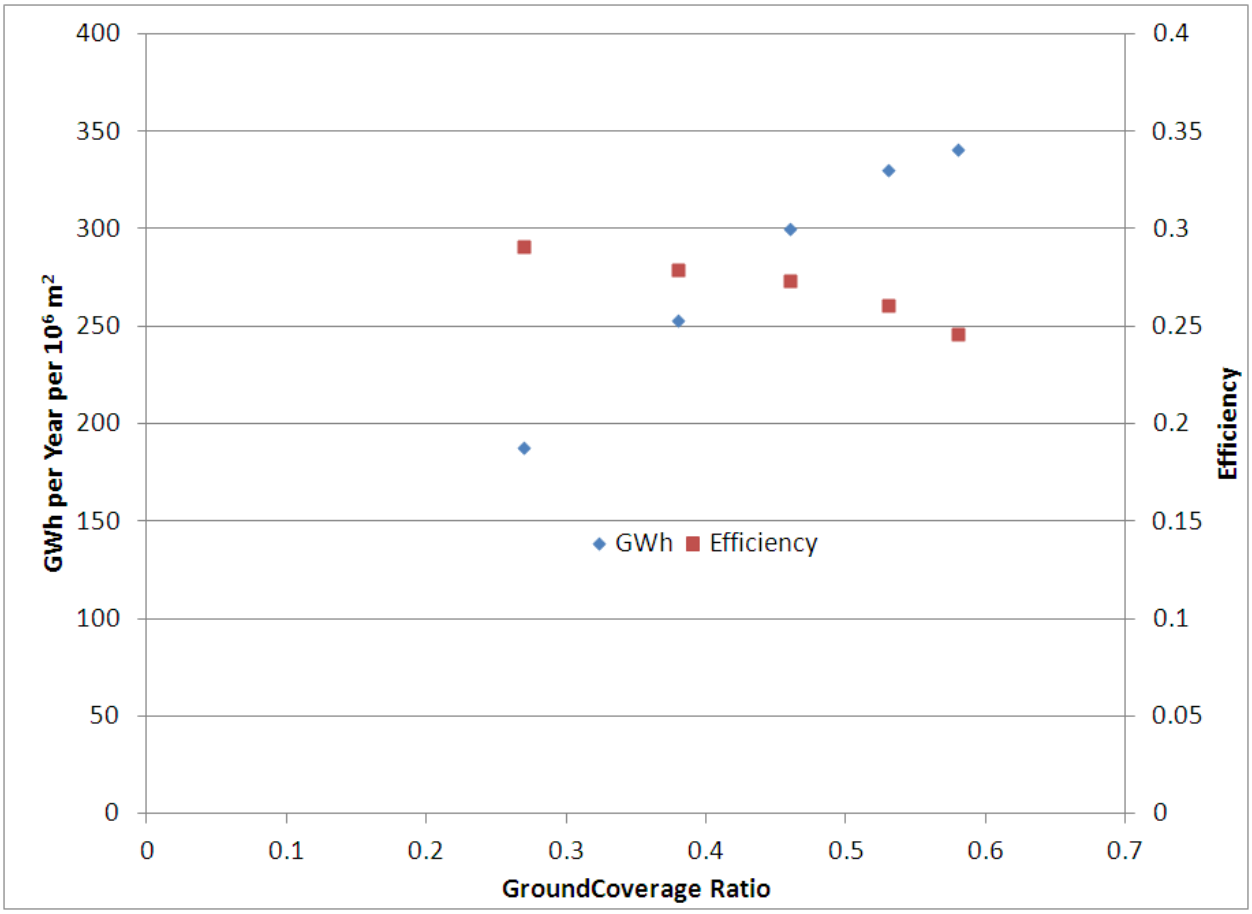

Figure 4-14. Close packing CPV array model power and efficiency vs. ground coverage ratio.

With this in mind in 2011 we initiated an effort to model the effects of increasing array packing density on power plant output. As a standard of comparison Boeing at the time was carrying out a detailed assessment of a potential flat panel silicon PV power plant in the California Imperial Valley. The performance metric at that plant was about 150 GWh/mi^2/yr. The limit to packing density at the site was access space for panel cleaning equipment. This in fact represented a real potential advantage for CPV as the two axis tracking obviates the need for discrete access roads.

The CPY based model employed TMY2 data for the Imperial Valley. Shadowing is treated with the appropriate geometry and published sun elevation data for the Imperial valley latitude. The results of the effort are provided in Figure 4-14. There are two conclusions from the data in Figure 4-14:

- CPV can easily far exceed the energy production from a fixed panel system. This could be of particular consequence for enabling power plant siting near major metropolitan areas as the impact of higher land cost will be offset by the higher output as well as the savings resulting from lower transmission costs;

- There is a price to be paid for this. As Figure 4-14 shows higher packing does lead to lower efficiency thereby raising equipment cost contribution to LCOE. However, note that at a module pitch of 9.5 m the efficiency is reduced by 10% but the field power density is more than doubled relative to conventional PV.

5 CPV System Manufacturing Maturation – SOPO Tasks 1.8, 2.8, 3.8

Task Objectives

The objectives of this task were:

- Perform manufacturing analysis of the candidate designs.
- Perform design for manufacturing/assembly studies to assess opportunities for manufacturing cost improvement.
- Develop factory implementation plans for all system elements to meet initial production capacity targets.

Highlights

- The 260 kW PVPowered inverter as a result of the SETP effort is now a standard PVPowered product with an available 20 year warranty.
- Robotic factory commissioned and operated for the production of 33 CPV panels with a total design capacity of 114 kW. The panels were delivered to the demonstration power plant and mounted on per-positioned trackers at the rate of 2 per hour
- Detailed planning studies have been carried out for the components and assembly infrastructure required to support a 150 MW per year production rate at the target $0.15 per kWh.
- Low CAPEX manufacturing concepts have been developed for advanced low designs that support a mature commercial price of $0.07 per kWh.

Table 5-1. CPV System Manufacturing Maturation

Period	Criterion	Results
2	2c-2) Demonstrate pilot production of inverter	Achieved, the 260 kWh inverter is now a production item with an optional 20 year guarantee
3	3d-1) Demonstrate system with 100 kWp capability produced with production tooling	All CSUN power plant panel hardware was manufactured in a robotic factory at a final production rate of 2MW per year.
	3d-2 Demonstrate volume production capability of all system elements	Studies carried out by Magna and Advanced purchasing Dynamics validated the availability of all elements at a cost that supports the $0.15 per kWh target. Automation studies validate the capitalization and labor required to meet the LCOE target’

Technical Accomplishments

5.1 Automated Production Facility Design and Demonstration

To meet rate and quality requirements, automated assembly was considered and selected as the going-forward approach for higher rate production. Within the time and cost constraints of the program, Boeing, working with Comau, Inc. in Detroit, Michigan, developed a partnership to develop an automated pilot factory to demonstrate that manufacturing technologies and operational requirements could be consistently met using automated assembly.

To provide the greatest value, the pilot factory concentrated its automated assembly on areas of the design where automated assembly would provide the most benefit to overall product accuracy and production rate. Material handling and detail part presentation were kept as manual tasks because these tasks have a solid automated history and are well understood in the automated realm.

Comau, needing to better understand the product design and requirements, colocated a team of designers to work with Boeing designers while the individual part and assembly designs were finalized. The Comau automation engineers developed specific designed-in areas on the parts with which the robotic end effecters would interface. This methodology not only provided a stair-stepped approach to enabling automated assembly, but it also provided valuable ownership to Comau.

Figure 5-1. Automated Receiver Wall Assembly

The pilot factory was designed at Comau's Arlans, Michigan, facility and constructed at its Novi, Michigan, facility located about 20 miles from the design center. Automated operations were accomplished using six articulated-arm robots, with various end effecters and work stands to enable the 20 automated installation operations required to produce a module and install it onto a support frame. Most automated processes were supported by one or more manual process of less complexity. The primary goals of the pilot factory were to prove that optical bonding, bus strip soldering, and assembly alignment were possible in an automated environment and that they would yield an acceptable product that previously had been only manually assembled. Figure 5-1 is a photograph of the automated receiver wall assembly.

Final design of the production version of the modules and panels continued well into the development of the robotic factory. Automated trials were done with preproduction parts using developmental versions of the assembly software to validate that part/robot interfaces were adequate to position and handle the parts and assemblies as required to meet assembly alignment tolerances. When issues with these interfaces arose, changes were made to the part or end effecter designs before committing to production quantities or final fabrication. During these trials, Boeing representatives were on-site to document the changing requirements and communicate those changes back to the design team for incorporation into the final design drawings. Only when the design was finalized were purchase orders placed for production quantities.

Figure 5-2. Pilot Automated Assembly Factory

The pilot factory (see Figure 5-2) was designed to have a capability of 1 MW/year production, with an option to increase the output to 2 MW/year by adding a second work shift. Initial low-rate production was 34 panels, or 100 kW. This rate was equal to roughly one panel per day, a rate that was achieved by the pilot factory at panel 27 and subsequently maintained. Panels previous to that were run at a slower pace, with each process scrutinized for compliance. Initially, each operation was run with a human-in-the-loop and modified incrementally until robust compliance was achieved. Only then was the process run in the automatic mode, with rates increased incrementally until the target rate was realized. Because of the complexity of the assembly, this ramp up took longer than anticipated, with some issues centering on adhesive cure times uncovered, leading to some additional process optimization before system commissioning. With these changes made, the system ultimately proved that the fundamental assembly requirements could be met or exceeded using high-speed automation.

Some operations proved to be more successful automated than when manually performed. For example, the pilot factory was far more successful with automated optical bonding than was demonstrated manually, with nearly perfect optical bonds being common and only a small fraction of the bonds deviating. Thermal bonding, including cell placement on the heat sink, was also highly successful. Primary optical element alignment and module alignment onto the frame were demonstrated and both were highly successful. However, bus strip soldering and primary optical element retention proved to be problematic, with an increased level of surveillance and inspection incorporated throughout the build cycle to validate their compliance.

Comau's experience in factory automation served to further educate Boeing in how to design for automation and high production. It is to be noted that in order to fully capitalize on the benefits, robotic interface and automated assembly processing must be implemented as a stringent design requirement from the initial design concept, with automation designers and programmers being an active element of the design team. Manual assembly, even with production parts, fails to adequately replicate the process nuances that successful automated assembly requires. Comau's design flexibility and available solutions enabled the important step to the higher production rates at the target cost.

5.2 Commercial Sized Factory Design

In parallel with the pilot production facility development and production demonstration Comau was contracted to carry out a concept design for a 150 MW volume production plant to support the commercial market. The facility layout presented in Figure 5-3.

In order to minimize product overall cost the facility in Figure 5-3 is vertically integrated with stations for fabrication of the plastic chassis, the POE, the heat sink, and the steel frame. The labor mix and total employees for two shift operation of the plant are summarized in Figure 5-4. The labor estimates, materials costs and proposed capital costs for the plant all agree with the input used in the cost modeling work described in Section 4.3.

In addition to developing a concept plan for the full scale production plant Comau carried out a detailed cash flow analysis for the plant for the first five years of operation. The cash flow analysis is summarized in Table 5-2. This analysis was based on the following input.

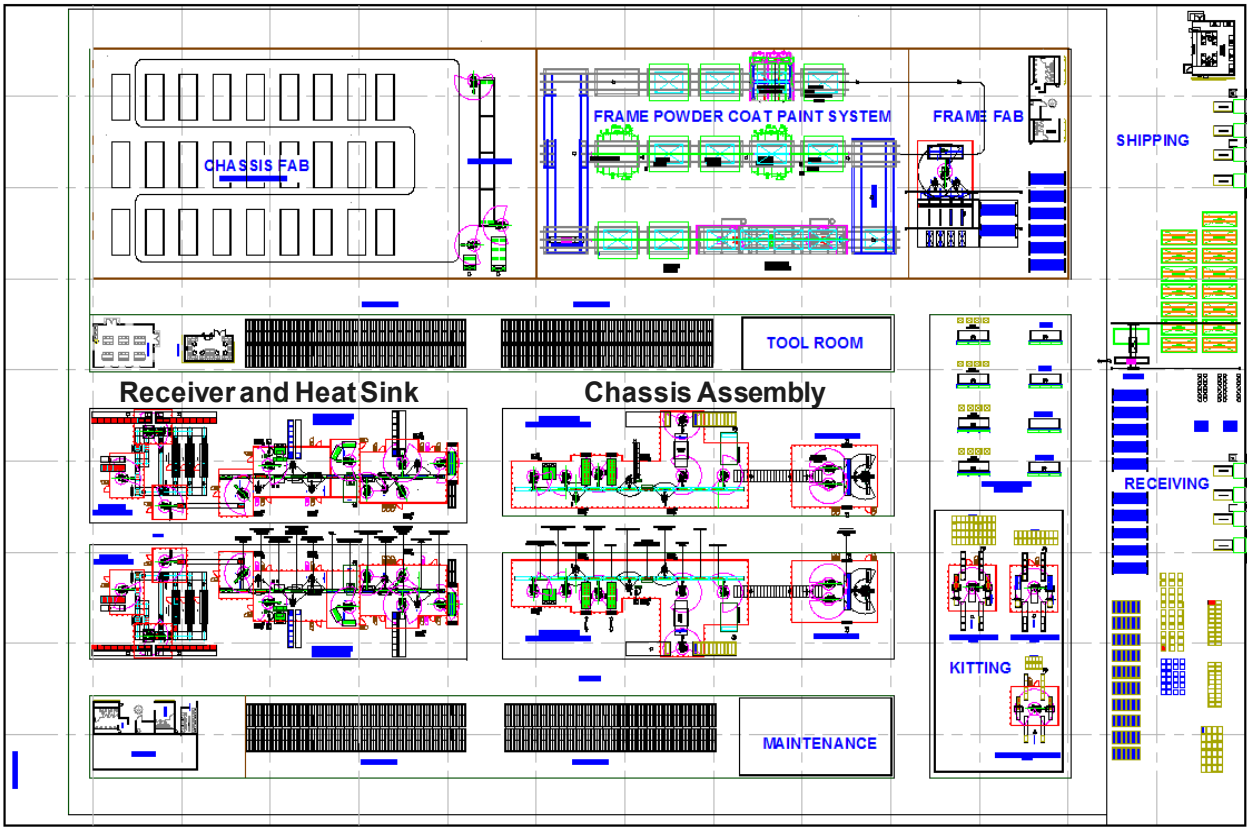

Figure 5-3. Concept layout for a 120,000 sq. ft., 150 MW per year CPV panel production facility.

- Plant capital cost was $110,000,000.
- The plant would be located near a high DNI continental United States site in order to minimize shipping costs to likely power plant sites.
- Target states for the plant location included Texas, New Mexico, Arizona and Utah based on DNI, availability of skilled workers, and state tax and incentives.
- Construction time was estimated as 16 months from the point at which financing is obtained.
- The initial target price for the power plant is assumed to $4 per watt which is compliant with the $0.15 LCOE.
- Based on the total Boeing cost model the panel price is calculated to $1.70 per watt for the first production year.
- Comau assumed that over the five year write down of the plant that the competitive price of the panels would have to be reduced to $1.20 per watt.
- Based on the Boeing and Advanced Purchasing Dynamics component cost analyses component costs are assumed to be reduced as shown in Table 5-2.

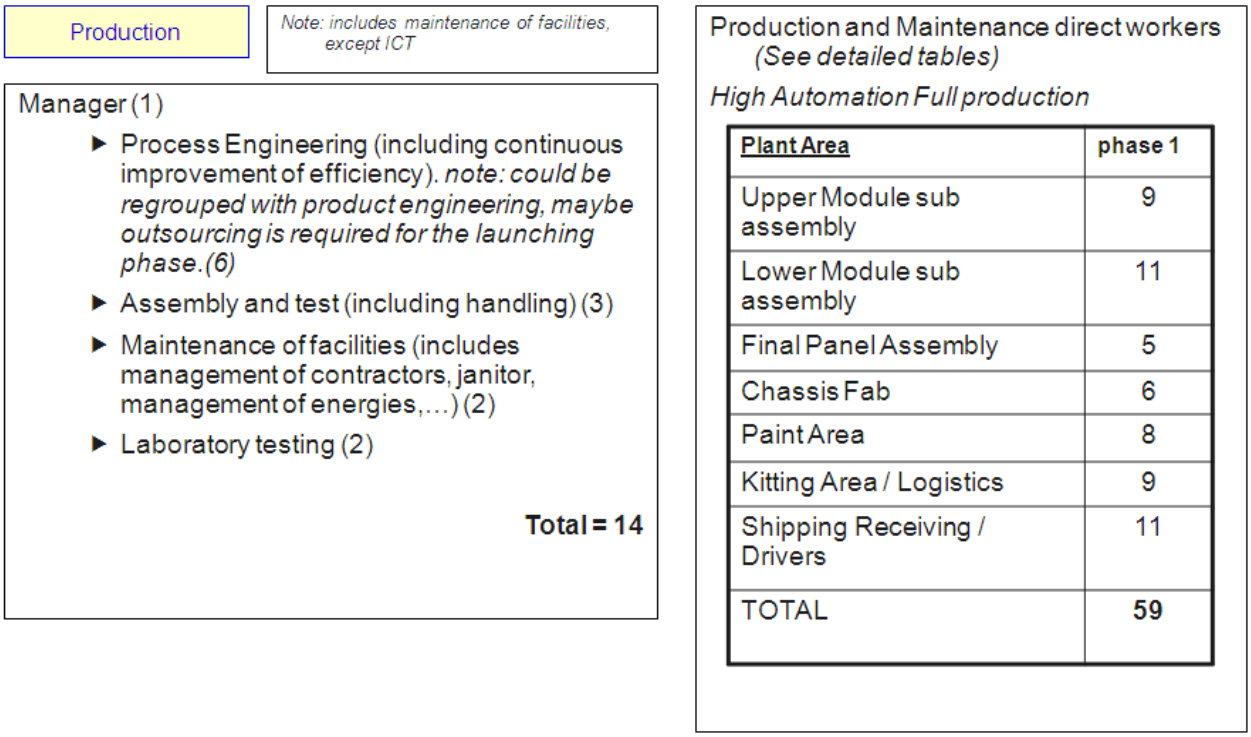

Figure 5-4. Labor mix and totals for a two shift operation of the commercial scale (150 MW/year) CPV panel production facility.

These input conditions lead to the final output in Table 5-2. As can be seen while the operation is profitable there is significant out year pricing pressure and reduced margins owing to the assumed improvement is competitive technology. Per watt panel price is falling from $1.70 to $1.20. This is only partially compensated for by learning curve driven lower materials costs.

Two approaches for improving financial performance were not considered in this analysis:

- Future improvements in cell technology. Spectrolab projects a 5 year growth in cell performance from 40% to 45%. All other conditions staying the same such a performance impact could increase total 5 year EBT by a factor of 4.
- Examining Table 5-2 it is clear that capital cost plays a major role in profitability. In Section 4.4 advanced design approaches were described which may lower both material and factory cost.

5.3 Advanced Factory Design for a Low Cost Receiver Assembly Module

Factory capital cost critically effects successful commercialization. Consider a $100M factory capable of producing 100 MW per annum. With a 7 year depreciation schedule and a 5% cost of money, this represents a $17.3M annual cost of the product which might have a parts and labor cost of $1 per watt. It plays not only an important role in the recurring cost of the current product but in the “go forward” decision for commercialization of a new product. Therefore, to make CPV successful, a new approach is desirable for factory capitalization that substantially reduces the investment required.

Table 5-2. Projected profit and loss analysis for the 150 MW per year plant.

		Year 1	Year 2	Year 3	Year 4	Year 5
Revenue						
Gross revenue		*$261,000,000*	*$218,566,176*	*$197,242,647*	*$187,913,603*	*$181,250,000*
Direct Labor costs		*$2,617,600*	*$2,669,952*	*$2,723,351*	*$2,777,818*	*$2,833,374*
Componet Material costs (Boeing 2010 cost est.)		*$220,339,080*	*$184,515,978*	*$166,514,419*	*$158,638,737*	*$153,013,250*
Cost of goods sold	Sub total:	*222,956,680*	*187,185,930*	*169,237,770*	*161,416,555*	*$155,846,624*
Gross margin		*$38,043,320*	*$31,380,247*	*$28,004,877*	*$26,497,048*	*$25,403,376*
Other revenue [source]		$0	$0	$0	$0	$0
Interest income		$0	$0	$0	$0	$0
Total revenue		*$38,043,320*	*$31,380,247*	*$28,004,877*	*$26,497,048*	*$25,403,376*
Operating expenses						
Sales and marketing		$250,000	*$255,000*	*$260,100*	*$265,302*	*$270,608*
Indirect Payroll and payroll taxes		2,105,000	*$2,147,100*	*$2,190,042*	*$2,233,843*	*$2,278,520*
Depreciation		*7,585,378*	*7,585,378*	*7,585,378*	*7,585,378*	*7,585,378*
Insurance		250,000	*$209,355*	*$188,930*	*$179,994*	*$173,611*
Maintenance, repair, and overhaul		*400,000*	*408,000*	*408,000*	*408,000*	*408,000*
Utilities		720,000	*$602,941*	*$544,118*	*$518,382*	*$500,000*
Property taxes		150,000	*$125,613*	*$113,358*	*$107,996*	*$104,167*
Administrative fees		180,000	*$150,735*	*$136,029*	*$129,596*	*$125,000*
Shipping		5,625,000	*$5,737,500*	*$5,852,250*	*$5,969,295*	*$6,088,681*
Total operating expenses		*$17,265,378*	*$17,221,622*	*$17,278,204*	*$17,397,786*	*$17,533,964*
Operating income		*$20,777,942*	*$14,158,625*	*$10,726,672*	*$9,099,262*	*$7,869,411*
Interest expense on long-term debt		*5,341,071*	*5,258,288*	*5,171,366*	*5,080,098*	*4,984,266*
Operating income before other items		*$15,436,871*	*$8,900,337*	*$5,555,307*	*$4,019,164*	*$2,885,145*
Loss (gain) on sale of assets		0	0	0	0	0
Other unusual expenses (income)		0	0	0	0	0
Earnings before taxes		*$15,436,871*	*$8,900,337*	*$5,555,307*	*$4,019,164*	*$2,885,145*
Taxes on income	*30%*	*4,631,061*	*2,670,101*	*1,666,592*	*1,205,749*	*865,544*

With respect to capitalization, the receiver assembly design plays a critical role. Its size and ease of assembly allow the rapid tailoring of existing high speed machinery. Co-mau manufactures the Smart Cell® product line which can be readily adapted for the re-ceiver assembly. The overall layout for a receiver assembly Smart Cell®-based work station is pro-vided in Figure 5-5.

The process begins with an operator loading trays of individual component material to the Comau assembly cell. There are four inbound conveyor systems to accept this component material. The operator is responsible to keep the inbound conveyor lanes full of component material. Once the incoming material enters the Comau assembly cell, the entire operation is automated and requires no manual intervention during nor-mal operating conditions.

The layout in Figure 5-5 assumes that the CCA/heat sink assembly is manufactured as a separate subassembly prior to being merged into the receiver assembly. For the POM XR700 design this was accomplished with thermal adhesive and thermal curing of the bond. This same process is assumed for the receiver assembly design; however, we are actively investigating simpler design approaches.

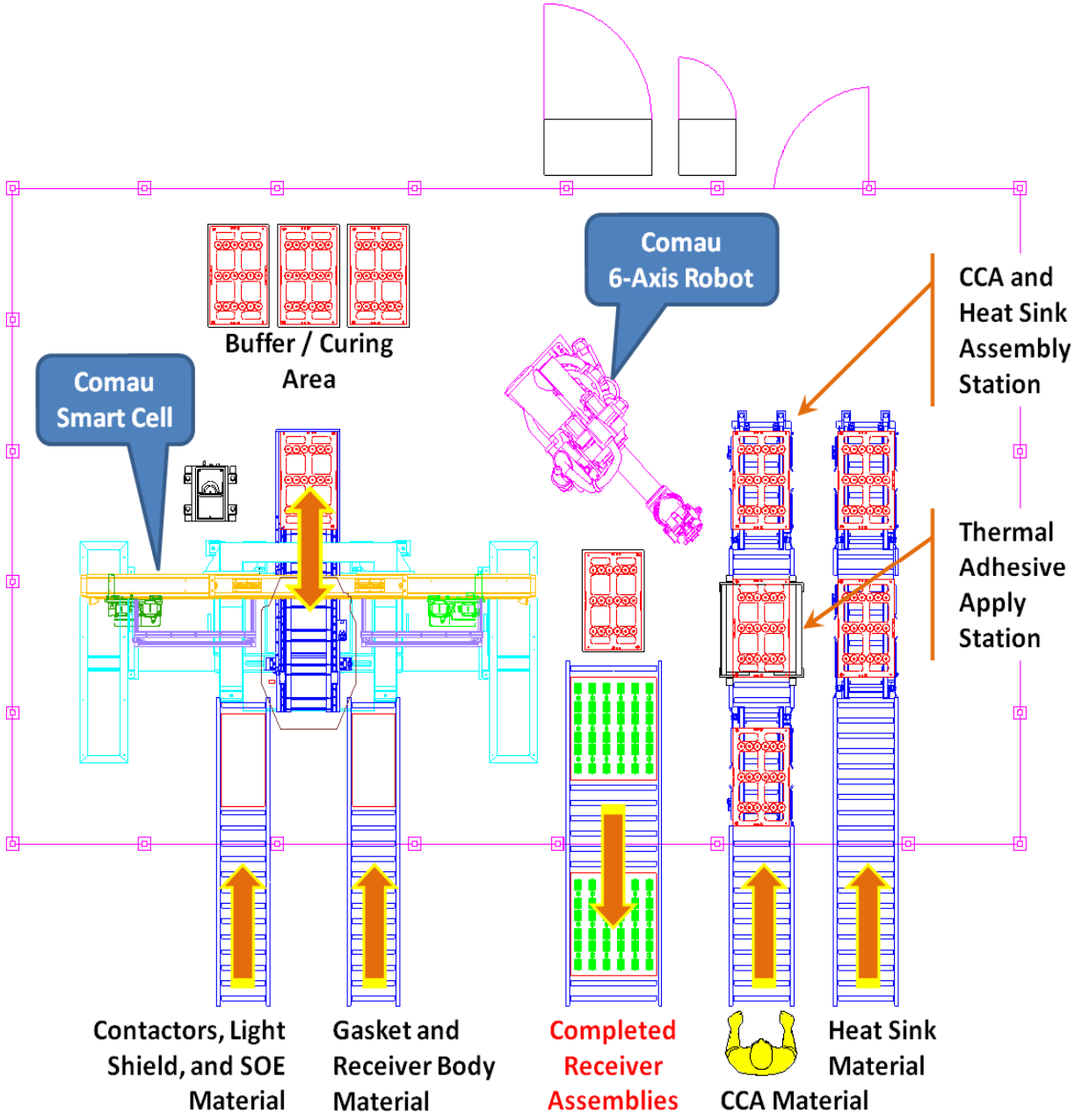

Figure 5-5. Receiver mechanized production cell sized for one part per minute. A six part per minute cell would implement more automatic handling equipment.

When the subassembly is complete, the robot will once again pick up the CCA/heat sink assembly. The robot will rotate this assembly to reposition the CCA/heat sink for the next operation and place it at the entrance to the Smart Cell®.

The CCA/heat sink assembly will now enter the Comau Smart Cell® for the remaining assembly operations. The Comau Smart Cell® is a patented high speed precision assembly machine utilizing two Z-Axis servo arms to assemble the product. The Comau Smart Cell® technology allows one Z-Axis servo arm to assemble a component to the product while the second Z-Axis servo arm is preparing for the subsequent operation.

Once the first Z-Axis servo arm finishes the first assembly step, the second Z-Axis servo starts the next assembly step. This process continues until all assembly steps are completed.

At the completion of this assembly process, the finished receiver assembly exits the Comau Smart Cell®. The robot picks the completed receiver assembly along with the nesting tray and repositions this assembly to an unloading buffer. The Comau robot then picks each receiver assembly from the in-process tray and packs the completed receiver assembly into a shippable container. Once this shippable container is full, the completed receiver assemblies exit the Comau assembly cell and can be unloaded by the operator. All of the empty material trays are automatically returned to the operator for refilling. The empty in-process trays are automatically returned to the beginning of the process for refilling.

Based on this current process, the receiver assembly work station can produce a completed receiver assembly every minute. This entire cell can be operated by one person under normal operating conditions. General maintenance will require additional support. The receiver assembly work station utilizes minimal floor space of approximately 1,200 square feet (112 square meters), not including incoming material inventory and completed receiver assembly inventory.

An ROM price for the manufacturing equipment required by the receiver assembly work station is $2.5M. A one-per-minute production rate corresponds, based on a 6 day per week double shift operation, to an annual yield of 10 MW per work station. It is assumed for purposes of this discussion that the chassis/mirror assembly is a purchased part and receiver assemblies are manually inserted in the chassis/mirror assembly to yield a completed module. Based on this model, the net capitalization cost for the whole factory is on the order of $5M, or about half the capital cost to product ratio used in the example presented at the beginning of this section. Higher rate tooling based on the same model would lead to an estimated further 50% improvement in the ratio.

6 Proof of Concept (POC) Fabrication – SOPO Tasks 1.9, 2.9, 3.9

Task Objectives

Test POC design elements and perform field demonstration to validate projected system performance

Highlights

- Demonstrated the required acceptance angle at the single receiver level, the multi-receiver module level and the array level.
- Increased conversion efficiency from 22% to 33% through a combination of optical refinement, improvements in triple junction cell technology, optimization of the thermal subsystem, improved geometric accuracy, and improved manufacturing tolerance. These improvements were demonstrated in six receiver modules. In 24 module arrays a maximum conversion efficiency of 30% has been demonstrated.
- Met the thermal performance specification of the contract as demonstrated in laboratory testing of the production configuration. These results have been verified by module tests under sun.

Table 6-1. Proof of Concept (POC) Design and Fabrication

Period	Criterion	Results
1	1e-1) Demonstrated Proof of Concept module design performance 1) Efficiency. minimum acceptable module-level power conversion efficiency is 20% 2) Acceptance Angle. Minimum acceptable angle is 1.0 degrees . 3) Thermal performance. Maximum acceptable solar cell operating temperature is 100° C	1) Best module efficiency demonstrated at +33%. Consistent performance at 30%. See Section 6.4.1. 2) On axis and off axis acceptance angles were demonstrates at 1.7° and 1.3° respectively. Six receiver off axis half acceptance demonstrated at 1.5°. Array half acceptance angle demonstrated at 0.98° azimuth and 0.83° elevation 3 Thermal compliance demonstrated by analysis (see Section 3.2.1) and test (see Section 6.4.3)

Technical Accomplishments

Proof of concept testing occurred throughout the course of the program. As the program progressed it became clear that the performance bar needed to be raised to assure a market competitive advantage in the CPV space, and continuous product improvement was pursued through the implementation of advanced triple junction cells, improved optics and improved thermal management. These activities went well beyond contract requirements with the goal of demonstrating an industry leading product with respect to cost, performance, and life.

6.1 Proof of Concept Test Configuration

All POC testing was carried out or at least the results verified in full size engineering modules of the basic design discussed in Section 3.2.2.

6.2 Fabrication Methodology / Process

Test modules were all hand built employing either released parts or parts built to a controlled design derived from a released part design. The assembly process was carried out with released process as follows:

- The chassis assembly was generally carried out by experienced mechanical technicians in an engineering lab environment. As required short run jigs and fixtures were employed;
- Mechanical aspects of receiver wall fabrication (mechanical attachments and soldering) were also carried out in the engineering lab;
- Critical adhesive bonds (thermal and optical) and well as CCA conformal coating (employing the same material as the optical bond to minimize cross contamination) were carried out in a clean chemical laboratory environment. Module assembly generally occurred in this environment although engineering lab and field assembly at the test site were also employed;
- During final receiver wall assembly the electrical integrity of each receiver was verified. The finished receiver wall was HIPOT tested at 2000 V above ground. The same test was carried out on the once the fully assembled module.

Engineering shop orders were employed for all POC fabrication to document the as built versus as designed configuration. Engineering release drawing for both parts and assemblies were employed

6.3 Module and Component Test Plan

The general module test plan consisted of the following steps:

1. Modules were mounted to a rack on a development tracker and aligned normal to the sun;
2. The module was connected to a purging system and programmable electronic load;
3. Thermocouples were attached to the chassis external wall and at least one of the heat sink blocks;
4. Four wire connections were made to the two modules terminals for the electronic load and the data acquisition system;
5. Initial module IV curves were taken to verify solar alignment and standard operation initiated which consisted of:
    a. Continuous daylight operation at peak power. Peak power and DNI were recorded on a 5 minute frequency;

b. Periodic daylight IV measurements (generally once every 30 minutes). The IV measurements were thus characteristic of an operating module.

6.4 Results

6.4.1 Efficiency

The Performance of the first POC module is presented in Figure 6-1. Performance data are enumerated in Table 6-2. Two features should be noted about these data and were to become major elements of the technical effort:

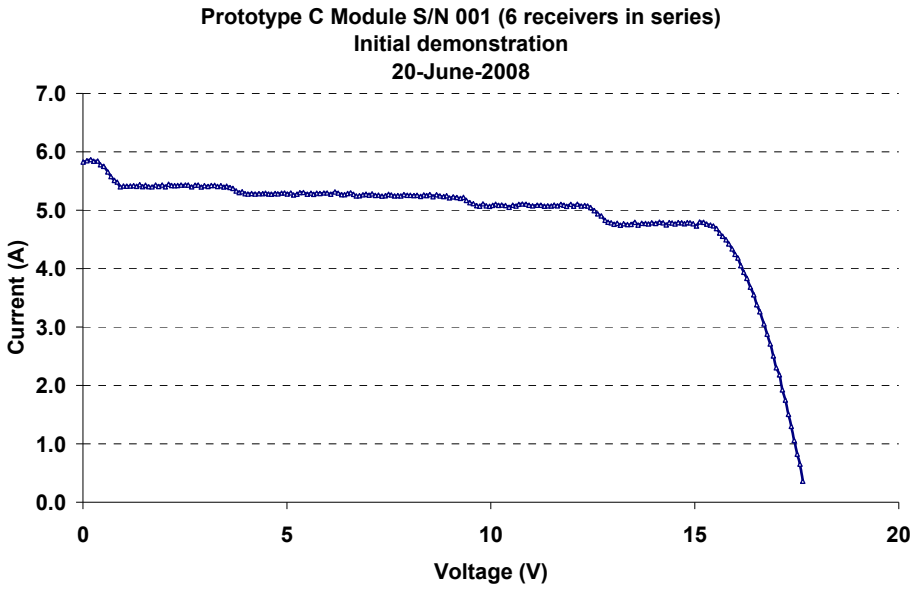

Figure 6-1. IV Curve for the first prototype C module demonstrated in 2008

Table 6-2. Data summary for the first POC module.

Isc (A)	5.826
Voc (V)	17.726
Imp (A)	4.732
Vmp (V)	15.457
Pmp (W)	73.14
FF	0.708
Efficiency**	17.3%
DNI, W/m2	872

- The IV curve of the module was composed of five distinct steps. This indicated a substantial mismatch between the 6 series receive sets which comprised the module.

- The measured Imp corresponded to a ~50% quantum efficiency, estimated from the subsequently developed quantum model.

Over the next 6 months the cause of the receiver mismatch was traced to poor receiver fabrication processes and mechanical misalignment. These were resolved by the fabrication processes described in Section 3.2.2. In parallel and as part of the same process a cleanup of the optical design was carried out. The windows were replaced with AR coated low iron glass (Schott, see Figure 6-3), a controlled optical adhesive bond line was implemented using the Nusil 6140 optical adhesive, and prototypes of the future production heatsink design were implemented. The results of these improvements are shown in Figure 6-1. The efforts led to a 10% absolute increase in module efficiency. IV curve has only small steps, a fill factor of ~80%, and the quantum efficiency is 88% of the optically attenuated limit.

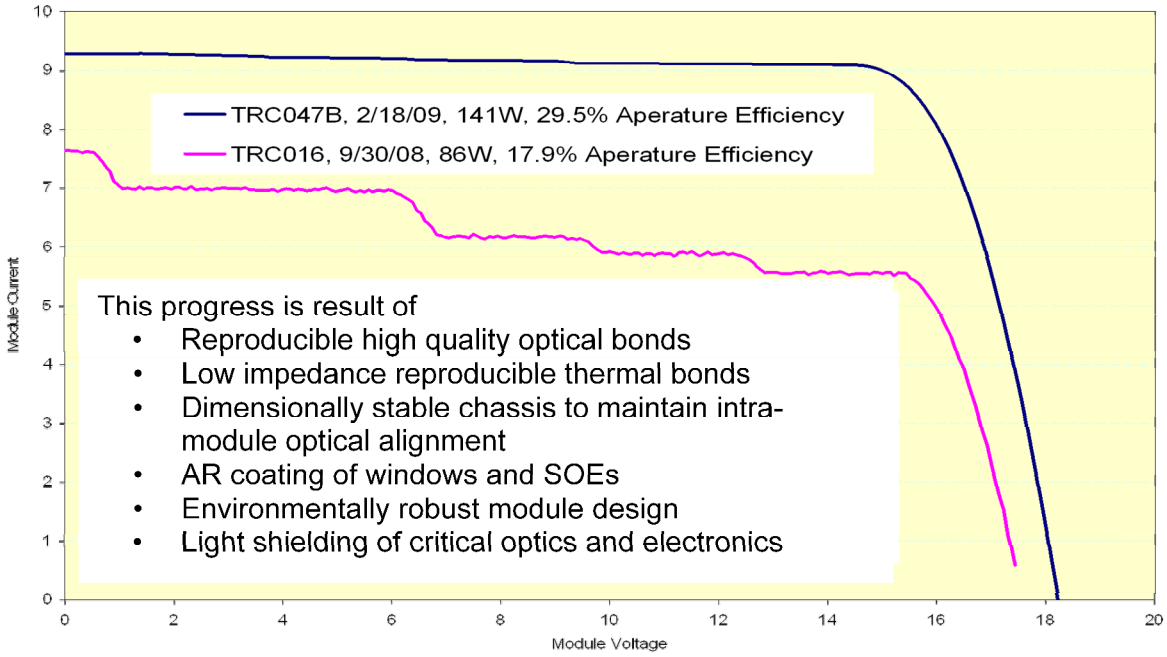

Figure 6-2. Performance of module TRC47B.

TRC47B basically represents the design point that was to become the POD array, for which module construction began in March of 2009. Future efficiency efforts focused on the upcoming POM and were centered on two design improvements.

- Implementation of advanced Specrolab cells.
- Further improvements in the optical efficiency through the use of AR coated SOEs.

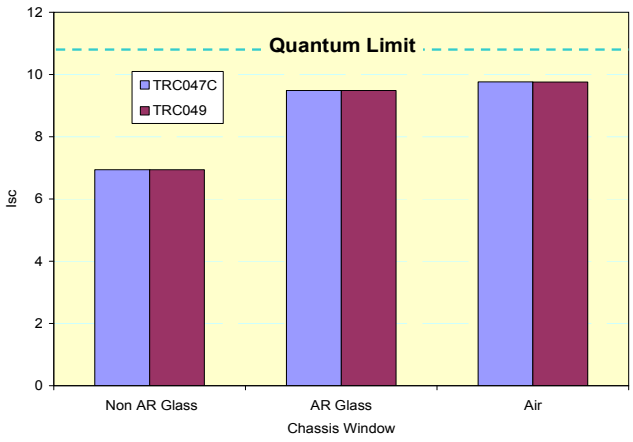

Figure 6-3. Effect of the AR coated window

The modules placed under test in this final phase of the proof of concept task are listed along with design and performance details in Table 6-3. Note that all modules in the table achieved fill factors of at least 80%. Also note that by this point the Nusil 3351 optical adhesive had been baselined. This decision was based on the successful qualification tests described in Section 3.1.2.3 and successful life test of the model that was shipped to NREL for independent testing (see Figure 6-4).

Table 6-3. POC modules tested to define the POM design.

	Module A	Module B	Module C	Module D	Module E	Module F	Module G
Cell	C3MJ	C3MJ	C3MJ	C3MJ	C3MJ	C3MJ	C4MJ
Optical Adhesive	3351	3351	3351	3351	3351	3351	3351
Thermal Adhesive	6534	6534	6534	4173	6534 @150°C	4173	6534 @150°C
SOE	Korea	Korea	Aura Coated	Comau Production	Comau Production	Comau Damaged	Aura Coated
Isolation			No RW tape	Kapton on RW to CCA Edge	Kapton Window on Heat Sink, Kapton on RW edge	Qualified HIPOT Design with Glass Beads in 3351	Qualified HIPOT Design
Mirrors	Stanley	EMF	Stanley	Stanley	Stanley	Stanley	Stanley
Heat Sink	Standard	Standard	Standard	Standard	Standard	Standard	Standard
Hipot			600	2000V	2200v	2200V	
Status	On test	On test	On test	On test	On test	On Test	On Test
FF	84%	80%	82.40%	83.80%	82.56%	82.70%	82.27%
Isc	9.28	9.72	10.3	9.57	9.62	9.69	10.75
Vmp	16.16	16.28	16.32	15.92	16.33	15.95	15.45
Pmp	144.4	142.5	158.4	147	147.8	146.06	156.28
Efficiency	30.1%	29.7%	33.0%	30.6%	30.8%	30.4%	32.6%

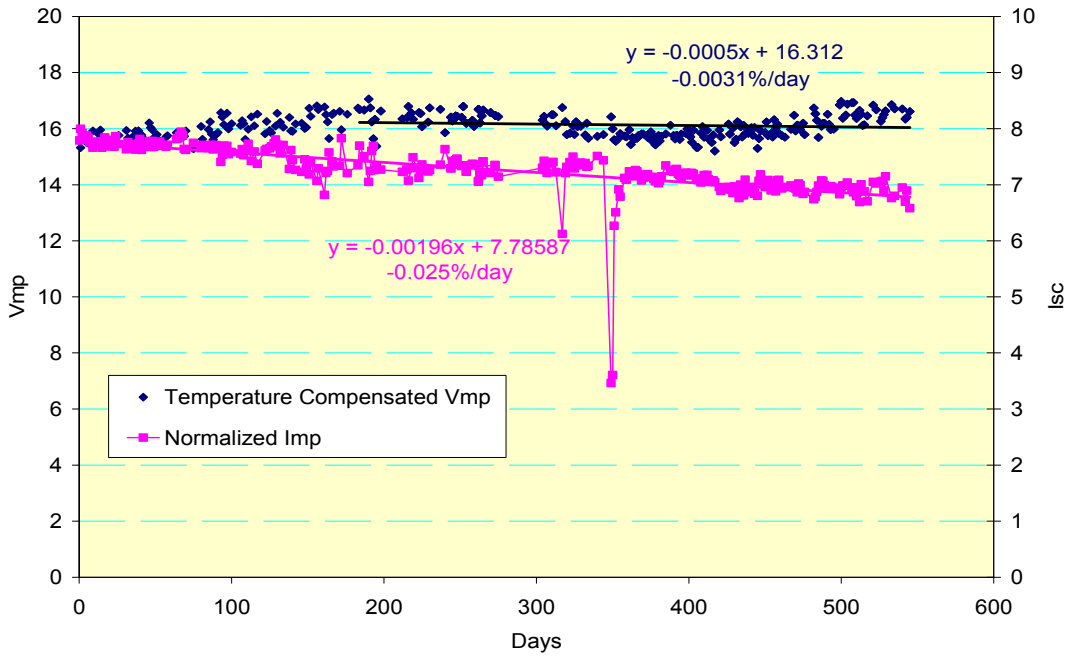

Figure 6-4. NREL module performance evolution. This module employed the LS 3351 optical adhesive. Note that the decline in Imp has been shown to arise for interior window contamination due to use of a non qualified caulking adhesive.

As can be seen in Table 6-3 the main variables in the design matrix are the triple junction cell, the SOE AR coating and the POE manufacturer. Only the first two would be expected to have a performance impact. The evaluation of the Stanley mirror was part of its qualification as lower cost alternative to the EMF POE.

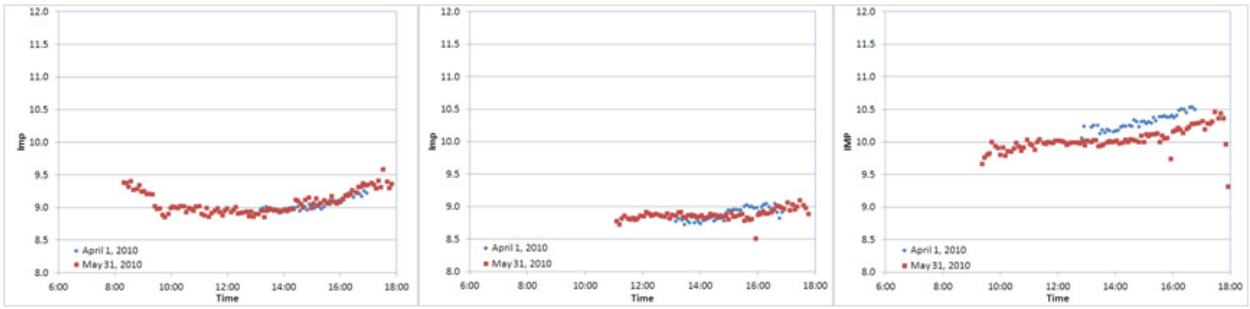

Figure 6-5. Variation in normalized peak power current for (left to right) C3MJ module D, C3MJ module E and C4MJ module G

Three of the modules in Table 6-3 deserve particular note:

- Module C - This module consistently demonstrated truly outstanding performance. At the time this was attributed to use of the new Auer AR coating on the SOE. This conclusion is supported by the outstanding Isc (10.3 A) which as determined with the Quantum Model was equivalent to optical 96.5%. Note that we were unable to duplicate this result in subsequent module built with the claimed equivalent Comau production SOE, however, other issues with this SOE may indicate that the design was not correctly transferred to the production process;
- Module D - This module is noteworthy as it incorporated all the design features of the POM module. While its performance can only be described as in family, it did promise a 116 kW demonstration power plant. It also served as a useful front runner yard stick for the performance over life of the demonstration power plant;
- Module G – This was the first module tested with the ultra high performance C4MJ cell. The Spectrolab development cell data indicated up to a 11% current increased partially counter balanced by a 5% experimental voltage decrease. In fact the quantum model optical efficiency of this cell is 92% indicating once again more run of the mill optics but with a much higher theoretical current. By the time of the Module G test we had been forced to commit to a POM design and thus the C4MJ cell did not make it to the power plant. Nonetheless its outstanding performance points to one of the most effective ways to increase module performance and lower LCOE.

One of the issues in classifying design performance is control of the test conditions. This has been a particular frustration in solar energy development where changes in both the DNI and the solar spectra lead to variations in the test data for multijunction cells. This issue is illustrated in Figure 6-5. The data illustrate the change in efficiency with time of day for early and late spring. What is changing between the three modules is the semiconductor and the SOE AR coating. Module D employed a first generation Auer coating and a C3MJ cell. As can be seen in Figure 6-5 there is a 7% relative efficiency diurnal change. This was brought to Auer's attention and a request made to

augment the transmittance of mid wavelength (500 to 1000 nm) light through their AR coating.

This was done for module E and as can been there is a 50% decrease in daily variation.

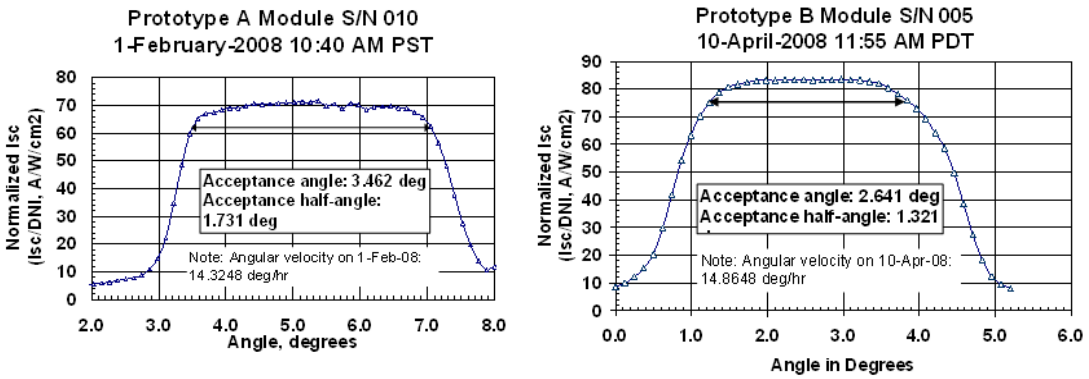

Figure 6-6. Azimuth acceptance angle axial (left) and off axis (right)receivers.

Module G employs the same SOE design as in E yet the variation in efficiency is, if anything, more pronounced through the course of the day. There is again 7% relative change in efficiency between 12:00 and 17:00. The reason for the reoccurrence (and in fact increase in total variation) is most probably due to the design J ratio greater than 1 in the C4MJ cell. In optimizing this cell Spectrolab boosted current of the blue top junction cell, which would have a favorable impact on designs which employ PMMA as the window.

6.4.2 Acceptance Angle

Compliance with this requirement was first demonstrated in early in feasibility hardware for both axial or off axis optics. These data are provided in Figure 6-6.

After we had achieved a mechanically and process stable design for POM and POF the test was repeated on TRC 47B as illustrated in Figure 6-7. Note that the half acceptance angle for the off axis design has increased from 1.32° to 1.48°, an indication of the improvements achieved in module design and fabrication.

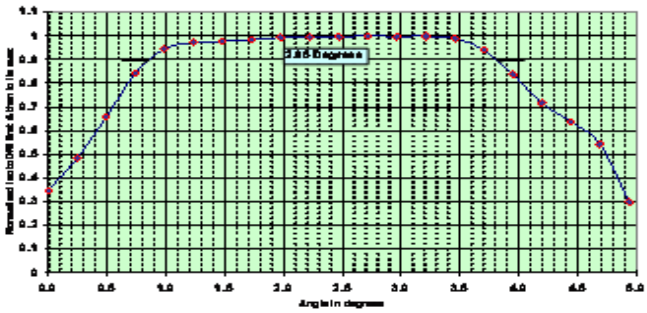

Figure 6-7. TRC47B acceptance angle

Once the POD array was complete we repeated the acceptance azimuth acceptance angle measurements and for the first time carried out an elevation acceptance angle measurement on the full array. The results are illustrated in Figure 6-8. Note that the half acceptance angle had decreased to 0.98° for the azimuth, an indication of problems encountered in building the POD hardware (see Section 7). The elevation half acceptance angle is slightly less (0.83°). The elevation angle is a more difficult measurement (the array must be moved) which may account for the lower value. In any event, once again the real issue was the variability of the hand build modules.

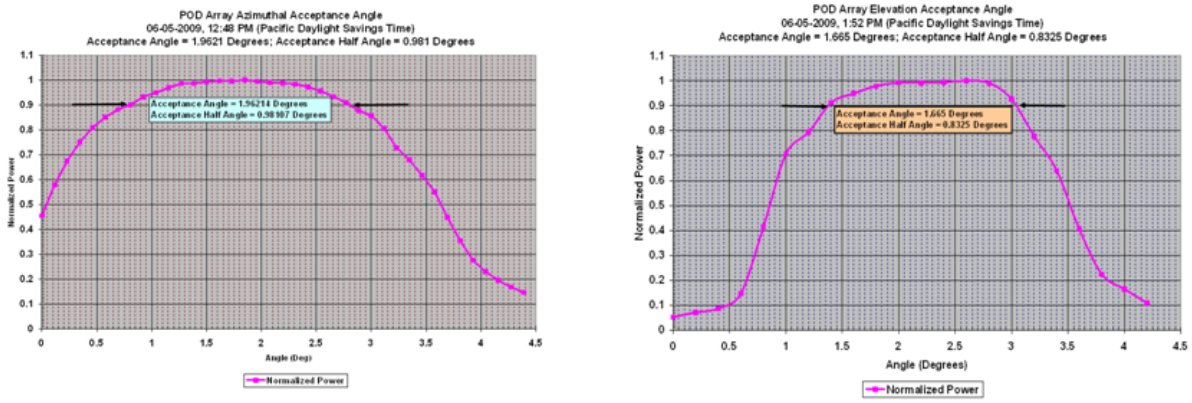

Figure 6-8. Azimuth and elevation acceptance angle measurements on the POD array.

6.4.3 Thermal Performance

The thermal design was validated in proof of concept tests for both the DC 4173 (thermal conductivity of 1.5 $Wm°C^{-1}$) and DC 6534 (thermal conductivity of 6 $Wm°C^{-1}$) adhesives. These measurements were carried out by:

- Converting the measured the measured quasi instantaneous Voc of a module operated under continuous peak power extraction to a temperature based on the Voc versus temperature measurements reported by Spectrolab as part of cell qualification;
- Scaling this temperature to the standard 1000 W/m^2 DNI from the measured DNI;
- Off setting the temperature to a 50°C ambient representing the worst case specification condition;
- No attempt was made to correct for wind speed but it was low, ranging from 2 to 5 mph during the course of the day for we report measurements.

The results for these measurements are presented in Figure 6-9 for module D employing the DC 4173 adhesive and module E with the DC 6534 adhesive. The figure also provides module efficiency, a good measure of thermal output. Based on average efficiency the two modules were operating with normalized average operational thermal outputs of 50.4 W and 50.7 W respectively (this number is based on out estimate of a 90% optical efficiency). The data in Figure 6-9 can be summarized as follows:

- Module D operated with an average cell temperature of 79°C (ΔT = 29°C). Our laboratory measurements had predicted a temperature gradient between the cell and heat sink of about 25°C with an additional 5°C gradient due to the heat sink. The results agree well with the lab test and certainly validate the integrity of the design;
- Module E operated with an average cell temperature of 70°C (ΔT = 20°C) as would be expected with the higher thermal conductivity adhesive. Once again the date agree well with development tests and validate the design against requirements.

Both modules show a higher ΔT in the morning than in the afternoon. We have observed this in numerous tests and attribute it to the start up of heat pipe as it basically "wakes up" and eventually reaches an equilibrium operation between heat source evaporation, heat sink condensation and wicking return of condensed water to the heat source.

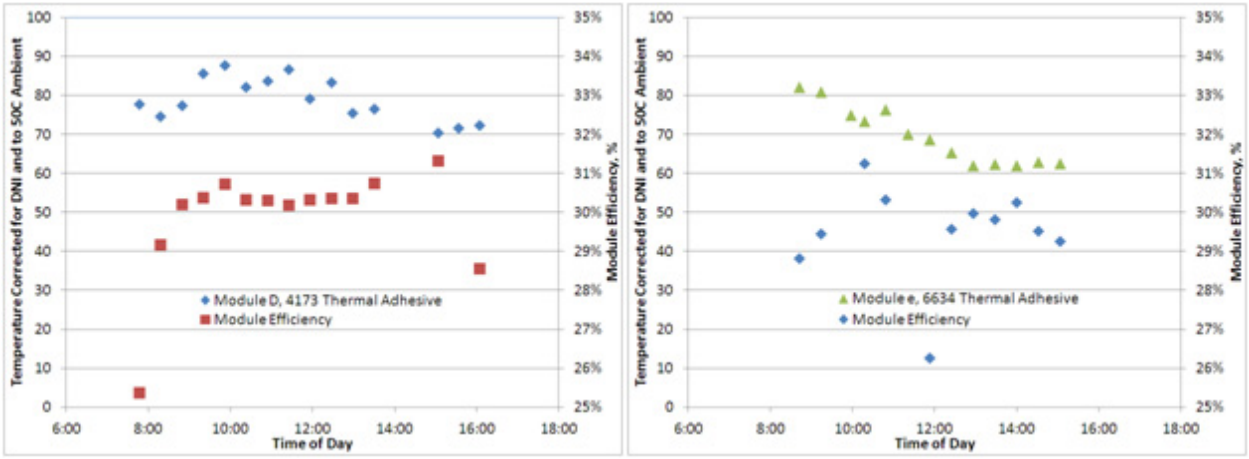

Figure 6-9. Verification of the thermal design for DC 4173 and DC 6534 thermal adhesive in POC testing.

As a final comment the temperature coefficient of the triple junction cell is 0.1% performance per °C. Thus a 40% cell becomes a 39.6% cell at 10°C above qualification. A module contains about $9.00 of the silver conductor DC 6534 adhesive and $1.00 of the alumina conductor DC4173. The value of 1% improved efficiency in a 160 W module with a $1.00 per watt metric is $1.60, far less than the added cost of the DC 6534.

6.4.4 Lessons Learned

Cell Tailoring – As described in this section based on the experimental behavior of Boeing test articles it appears that performance would be improved if the current balance between the top and middle cell were optimized with respect to the optical design of the hardware and actual (as opposed to an arbitrary standard) input spectrum.

Module Mechanical Stability – Cited in this section was the desirability of a self supporting module to assure correct module-to-module alignment. Not only is this critical, but an additional lesson learned was the criticality of maintaining the alignment of the intra-module optical components. Subsequent to this effort approaches have been developed for support the six receiver module in a non-stressed fashion which should reduce the requirements for module rigidity, and these approaches must be assessed with additional development.

Bond Design – During the development test activity many instances were encountered where inadequate attention had been applied to the engineering of adhesive bond lines. The first instance was when it was discovered that the optical and thermal bonds were not thickness controlled, rather, for example, the SOE rested literally on the tops of the gridlines to yield a bond line as thin as 10 microns. This in turn led to a highly inflexible bond wherein severe stress was transmitted by the glass kaleidoscope to the semiconductor as a result of CTE mismatch during temperature cycling and was ultimately able

to destroy the semiconductor. The mechanical, chemical, optical and thermal properties of a bond are critical to the performance of the hardware and must be correctly engineered in consultation with all relevant disciplines.

Solder Connections to the CCA – In the Boeing design with an integral heat sink soldering to the CCA has proven to be a very difficult and expensive process. While this process was successfully scaled up to automated production its reliability is uncertain and solder joints cannot in this assembly cannot be easily tested. A different approach to electrical connections such as that described in Section 4.4.1.is required.

Receiver Assembly – While high performance levels have been achieved with the Boeing receiver assembly, it has also been the source of numerous performance and reliability issues. This is true even of the finally evolved design built with automated equipment and deployed in a 100 kW demonstration plant. It is difficult to assemble reliably, difficult to test, and even in the receiver wall configuration difficult to handle and assemble into the module. A further redesign of this part is required to resolve these issues. Such a design has been demonstrated and is described in Section 4.4.

7 Proof of Design (POD) Fabrication – SOPO Tasks 1.10, 2.10, 3.10

Task Objectives

The objective of this task is to assemble proof-of-design arrays as required to demonstrate the production design performance and manufacturability. Subjectives include:

- Assemble proof-of-design arrays, modules, and other components as required to support system qualification tests;
- Itegrate POD arrays with trackers, inverter(s), and balance of plant;
- Perform field demonstration of the POD system to validate system performance.

Highlights

- Manual production facility established and 24 panel quality modules produced.
- 2.7 kW array demonstrated
- Boeing tracker and software demonstrated with the POD panel
- 216 W/m^2 demonstrated with C2MJ cell projects to 252 W/m^2 with C4MJ and improved mechanical assembly.
- High margin inverter design and rigorous testing complete.
- 260 kW inverter demonstrated and functional testing complete and independently witnessed by ELT.
- Commercial inverter deliveries initiated in 2009.

Table 7-1. Proof of Design (POD) Fabrication.

Period	Criterion	Results
2	2c-1) Demonstrate POD Array design performance with power output >250 W/m2 peak produced with pre-production tooling.	PPD array has been complete and on test since 2009. The demonstrated normalized peak power (2.8 kW) corresponds to 250 W/m^2 with a 40% cell and improved mechanical assembly. With demonstrated improved optics performance increased to 300 W/m^2.
	2c-2) Demonstrate pilot production of inverter.	260 kW inverted demonstrated and commercialization initiated.

Technical Accomplishments

7.1 Proof of Design Hardware and Test Configuration

The configuration of the POD modules and panel are as described in Section 3 with the following specific configuration details noted in Table 7-2.

Table 7-2. Configuration of POD Array

Design Element	Configuration	Section
Cell	C2MJ	1
Thermal Adhesive	DC 4173	3.2.1
Optical Adhesive	LS 6140	3.2.1
Window	Schott	3.2.2
SOE AR Coating	Korea	3.2.1
POE	EMF	3.2.2
Frame and Panel	Steel torque tube. Aluminum small beams	3.3.1
Module Attachment	Bolted	3..3.2
Environmental Control	Purging	3.2.3
Tracker	Inspira and Boeing	3.3.3

7.2 Fabrication Methodology / Process

7.2.1 Modules

A reprise of the module assembly procedure is provided below, Design details are provided in Section 3.

The first panel was manually assembled. Chassis assemblies (chassis, POEs, windows, etc.) were assembled by skilled mechanical technicians in an engineering lad environment. Low run wooden jigs were employed to assure correct assembly alignment.

Receiver wall assembly was split in two:

- Heat sinks CCAs were bonded together in a clean chemical lab environment and the adhesive cured in a laboratory oven;
- Completed heat sink / CCA assemblies were shipped to the engineering lab where they were sealed with caulk and mechanically attached the receiver wall and the inter-receiver and terminal bus strips solder to the CCA;
- The receiver wall was then returned to the clean assembly area and the receiver assembly completed by attachment of the SOE and light shield. This step included formation of the optical bond, structural attachment of the SOE and addition of a white caulking bead between the SOE and the receiver wall to act as a secondary external light shield.

The completed receiver wall was now returned to the engineering lab for final mechanical attachment and sealing of the receiver wall to the.

7.2.2 Panel

During the building phase of the array, the modules were installed symmetrically about the center torque tube to keep the structural loads balanced and minimize structural deflection, Table 7-3 shows the installation sequence. Figure 7-1 shows module number, module position number and module polarity configuration on the array tracker.

All the modules were individually aligned when mounted to the tracker. This .was accomplished by normalizing the tracker with respect to the sun, loose mounting of the module to the panel frame mounted on the tracker and finally careful alignment and firm attachment to frame with a manual sun site mounted on the module window surface.

After installation and alignment each module was performance tested a minimum of three times daily. Each test consisted of an I-V curve performed with an Agilent N3300A DC electronic load.

Table 7-3. Array tracker module installation sequence

Installation	Qty	Modules
1	3	1,2,12
2	3	13,23,24
3	6	3,4,11,14,21,22
4	6	5,6,10,15,19,20
5	6	7,8,9,16,17,18

Several checkouts were performed per document number SAI_SOP000008 (SB Test Site POD Array Test Procedure) in preparation for 24 modules in series connection, see section 3.4.2. The fully assembled array (1 array =24 modules) is shown in Figure 7-2.

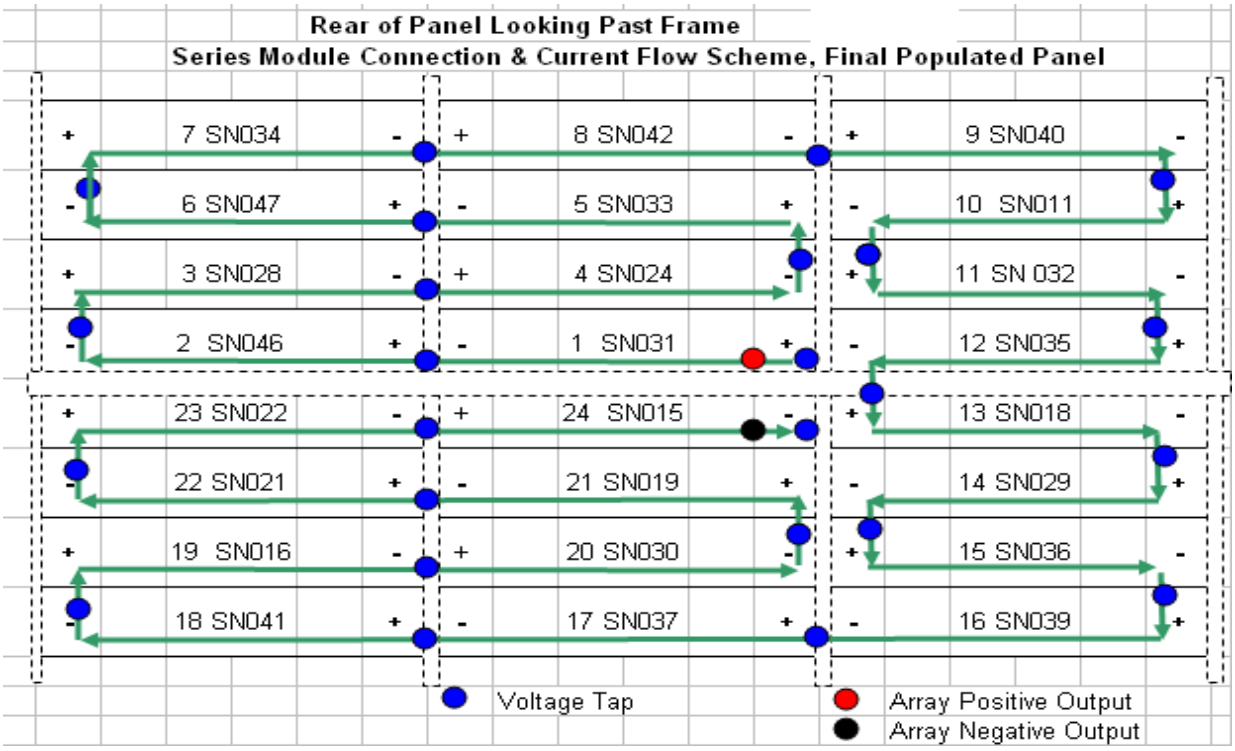

Figure 7-1. Fully assembled array configuration

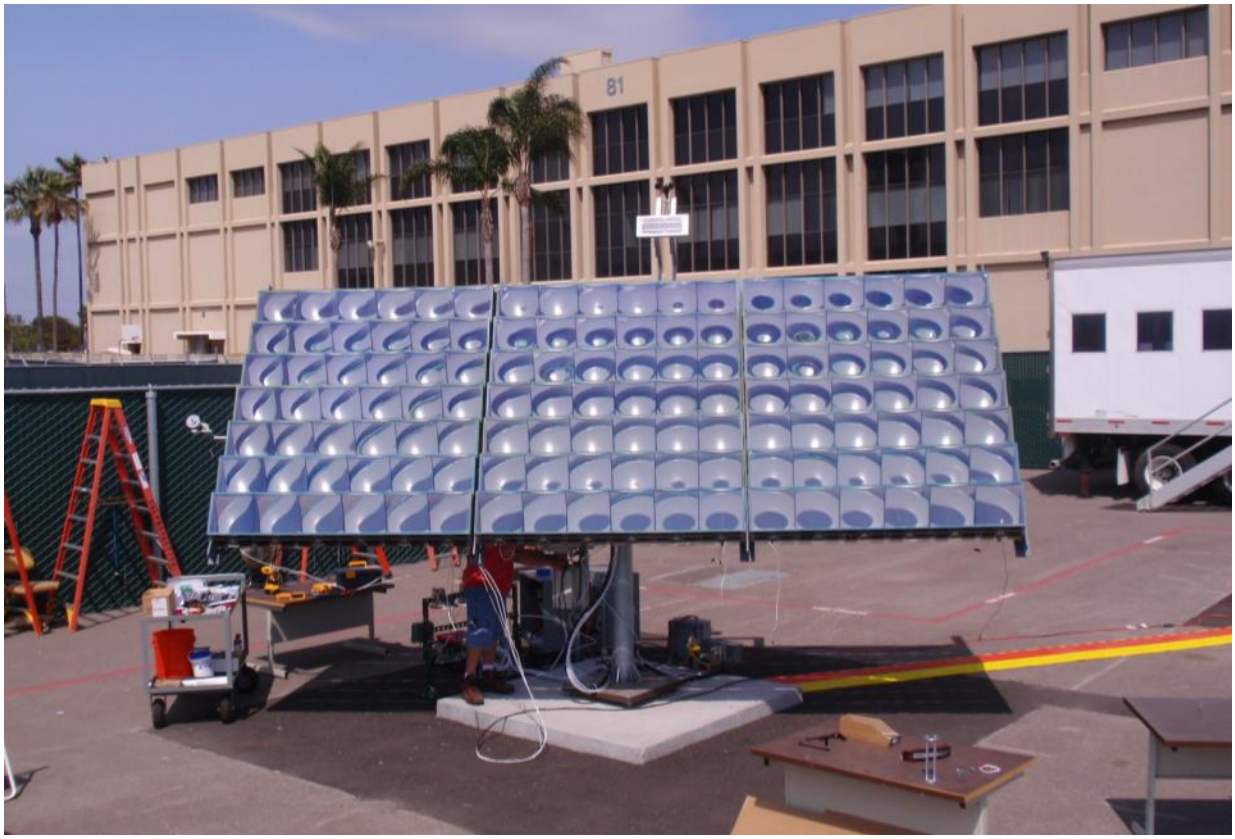

Figure 7-2. POD array at full assembly.

7.3 Component and Module Test Plan

7.3.1 Component Test

All components were built to released engineering documentation. As appropriate they were subjected to first article inspection and in process inspection by the assembly technicians. In general this problem worked, defective parts rejected and no assemblies were identified as result of use of bad parts. No doubt this is large part due to the determinate assembly

7.3.2 Module Test

A great deal of effort in both POD and POM was put into developing a means of in line module acceptance test in the production environment.

7.3.2.1 In Line Searchlight Module Acceptance Testing

The intended purpose of the spotlight test was to verify that the power generating circuit of each receiver on a fully assembled module is functional (generating electrical power) and that receiver to receiver Isc was matched to within 0.25 A. The acceptance criteria for each module is for each receiver in the power generating circuit to generate an electrical current of two amps (2 A) or greater.

An SPL SX-5 (500W xenon lamp 2deg – 10deg adj. focus at 15 ft) searchlight positioned 7’10.5’’ from the glass surface of a module was used to perform a search light test. The module was set in the test setup with the receiver wall facing up, this ensured

that there was no damage done to the receiver wall during module test set up installation, Figure 7-3 shows a module mounted on the test setup. Using a digital level the alignment of the module was verified by measuring the angle on the glass face of the module. The alignment was within half a degree of vertical. The glass face of the module was covered in such a way that only the mirror to be tested was exposed to light. If facing the module, position one is on the right end of the module.

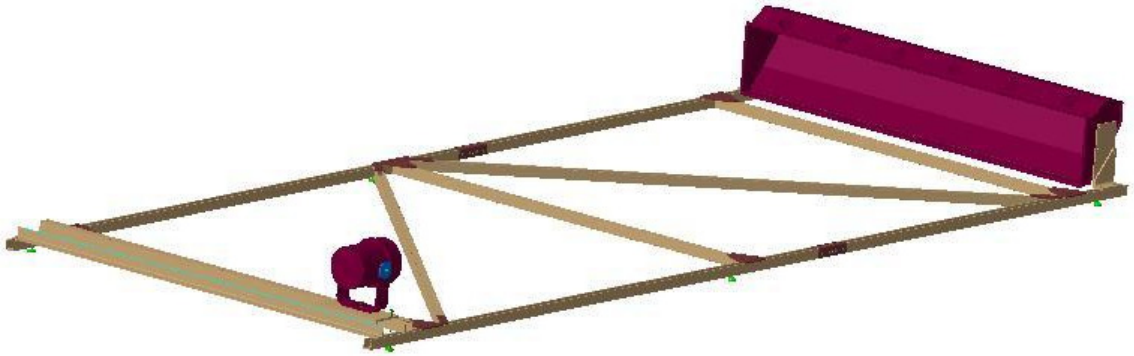

Figure 7-3. Search light test set up.

The searchlight was positioned in front of the mirror-receiver to be tested. Current and voltage (voltage sweeps) data was acquired through an Agilent N3300A system DC electronic load. The left side of Figure 7-4 shows a typical IV curve for one receiver. The search light test was continued until the remaining five receivers were individually tested, as shown on the right side of Figure 7-4.

As mentioned the objective of the test was to assume matching of receiver to receiver Isc within a given module to assure that the high fill factor. Unfortunately, the accuracy of the search method was not sufficient to achieve this as determined by in sun module acceptance testing.

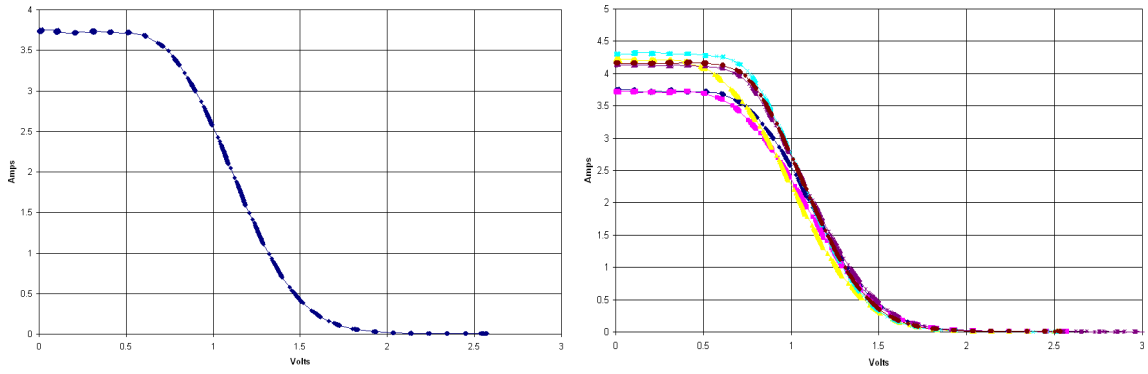

Figure 7-4. Search light IV curves for a single receiver and all 6 receivers in a module.

7.3.2.2 In Sun Module Acceptance Testing

The purpose of the sun exposure test was to verify that the power generating circuit of each fully assembled module is generating electrical power. The acceptance criteria for

each fully assembled module was that it generate an electrical current of six amps (6 amps) or greater and a power of 110W.

Figure 7-5. Sub exposure test using the module wooden cradle

There are two different setups for doing sun exposure test on a module. The first setup allows for a quick sun exposure test. It was performed by mounting a module on the module wooden cradle and placing the module wooden cradle to a flat surface (table with wheels or cart, see Figure 7-5). The module was set in a location where it was fully exposed to sunlight. The glass face of the module was aligned to the sunlight using the module alignment tool. The module alignment is correct (optimum) when the sun spot is centered at the target location of the module alignment tool.

Figure 7-6. Modules mounted on the array tracker for testing.

Current and Voltage (Voltage Sweeps) data was acquired through an Agilent N3300A system DC electronic load. The data was reduced and plotted to show I-V and Power curves.

The second sun test was carried out at the test site. The modules were mounted and aligned to the array tracker. Module performance (IV curves) was measured over the course of at least a day against the previously mentioned pass fail criteria. Modules which had passed the acceptance test were generally left in place for what would eventually become the POD panel assembly. Figure 7-6 shows modules mounted on the array tracker which have undergoing the acceptance test and have become part of the partially assembled POD panel.

Current and Voltage (Voltage Sweeps) data was acquired through an Agilent N3300A system DC electronic load. The Data was reduced and plotted to show I-V and Power curves, Figure 7-7 shows typical I-V and power curves of a module installed on the array tracker.

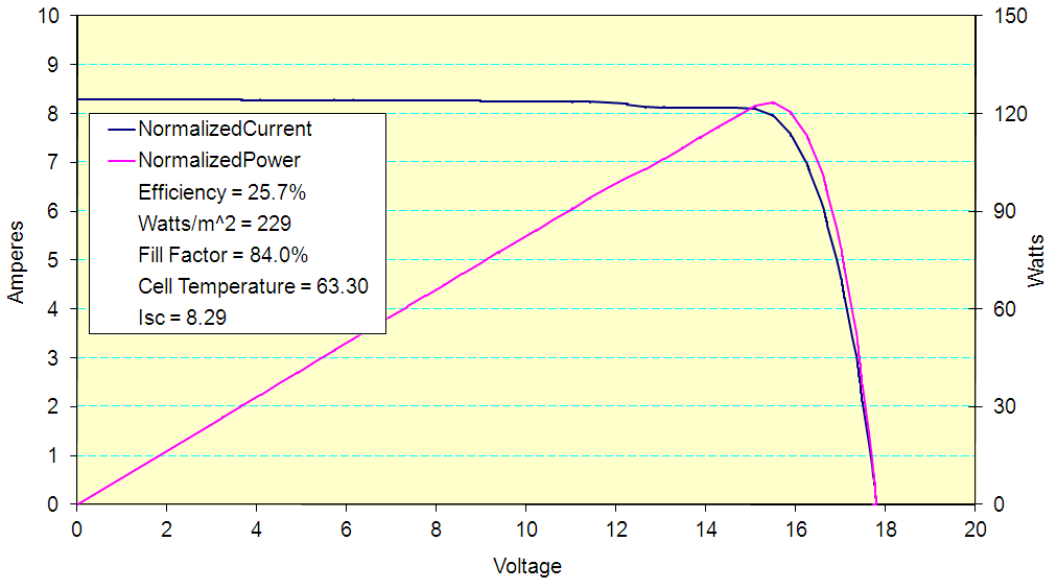

Figure 7-7. Typical IV and power curves for a module installed on the array tracker.

This method clearly yielded unequivocal results with respect to the module performance. Its application to array assembly is described in Section 7.4.1.

7.4 POD Array Test Results

7.4.1 Module Acceptance Test

Final acceptance testing of all modules took place in Seal Beach on the Array tracker. The test data for the 24 modules accepted for array assembly are provided in Table 4

The Isc and Voc of the modules are pretty tightly grouped, particularly when compared to the maximum power, fill factor and efficiency. This is a clear indication of the already described mechanical issues encountered in the hand assembly of the modules. These assembly issues lead to misaligned receivers within modules, voltage steps and a reduced fill factor. As can be seen in Figure 7-8 there is a very direct correlation between fill factor and conversion efficiency.

7.4.2 Array Test

7.4.2.1 Grid Connection

The Boeing Seal Beach Solar Test Site has been equipped with a 3KW grid connection system to demonstrate the capability of the Boeing CPV Array to connect to the grid; for such demonstration an inverter has been installed and connected between the POD Array and the utility grid.

Table 7-4. Acceptance test data for the 24 modules built into the POD array.

SN	Temp	DNI	Isc	Voc	Pmp	Fill Factor	Efficiency
11	20.01	802.3	8.33	17.67	118.3	80.3%	24.6%
15	20.85	908.8	8.52	17.75	120.2	79.5%	25.0%
16	20.56	808.7	8.41	17.62	111.6	75.4%	23.2%
18	20.26	917.4	8.58	17.81	119.2	78.0%	24.8%
19	20.97	910.2	8.40	17.77	119.7	80.2%	24.9%
21	20.62	889.3	8.60	17.74	127.3	83.4%	26.5%
22	20.69	898.7	8.38	17.73	108.0	72.7%	22.5%
24	20.30	810.2	8.57	17.49	116.7	77.9%	24.3%
28	20.42	813.1	8.64	17.51	118.6	78.4%	24.7%
29	20.40	910.2	8.54	17.74	114.3	75.5%	23.8%
30	20.44	809.5	8.57	17.79	119.7	78.6%	24.9%
31	20.29	810.2	8.43	17.84	105.2	69.9%	21.9%
32	19.83	805.9	8.69	17.61	114.8	75.0%	23.9%
33	20.28	809.5	8.38	17.56	115.2	78.3%	24.0%
34	20.43	909.5	8.74	17.42	118.6	77.9%	24.7%
36	20.07	807.3	8.20	17.85	114.3	78.0%	23.8%
37	20.52	805.9	8.61	17.94	122.2	79.1%	25.5%
39	20.13	801.6	8.62	18.10	123.9	79.4%	25.8%
40	20.25	804.4	8.41	17.74	119.5	80.1%	24.9%
41	20.85	806.6	8.59	18.06	126.9	81.8%	26.4%
42	20.25	808.0	8.48	17.49	123.3	83.1%	25.7%
45	20.83	797.2	8.55	17.73	104.6	69.0%	21.8%
47	20.64	798.0	8.77	17.48	121.0	78.9%	25.2%
48	20.73	809.5	8.69	17.75	122.2	79.2%	25.4%
Average			8.53	17.72	117.71	77.9%	24.5%
% St. Dev.			1.6%	1.0%	5.1%	4.6%	5.1%

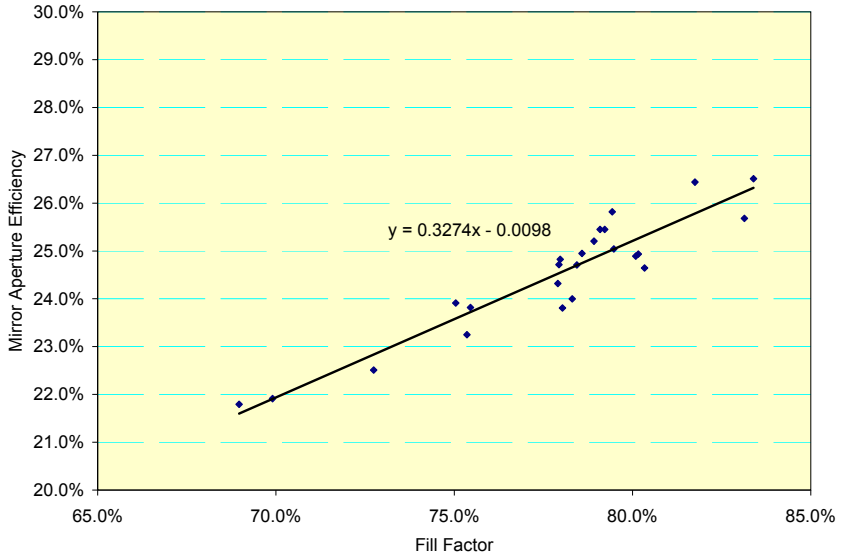

Figure 7-8 Relation between fill factor and efficiency for POD array modules

Inverter System – The inverter system selected is model PVP4600 manufactured by PVPowered, Bend, OR from their Grid Tied Residential Inverters Series which are utility interactive inverters for photovoltaic (PV) systems.

The inverter is tied to an electrical source provided by the local utility company as well as to the CPV system. The inverter contains everything needed to convert the DC voltage generated by the Boeing POD Array into the proper AC voltage required for grid connection.

A PVP4600 System Block Diagram is shown in Figure 7-9

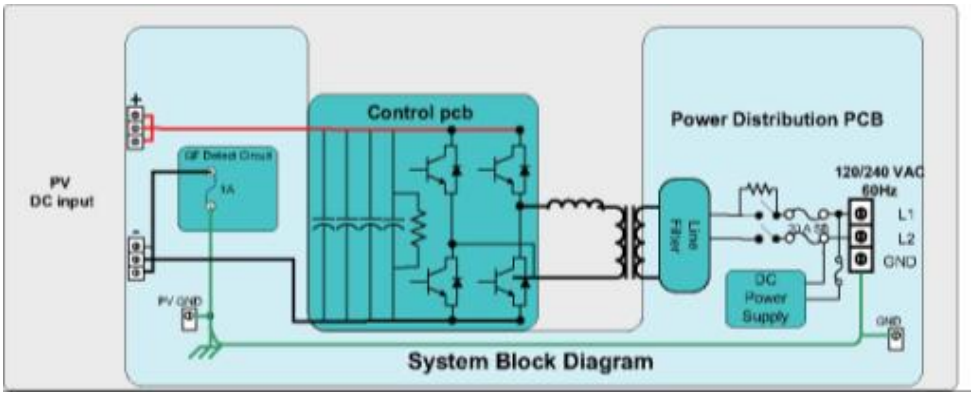

Figure 7-9. Inverter block diagram.

The PVPowered inverter has the following features:

- It is suitable for both indoor and outdoor installation in a NEMA 3R rated enclosure.
- The operating and non-operating environmental ambient temperature range is -15°F to 105°F (-25°C to 40°C).
- A Ground Fault Interrupter (GFI) circuit is to detect a ground fault (unintended current flow from the PV arrays to earth ground). The GFI works by using a fuse to connect or bond the PV array negative to earth ground through the 1A fuse.
- The PVM1010 Data Monitoring Module which is a data acquisition and communications interface accessory for on-site monitoring to access inverter performance information using standard open UDP protocol.

Inverter/eLoad Relay –_During array testing, the inverter is connected and disconnected from the array by a relay that, under load, switches the output of the array from the inverter to the electronic load to collect I-V curve data. The relay is controlled by a discrete output generated by the data and control system. The relay is a 500VDC make/break load switching relay rated at 30A. The Gigavac model G18WP was selected for its tungsten contacts, its internal dielectric shield and its user interchangeable coil features.

Electrical Instrumentation – The electrical instrumentation box (Figure 7-10) contains:

The shunt – interfaces to the instrumentation system to read current data from the voltage of the array under test.

The inverter/eload relay – selects the destination of the array voltage during performance testing.

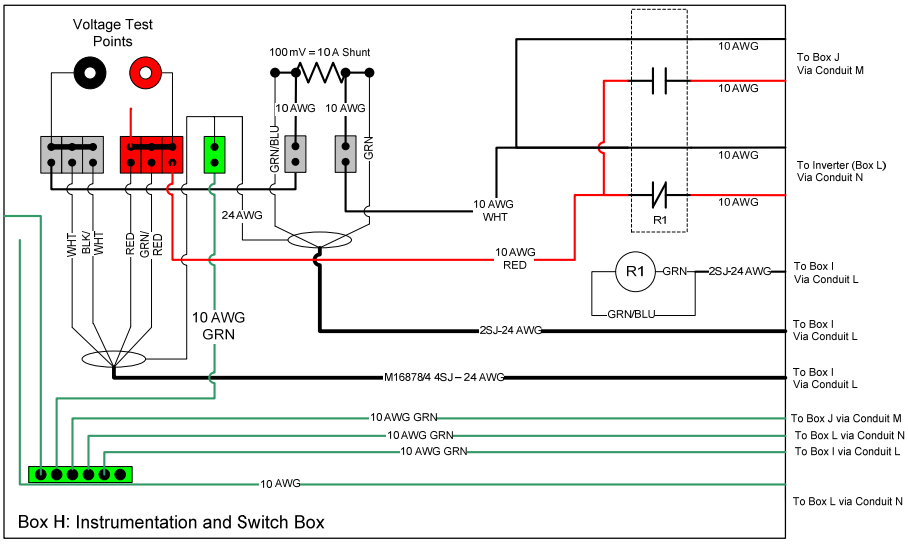

Figure 7-10. Electrical instrumentation box

Array Disconnect Switch – The array disconnect switch (Figure 7-11) is a 3-position Square D double throw safety switch, p/n DTU 362RB to allow control of the array high voltage.

The disconnect switch positions are:

- Short : to connect the positive and negative leads together therefore creating a safe working environment
- Open: to open the connection between the array and the load (inverter or eload) for Voc measurement.
- Active: to connect the array in test to the inverter/eload relay that will direct the array output as selected by the system operator.

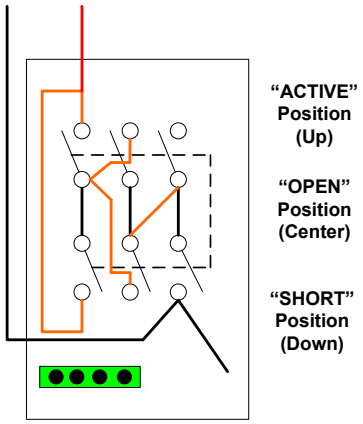

Figure 7-11. Array disconnect switch.

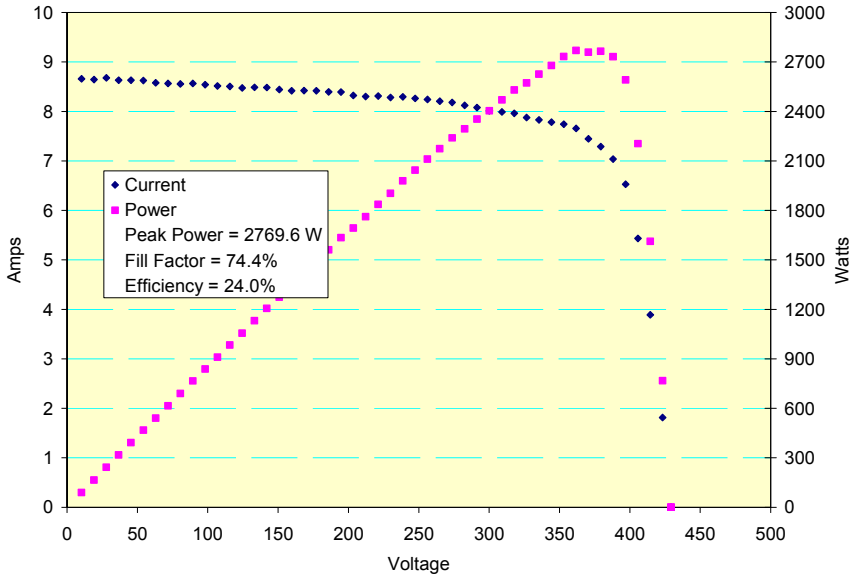

Figure 7-12. Initial array performance.

7.4.2.2 Operational Electrical Characteristics

Startup – The array reached full voltage on the afternoon of 5/14. A typical IV and power curve for the afternoon of 5/22 is presented in Figure 7-12. The array is delivering a 1000 W/m^2 normalized 2770W with a 37.5% cell. Normalized to a 40% cell the array would deliver 2955 W or 219 W/m^2 based on window area. The measured power is 54 W less than that predicted by simple addition of the individual power values listed in Table 7-4.

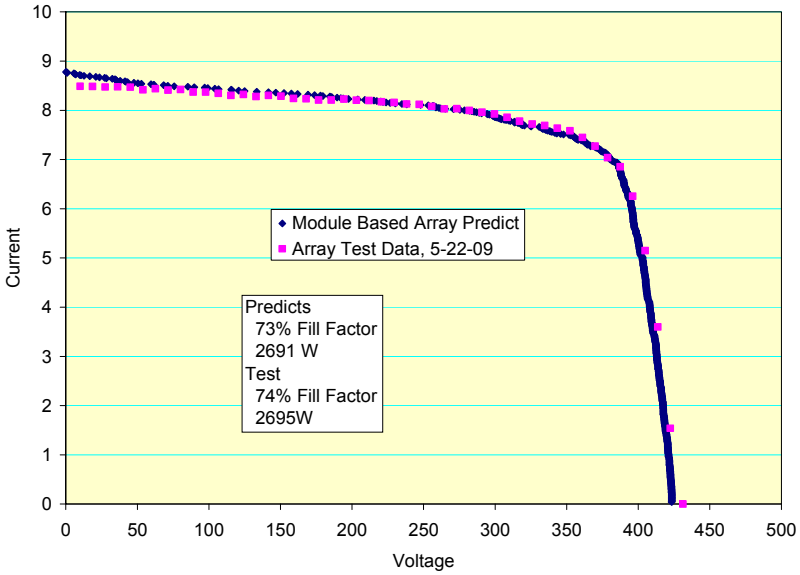

Figure 7-13 Output of the array tool compared with array experimental IV data.

In order to analyze the performance of the array and develop means of improving both its performance and that of future modules an array prediction tool was implemented to predict array performance based on module acceptance test. The tool computes at fixed current the output voltage of all array modules based on empirical acceptance test data. The agreement of the tool with measured performance is shown in Figure 7-13.

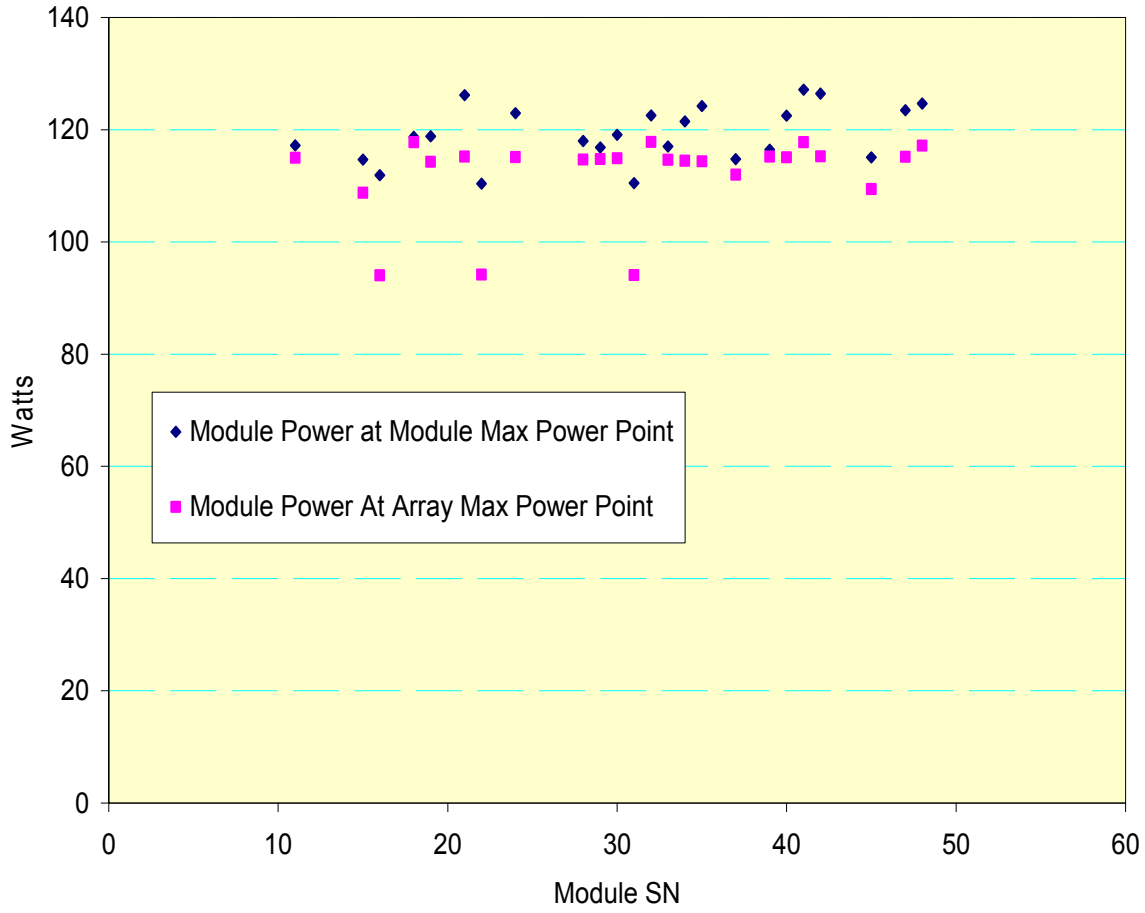

Figure 7-14. Module performance at the array and the module peak power points.

The first use of the tool was examining if there was any value in replacing some of the weak modules used to build up the array with stronger modules. The answer was basically to with respect to achieving a significant benefit. Examining Figure 7-14 it is clear that three of the modules (16, 22, and 31) are significantly out of family. Analysis of the array using the tool showed that replacing these three modules with clones of module 41 yielded a array peak power increase of 71 W (as compared with increase in individual module peak powers 50 W at their individual Vmps).

One characteristic that is worthy of comment is the time of day dependency of the peak power. In Figure 7-15 it can see that the output power of the array increases by about 100 W between 2:00 pm and 5 pm. For purposes of criteria reporting we employ a 3:00 pm value. This characteristic of the array is almost certainly a result of changes to the solar spectra with time of day

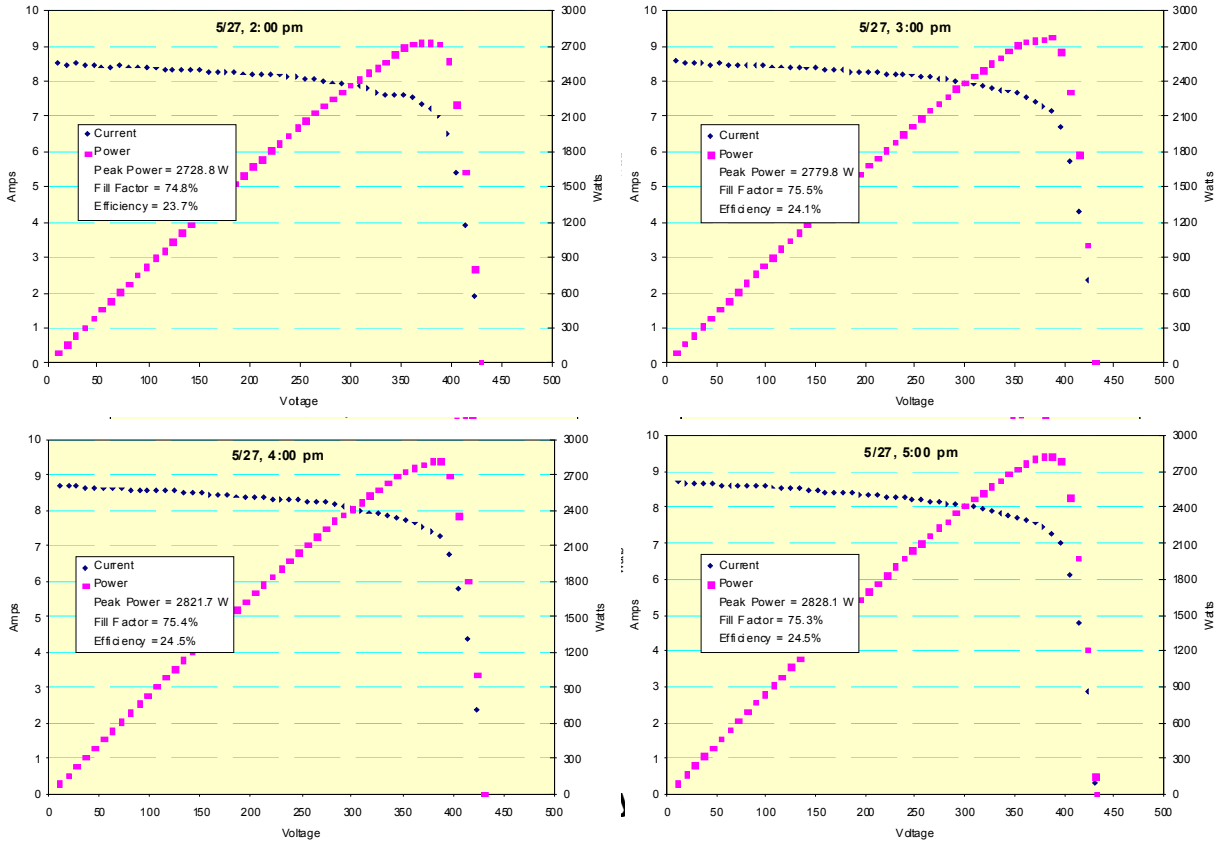

Figure 7-15. Effect of time of day on panel performance

The array was first put on the grid on 5/14/09, the day it reached full voltage. Teething problems delayed routine grid connecting for about 10 days but by the end of May the array was routinely connected to the grid. Except for special tests and O & M the array has since been continuously grid connected.

Table 7-5. Performance improvement road map

	Measured	40% cell	Fill factor	Optics
Array W/m^2	218	230	253	265
Panel W/m^2	243	260	283	298

The peak BOL power measured on the POD array was 2800 W after normalization to 1000 W/m^2. This corresponds to 218 W/m^2 for the array and 243 W/m^2 for the collector (POE) aperture. Normalized to a 40% cell the two values are increased to 230 W/m^2 and 260 W/m^2. This demonstrates compliance with Criteria 2c-1. As shown in Table 7-5, technologies subsequently demonstrated in the pre-POM concept maturation substantially increased the values achieved in POD. In this later phase modules were tested at up to 340 W/m^2.

7.4.3 Array Life and Life Analysis

Since commissioning the POD array has been on test for approximately 2.5 years. Its performance history through life is provided in Figure 7-17. Peak power has decreased by approximately 20% over the 2 plus years of test data in the figure. Early in the life of the array it was determined that there was a gradual obscuration of the window occurring because caulking employed at the circumference of the SOE was out gassing and the products of the out gassing condensing on the window.

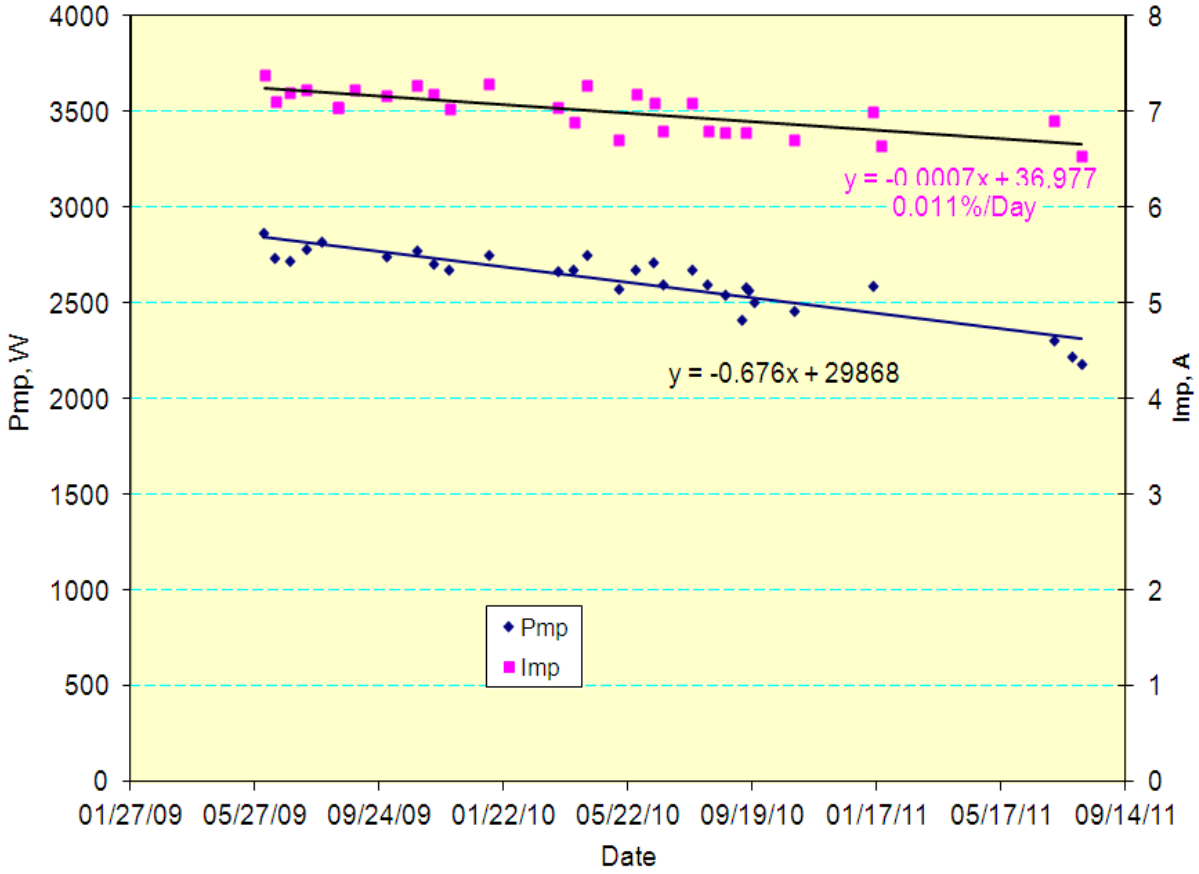

Figure 7-17. Performance of the POD array over its first 2.5 years of life.

In 2011 further characterization of this was carried out through a DPA of one of the modules. The module was removed from the array, its window and receiver wall removed and the POE and receiver separately tested against well characterized substitute components. The results of this characterization are provided in Table 7-6.

As can be seen in Table 7-6 the component performance of both the receiver wall and the chassis assembly (less window) are actually superior to the performance measured in 2009. Thus we can unequivocally establish that the cause if the performance decline is due to the window fogging. Nothing in the performance of these components detracts from the ultimate promise of the technology as a long life renewable power source.

Table 7-6. Component characterization results for a POD array module.

	Date	Isc	Voc	Imp	Vmp	Pmp	FF	DNI	Eff.
Performance April 2009	9-Apr	8.71	17.75	8.18	15.08	123.57	79.99	878.54	25.7%
Performance January 2011	11-Jan	8.47	17.49	7.31	15.30	111.71	75.40	878.73	23.3%
Performance of 24D Receiver Wall	11-Jan	9.51	17.58	9.71	15.05	132.66	79.22	907.64	27.6%
Performanc of 24D w/o Window	11-Jan	9.48	17.77	8.55	15.39	131.51	78.18	903.94	27.4%

[redacted] Test Data.xls

7.5 Inverter Demonstration

7.5.1 Overview

The SETP 260kW solar inverter has been designed, prototyped, and tested through the first of three phases of product release testing. Overall performance has been achieved consistent with the initial design, performance, and reliability specifications. Functional testing is underway in PVP's new engineering lab. PVP's new facility has all the space and power required to support and manufacture large commercial-sized inverters. UL compliance certification to UL1741 is expected to be completed by mid-July 2009.

7.5.2 Functional Testing Schedule

PVP employs a three stage process for moving an inverter design through the final stages of engineering and though UL compliance testing. The detailed test matrix for all phases has been shared by PVP with Boeing previously. A high level summary of the test matrix is provided below for edification:

Table 7-7. Summary of inverter qualification test matrix.

Function	Pre-Functional	Functional	Compliance
1.0 External			
1.1 DC input	✓	✓	✓
1.2 AC output	✓	✓	✓
1.3 Power generation, tracking and efficiency	✓	✓	
1.4 Thermals	✓	✓	✓
1.5 Monitoring and control	✓	✓	
1.6 Electrical safety and grounding	✓	✓	✓
1.7 Install error protection	✓	✓	✓
1.8 Physical	✓	✓	✓
1.9 State machine	✓	✓	

1.10 Fault and state handling	✓	✓	✓
2.0 Internal			
2.1 DC input	✓	✓	
2.2 AC output	✓	✓	✓
2.3 Thermal	✓	✓	✓
2.4 Monitoring and control	✓	✓	
2.5 Electrical safety and grounding	✓	✓	✓
2.6 Install error protection	✓	✓	✓
2.7 Subsystems	✓	✓	

The first phase was pre-functional testing, the initial 200-step test cycle designed to insure that the inverter performs according to requirements as specified in the Market Requirements Document (MRD) and UL1741 standard. This stage was performed by the design team at PVPowered. All issues uncovered during pre-functional testing closed via subsequent control algorithm tuning, firmware bug fixes or other small modifications.

The second phase, called functional testing, was performed by the reliability at PVPowered. This 175-step test cycle was designed to confirm the inverter meets all functional test requirements

The third test phase, UL Compliance testing (UL1741), will begin immediately after functional testing is completed. The test plan that ETL/Intertie has proposed to PVP is expected to require three weeks of testing. This suggests that UL certification will be completed the week of July 13th.

7.5.3 Thermal Systems Results

Over the period of this program, PVP collaborated with Boeing on reliability engineering of the 260kW inverter. PVPowered's overall approach to using thermal studies as part of reliability engineering is summarized in Figure 7-18 below.

The 260kW time-dependent thermal model is essential for developing and validating the blower control algorithm and for simulating climates that are not reproducible in our lab (e.g. very cold climates).The time-dependent thermal model takes into account self-heating, conduction, and convection using standard physical relationships. The differential equation set is solved in Matlab using simple forward-difference discretization with a time step of 1 second. Thermal coefficients are determined by matching steady state solutions to long-duration thermal tests. An example of the data output from a thermal modeling run is shown in Figure 7-19. Temperatures from specific points within the inverter are tracked, which enables assessment and refinement of thermal control algorithms in software prior to coding them into inverter firmware.

Physical measurements on an operating inverter are then performed, and compared to the modeled predictions. Some thermal performance issues were revealed in early thermal systems tests. Most issues were addressed with simple tuning and refined parameterization of the thermal controls. Concerns about magnetics temperatures necessitated the addition of a temperature sensor on the output inductors. Table 7-8

summarizes recent measurements and compares them to predicted values. It can be seen by inspection between the measured and predicted values that the overall thermal model is accurate, and suitable for thermal controls development.

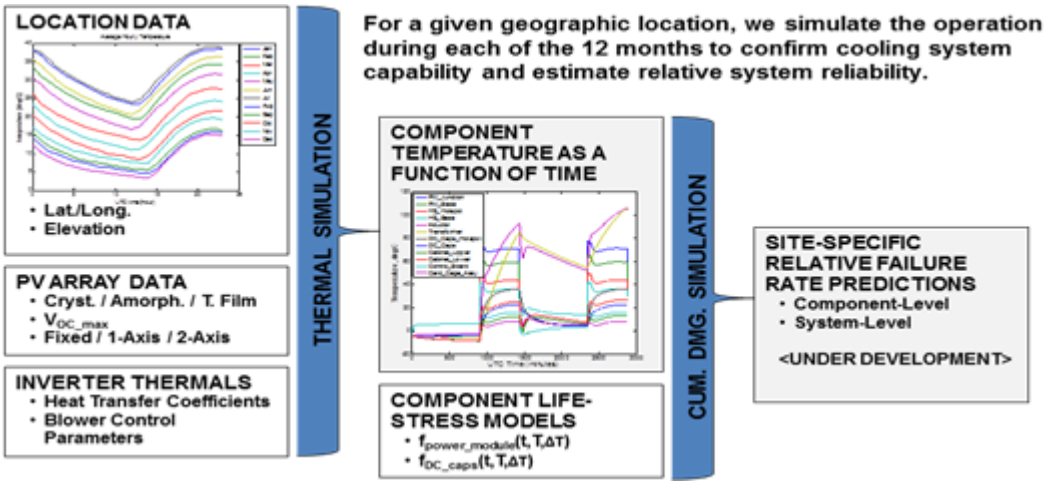

Figure 7-18. Time-dependent thermal and reliability modeling approach used in the development of the SETP 260kW inverter

7.5.4 Electrical Systems Results

The electrical systems of the SETP 260kW inverter have been completed and thoroughly tested. A few of the key results are summarized here.

7.5.4.1 Power Drive Protection Tuning

The inverter power drive must be tuned for over-current and desaturation protection. The over-current condition is determined by monitoring the CTs which measure the output currents (LEMs). The IGBTs are rated to sustain 2X the 2800A rated current indefinitely. The SAI 260kW inverter uses two IGBTs per phase, and the maximum current experienced by an IGBT at full power output is 1510A. The over-current protection threshold was set to 2000A within the inverter firmware.

Desaturation is also monitored to protect the IGBTs against voltage overshoot conditions. PVP is using a Powerex gate drive circuit in the 260kW inverter, and this circuit has built-in desaturation detection. Desaturation can occur during a short circuit condition. The test results shown in Figure 7-19 reveal that voltage overshoot does not exceed 440V, thus ensuring that damaging overshoot will not occur under the worst case conditions.

7.5.5 Ripple Filter

In order to minimize injection of excessive harmonics into the AC output of the inverter, a ripple filter is required. This filter must be stable under all operation conditions, including those with multiple inverters in close proximity. It must attenuate the ripple current on the grid by at least 2.5X, or 8dB. The design was guided by using stability criteria from control theory, which suggests the phase angle be greater than 135° when the gain is 1 (0dB), and the gain should be attenuated by greater than 8dB when the phase angle reaches 180°. The inverter switching frequency is 8kHz, so this is the primary target for attenuation, along with expected harmonics. Mathematical modeling was used to

design the appropriate filter, and the predicted performance was correlated to experimental results. The attenuation achieved is approximately 6X (16dB) at 8kHz. The output power loss varies between 370 to 470W total. Further attenuation is possible, but will require higher power dissipation. So the end result is a trade-off between sufficient attenuation of harmonics and minimal power loss.

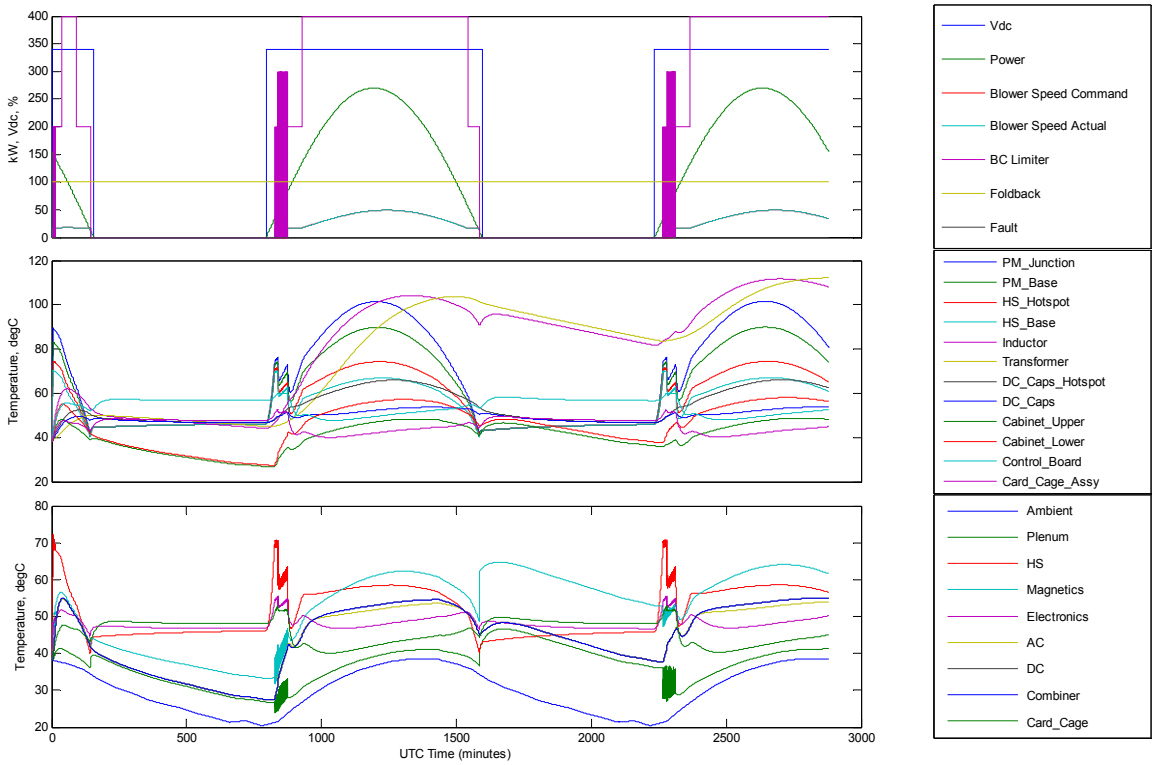

Figure 7-19. Temperature simulations taken at a variety of test points within the 260kW inverter. These behaviors are analyzed and used to tune the thermal controls for maximum performance and inverter lifetime.

Table 7-8. Airflow temperatures at exit of compartments.

	TC	MEAS	PRED
Ambient Inlet	201	16.1	16.1
Plenum	219	17.4	17.1
Heat sink	220	27.2	26.8
Magnetics	119	29.0	30.8
Electronics	203	24.1	20.1
AC	102	23.6	22.1

DC	101	26.8	22.7
Combiner	202	28.6	22.7
Card_Cage			17.8

Parts Temperatures	TC	MEAS	PRED
PM_Junction			70.6
PM_Base			58.9
HS_Hotspot			43.5
HS_Base	<AVG>	36.2	36.3
Inductor	120	53.5	54.1
Transformer	206	46.0	45.9
DC_Caps_Hotspot			36.8
DC_Caps	<AVG>	22.1	23.3
Cabinet_Upper	104	16.1	21.6
Cabinet_Lower	105	24.5	27.1
Control_Board	112	24.1	24.6
Card_Cage_Assy			17.9

7.5.6 Transformer Efficiency

One of the primary factors in determining overall inverter efficiency is the efficiency of the isolation transformer. PV Powered has assessed many vendors over the last two years seeking one that can provide industry-leading efficiency within an economical product. PV Powered has specified 99.2% CEC weighted efficiency, and has had difficulty finding vendors who can meet this requirement in a cost-effective transformer. We have narrowed the field down to two vendors, Eaglerise and Acme. Currently, the Eaglerise is the leading performer, achieving 99.35% CEC weighted efficiency at the 295V tap, and 99.3% at the 265V tap. This is outstanding performance, and will assist in achieving an overall high CEC inverter efficiency (96.0% specified, with 96.5% as a stretch goal). This was achieved using a metglas-cored transformer design. Acme's prototype is a steel-core transformer, and as can be seen in Figure 7-22, falls short of the Eaglerise performance by approximately 0.5%. After these results, Acme has requested a chance to compete with a metglas design, and we have agreed to test another unit. It has not yet been received.

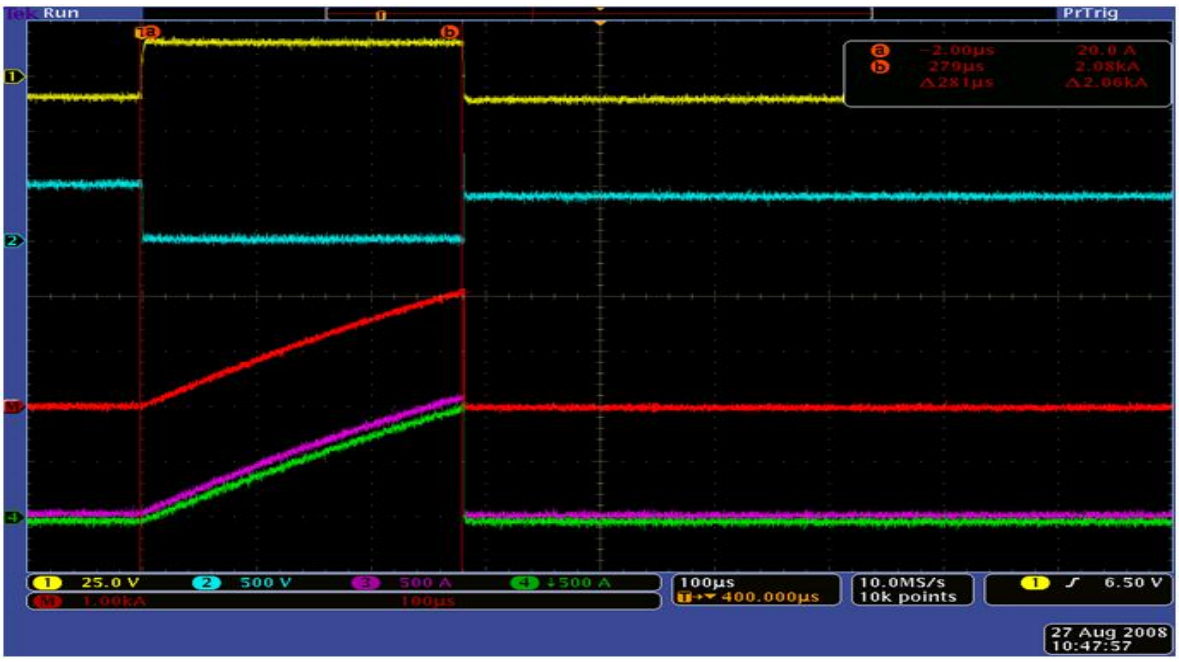

Figure 7-20. Waveforms for over-current testing. Ch1: V_{GE} (high side IGBT, 25V/div), Ch2: V_{CE} (high side IGBT, 500V/div), Ch3: Left module current (500A/div), Ch4: Right module current (500A/div), Match: Total module current (1000A/div).

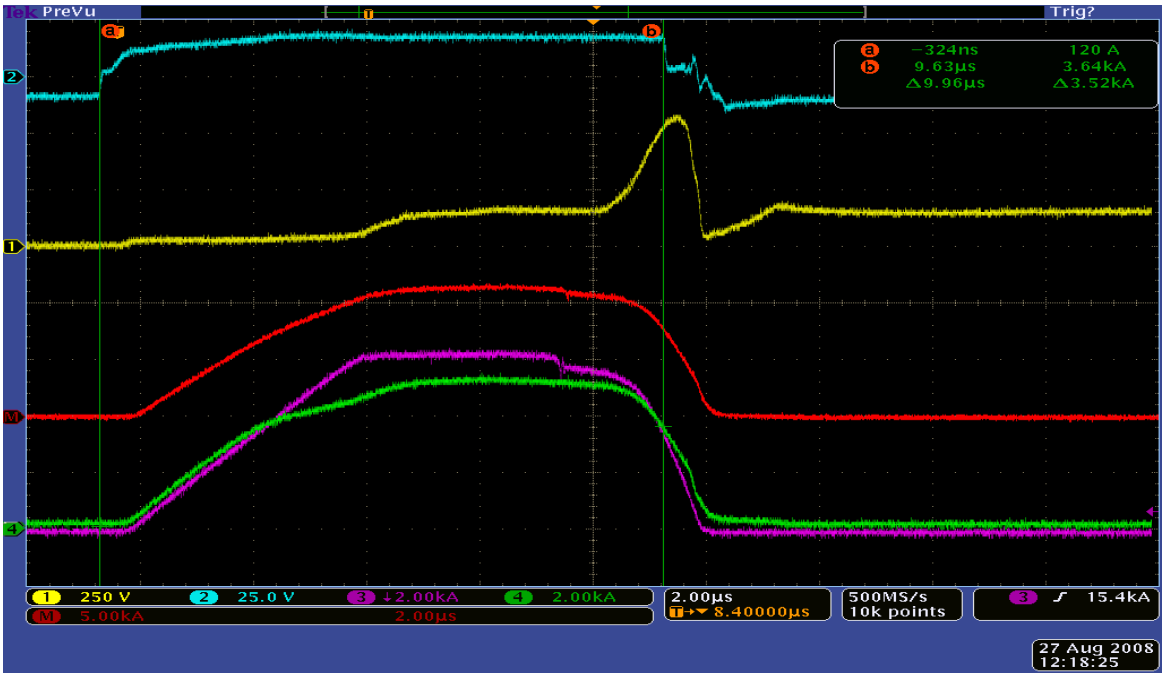

Figure 7-21. Switching waveforms for de-saturation circuit testing. Ch1: V_{CE} (high side IGBT, 250V/div), Ch2: V_{GE} (high side IGBT, 25V/div), Ch3: Left module current (4000A/div), Ch4: Right module current (4000A/div), Math: Total module current (10kA/div)

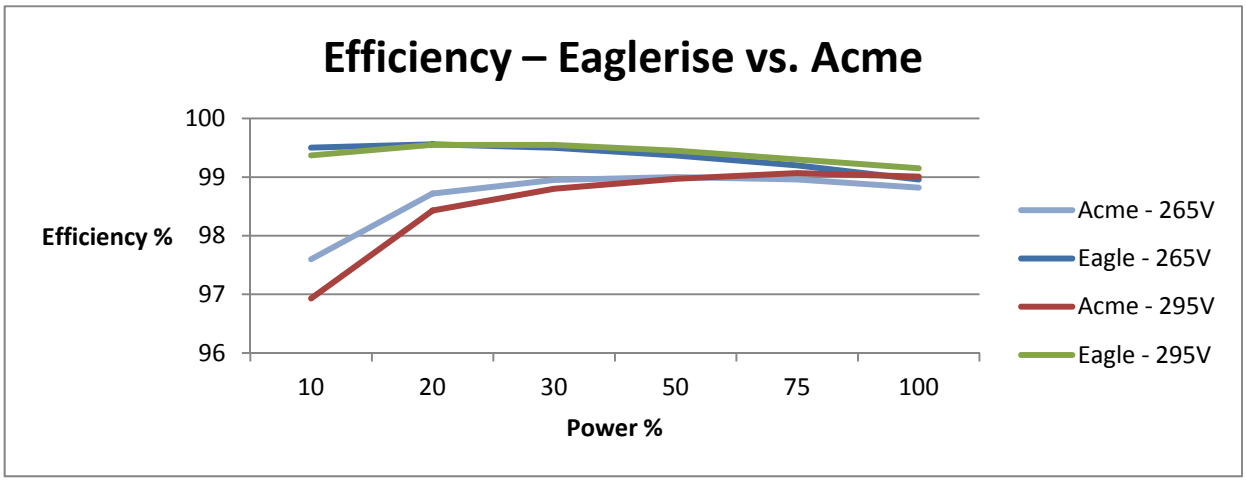

Figure 7-22. Comparison of isolation transformer efficiency

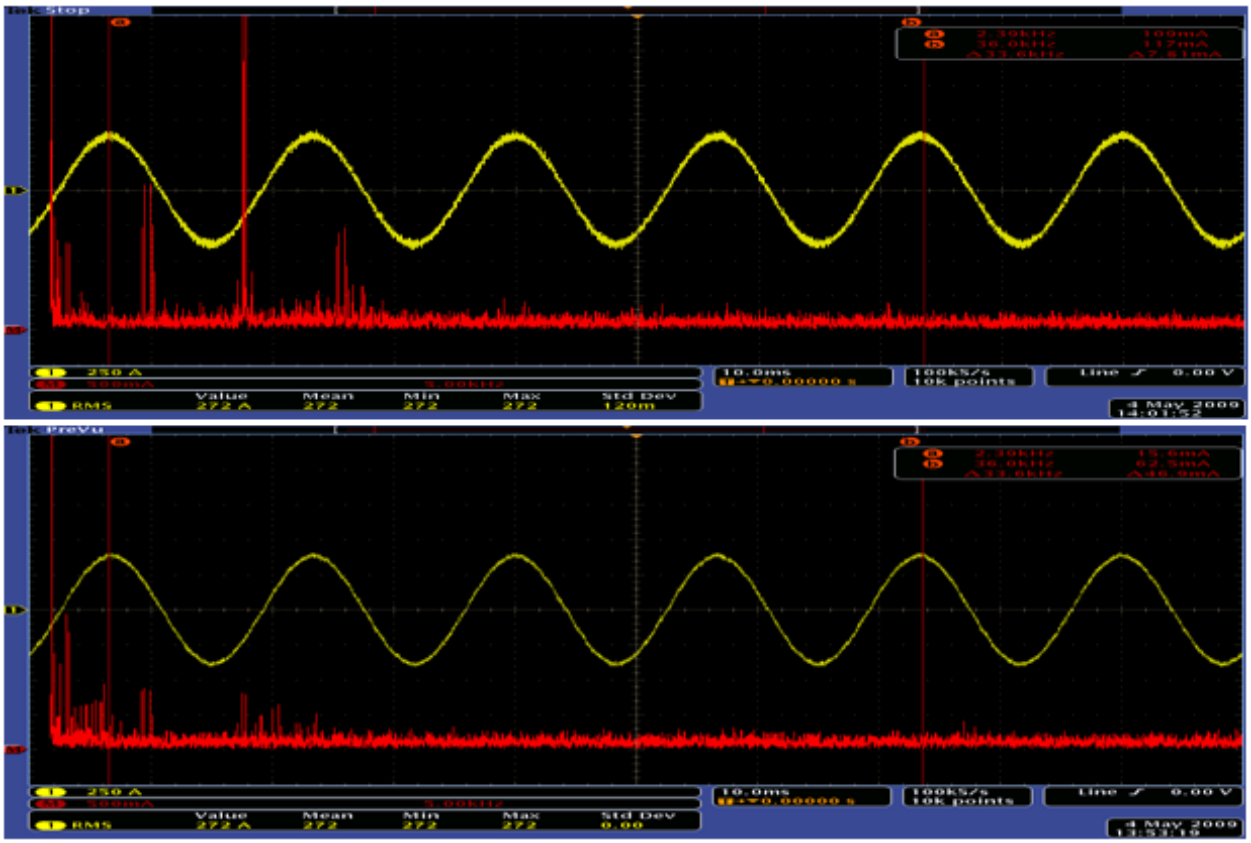

Figure 7-23. AC harmonics without (above) and with (below) the output ripple filter.

7.5.7 Reliability Engineering

The design approaches used to maximize reliability are:

- Connector derating derived from military / aerospace standards: 50% of rated current, 50% of rated voltage, 50 deg C below rated temperature

- Board-level resistor derating: 10% of rated power
- Board-level capacitor derating: 50% of rated voltage
- Smart Air Management – continuously adjusts blowers to minimum speeds necessary to cool the most critical components (power module, card cage, magnetics) to levels required for high long-term reliability
- Bus bar spacing 1" (double what UL standards require)
- Redundant blowers (3) with onboard fault detection
- Additional onboard health and fault monitoring (current balance, PV-DC delta)
- Power fold back in extreme cases (loss of blowers, clogged filter, etc.)
- Enhanced remote monitoring data stream
- Secondary air filter for card cage air
- Dual redundant two-tiered surge suppression

Four areas of prime concern in producing a reliable inverter are IGBT thermal control, DC capacitors, cooling fans, and magnetics. Some details on these subsystems are provided below.

7.5.7.1 IGBT Thermal Control

Significant effort has been applied to the design of the IGBT cooling system and algorithms. We have concluded that to achieve long-term reliability, the power module temperatures must meet the following constraints:

- IGBT junction temperature must be less than 109°C
- IGBT junction temperature excursion must be less than 106°C
- Power module case temperature excursion must be less than 71°C

Meeting these constraints should result in a 20-year power module lifetime under the worst-case environmental conditions (such as China Lake, CA) with less than 2% cumulative power module failure rate per inverter. Additional temperature reductions will result in decreased failure rates.

7.5.7.2 DC Capacitors

We have chosen a Cornell-Dublier DC capacitor with outstanding lifetime and performance. The CDE 947C231K102CAIS capacitor (1000V, 230µF) used in the 260kW inverter is based on a metalized polypropylene construction. Their operating temperature range is -40°C to +85°C, and they contribute a mere 60W of total power loss at full inverter power. The low ESR also means that temperature hot spots are minimal, with the hot spot to ambient temperature rise of only 19°C with no airflow based on manufacturer thermal data. If you apply the 29°C stress-equivalent temperature of our worst-case environment (China Lake), the DC capacitor hotspot would be ~48°C. In this worst-case environment, the manufacturer's expected lifetime at this temperature and derating is greater than 800,000 hours.

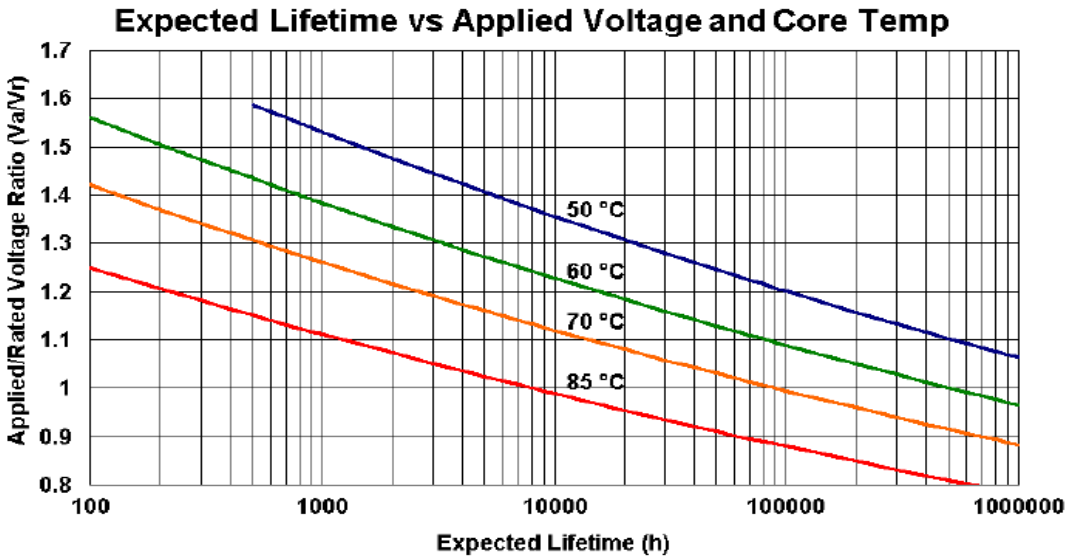

Figure 7-24. Lifetime curves plotted versus applied voltage ratio and temperature for the Cornell-Dublier DC capacitors used in the SAI 260kW inverter.

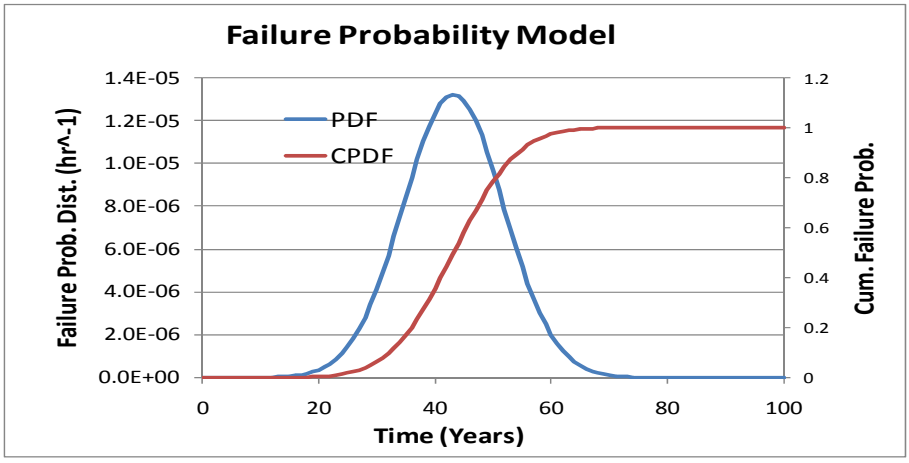

Figure 7-25. An exponential life temperature model fit to the EBM Pabst cooling fan used in the SAI 260kW inverter.

1.1.1.1 Cooling Fans

The SETP 260kW inverter uses three EBM Pabst blowers. They are DC, variable speed, highly balanced axial fans, controlled in a redundant fashion that permits full inverter output power even with the loss of one fan. EBM Papst provided L10 life expectancy for full speed operation at 40 and 60°C. Life expectancy in inverter hours is calculated based on average 56% speed while inverter is operating. The cooling system is designed so that the fans will run at this derated value under normal conditions, and spin up to full speed only under abnormal conditions such as the loss of one of the fans. The EBM failure data was fit to an exponential life-temperature model.

The predicted lifetime of the EBM cooling fans is 32 years (see Figure 7-25), which exceeds the required service life of the inverter.

7.5.7.3 Magnetics

The transformers and inductors used in the SETP 260kW inverter are custom designed and built in order to achieve the exception performance required to maximize overall inverter efficiency. As such, manufacturer reliability data is not available. Therefore, we use MIL-HDBK-217 as guidance (Figure 7-26):

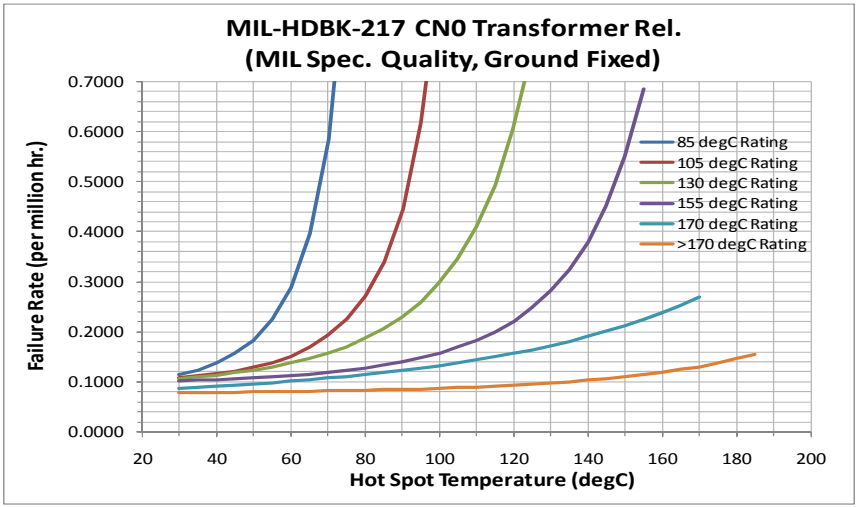

Figure 7-26. MIL-HDBK-217 transformer failure rates predicted versus hot spot temperature and magnetics rating.

There are two key assumptions inherent in this approach, which is that the quality is MIL-SPEC and the environment is ground fixed. PV Powered has specified the following for their inverter magetics:

- Magnetics hot spot not to exceed 55°C
- Insulation rated for 180°C or higher
- Surface temp not to exceed 135°C

Using MIL-HDBK-217 and the 155°C Rating Curve at the knee of the curve, a hot spot temperature of 110°C and a failure rate of 0.184 failures per 10^6 hours is indicated. This translates to a 1.3% cumulative failure rate per part over 20 years. Given the MIL-217 analysis is conservative, this is deemed adequate.

7.5.8 Testing Facility

In order to access sufficient electrical power to test a 260kW inverter, PVP moved from their small Bend, Oregon Scalehouse Loop facility to a new facility in Bend on Brinson Blvd. This 105,000 square foot former window factory is outfitted with 1.5MW of 480V electrical service, which is adequate to support development, compliance testing and manufacturing of PVP's full commercial and residential inverter product lines. The construction and wiring of this new laboratory is now complete, and it is being used for inverter functional and compliance testing.

7.5.9 Summary

The SETP 260kW solar inverter (see Figure 7-27) has been designed, prototyped and tested through the first of three phases of product release testing. Overall performance

has been achieved consistent with the initial design, performance and reliability specifications. Functional testing is underway in PVP's new engineering lab. PVP's new facility has all the space and power required to support and manufacture large commercial-sized inverters. UL compliance certification to UL1741 is expected to be completed by mid-July 2009. The production line for the 260kW inverter is currently being put in place, and will be ready by early July. Product shipments to commercial customers will begin immediately after UL certification is completed. Demand for the 260kW product is high, and we anticipate strong acceptance from the marketplace for this product.

Figure 7-27. A 260kW inverter prototype wired up within a thermal test chamber within PV Powered's new engineering facility.

7.6 Lessons Learned

Module Fabrication – Achievement of consistent performance from hand assembled modules was first noted in the proof of concept phase. Design changes, of course, were made to improve manufacturability and performance in the POD phase but many issues lingered (e.g., assembly accuracy requirements to achieve performance goals). These had substantial influence on the design the machinery used for fabrication in the POM phase.

Need for Module Uniformity – A new issue only appreciated in the POD phase was the need to use matched modules in an array. As described in this section, lack of

matching leads to a higher than arithmetic performance loss. The manufacturing process must yield uniform modules.

In-Line Module Performance Testing – The desirability of this was manifest to all. We were unable to accomplish this in the POD phase (search light test) and ultimately defaulted to off line in sun testing of individual modules which is not in a high speed production environment.

8 Proof of Manufacturing (POM) Fabrication – SOPO Tasks 1.11, 2.11, 3.11

Task Objectives

Conduct planning for manufacturing, test, test site selection, site design, site permitting and approval by applicable authorities, and installation for POM demonstration system. Develop, fabricate and/or procure critical long-lead items of hardware and/or production tooling as required to support the POM demonstration schedule.

Highlights

- Robotic factory designed, developed and commissioned. Demonstrated production rate of 1 panel per 8 hour shift, 60 X that of hand assembly.
- Robotically assembled panels demonstrated at up to 3400 W of normalized power, 21% above POD
- 100 kW power plant design, site prepared, tracker installed, panels installed and plant placed on the grid. Peak normalized power generation 83 kW.
- Power plant operated for 3 months, decommissioned due to unexpected component aging.
- Failure analysis completed on critical components, root cause of the two dominant failure modes (mirror corrosion and SOE failure) identified, and corrective action for each demonstrated.

Table 8-1. Proof of Manufacturing (POM) fabrication

Period	Criterion	Results
3	3d-1) Demonstrate system with 100 kWp capability produced with production tooling	Robotic factory commissioned and operated through the production of 33 panels. Panels deployed on Boeing trackers at California State University (CSUN).

Technical Accomplishments

8.1 Proof of Manufacturing Test Configuration

The module configuration for the POM effort is as described in Section 3.2 with the implementation of the specific details enumerated in Table 8-2.

Table 8-2. Configuration details for POM robotically manufactured modules

Design Element	Selection	Justification
Cell	C3MJ, efficiency = 38.5%	Best qualified design
Thermal Adhesive	DC4173, κ = 1.5 WmC$^{\circ -1}$	Predictability greater performance and cost lower than DC6534

Design Element	Selection	Justification
Optical Adhesive	LS3351, n = 1.51	Qualified by test and in 18 month NREL module test
SOE	Schott B270 glass, cold form sharp kaleidoscope corners, Auer AR coating	1 to 2% absolute performance improvement demonstrated
POE	Stanley mirror with 25Å metallic protective coating and proprietary alloy A	Successful qualification testing at Boeing
Window	Centrosolar AR coated and tempered low iron glass	Commercial solar module product

The panel / array configuration for the POM effort is as described in Section 3.3 with the implementation of the specific details enumerated in Table 8-3.

Table 8-3. Configuration details for POM robotically manufactured panels and demonstration power plant arrays

Design Element	Selection	Justification
Frame	All steel	Lower cost than POD steel aluminum
Module Attachment	Spot welding	High speed production approach
Environmental control	Continuous purging at a low flow rate	Perception of equivalency to period five volume change purge
Tracker	Boeing tracker and software design	Lower cost

8.2 Plant Design

One of the key goals for the program was the installation of a 100 kW demonstration power plant. Boeing originally planned to install the power plant on Southern California Edison (SCE) owned land in Daggett CA near the Solar 1 site. SCE made every effort to accommodate the project in selecting this site however, the requirements for road and infrastructure improvements exceeded the available budget for the project. In addition, the program team determined that it was desirable to have the demonstration site closer to a local Boeing facility in order to facilitate visits by Boeing management, potential licensees, or Spectrolab customers. The team evaluated sites in Irvine California, Mesa Arizona, Northridge California, and San Diego California.

The project selected a site at California State University – Northridge (CSUN) for deployment of the POM test site (see Figure 8-1). CSUN has a renewable energy grid in place and is a college with which Boeing has a long standing relationship. In addition,

CSUN had a site that was nearly construction ready as well as a long standing relationship with the Los Angeles Department of Water and Power (LADWP.)The plan was designed to provide 100 kW of solar power to the grid. LADWP provided the substation interface for the power plant. The plant was designed to accommodate 40 panels. The baseline plan (see Figure 8-2) was to install 32 panels with the spare space available in the event it was required to meet the 100kW goal.

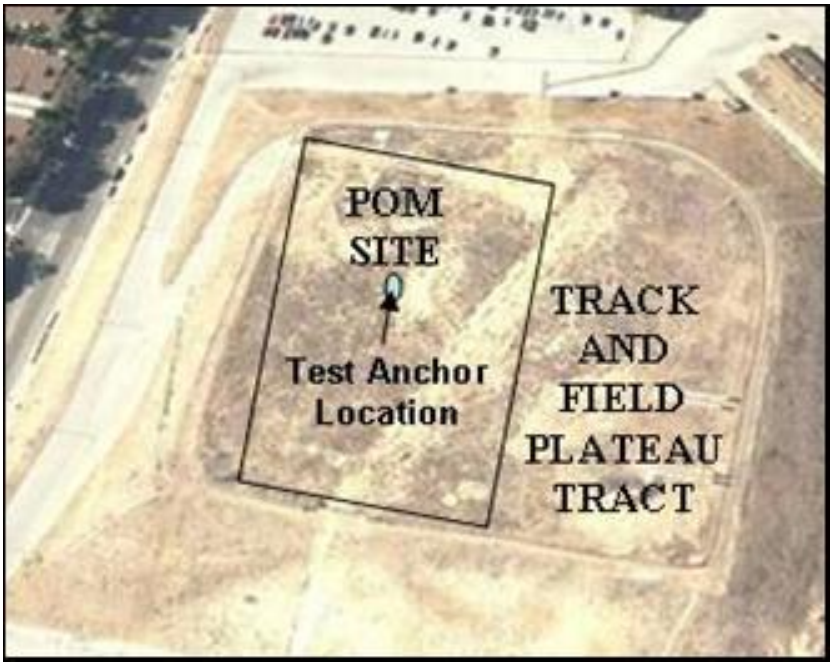

Figure 8-1 CSUN site.

Complete the Schematic design of the Proof of Manufacturing Plant

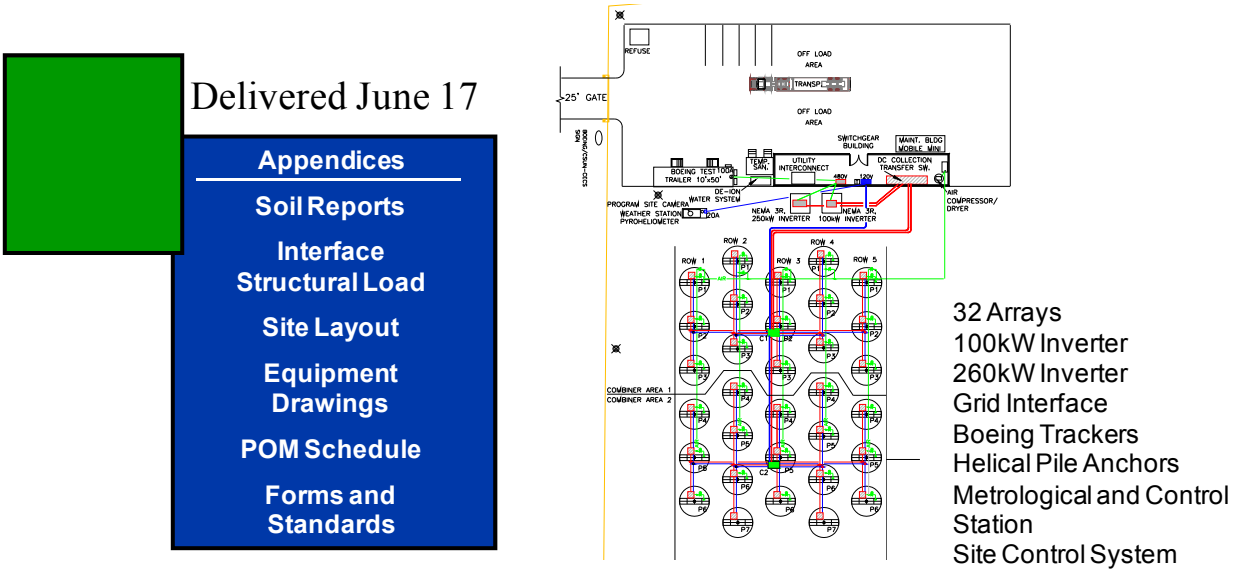

Figure 8-2 CSUN Plant design

Originally a minimum of 32 arrays were planned for the CSUN site. Expansion space was available for up to 40 arrays. The final number of arrays depended upon the output losses in the robotic manufacturing. If that rate were low we could install all available panels at CSUN with no impact. Ultimately the production losses were higher than plan and only 33 arrays were installed at CSUN.

In order to minimize the helical pile costs, test piles were installed at the site and load tested. This allowed the soils engineering company to reduce the required length of the pile at a substantial cost savings.

8.3 Fabrication Methodology / Process

8.3.1 Panel Production Campaign

The production of the CSUN panels occurred in a single campaign between January and June of 2010 at the Comau Novi, Michigan facility. During this period Boeing provided essentially full time on site monitoring by manufacturing and/or process engineers. Issues which arose, particularly in the early phases of the campaign include,

Incoming Parts Quality – The most serious example of this was the discovery by Comau incoming inspection of what appeared to be cracks on the lower surface of the SOE. This lead to a 100% inspection of the parts, rejection of parts with cracks and analysis by LPI (the contract parts supplier) of the thermal consequence of the cracks. In this latter process it was determined that the cracks did decrease the thermal robustness of the parts but that this could be largely restored by grinding out the cracked area, and this rework was carried out as a rework to print on 100% of the rejected parts.

Soldering – Soldering of bus leads to the CCA was an issue throughout the development of the module. It was critical for a realistic production demonstration that the soldering step be implemented as a robotic process. This was designed into the plant but with (at least initially) very poor yields. Boeing process engineering spent over a week at the plant fine tuning the process and eventually it did achieve the required throughput.

Screw Fastening – Automatic fastening issues were encountered with both the attachment of the heat sink CCA assembly to the receiver wall and the receiver wall to the chassis. The former issue was a consequence of the use of #2 self tapping fasteners with minimal thread engagement. The solution implemented was reworking of the pilot holes prior to assembly to provide a lead in for the self tapping screw.

Difficulties with the attachment of the receiver wall to the chassis arose as a robot is not capable of “finding” a female insert with a screw. Typically this issue would be addressed with either highly accurate female thread location, a self tapping sheet metal fastener, or use of a screw with an unthreaded pilot lead. The unthreaded pilot lead was shown to be effective; however, the time and expense of its implementation as an automatic process when compared to leaving this step to human execution led to selection of the latter approach. As this was not a rate determining process there was no consequence to the throughput.

The above issues were all resolved in the course of the campaign and the final as-designed one panel per 8 hour shift throughput was demonstrated.

8.3.2 Plant Assembly

There were three phases to the plant assembly. In the first the site was prepared for receipt of the panels which entailed mounting of helical piles and trackers, trenching electrical and purge gas connection, installing the connections, final grading and land preparation, and installation of centralized facilities (compressor/drier for purge gas, inverter and grid connect and central control building). The fully prepared site is displayed in Figure 8-3.

Figure 8-3. CSUN site prepared for panel mounting. Note the helical piles are topped with trackers and attached junction boxes

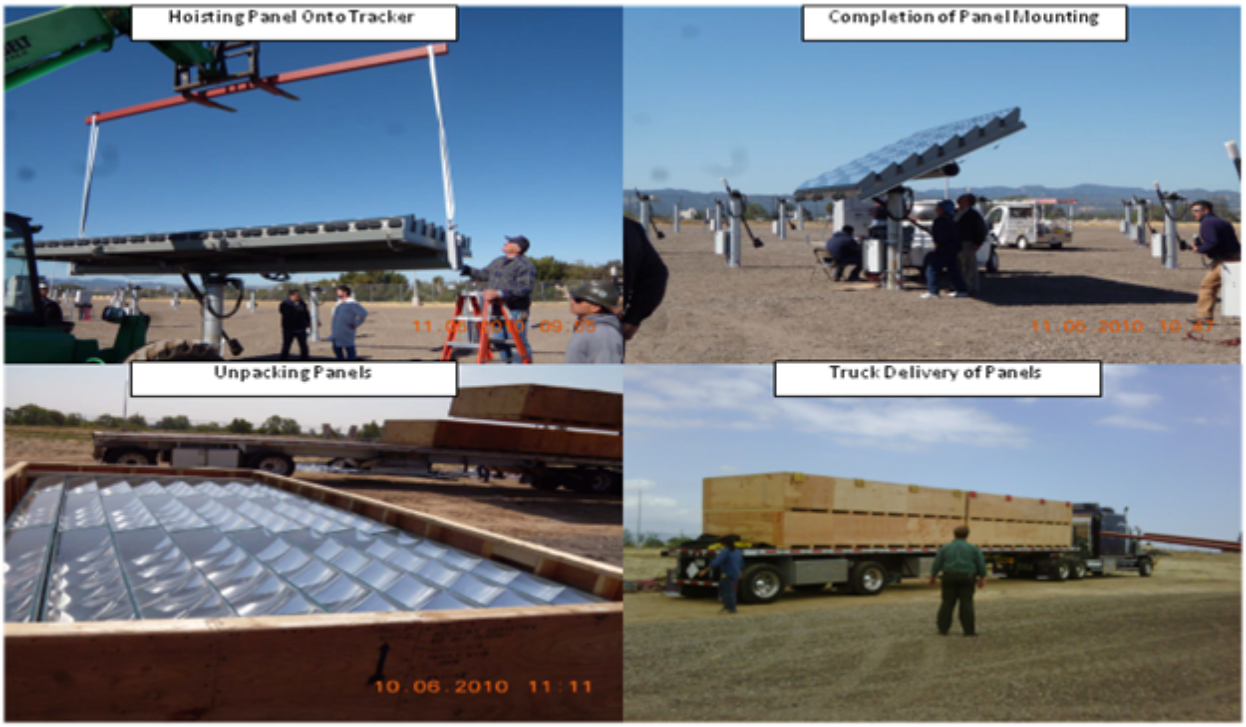

Figure 8-4. Illustrated assembly process at the site of the CSUN power plant.

In the second phase completed panels were delivered by truck from Comau, removed from their shipping containers, and mounted on the helical pile – tracker, and inspected for performance. This step occurred between early May and the end of June 2010. The various steps of the process are illustrated in Figure 8-4. In general the assembly went very smoothly. A truck load of four panels arrived at the site after a 3 to 4 day cross country journey. Unpacking and receiving inspection would require on the order of 30 minutes per panel with another 30 minutes for hoisting to and mounting on the tracker. The final step in receiving inspection was an acceptance IV after which the panels were sun tracked at open circuit until the entire field was assembled and grid connected (as discussed in Section 8.5.2 this was probably not the most prudent course). The final result of the assembly effort is shown in Figure 8-5 for the fully populated power plant.

Figure 8-5. CSUN power plant at assembly complete.

8.4 Test Plan

The 100kW plant installed at CSUN was intended as a life test article. Initial performance testing was performed on each panel as it was installed. Plant level performance is measured at the inverter. The 100kW inverter was connected to the field prior to grid connection. Upon approval by LADWP the system was connected to the grid. CSUN agreed to monitor performance for 5 years. Later events proved this unnecessary.

8.5 Results and Analysis

8.5.1 Panel acceptance testing

8.5.1.1 Front Runner Panel

Prior to releasing the factory for full scale production one first article panel was produced and shipped to Seal Beach for verification testing. This panel was placed on test in mid April of 2010. Typical initial performance data is provided in Figure 8-6.

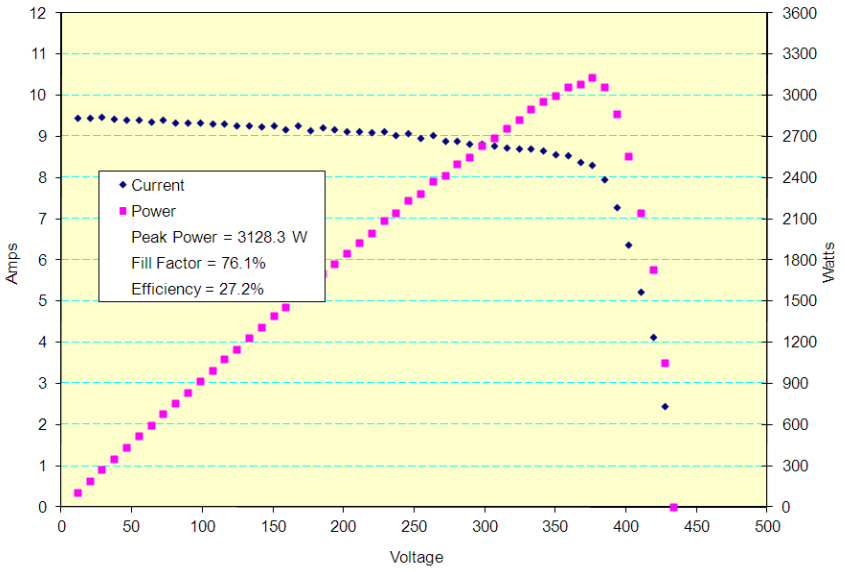

Figure 8-6. Typical initial performance data for front runner panel CP01.

The data are below our expectations for the technology owing to module-to-module mismatch as evidenced by the low fill factor. The mismatch is also apparent in the acceptance angle measurements (see Figure 8-7) which are nearly identical to values obtained for the POD panel. Difficulties in production acceptance testing are discussed in Section 8.3. We were unable to improve module matching in this panel, although as production matured there was evidence module uniformity did improve.

The first production panel was tested on-sun for two weeks prior to approving full production. In the two weeks of testing in Seal Beach panel performance was stable with an average power of 3100 W and production was authorized.

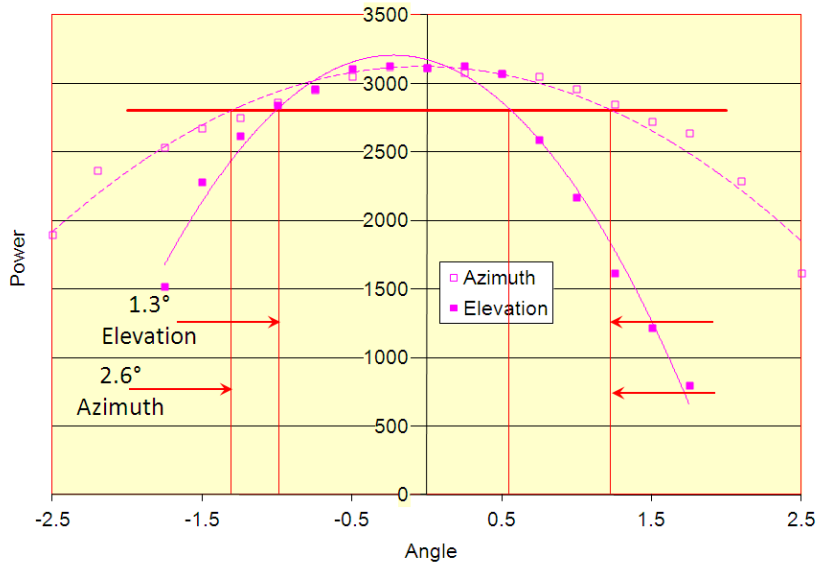

Figure 8-7. Azimuth and elevation measurements of the acceptance angle vs. relative normalized peak power for POM panel CP01

Panels were received at the CSUN power plant site over a six week period in May and June of 2010. As each panel was received (typically in batches of four) it was removed from its shipping container, inspected for transportation damage and, if accepted, mounted to the pre-installed tracked-pole. At this point the tracker software automatically aligned the panel to the sun and an IV curve was recorded. The results of these measurements normalized to 1000 W/m^2 are given in Figure 8-8 for all the production panels.

As can be seen, individual panel performance values as high as a normalized 3400 W were obtained, surpassing by 21% the peak observed for POD and representing a 30% aperture efficiency. Fill factors as high as 79% were likewise observed but no fill factor equivalent of a good module (≈83%) was seen. Modeling the projected performance of the plant based on a parallel connection of the 33 array yield a predicted performance as shown in Figure 8-9.The projected peak power of 106 kW exceeds the contract goal.

8.5.1.2 Production Panel Acceptance Testing

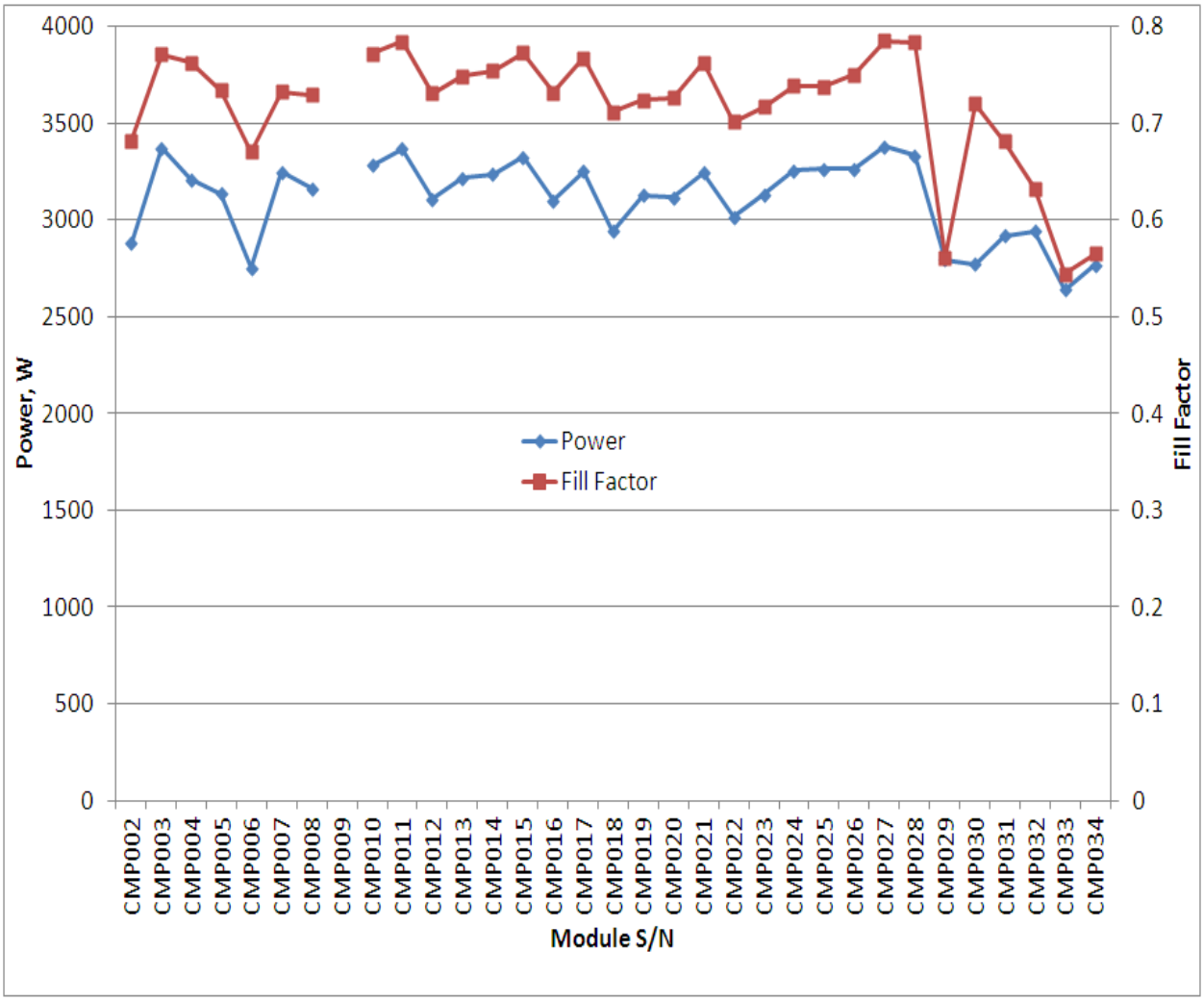

Figure 8-8. Receiving inspection data for the CSUN power plant panels.

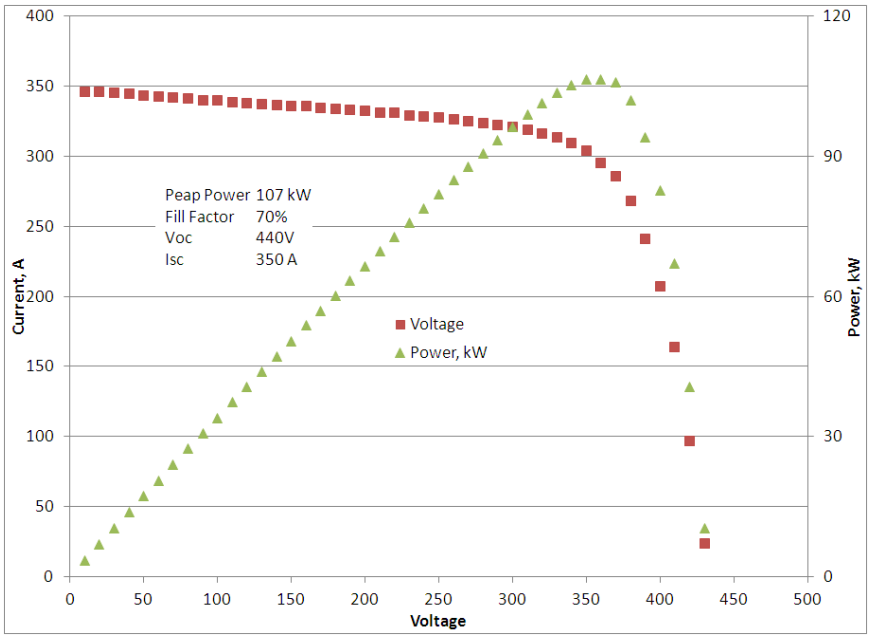

Figure 8-9. Projected performance of the POM power plant based on the acceptance test data of the individual modules.

8.5.2 CSUN Performance and Analysis

After physical completion of the power plant a full month elapsed while negotiations were completed with the local power company for the grid connection of the power plant. The first normalized plant peak power was 83 kW. The Individual panels were then measured and the data are shown in Figure 8-10. As can be seen, the Imp of at least the oldest panels had markedly decreased. Imp is a measure of the optical transmission to the solar cell and thus the data in Figure 8-10 imply that sun exposure led to a deterioration of the optics.

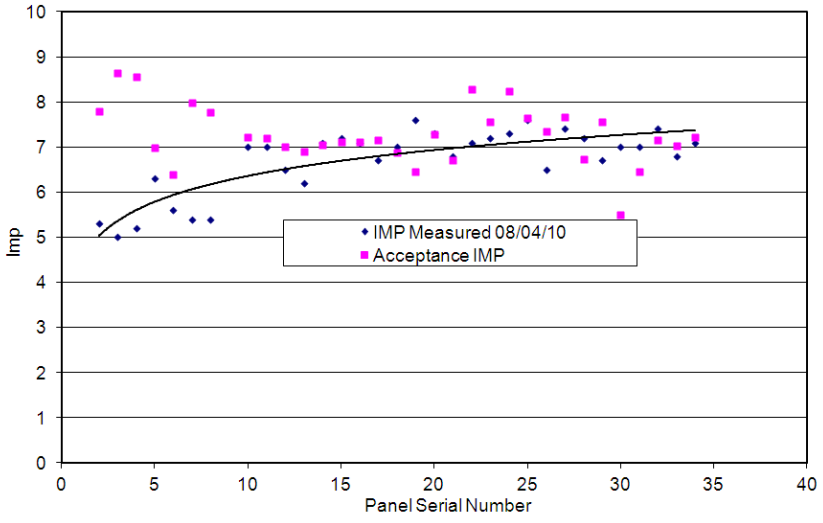

Figure 8-10. Comparison of the Imp of the individual power plant panels as received and after commissioning of the demonstration power plant at CSUN

Based on plant output and the data in Figure 8-10 an effort was immediately launched to determine the root cause(s) of the apparent anomaly. This effort included:

- Close monitoring of performance trends in the power plant;
- Immediate and periodic physical examination of the power plant hardware;
- DPA on sample hardware;
- Contact with and support by key suppliers, particularly Stanley Electric;
- Comparison of data and design features to those of earlier hardware;
- Analysis of possible root causes (fish bone);
- As required, development of test matrices to elucidate anomaly root cause and demonstrate solutions.

8.5.2.1 Performance Trends

The output of the power plant was monitored over the next several months and these data are provided in Figure 8-11. Two things stand out:

- There appears to be something different about operation at CSUN (power plant) vs. Seal Beach (front runner);
- POM module D built at Boeing has a much lower rate of power loss than the factory built hardware (although it ultimately failed for reasons similar to what was observed in the factory built hardware).

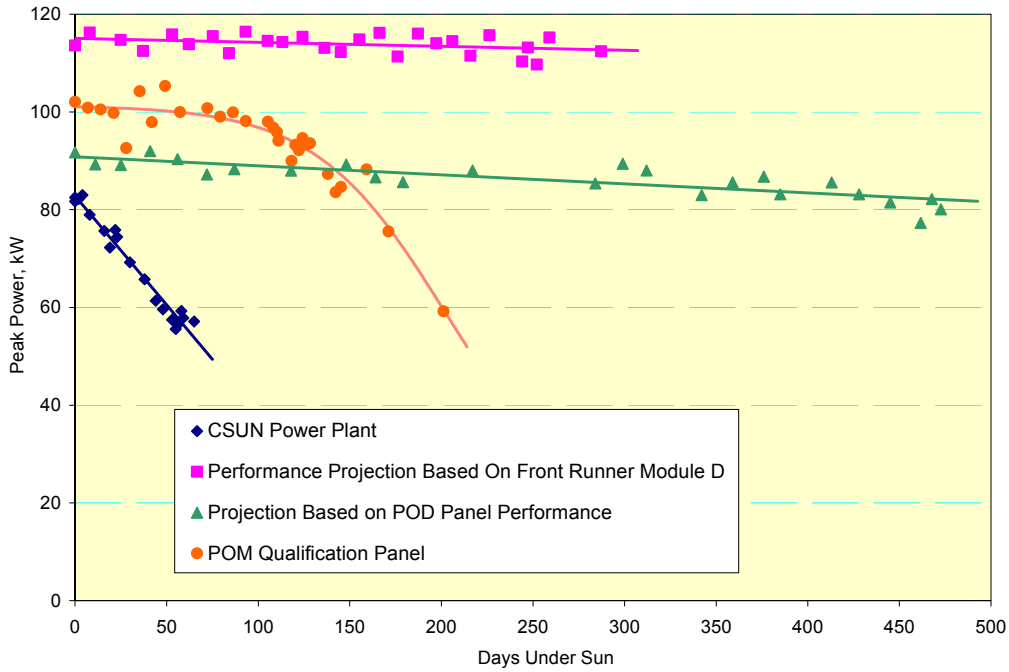

Figure 8-11. Comparative normalized life test data for the POD array, The POM CSUN power plant and front runner POM module D. All data are scaled for 32 arrays.

The site difference may be due to:

- Differences in temperature (CSUN is located in the San Fernando Valley, considerably warmer than Seal Beach);
- The fact that the power plant panels stood at open circuit under sun (≈30% warmer) for between 1 and 3 months whereas the front runner was always under load;
- The difference in environmental control implemented at the power plant (slow continuous bleed of dry air) vs. the front runner (periodic purging every 5 days at 5 volumetric changeovers per hour for one hour).

8.5.2.2 Nondestructive Examination

Three formal inspections of the power plant hardware were carried out in the first and third weeks of August and in mid September 2010. The most immediate observation was that the front surface silver mirrors showed clear discoloration when compared to their as-received condition and to the POD panel (see Figure 8-12). Furthermore, closer examinations slowed that there appeared to be a general trend wherein mirrors at the right hand side near the module vent tended to show more discoloration (see Figure 8-13).

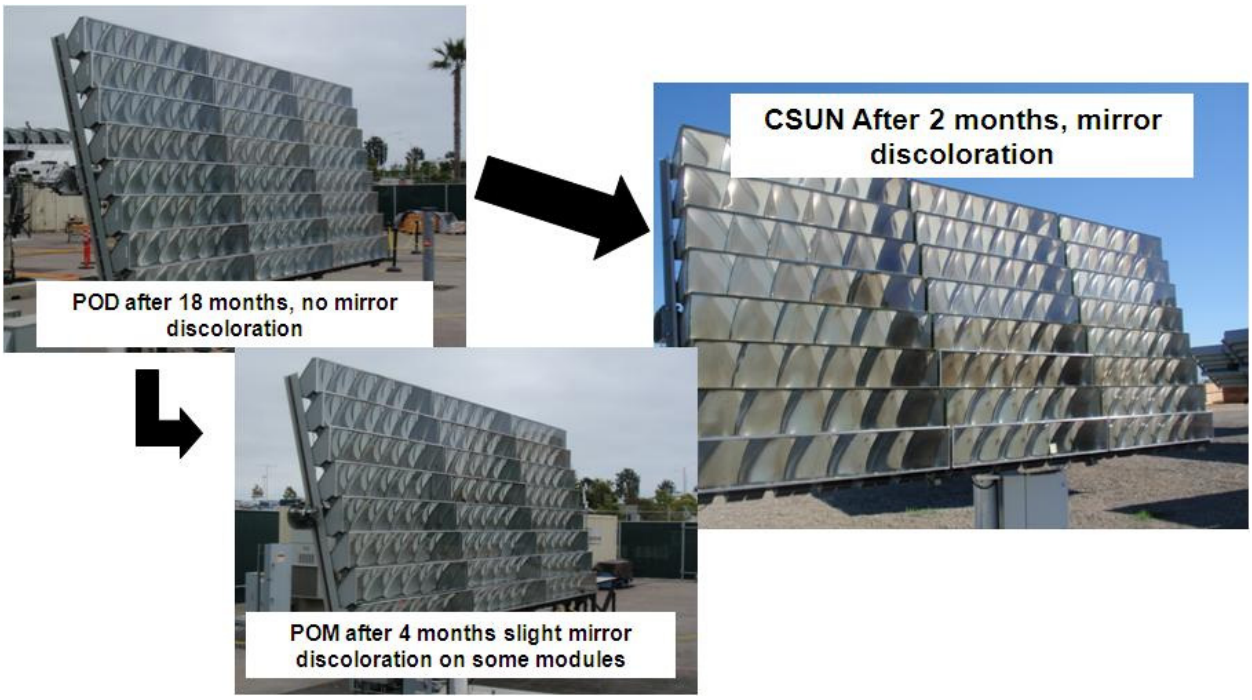

Figure 8-12. Seal Beach POD and POM panels and a CSUN power plant panel.

The second significant observation was that the kaleidoscopes on many of the SOEs appeared to be cracked. In addition many of the cells showed what appeared to be burn marks. Finally, under sun some of these burn marks appeared to glow white hot. The definitive observations of the same hardware showed that the burn mark – hot spot turned into a cracked kaleidoscope as shown in Figure 8-14. The observations obviously point to something at the cell to kaleidoscope interface which evolved with time

and under high intensity solar radiation, absorbing energy and thus leading to a hot spot. The mechanical integrity of glass is clearly comprimised due to stress under such conditions.

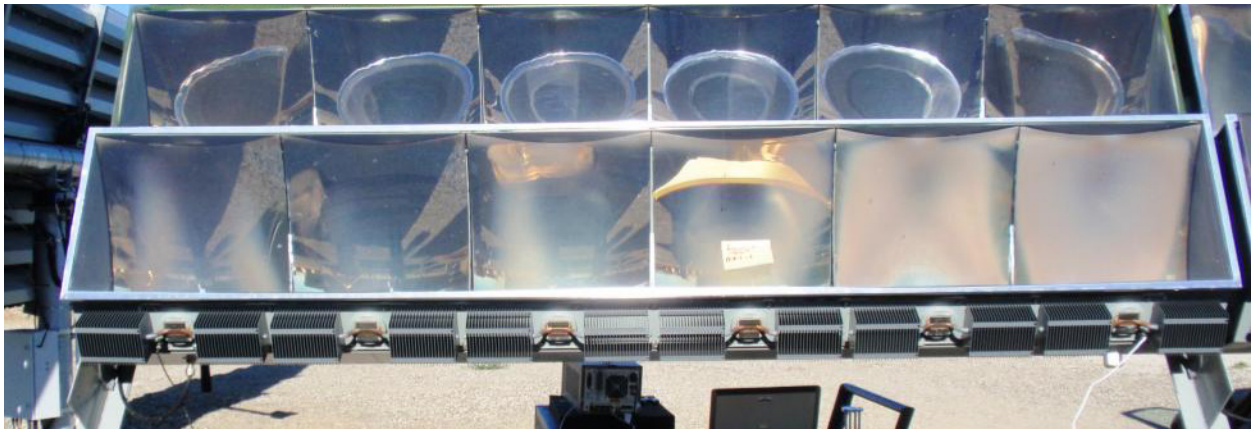

Figure 8-13. Preferential mirror discoloration near the right hand side adjacent to the module vent.

Figure 8-14. Evolution of the cracked kaleidoscope.

8.5.2.3 Sample Hardware DPA

Based on the CSUN observations two modules were removed. One was provided to Stanley for analysis of the mirror. This is reported on in Section 8.5.2.4. The second module was examined by Boeing with the focus on the SOE / kaleidoscope issue.

The first thing established by the Boeing examination was that the kaleidoscope was indeed cracked. The kaleidoscope–cell interface and initial observations are provided in Figure 8-15. As can be seen the cell looks as built. Parts of the optical adhesive appears to have changed (become crystalline), however, we can't say if this is the root cause or a result of the hot spot heat.

8.5.2.4 Stanley POE DPA and Root Cause Determination

Stanley carried out an admirable DPA analysis of the mirrors from a CSUN module. Their most critical step was an XPS examination of the discolored mirror surface. The results of this examination are provided in Figure 8-16. The test discovered chlorine

which is a well known corrosion catalyst. With even trace amounts of water in the presence of a reactive metal, chlorine will form metal chlorides which are Lewis acids and will form a cycle with water. The end products are a metal hydroxide corrosion product and hydrogen chloride which will continue the corrosion cycle as shown below.

$$XHCL_2 + YM \rightarrow M_YCl_{2X} + \frac{X}{2}H_2$$

$$M_YCl_{2X} + XH_2O \rightarrow \frac{X}{2}HCl + M_YOH_{2x}$$

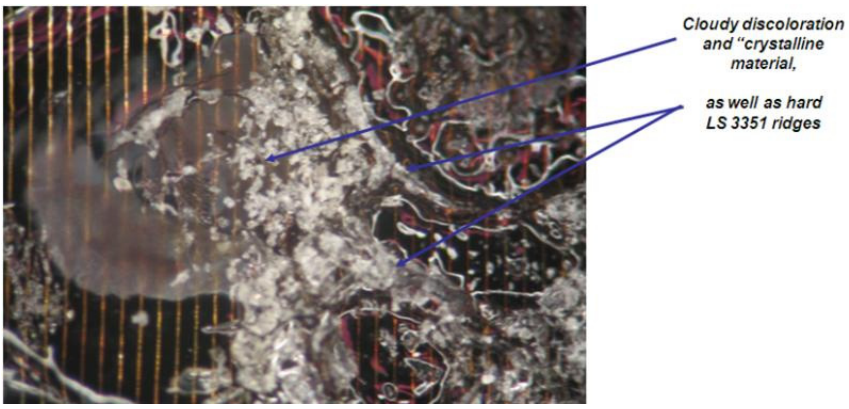

Figure 8-15. Post operation examination of the of the optical bond from hardware with a cracked kaleidoscope.

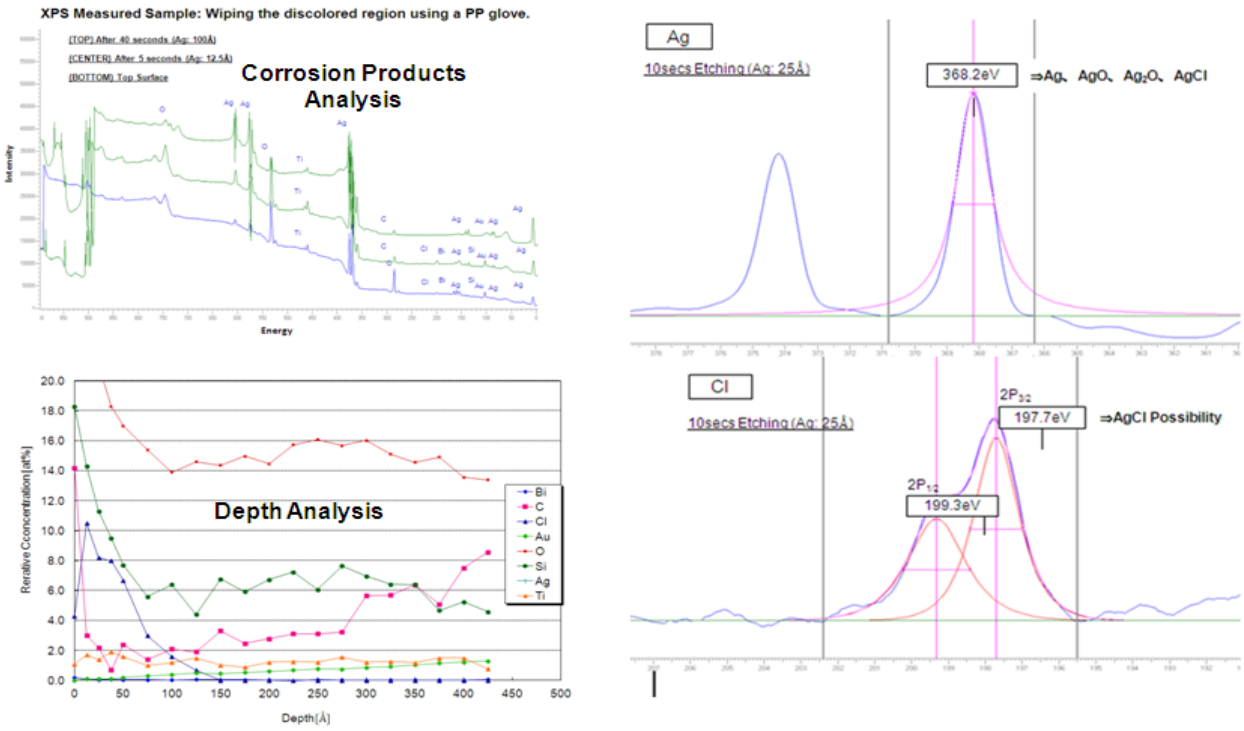

Figure 8-16. Results of the XPS examination by Stanley of the power plant POE.

The next question was, therefore, where did the chloride come from? And why hadn't this been observed in early testing at Seal Beach? Stanley examined all the components of the module and determined that only the adhesive employed to attach the window to the module contained chlorine. It was immediately realized that during the three month assembly campaign at CSUN there had been numerous instances of panel off-pointing and that, during these events, reports had been received of overheating the adhesive and the generation of smoke (undoubtedly containing chlorides) from the overheated adhesive.

Owing to the much shorter duration of uncontrolled hardware sun exposure at the smaller, technician-managed Seal Beach test site this did not occur with sufficient frequency to lead to immediate damage. Seal Beach is, however, a marine environment and some chloride intrusion must inevitably occur.

Two other differences between Seal Beach and CSUN critically delayed or stopped the chloride corrosion process. First the POD hardware employed EMF mirrors with a thick metal oxide outer protective layer. Stanley's original mirror design employed a thinner metallic protective coating which is likely less protective. A discriminating test was not carried out as the module is environmentally protect against salt fog and a "dry" salt fog test hadn't been developed. Second, the early Stanley hardware (e.g., module D) employed preproduction POEs manufactured in Stanley's Japanese corporate laboratory. The production mirrors were built in the Stanley Battle Creek, MI factory and only evaluated in the POM front runner panel which of course was tested more carefully.

At the end of the day, however, the "dry" salt fog environment is real. All the preproduction test modules and the front runner did eventually fail after at most a year of operation in Seal Beach. Only the POD POEs with the metal oxide protective coating are still fully operational after three years with no evidence of mirror corrosion.

8.5.2.5 Comparison with Successful POD Hardware

The titled comparison is provided in Table 8-4. As will be noted many of the differences are applicable to the POE issue which as described in Section 8.5.2.4 Stanley has effectively closed. Table 8-4 therefore really serves a reference point for the upcoming fish bone analysis of the kaleidoscope issue.

Table 8-4. Comparison of relevant design changes between POD and POM arrays.

Feature	POD	POM
SOE-chassis adhesive	Silicone with volatile contaminant	Silicone without volatile contaminant
CCA	C2MJ	C3MJ
Mirror	EMF with +1000Å metal oxide protective layer	Stanley with 25Å metallic protective layer
Feature	POD	POM

Optical adhesive	Silicone with alkyl group substitution, n= 1.40, glass bead line control, not qualified	Silicone with phenyl group substitution, n = 1.53, glass bead bond line control qualified by accelerated lab test and real time module test at NREL
Window adhesive	Chloride bearing with protective Al tape masking	Chloride bearing without Al tape masking
Location	Seal Beach, CA	Northridge, CA
Window AR coating	Schott	Centrosolar

8.5.2.6 Fish Bone Analysis of the SOE / Kaleidoscope Anomaly

The SOE kaleidoscope fish bone is provided in Figure 8-17. An anomaly analysis criterion was that any proposed root cause should not only lead to cracking of the kaleidoscope but also develop the observed precursors of a crack (cell burn marks leading to hot spot leading to crack) and demonstrate hockey stick kinetics based on the observation that cracking at Seal Beach would not develop for months and suddenly appeared on several receivers of a module within a month. While having all the features was not required to be put on the fish bone it certainly influenced the priority of the testing program to establish the root cause.

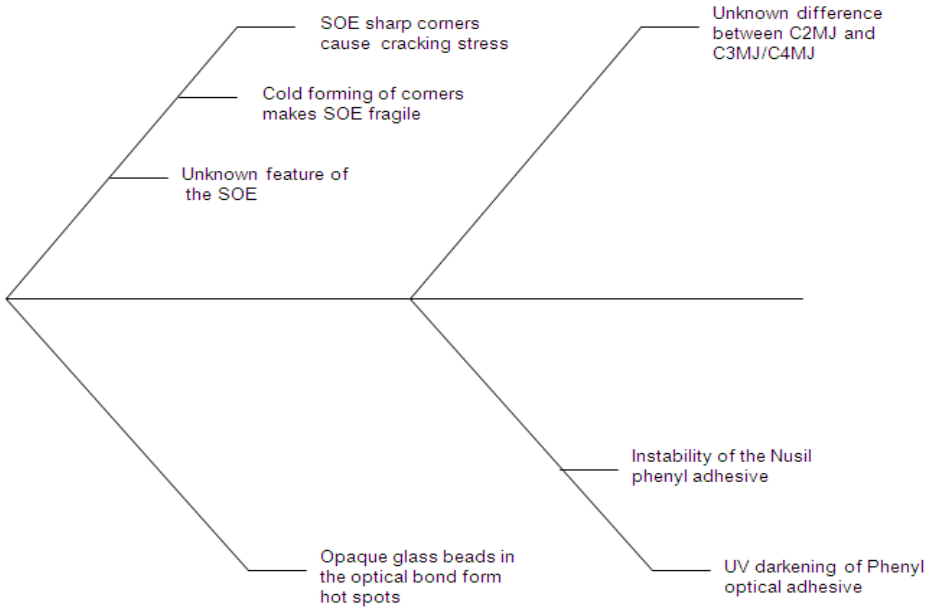

Figure 8-17. Fish bone for the anomaly analysis of the kaleidoscope cracking problem.

The following explores the potential failure mechanisms identified:

Opaque glass beads – During the anomaly analysis it was microscopically observed that not all the glass beads used in controlling the optical bond thickness (≈5 v%) were clear. A opaque bead would therefore absorb solar radiation and run hotter, and ould form an ever expanding hot spot as the silicone matrix would tend to darken more near the micro hot spot.

UV darkening of the LS3351 phenyl optical adhesive – There was certainly a body of knowledge that phenyl adhesives tended to darken with UV exposure. We had carried out extensive laboratory qualification of the adhesive which showed no loss of transmissivity after the equivalent of several years of exposure. In addition in 2009 we supplied a module to NREL which was tested for 18 months without SOE failure (the window adhesive, which was changed for POM, eventually failed and the test terminated).

UV darkening of any phenyl optical adhesive – Shin Etsu markets into the solar power industry KER 6000 phenyl bearing adhesive with a refractive index or 1.51. This adhesive has been shown to be stable under intense UV illumination at 150 °C.

An SOE manufacturing defect – During the hardware assembly phase of the CSUN power plant Comau incoming inspection discovered what appeared to be cracks on the lower, non optical surface of the SOEs from LPI / Ecoglas. This was brought to LPI's attention and thermal stress testing was carried out. The result was that indeed the parts were more sensitive to repetitive thermal stress, and they were reworked by supplier grinding off the cracked area. This did lead to more robust parts but still not as good as the original. Given the schedule demands of the program the solution was accepted. It is not clear how the observed parts issue would have led to the failure. However, older parts never failed (at least in mid 2010).

C2MJ vs. C3MJ / C4MJ – There no reason to indict the triple junction cell other than it is different. Strongly arguing against this is that it is the same cell used by commercial suppliers of CPV hardware and they don't (to our knowledge) have our problem.

8.5.2.7 Anomaly Test Matrix

To sort out the above possibilities, tests were conducted according to the test matrix shown in Table 8-5. The various issues on the first bone were addressed as follows:

- Three different SOEs are tested, The Star SOE is basically the POD design. The New Auer Red is the POM design reworks by the manufacturer with grinding. The Star SOE is the built with the original process;
- Numerous modifications of the optical bond are evaluated:
    - Designs were evaluated employing the Shin Etsu KER 6000 optical adhesive which is claimed to have superior thermal and UV stability.
    - The design with Nusil LS 3351 is evaluated side by side with Shin Etsu;
    - One module was tested with the original and successful Nusil LS6140.
    - Both the KER 6000 and the LS 3351 are evaluated with optical bonds design based on 5 v% glass beads, 4 glass beads only physically placed at the corners of the cell, and designs in which the glass beads are replaced with a 100 µm shim made with optical adhesive.

Table 8-5. Module test matrix to isolate the root cause of the CSUN power plant anomaly.

Module S/N	Cell Tap	Heat SinK	POE	SOE	CCA	Window Adhesive	Thermal Adhesive	Optical Adhesive	AT Efficiency
Module L	Yes	Avid	Stanley	New Auer Red	C3MJ	POM P1 (exisitng)	DC6534	LS6140	29.3%
Module M	Yes	Avid	Stanley	New Auer Red	C3MJ	POD GM-1	DC6534	ShinEtsu 6000 100° Cure	32.0%
Module N	Yes	Avid	Stanley	Star	C3MJ +	POD GM-2	DC6534	ShinEtsu 6000 100° Cure	31.1%
Module O	Yes	Avid	Stanley	Star	C4MJ	Epoxy	DC6534	ShinEtsu 6000 100° Cure	32.1%
Module P	No	Avid	Stanley	New Auer Red	C3MJ	Epoxy	DC6534	LS 3351, 4 Glass Beads	31.0%
Module R	No	Avid	Stanley	New Auer Red	C4MJ	Epoxy	DC6534	LS 3351, 4 Glass Beads	32.0%
Module S	No	Avid	Stanley	New Auer Red	C4MJ	Epoxy	DC6534	ShinEtsu 6000, 100°, 4 Beads	29.8%
Module T	No	Avid	Stanley	New Auer Red	C4MJ	Epoxy		LS 3351 100µ Shim, No Beads	33.4%
Module U	No	Avid	Stanley	New Auer Red	C4MJ	Epoxy		KER 6000, 100µ 100°C Shim	33.1%

With the exception of the C2MJ option these variants encompass the fish bone analysis.

The modules were placed on life test in March of 2011. The results by the end of the Program (December 2012) are presented in Table 8-6. The results are definitive, everything has failed except the module employing the LS6140 optical adhesive. The root cause of these failures wasn't the bond design, nor the SOE but rather the phenyl substituted optical adhesive.

Table 8-6. Results for the corrective action matrix of modules.

Date 11/30/2011	SB Module Survey	BR =	Burnt RTV Seal (SOE)	LG =	Loose Glass	DS=	Dark Spots	FS = Foggy SOE
		B =	Burn Marks on Cell	C =	Cracked (SOE)	BKT=	Burnt Kapton Tape	
		LM =	Loose POE	D =	Optical Adhesive Debond/Kaleidoscope failure			
	View from Front of Panel	H =	Hazing of Glass Windo	BM =	Browning of PO	AB=	Adhesive Bubbles	

GM-8 T	BM FS AB	BM D AB FS	D BM FS	D AB B FS	D B AB FS BM	D AB FS BM	GM-1 L	BM FS	AB BM FS	AB BM FS	AB BM FS	AB BM FS	AB BM FS	GM-5 P	D B BM FS	AB BM FS	AB BM FS	BM FS	BM FS	D BM FS
GM-9 U	D AB FS BM	D AB FS BM	D AB FS BM	D AB FS BM	D AB FS BM	AB FS BM	GM-3 N	AB BM D	AB BM	AB BM	AB BM	AB BM	AB BM	GM-6 R	AB	OK	B AB	B BM	DS AB BM	B
GM-10 M	AB FS	AB FS B	AB FS B	D FS	D FS	D FS	GM-4 O	D B	B AB	B AB	D AB	D B AB	D B AB	GM-7 S	D BM FS AB	AB BM FS	B AB BM FS	B AB FS	D AB BM FS	D AB BM FS

8.5.3 Corrective Action

8.5.3.1 POE

While there were several contributing causes to the corrosion of the mirrors at the CSUN power plant, subsequent testing at Seal Beach (both the continued testing of development modules and the module test matrix) demonstrated eventual darkening of the Stanley mirrors. Based on these data Stanley has revised its mirror formulations to provided improved environmental tolerance.

As a result of this development work Stanley has developed several revisions that promise both improved life and possibly lower cost. Their test data showed great promise and Boeing independently evaluated the promising samples. Two different tests have been carried out Boeing:

- A “soft salt fog” test with the duration limited to one hour;
- UV exposure.

Results for the first set of tests on three different samples are provided in Figure 8-18. The CSUN power plant alloy was ABA + M. While this formulation was not retested the expectation was that the left hand configuration would represent an improvement. While this may be the case it clearly fails the test. On the other hand both ABC alloy with either an M or M + MO_x formulation showed great promise in this test.

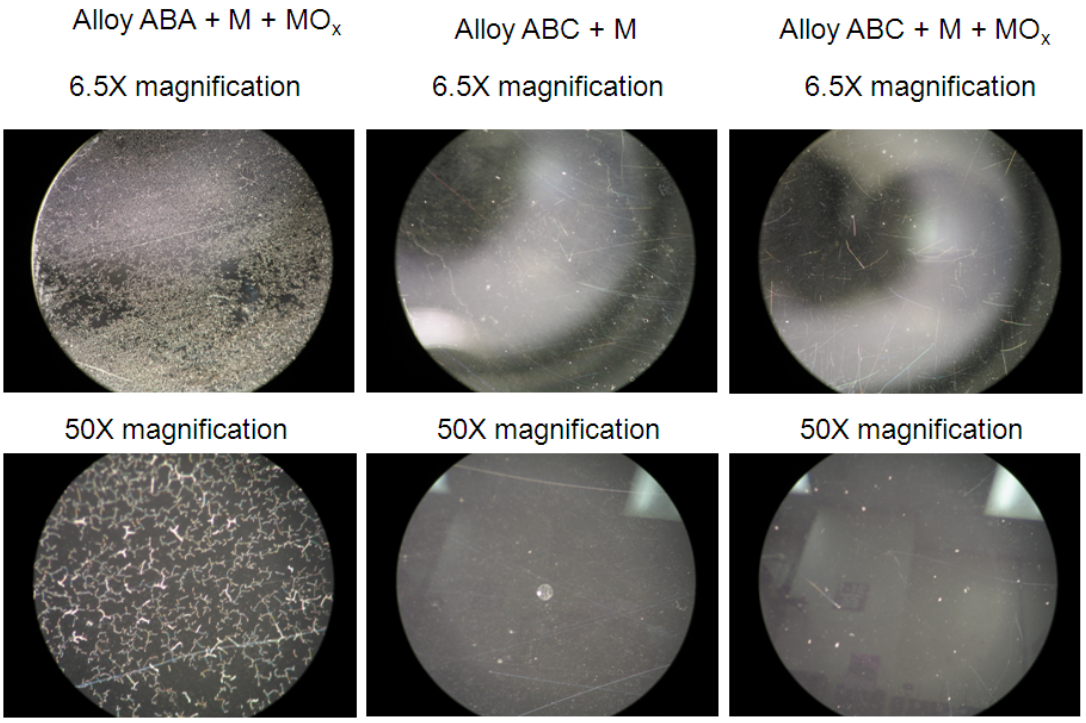

Figure 8-18. “Soft salt fog” test results for three different Stanley mirror formulation.

The next tests involved UV exposure of the samples. The ABA + M configuration had previously passed this test. As shown in Figure 8-19 both ABA + M + MO_x and ABC + M + MO_x pass the test but ABC + M does not.

Based on these results Stanley has provided Boeing with POE samples of the ABC + M + MO_x alloy. The samples were received. These samples were received last year and placed on module test with fully passive environment control. Over five months no change in mirrors has been noted.

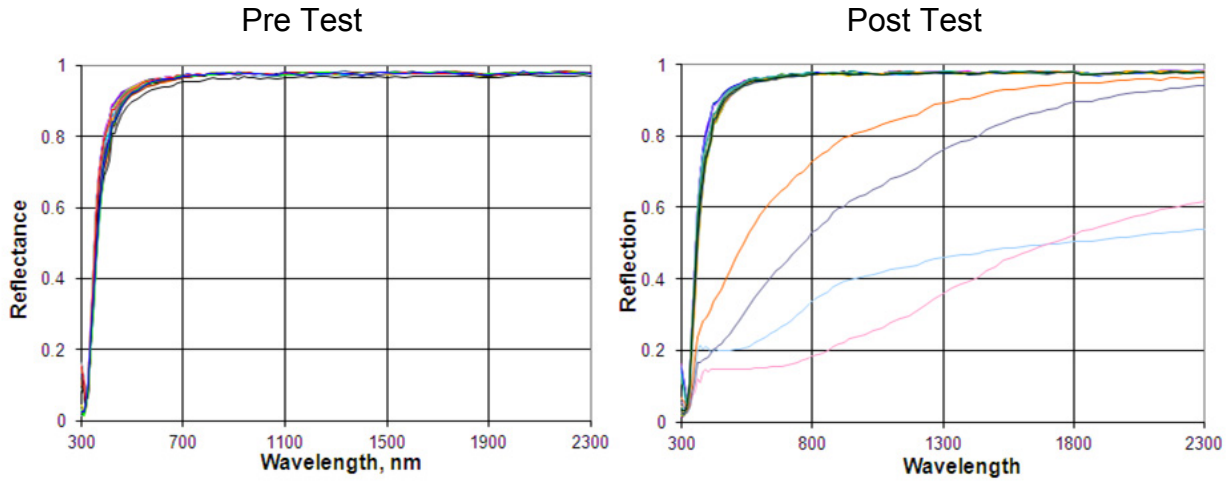

Figure 8-19. Pre (left) and post (right) UV exposure reflectivity test results on new Stanley mirror formulations. Of the new formulations only the ABC + M formulation fails as shown on the right.

8.5.3.2 SOE Kaleidoscope Failure

The SOE anomaly analysis was not complete until December 2011, the end of the contract. Nonetheless the results of the anomaly resolution can be fairly said to define and demonstrate the solution. Future CPV hardware which employs silicone optical adhesives should not employ phenyl substituted versions of these materials, at least not without pre-filtering of the UV spectrum.

Figure 8-20. CSUN Power Plant After Retrofit With Flat PV Panels.

The CSUN CPV power plant was operated through all of 2010. As time progressed the performance continued to deteriorate. There were a limited number of failures of the Centrosolar AR coated window (due probably to both adhesive failure and stress failure of the tempered window). These failures led to ground faults in the system creating a potential electrical hazard. In view of these considerations Boeing strongly urged the decommissioning of the CPV power plant and as a Boeing act of good will replaced the CPV panels with commercial flat panels mounted to the two axis Boeing trackers. The retrofit is illustrated in Figure 8-20.

8.6 Lessons Learned

Schedule compression – While not strictly a technical lesson, most of the issues encountered at in both performance and life of the CSUN power plant were a consequence of a first pass success program approach. This is not intended as a critique of the approach but rather an observation that resources were not available to either fully demonstrate solutions to the issues encountered or more critically to rework the power plant after a complete failure analysis. In particular, budget-driven delays in the start of the manufacturing effort precluded a through resolution of assembly quality and inspection issues which in turn led to performance levels not matching development hardware.

Close coordination between hardware production and deployment – Although this did not affect the final outcome at the CSUN power plant it did lead to initial reduced performance levels achieved owing to prolonged high temperature exposure.

- Delivery of fully completed panels from a distant factory to the power plant site is probably a false economy. Shipping and packaging cost are obvious but even more significant may be artificial design limitations which, for example, may sub-optimize the panel size and tracker to meet transportation load requirements.
- A full understanding of the materials requirements must include both normal and off-normal conditions. During development we were able to minimize off-normal testing. This is not always the case at a construction site and can lead to damage to the hardware.
- Full understanding of all the quality requirements for incoming parts and materials prior to initiating full scale assembly is critical in order to avoid surprises in the field.

Environmental Control – Maintenance of the relative humidity at acceptable levels in the internal module volume is a subtle problem. Local internal humidity distributions may arise leading to premature failure.

Materials requirements – A full understanding of the materials requirements must include both normal and off normal conditions. During development we were able to minimize off normal testing. This is not always the case at a construction site and can lead to damage to the hardware.

Quality requirements – A full understanding of quality requirements for incoming parts and materials prior to initiating full scale assembly is critical in order to avoid surprises in the field. However, such requirements cannot be arbitrarily imposed on a cost critical part but must be based on either analysis, test or field experience.

9 System Testing – SOPO Tasks 1.12, 2.12, 3.12

Task Objectives

The objective of this task was to conduct qualification tests of arrays, modules, and other components as required to qualify the system to applicable design standards.

Highlights

- The 260 kW PVPowered inverter has been both life and endurance qualified. The inverter is now a commercial product with a 10 year base life warranty and an available 20 life warranty.
- IEC 62108 receiver and module qualification has been carried out with POM hardware. The lessons learned from the first exposure to the qualification process will be of great value in the qualification of the final commercial product.
- A remote site module testing program has been carried using POD hardware with the objective of a) debugging the process to facilitate future larger efforts and b).assessing the environmental impact on module life and performance. The lessons learned will be of great value towards eventual wide spread deployment.

Table 9-1. Task 9, System Testing.

Period	Criterion	Results
1	1d-2) Inverter qualified per SCE standard	260 kW inverter qualified and commercialized with a 20 warranty option.
3	3c-2) Array, module and receiver qualified per IEC-63108 standard	Receiver and module qualification program carried out 2010. Multiple lessons learned for eventual commercial qualification

Technical Accomplishments

9.1 Inverter Qualification and Life Testing

The inverter qualification and life testing that is performed during and after the design phase can be summarized as four phases;

- Pre-Functional Testing;
- Functional Testing;
- Compliance Testing;
- Endurance Testing

9.1.1 Pre-Functional Tests

Pre-functional testing is performed during the design phase by engineers responsible for the design. This testing is designed to identify any issues prior to formal qualification of the inverter. The pre-functional test list is given in Appendix B: 260kW Functional Test Matrix. The 260kW inverter completed passed the pre-functional test in April 2009.

9.1.2 Functional Tests

After passing pre-functional testing, functional testing was performed by the PVP Quality and Reliability Group. It is meant to put the inverter through all functions for which it is designed, and verify that it performs those functions properly. The 260kW inverter completed passed the pre-functional test in June 2009.

9.1.3 Compliance Testing

After passing functional testing, the 260kW inverter was subjected to testing against UL 1741 by Nationally Recognized Testing Laboratory Intertek ETL.

9.1.4 Endurance Test Plan

The endurance test for the 260kW inverter design is effectively an accelerated life test using two units. A summary of the endurance test is provided in Table 9-2. The acceleration factors were derived from reliability analysis performed during the inverter design phase.

Table 9-2. Inverter qualification endurance test

Unit A	Unit B
Power Cycling 54,750 cycles idle to full power	Temperature Cycling Test 1,000 cycles Tcc = -40 to 75 °C ΔTc = 130±5
High Temperature Operating Life 1,000 hours, then to failure Ta = 66±3 °C Tj = 147±3 °C	85-85 1000 hours, then to failure 85 °C 85 % relative humidity

9.2 Module Qualification Testing

9.2.1 IEC 63108 Qualification Testing

An abbreviated qualification test program was performed using the SETP program developed, Proof of Manufacturing (POM) modules manufactured in the Spring of 2010 in the Comau robotic assembly line demonstration plant. The objectives of this abbreviated qualification test program were:

- Early evaluation of the environmental robustness of the POM module's as-built design and use test results to clarify key design requirements for the final commercial production design
- Early evaluation or shakeout of the IEC 62108 module qualification test process itself, including setting up the subcontract with the test agency, shipping and handling, test setup and test article installation, test standard interpretation, test agency operations and services, and overall test schedule duration.

The test conditions for the IEC 62108 qualification test regime are summarized in Table 9-3. These tests were performed (in many cases more than once) through the six test sequences listed in Table 9-4. A summary of each specific test sequence follows.

Table 9-3. Qualification evaluation test conditions

Test No.	Test Title	Sample m: module r: receiver	Test Condition
10.1	Visual Inspection	All	Visual Inspection
10.2	Electrical Performance	All	Outdoor side-by-side I-V with DNI > 700 W/m^2 Wind speed < 6 m/s, clear sky
10.3	Ground Path Continuity	All	Measure resistance between grounding point and other conductive parts with 2 X I_{sc} current passing through. I_{sc} specified as 10 A.
10.4	Electrical Insulation test	All	At ambient temperature, 25°C +/- 10°C and RH < 75%, apply 2 X V_{SYS} + 1,000V for 2 min (hi-pot) Vsys specified as 600 V. Measure R at 500V
10.5	Wet Insulation Test	All	Measure R at 500V when the sample is wetted by surfactant solution with resistivity < 3,500Ω /cm
10.6A	Thermal Cycling Test	2r	500 cycles, -40°C to 110°C Apply ***0.38 A*** when T > 25°C Current cycling rate is 10 electrical/thermal
10.6B	Pre-HF Thermal Cycle	1m	400 cycles, -40°C to 65°C
10.7	Damp Heat Test	1m	1755 hours at 65°C and 85% RH
10.8	Humidity Freeze Test	1m	23 cycles as follows: 20 hours at 65°C and 85% RH, followed by cool down to -40°C, dwell at -40°C 0.5 hours min.
10.9	Hail Impact Test	1m	At least 10 shots of 25.4mm diameter ice ball at 22.4 m/s on areas where an impact by hailstone falling from 45° around the vertical line is possible

Test No.	Test Title	Sample m: module r: receiver	Test Condition
10.10	Water Spray Test	1m	1 hour of water spray in each of the following orientations, with at least 15 min. between tests: a. Front surface 45° to the horizontal b. In the stow position c. At the normal limit of its allowed tracking d. Upside down, if appropriate for module operation
10.11	Bypass Diode Thermal Test	1r	At 75 °C sample temperature, apply 10 A through the receiver for 1 h, then measure bypass diode temperature. Apply 12.5 A for additional hour.
10.12	NA		
10.13	Mechanical Load Test	1m	10.4 PSF on front and 23.625 PSF on back 1 hour each, total of 3 cycles.
10.14	Off-axis Beam Damage Test	1m	Light aimed at suspect locations for at least 15 minutes when DNI > 800W/m^2, or walk-off for 3 hours
10.15	UV Conditioning Test	1m	Expose to UV accumulation of **15** kWh/m^2
10.16	Outdoor Exposure Test	1m	Expose to DNI accumulation of **363** kWh/m^2 when DNI > 600W/m^2
10.17	NA		

As shown in Table 9-4, four modules failed the initial dry high potential (hi pot) electrical insulation test at 2200 Volts. It should be noted that the 2200 volt test criteria is defined in the IEC 62108 standard as 1000 volts plus two times the specified system voltage and Boeing's specified system design voltage is 600 volts. Boeing conservatively chose to evaluate the POM modules against the design specified system voltage instead of the lower actual system voltage for the purposes of this test. The POM panel and array field configuration actual system open circuit voltage is ~ 432 volts. Using a conservative round-up to 450 volts would result in a high pot test voltage of 1900 volts (1.9 kV). The actual voltage where the breakdown or arc occurred, if recorded during the test, is shown in Table 9-4 for cases where the test failed to meet the 2200 volts level. The POM appears to pass the dry hi pot test if the actual system voltage is used to derive the test criteria instead of using the design requirement value.

Table 9-4. POM module qualification evaluation test summary, green indicates the test was passed, red that the test was failed.

	Sequence No.	A	B	C	D	E		F
	Test Article No.	0QT1: r1,r2,r3 R_"Kapton"	0QT3	0QT2	0QT7	CM11	0QT4	CM10
Code	Test	Receiver Thermal and Current Cycling	Humidity Freeze	Damp Heat, Mech Load	MST26, Hail Impact	UV and Outdoor Exposure	Control	Safety, CEC, Off Axis, Water Spray
10.1	Visual Inspection							
10.2	Elec Perf SBS (outdoor IV)							
		Incident 1						
10.3	Ground Path Continuity							
10.4	Dry Hipot-500V							
10.4	Dry Hipot-2200V				1.95 kV	2.1 kV	2.02 kV	1.98 kV
10.5	Wet insulation (wet hipot)							
10.6	**Thermal Cycling (Rcvr)**	500 cycles						
10.11	**Bypass Diode Test**							
10.6	**Pre-HF Thermal Cycling**		500 cycles					
10.1	Visual Inspection							
10.8	**Humidity Freeze**		23 cycles					
10.1	Visual Inspection							
10.7	**Damp Heat**			1755 hours				
10.4	Dry Hipot-500V							
10.4	Dry Hipot-2200V			2.15 kV				
10.5	Wet insulation (wet hipot)							
MST26	**Reverse Current Overload**							
10.5	Wet insulation (wet hipot)							
10.9	**Hail Impact**							
10.4	Dry Hipot-500V							
10.4	Dry Hipot-2200V							
10.5	Wet insulation (wet hipot)							
MST11	**Accessibility**							
10.15	**Ultraviolet conditioning**					15.1 kWh/m^2		
10.16	**Outdoor exposure**					363 kWh/m^2		
10.4	Dry Hipot-500V							
10.4	Dry Hipot-2200V							
10.5	Wet insulation (wet hipot)							
						Incident 2		
8703	**Temperature**							
8703	**Elec Parameter Test**							
CEC	**Performance @ PTC**							
10.14	**Off Axis Beam Test**							
10.1	**Water Spray**							
10.4	Dry Hipot-500V							
10.4	Dry Hipot-2200V							
10.3	Ground Path Continuity							
10.2	**Elec Perf SBS (outdoor IV)**	For Info Only				For Info Only	Control	
10.13	**Mechanical Load**			Incident 3				
10.4	Dry Hipot-500V							
10.4	Dry Hipot-2200V							

9.2.1.1 Sequence A

Two receiver pairs from a POM module passed the Receiver Thermal Cycling Test. The test exposed the receiver assembly sections to the required 500 cycles from -40° C

to +110° C (as referenced from the cell temperature). No discontinuities in current were observed during the powered portions (0.38A) of the test when the cell temperature rose above 25° C.

A Seal Beach manufactured POM single receiver assembly passed the Bypass Diode Test. The test exposed the single receiver to the specified rated short circuit current of 10 Amps for 1 hour and 12.5 Amps for 1hour with initial device temperature set to 73° C. The calculated maximum diode junction temperature reached 91.8 ° C versus the rated max junction temperature of 150° C. This same single receiver special test article had been exposed to the 500 cycle receiver thermal cycling test and was used as a solar cell temperature monitor to control the test chamber setting.

Test "Incident 1" occurred during Test Sequence A as the 0QT1 module fell off the outdoor test frame following initial electrical side by side performance tests. This was caused by an improperly mounted module. While the receiver assembly sections passed thermal cycling, the post test electrical side by side measurement was not valid as the 0QT1 module chassis optical alignment had been impacted by the incident.

9.2.1.2 Sequence B

POM module 0QT3 failed the Humidity Freeze Test Sequence. The module passed the initial series of dry and wet hi pot electrical insulation tests. The module passed the required 400 pre-conditioning thermal cycles from -40° C to +65° C. The Humidity Freeze test was executed for 23 cycles of 20 hours at +65° C and 85% RH followed by at least 30 minutes of no humidity control and -40° C temperatures. The test failure was observed upon inspection of the module in the chamber after stopping the test. The module glass cover had shattered. Broken glass had fallen into the cavity of the module.

9.2.1.3 Sequence C

POM module 0QT2 failed the Damp Heat and Mechanical Load test sequence. The module passed the initial series of dry and wet hi pot electrical insulation tests. The module completed 1755 continuous hours of damp heat exposure at +65° C and 85% RH. The post test dry hi pot test passed at the 500 V level but experienced breakdown or arcing before reaching the 2200 V level. As shown in Table 9-4, other modules failed dry hi pot when approaching the 2200 V level before environmental exposure. The module passed the post test wet hi pot test. The final side by side electrical test indicated the performance of the module had degraded by 27%.

POM module 0QT2 was then exposed to the default test requirement from IEC 62108 attempting to apply 2400 kPA (50.124 PSF) load across the front then the back of the module. "Incident 3" occurred when the module collapsed before the final load was applied. Unfortunately this was an over test. The requirement permits the manufacturer to specify the design load of the module. Boeing plans to qualify to lower loads (10.4 PSF front and 23.6 PSF back) as our design requirements target is a more benign ice & snow load based on historical data in the Southwest USA. In an actual qualification certification test, TÜV Rheinland PTL would have insisted on a module installation and loading manual for this test from the manufacturer prior to running the test. While the intent was to perform this evaluation test to the Boeing design loads, it was an oversight on the part of Boeing to not provide the intended load condition formally (It should be

noted that Boeing had previously conducted and passed the mechanical load test on POD series modules to the Boeing design loads.). A formal module installation and mechanical loading specification will be provided to the CPV test provider in the future.

9.2.1.4 Sequence D

POM module 0QT7 passed its test sequence which included Reverse Current Overload and Hail Impact Tests. The module passed the post stress test evaluation tests including dry and wet hi pot electrical insulation tests, ground path continuity, and final side by side electrical performance test even though the pre-stress dry hi pot test did not reach the 2200V level before arcing or breaking down.

9.2.1.5 Sequence E

POM Module CM11 accumulated 15.1 kWh/m^2 UV and 363 kWh/m^2 outdoor exposures. The initial pre-environmental dry hi pot test did not reach the 2200V level before arcing or breaking down yet passed completely both the dry and wet post environment hi pot electrical insulation tests. "Incident 2" occurred when pulling the module out of the water bath after the wet hi pot test. The module cover glass was not supported properly and the glass broke off from the suction force. This is considered by TÜV Rheinland PTL and Boeing as a test operator error. Unfortunately with the glass breakage, module optics became misaligned, water exposed, and prevented a valid post environment side by side performance test.

9.2.1.6 Sequence F

POM module CM10 was used for a series of safety related tests. The initial pre-environmental dry hi pot test did not reach the 2200V level before arcing or breaking down and wet hi pot electrical insulation tests also failed.

The UL8703 based Temperature test, Electrical Parameter Test, and CEC performance measurements were performed for engineering information.

POM module CM10 failed both the off axis beam test and the water spray tests specified in IEC 62108.

9.2.1.7 IEC 62108 Module and Receiver Test Conclusions and Lessons Learned

The qualification evaluation test results indicated that the Spring 2010 POM modules do not pass the environmental robustness standards defined by the industry accepted IEC 62108 test program. Failed events include module window damage due to Humidity Freeze Test, high performance degradation due to Damp Heat Test, and water incursion due to Water Spray Test. Key test successes include Hail Impact Test, Receiver Thermal Cycle Test, and Bypass Diode Thermal Test

The module qualification evaluation test program, conducted June 29th to Dec 1st 2010 by TÜV Rheinland PTL at their test facilities in Tempe, Arizona, accomplished these test objectives. Boeing experienced the qualification process of every applicable test and established a working relationship with a CPV industry respected and accredited test laboratory. Important lessons learned about the test process itself, to be incorporated for future evaluation or formal certification testing includes.

- Provide spare modules to replace damaged equipment due to operator error

- Account for seasonal weather impacts to outdoor performance test schedule.
- Incentivize early completion of non critical path tests
- Provide formal spec and loading instructions for mechanical load test

9.2.2 Remote Site Testing

This was a complex task performed during the second budget period. Rather than attempt to duplicate the report it is included in its entirety as an Appendix B to this report.

9.2.3 Lessons Learned

The lesson learned from this effort is the criticality of adequate planning prior to engaging in an expensive and high visibility test. This manifest itself in at least two major issues:

- The failure of the off site test program to have a major influence on the main program. This was a result of the low visibility of the effort, its execution with hardware of an obsolete design and employment of inadequate test instrumentation.
- The second examples were the failures that occurred at TUV due to human error as opposed to hardware failure. At the very least spare hardware should have be provided for the effort

10 Deployment Facilitation – SOPO Tasks 1.13, 2.13, 3.13

Task Objectives

The objectives of this task is to develop a project plan in collaboration with a utility partner for a multi-megawatt system installation, including project definition, site preparation, shipping, installation, grid integration and testing.

Highlights

- Licensed the technology to Stirling Energy Systems.
- Continued broad effort to negotiate multiple non-exclusive licenses for technology commercialization.

Table 10-1. Deployment Facilitation

Period	Criterion	Results
1	1g-1) Identification of deployment and marketing partner	A licensing agreement of the Boeing XR700 technology was negotiated with Sterling Energy Systems, and technology transfer engineering services agreement entered into.

Technical Accomplishments

10.1 Overall Plans

Spectrolab's core business will be expanded with large-scale terrestrial solar cell production to generate substantially higher multifunction solar cells suitable for the Boeing XR700 CPV System. Spectrolab will continue to challenge the world in terrestrial solar cell efficiency and manufacturing volume. Boeing has invested $55M to expand the capacity of the Spectrolab solar cell business.

To support and stimulate demand for the Spectrolab suite of high-efficiency products and the Boeing EPC services business, Boeing developed a CPV system with the highest acceptance angle and concentration that is on the market. The Boeing CPV product is a system suited for highly automated production that leverages high-efficiency solar cells and innovative low-cost manufacturing processes. Multiple product evolution strategies have been developed that will continue to drive down overall system cost. The recent Navigant review (Appendix A) attests that Boeing can meet the LCOE goal of $0.15/kWh, and approaches have been developed to meet future LCOE goals.

10.2 Stirling Energy Systems

Commercialization of the SETP technology is of key interest to Boeing and DOE. To maximize the value of the technology developed during the SETP program and ensure CPV XR700 commercialization, Boeing launched a rigorous search for a license partner that would bring the requisite manufacturing skills and solar business focus to succeed with this CPV product through a targeted invitation process. The search involved finding, examining, validating and negotiating more than 10 potential licensees. That list was reduced to four by a process of requests for proposal (RFP) and in-depth back-

ground investigations. Boeing selected Stirling Energy Systems as the logical licensee. SES, in collaboration with Tessera, was determined to have the necessary expertise and market focus to address the CPV market. In addition, the SES vision for a market segmentation wherein the CPV product would address the distributed power market while its core dish product would address the larger scale (>50MW) utility market was attractive.

Boeing would take the role of the power plant EPC. In December 2009, SES signed a license agreement to develop and deploy the XR system as a complement to its existing dish system. Subsequently, SES provided Boeing with an engineering services agreement whereby SES funded Boeing to work with SES' chosen manufacturing partner, Magna International, to start work on the next-phase design. SES' manufacturing model focused on the use of world-class automotive manufacturing partners to produce its products. Magna International, a leading tier 1 automotive component supplier, identified a team to support Boeing's design team to work on the development of a next-generation design. The goal of this effort was to reduce cost to $2.50/W for the CPV components, including the tracker, pole, and array. This decision was based on the assumption that PV prices will continue to fall to installed costs below $3.00/W.

SES concluded that the system required capital investment not affordable by Stirling Energy Systems because of SES financial constraints and management strategies. Boeing was informed that Stirling Energy Systems could not pursue commercially developing the XR700. After 10 months Stirling Energy Systems ended its commercial development support for the XR700 system. This decision occurred in a period of tightening cost constraints which lead within a year to the bankruptcy of SES.

Negotiations completed with Stirling Energy Systems resulted in the return of the intellectual property (IP) control to Boeing.

10.3 Current Partnership Initiatives

Boeing remains committed to securing a commercialization partner for the XR700 CPV product and has completed an independent review of the XR system cost model. The Company concludes that the product is very competitive with PV, and, when LCOE is calculated for the CPV product, it can be shown to be competitive with current or forecast PV costs. In fact, the greater kW-hr/kW installed fraction makes CPV the technology of choice in the US Southwest as well as in other high DNI locations. In 2011, Boeing was able to extend the SETP contract at no cost to DOE to enhance the performance and improve the system design based on previous testing results that can reduce cost of the XR700 system to competitive projected levels.

Boeing continues to negotiate with prospective partners to secure a license partner into the future. Boeing has several candidates with high interest in the XR700 CPV System. One US company has received a limited license and signed an option to acquire pending financial backing or leverage in the near- future. Others have serious interest to expand their business and enter the CPV solar market.

Conclusions

The success of the Boeing SETP program must be measured against the following goals

Technology Development:

Significant successes in this area include

- Advancement of multijunction cell performance by at least 3.5% (36.5% to 40%) and implementation of this advancement in commercial cells which have become the building block for the industry.
- Mechanization of cell production to a capacity capable today of supplying a 250 MW per year commercial CPV industry
- Demonstration of the real potential of non-imaging optics in module hardware operating at up to 33.8% aperture energy conversion efficiency.
- Demonstration of low cost, long life, state-of-the-art component technologies available to the industrial community in the areas of heat sinks, inverters, optics, environmental control, trackers, etc.

While the program experienced several technical and production challenges, all contributing issues were fully resolved and these experiences do not detract from the potential of the technology. CSUN was a test field and the numerous lessons learned from this experience have incorporated in the design.

Cost Control:

From the beginning the Boeing effort was managed with a clear understanding that the end state was not the highest conversion efficiency but the lowest LCOE. This management approach assured that technical success would be reflected in true national value. Boeing managed not only with a clear view of the contract requirement of $0.15 per kWh but saw over the horizon that a sustainable product worthy of true commercialization had to meet the out-year challenge of $0.07 per kWh. That this challenge can be met has been demonstrated not simply by analysis but by the demonstration of enabling technologies in the spheres of component hardware, producibility and balance of systems.

Manufacturing:

A 2 MW per year fully robotic manufacturing facility was built and demonstrated at the design production rate. This facility produced the initial 100 kW of tracker ready arrays and demonstrated key production aspects of achieving low manufacturing cost goals. With this facility the commercial potential of the Boeing design and the manufacturing expertise of U.S. industry were demonstrated.

Commercialization:

Finally, with the commercialization potential of the Boeing of the CPV system technology being demonstrated on the SETP program, the Boeing Company is continuing to pursue its technology licensing into the solar energy industry. It is hoped that this report

will serve to describe the program and technology in sufficient detail to develop potential licensing interest, and will prove of value to other CPV developers.

Patents and Disclosures

Case Reference	Submission Date	Inventors (List)	Proposed Title	Decision
07-0222	01 Mar 2007	Grip, Robert E. (290409);Jones, Russell K. (597921)	Assembly of High-Precision Solar Collector Array Using Low-Precision Supporting Structure	Protect with a Patent
07-0283	16 Mar 2007	Grip, Robert E. (290409)	Structurally Constrained Solar Receiver Assembly	Protect with a Patent
07-0424	8 Aug 2007	Kinsey, Geoffrey Mesropian, Shoghig	PV Cells with Selectively Patterned TCO Coatings and Associated Methods	Protect with a Patent
07-0548	25 May 2007	Grip, Robert E. (290409)	Structurally Isolated Thermal Interface ("Hairy Heat Sink")	Protect with a Patent
08-0371	15 Apr 2008	Hebert, Peter (1032050);Brandt, Randolph J (1036694)	Method for the Attachment of Solar Collectors to Structural Framework	Protect with a Patent
08-0453	06 May 2008	Hebert, Peter (1032050);Brandt, Randolph J (1036694)	Flexible Thermal Cycle Test Equipment for Concentrator Solar Cells	Protect with a Patent
08-0494	15 May 2008	Schwartz, Joel A. (1029362);Narayanan, Authi A (1417993);Benitez, Pablo (1726511);Minano, Juan-Carlos (INV-20975);Plesniak, Adam P (1501911);Grip, Robert E. (290409)	Enclosed Off-Axis Solar Concentrator	Protect with a Patent
08-1155	24 Nov 2008	Fetzer, Christopher M. (1077597)	Highly Doped Layer for Tunnel Junctions in Solar Cells	Protect with a Patent
09-0034	14 Jan 2009	Frericks, Jeff E (231555);Hightower, Charles H (245048)	Mitigation of Gridline Blockage Over a Wide Range of Incident Angles to Enhance Photovoltaic Photon Conversion Efficiency	Deferred

Case Reference	Submission Date	Inventors (List)	Proposed Title	Decision
09-0159	18 Feb 2009	Plesniak, Adam P (1501911)	Solar Concentrator Light Shield	Protect with a Patent
09-0174	24 Feb 2009	Plesniak, Adam P (1501911)	Sealed Concentrator Cell Assembly with Optically Active Cover	Protect with a Patent
09-0298	27 Mar 2009	Liao, Henry H. (235179)	2-AXES Tracker for Solar Panel and Reflector Antenna	Protect with a Patent
09-0317	04 Apr 2009	Plesniak, Adam P (1501911)	Non-Enclosed Off Axis Concentrator	Deferred
09-0452	26 May 2009	Hightower, Charles H (245048);Frericks, Jeff E (231555);Narayanan, Authi A (1417993)	Diode-less Terrestrial Photovoltaic Solar Power Array	Deferred
09-0522	19 Jun 2009	Rau, Scott J. (1036247)	Solar Tracker Shuffle Motor Drive	Protect with a Patent
09-0537	23 Jun 2009	Wilson, Kitchener (1953973)	A Means of Disconnecting a Photovoltaic Array from a Network of Arrays by Incorporating the Array and Inverter Electrical Characteristics	Deferred
09-0559	26 Jun 2009	Ventura, Mark C (221944);Davis, Kenneth F. (383532);Raetz, John E (305411)	Ice Blast Cleaning of Solar Power Systems	Protect with a Patent
09-0560	28 Jun 2009	Wilson, Kitchener (1953973);Rau, Scott J. (1036247);Oittinen, Karl C (280767)	No Sun Sensor Solar Tracker Controller	Deferred
09-0906	07 Oct 2009	Plesniak, Adam P (1501911);Hall, John C. (1031883)	Plastic Module Enclosed Off Axis Concentrator	Protect with a Patent
09-1116	04 Dec 2009	Grip, Robert E. (290409)	Solar Array Vane and Counterweight	Protect with a Patent
09-1178	18 Dec 2009	King, Richard R. (1030153);Boisvert, Joseph C. (1049873);Law, Daniel C. (1175208);Fetzer, Christopher M. (1077597);Krut,	Structures for Increased Photogeneration and Long-Wavelength Rejection in Photovoltaic Cells	Deferred

Case Reference	Submission Date	Inventors (List)	Proposed Title	Decision
		Dimitri D. (1036911);Edmondson, Kenneth M (1035002);Karam, Nasser H. (1031011)		
10-0213	25 Mar 2010	Plesniak, Adam P (1501911);Hall, John C. (1031883)	Glass Cover Design for Plastic Module Enclosed Off Axis Concentrator	Deferred
10-0330	06 May 2010	Grip, Robert E. (290409);Cameron, Michael S. (230409)	Ski-Lift Solar Array Tracker Configuration	Protect with a Patent
10-0336	11 May 2010	Plesniak, Adam P (1501911)	Rooftop / Ground Mounted Solar Concentrator Tracker	Deferred
10-0517	13 Aug 2010	Plesniak, Adam P (1501911)	No Chassis Off Axis Concentrator	Deferred
10-0696	29 Jul 2010	Frost, John (1491268);Brandt, Randolph J (1036694);Hebert, Peter (1032050);Al Taher, Omar (1863378	Solar Cell Interconnecting Method	Protect with a Patent
10-0790	15 Oct 2010	Jungwirth, Douglas R. (1489752);Quezada, Emilio (1035538)	Large area, high intensity, continuous solar simulator	Protect with a Patent
10-1370	13 Dec 2010	Zhang, Xiaobo (1634487);Bhusari, Dhananjay M (1684245);Lee, Hoon H (1105159)	Multiple Junction Solar Cell With No Mesa Damage	Protect with a Patent
11-0869	21 Jun 2011	Hall, John C. (1031883);Martins, Guy L. (234846)	Componentized Low Cost CPV Module Design	Protect with a Patent

Papers

A. Cvetkovíc, M. Hernandez, P. Benítez, J.C. Miñano, J. Schwartz, A. Plesniak, R. Jones, D. Whelan, “The Free Form XR Photovoltaic Concentrator: a High Performance SMS3D Design,” Proc. SPIE 2008, Vol. **7043, 70430E**.

Adam Plesniak, Russ Jones, Joel Schwartz, Guy Martins, John Hall, Authi Narayanana, David Whelan, Pablo Benítez, , Juan C. Miñano, Aleksandra Cvetkovíc, Maikel Hernandez, Oliver Dross, Roberto Alvarez,”HIGH PERFORMANCE CONCENTRATING PHOTOVOLTAIC MODULE DESIGNS FOR UTILITY SCALE POWER GENERATION”

R. R. King, R. A. Sherif, G. S. Kinsey, D. C. Law, K. M. Edmondson, H. Yoon, H. L. Cotal, C. M. Fetzer, J. H. Ermer, P. Hebert, P. Pien, and N. H. Karam, “New Opportunities in Concentrator Photovoltaics with Low-Cost, 40%-Efficient Multijunction III-V Solar Cells,” SPIE Optics & Photonics Conference, San Diego , California Aug. 26-30, 2007.

R. R. King, D. C. Law, K. M. Edmondson, C. M. Fetzer, G. S. Kinsey, H. Yoon, R. A. Sherif, D. D. Krut, J. H. Ermer, P. Hebert, P. Pien, and N. H. Karam, “Multijunction Solar Cells with Over 40% Efficiency and Future Directions in Concentrator PV,” Proc. 22nd European Photovoltaic Solar Energy Conference and Exhibition, Milan, Italy, Sep. 3-7, 2007.

R. R. King, D. C. Law, K. M. Edmondson, C. M. Fetzer, G. S. Kinsey, H. Yoon, D. D. Krut, J. H. Ermer, R. A. Sherif, and N. H. Karam, “The Physics of Terrestrial Concentrator Solar Cells with Over 40% Efficiency,” The Industrial Physics Forum 2007: The Energy Challenge, American Vacuum Society (AVS) 54th International Symposium, Seattle, WA Oct. 14-19, 2007.

G. S. Kinsey, P. Pien, P. Hebert, R. A. Sherif, R. Brandt, J. Lacey, J. Hanley, N. Beze, R. R. King, J. Hoskin, B. Stone, T. Cavicchi, and J. Peacock, “Multijunction Concentrator Photovoltaic Cells,” Solar Power 2007, Long Beach, CA, Sept. 2007.

G. S. Kinsey, P. Pien, P. Hebert, and R. A. Sherif, “Operating Characteristics of Multijunction Solar Cells,” 17th PVSEC Fukuoka, Japan, Dec. 2007.

G. S. Kinsey, P. Pien, P. Hebert, and R. A. Sherif, “Multijunction solar cells for CPV,” 1st Concentrating Photovoltaic Summit, Madrid, Spain, Apr 2008.

G. S. Kinsey, R. A. Sherif, P. Pien, P. Hebert, R. R. King, and D. Aldrich, “ Towards Commercialization of Concentrator Multijunction Photovoltaic Modules,” IEEE PVSC, San Diego, California, May, 2008.

G. S. Kinsey, P. Hebert, K. E. Barbour, D. D. Krut, H. L. Cotal, and R. A. Sherif, “Concentrator multijunction solar cells,” Progress in Photovoltaics: Research and Applications, June, 2008.

Geoffrey S. Kinsey and Kenneth M. Edmondson, “Spectral Response and Energy Output of Concentrator Multijunction Solar Cells,” Progress in Photovoltaics: Research and Applications, submitted June, 2008

P. Hebert, “Qualification and Reliability of High efficiency Multijunction concentrator solar cells for terrestrial applications,” SPIE Optics & Photonics Conference, San Diego, California, Aug. 11-14, 2008.

G.S. Kinsey, D. Bhusari, C. M. Fetzer, P. Hebert, R. R. King, R. A. Sherif, and P. Pien, “Multijunction Solar cells in HCPV Systems,” 23rd European PVSEC, Valencia, Spain, Sept. 2008.

R. R. King, A. Boca, W. Hong, D. C. Law, G.S. Kinsey, C.Fetzer, M. Haddad, K. Edmondson, H. Yoon, P. Pien and N. H. Karam, “High Efficiency Multijunction Photovoltaics for Low-Cost Solar Electricity,” IEEE Laser and Electro-Optics Society Annual Meeting, Newport Beach, CA, Nov. 9-13, 2008.

A. Boca, K. Edmondson, and R. King, “Concentrator solar cell performance enhancement by way of prismatic covers,” International Conference on Solar Concentrators for the Generation of Electricity, ICSC-5, Palm Desert, CA, Nov. 16-19, 2008.

R. Jones, “Terrestrial PV Technology from the Aerospace Industry,” IEEE SCV-EDS PV Symposium, October 2,2008.

R. King, et.al., “High-Efficiency Multijunction Photovoltaics for Low-Cost Solar Electricity,” LEOS Fall Meeting, November 9, 2008.

R. Jones, “Solar Cell Suppliers: Industry Perspective Spectrolab, Inc.,” ICSC-5 Palm Desert, CA, Nov. 16, 2008.

R. King, et.al., “High-Efficiency Terrestrial Concentrator Multijunction solar Cells- Research to Manufacturing at Spectrolab,” ICSC-5 Palm Desert, CA, Nov. 16, 2008.

R. Jones, “New Frontiers in Solar Cell Conversion Efficiency,” Council of Scientific Society Presidents, Washington DC, Dec. 7, 2008.

D. Krut, “Characterization fo Multijundtion Solar Cells for Concentrator Application,” 2nd Concentratin PV Optics and Power Workshop (CPVOP) Darmstadt, Germany, March 9-10, 2009.

D. Law, et.al., “Future Terrestrial III-V Multijunction Solar Cells: Practical Efficiency Ceiling and Technology Pathway,” Material Research Society Spring Meeting, San Francisco, CA, April 13, 2009.

R. Jones, et.al., “Spectrolab Progress in Multi-Junction Cell Performance and Cost,” CPV Summit, Toledo, Spain, April 27, 2009.

R. Jones, et.al., “Progress in High-Efficiency Terrestrial Concentrator Solar Cells,” IEEE Photovoltaic Specialists Conference PVSC-36, Philadelphia PA, June 7, 2009.

A. Boca, et.al., “Prismatic Covers for Boosting the Efficiency of High-concentration PV Systems,” 36th IEEE Photovoltaic Specialist Conference, Philadelphia, PA, June 7, 2009.

R. King, et.al., “Electronic Materials Science Challenges in Renewable Energy,” 51st Electronic Materials Conference, University Park, PA June 24, 2009.

R. King, “Raising the Efficiency Ceiling on Multijunction Solar Cells,” Stanford Photonics Research Center Symposium, Sept. 14, 2009.

R. King, “Band-Gap-Engineered Architectures for High-Efficiency Multijunction Concentrator Solar Cells,” 24th European Photovoltaic Solar Energy Conference, Hamburg, Germany Sept. 21, 2009.

N. Karam, “Ultrahigh Efficiency Multi-junction Solar Cells for Terrestrial Applications,” Arizona State University, AZ, Nov. 6, 2009.

Daniel C. Law, et.al., “Electric Energy Generation using Concentrating Photovoltaic III-V Solar Cell Technology,” Printed Electronics USA 09 San Francisco, CA, December 2, 2009.

P. Hebert, et.al., “Qualification and Reliability of High efficiency Multijunction Concentrator Solar Cells for Terrestrial Applications,” SPIE Reliability of Photovoltaic Cells, Modules, Components, and Systems, August 11, 2008.

N. Karam, “Recent Progress in Concentrating Photovoltaic solar Cell Technology and Manufacturing,” Solar Energy and Technology, SPIE Optics and Photonics, San Diego, CA, Aug. 2, 2009.

A. Plesniak, “Deployment and Performance of Boeing HCPV Modules and Arrays,” CPV Summit USA 2010 Proceedings.

P. Hebert, “Reliability of II-V Multi Junction Solar Cells in High Concentration Terrestrial Applications,” International Reliability Physics Symposium, Anaheim, CA, May 26, 2010.

C. Fetzer, et.al., “MOVPE Development of III/V Multijunction Terrestrial Solar Cells at Spectrolab,” CPV 6, Freiburg Germany April 7, 2010.

D. Larrabee, et.al., “Progress in High Efficiency III-V Multijunction CPV at Spectrolab,” CPV 6, Freiburg Germany April 7, 2010.

A. Zakaria, et.al., “Influence of the Degree of Order of InGaP on its Hardness Determinded Using Nanoindention,” Journal of Applied Physics, 2010.

M. Ventura, “High Efficiency XR-700 Concentrator Photovoltaic System,” Solar Energy Technologies Program Peer Review, May 26, 2010.

C. Fetzer, et.al., “MOVPE Development of III-V Multijunction Terrestrial Solar Cells at Spectrolab,” ICMOVP XV, Lake Tahoe NV, May 23, 2010.

R. King, et.al., “Energy Production in Next-Generation Multijunction Solar Cells,” Special Issue of Journal Progress in Photovoltaics, 2010.

R. King, et.al., “Multijunction Solar Cells: A Look Back and the Path Forward,” Cherry Award presentation, 35th IEEE Photovoltaic Specialist Conference, Honolulu, HI , June 20, 2010.

R. Jones, et.al., “Status of 40% Production Efficiency Concentrator Cells at Spectrolab,” 35th IEEE Photovoltaic Specialist Conference, Honolulu, HI, June 20, 2010.

Adam Plesniak, Guy Martins, and John Hall, “Production and deployment of high performance CPV panels for the utility scale marketplace,” Proc. SPIE 7769, 77690C (2010)

O. Al Taher, et.al., “Qualification Testing of 40% metamorphic CPV Solar Cells,” 35th IEEE Photovoltaic Specialist Conference, Honolulu, HI, June 20, 2010.

P. Hebert, et.al., “Reliability of II-V Multi Junction Solar Cells in High Concentration Terrrestrial Applications,” International Reliability Physics Symposium, May 26, 2010.

R. King, et.al., “Fundamental Efficiency Losses in Next-Generation Multijunction Solar Cells,” 25th European Photovoltaic Solar Energy Conference, Valencia Spain, September 6, 2010.

P. Hebert, “Proposed Thermal Cycle Test for IEC Bare Cell Qualification Standards,” NREL Reliability Workshop, Feb. 18, 2010.

N. Karam, “Progress in Concentrating Photovoltaic Solar Cell Technology & Production for Low-cost Energy Generation,” 2010 Photovoltaic Summit, San Diego CA, May 3-5, 2010.

J.H. Ermer, “III-V Multi-Junction CPV: A Look Forward at Challenges and Opportunities from 40% to 50%,” NIST Grand Challenges for Advanced Photovoltaic, Technologies and Measurements, Denver, Colorado, May 11-12, 2010.

R. Jones, et.al., “Multi-Junction III-V Solar Cells and CPV - The Next Big Thing in PV,” Solar Power International, Los Angeles, CA, Oct. 10-12, 2010.

D. Bhusari, et.al., “Wafer Processing Aspects of High Efficiency Multi-Junction Solar Cells,” CPV-7 (7th International Conference on Concentrating Photovoltaic Systems), Las Vegas, NV, April 4-6, 2011.

P. Hebert, et.al., “Qualification Testing of 40% metamorphic CPV Solar Cells,” CPV-7 (7th International Conference on Concentrating Photovoltaic Systems), Las Vegas, NV, April 4-6, 2011.

P. Hebert, et.al., “Improved Thermal Cycling,” CPV-7 (7th International Conference on Concentrating Photovoltaic Systems), Las Vegas, NV, April 4-6, 2011.

P. Hebert, “What not to Do,” NREL PV Reliability Workshop, Feb. 17, 2011.

R. King, et.al., “Raising the Efficiency Ceiling in Multijunction Solar Cells,” Institute for Energy Efficiency, and Center for Energy Efficient Materials Seminar, Univ. of California Santa Barbara, Feb. 16, 2011.

John C. Hall, Guy L. Martins, Michael Cameron, Stuart Marks. “Boeing High-Efficiency Low-Cost Concentrated Photovoltaic Technology” Solar Energy and Technology, SPIE Optics and Photonics, San Diego, CA, August, 2011.

Travel

Travel Date	Travelers	Head Count	Place	Purpose of the trip	Accomplishment
12/10/06-12/13/06	Peichen Pien	1	Taiwan	Receiver assembly supplier evaluation	Conducted process capability evaluation and finalized receiver assembly specification
3/12/2007	Beth Stone Jon Lacey Maggie Lau	3	St. George UT	Evaluate subcontractor (Sylarus) Ge substrate process capability	Conducted initial process capability evlauation
5/9/07-5/11/07	Jim Ermer Terry Cavicchi	2	Newark, NJ	MOVPE reactor supplier evaluation	Conducted equipment capability evaluation
9/1/2007	Richard King	1	Milan, Italy	22nd European Photovoltaic Solar Energy Conference and Exhibition, Milan, Italy, Sep. 3-7, 2007	Deliver invited plenary. Gain information on latest developments in photovoltaic technology, and business opportunities in photovoltaics.
8/25/07	Richard King	1	San Diego	SPIE Optics & Photonics Conference, San Diego, California, Aug. 26-30, 2007	Deliver invited talk. Gain information on latest technological developments in the fields of semiconductors and optics.
10/9/07 - 10/14/07	Peter Hebert	1	Frankfurt	IEC standards meeting	Started discussion of CPV rating standards
10/23/07	M. Lau/R.Cravens	2	St. George UT	Review Sylarus Qualification Readiness	Sylarus' process is frozen. Finalize Qualification split lots matrix
10/14/07-10/16/07	Richard King	1	Seattle Chicago	The Industrial Physics Forum 2007: The Energy Challenge, American Vacuum Society (AVS) 54th International Symposium, Seattle, WA, Oct. 14-19, 2007	Deliver invited talk. Gain information on latest technological developments in energy related fields.
9/25/07	Peter Hebert Peichen Pien	2	Long Beach, CA	Attend Solar Power 2007 Conference	Made contacts with ASU-PTL and improved

Travel Date	Travelers	Head Count	Place	Purpose of the trip	Accomplishment
					market awareness
12/7/2007	Geoffrey Kinsey	1	Fukuoka, Japan	IEC 62108/WG-7 Meeting	Meeting to finalize IEC-62108 qualification standard for CPV modules
3/1/2008	Geoffrey Kinsey	1	Madrid, Spain	1st CPV Summit	presented the state of the art to CPV community
4/1/2008	Peter Hebert, Jerry Kukulka	2	Denver, CO	Attend DOE Accelerated Aging Workshop	Provide feedback on needs to DOE laboratories. Gain and share information on reliability test status across PV industry.
6/11/2008	Chris Fetzer	1	Somerset, NJ	Training on New MOVPE Reactor software before system installation	Learned new Nexus operating system & programming language.
6/4/08 - 6/5/08	Randy Brandt Muhammad Afzal	2	San Jose, Ca	Visit (5) suppliers to related to the wafer prober test test development.	Able to make a recommendation to SPL team for wafer prober, integrator and probe card suppliers
6/8/08 - 6/11/08	Muhammad Afzal	1	San Diego, Ca	Wafer Test workshop	Gained industry information related to wafer testing techniques and equipment to help minimize development effort.
4/21/08 - 4/24/08	Don Aldrich Geoffrey Kinsey	2	Austin, TX	Attend SAI Solar Energy Technologies Program Review	Supported DOE SAI program review.
9/4/08- 9/5/08	Maggy Lau, Beth Stone	2	St. George UT	Review subcontractor (Sylarus) Ge substrate process capability before large production	Review Eng. Change notice (ECN) process change, update on new improvements projects

Travel Date	Travelers	Head Count	Place	Purpose of the trip	Accomplishment
10/2/2008	Russ Jones	1	Santa Clara, CA	IEEE SCV-EDS PV Symposium	Present paper
10/21/08-10/22/08	Maggy Lau	1	St. George UT	Compare Wafer inspection technique	Compare inspection technique difference bween SPL inspector and Sylarus inspectors
8/11/08-8/13/08	Pete Hebert	1	San Diego, CA	Attend SPIE reliability conference	Presented paper
11/17-11/19-08	Pete Hebert Peichen Pien Omar Al Taher	3	Palm Desert, CA	Attend ICSC-5 and IEC Stanadard Committee meetings	Technical conference for latest CPV technology and news; represent Spectrolab for IEC solar cell qualification test standard meeting
11/16-11/19/2008	Andreea Boca	1	Palm Desert, CA	ICSC-5	Presented poster
11/16-11/19/2008	Richard King	1	Palm Desert, CA	ICSC-5	Presented paper
11/16-11/19/2008	Russ Jones	1	Palm Desert, CA	ICSC-5	Presented paper
Dec. 7, 2008	Russ Jones	1	Washington DC	Council of Scientific Society Presidents	Presented paper
March 9-10, 2009	Peter Hebert	1	Darmstadt, Germany	Attend IEC standard writing meeting	
3/25-3/27/09	Eric Moloy	1	Horsham, PA	Evaluate SSEC's automated lift-off tool for metal lift off process	Evaluate lift off times as function of process conditions
4/1-4/3/09	Eric Moloy	1	Kalispell, Montana	Evaluate Semitool's automated lift-off tool for metal lift off process	Evaluate lift off times as function of process conditions
6/2-6/11/09	Chris Fetzer, Jeff Krogen	2	Aachen, Germany	MOVPE reactor supplier evaluation	Conducted equipment capability evaluation, comparison of Installed K475 tool base against novel G4-2800R reactor.

Travel Date	Travelers	Head Count	Place	Purpose of the trip	Accomplishment
3/19/2009	Krut, Dimitri	1	Golden, CO	Meet with NREL and Sylarus to determine a reliable way to measure Ge lifetime	Recommend a set up which has resolved the issue altogether. Sylarus has implemented in the procedure.
4/30 - 5/5/09	Peichen Pien	1	Shanghai, China Taiwan	CCA assembly houses, Amkor China & Delta capability review	Reviewed both companies' progress for their CPV CCA assembly capability development
6/08 - 6/12/09	Andrea Boca, Richard King, Pete Hebert	4	Philadelphia, PA	IEEE PV Symposium	Presented paper. Participated in IEC bare cell standard discussions.
6/22 - 6/26/09	Richard King	1	University Park, PA	Electronic Materials Science Challenges in Renewable Energy	Presented plenary talk
9/16/09	Richard King	1	Stanford, CA	Stanford Photonics Research Center Symposium	Presented symposium talk
9/21 - 9/25/09	Richard King	1	Hamburg, Germany	24th European Photovoltaic Solar Energy Conference	Presented paper
10/27/2009	Nuran Deyirmencian, Maggy Lau	2	Anaheim , CA	Visit Solar Power Conference 2009 to meet equipment vendors	Reviewed equipment needs with prospective vendors
2/17/10 - 2/18/10	Jim Ermer Pete Hebert	2	Golden, CO	Attend NREL Reliability Workshop	Participated in group sessions on CPV reliability issues charged to 20092 I believe.
5/21/10 - 5/28/10	Chris Fetzer, William Hong	2	Incline Village, NV	Attend and present at ICMOVPE conference on epitaxy of semiconductors, discuss with vendors of epitaxy equipment	presented paper, made vendor discussions to upgrade fab capability
5/23/10 / 5/27/10	Russ Jones	1	Washington, DC	DOE SETP Peer Review	Participated in review

Travel Date	Travelers	Head Count	Place	Purpose of the trip	Accomplishment
6/20/10-6/25/10	Omar Al Taher	1	Honolulu, HI	Presented poster on C4MJ qualification at IEEE PVSC 35	Presented poster, met with potential customers and vendors. Gathered information from technical presentations

Acronyms

BOL	Beginning of Life
CCA	Concentrator Cell Assembly
CDO	
COTS	Commercial off the Shelf
CPV	Concentrated Photovoltaic
CSUN	California State University at Northridgr
cte	Coefficient of Thermal Expansion
CYP	
DNI	Direct Normal Radiation
DPA	Destructive Physical Analysis
EPC	Electric Power Contractor
FF	Fill Factor
FFRDC	
FOA	
H/W	
Imp	Current at Peak Power
Isc	Current at Short Circuit
Jratio	The ratio of the top cell to middle cell current in a triple junction cell
LCOE	Levelized Cost Of Energy
PMMA	Polymethylmethacrolate
POC	Proof of Concept
POC	Point of Contact
POD	Proof of Design
POE	Primary Opt6ical Element
POF	
POM	Proof of Manufacturing
PPA	Power Provider Agreement
SAM	Solar Advisor Model

SES	Stirling Energy Systems
SOE	Secondary Optical Element
TIOS	
TMY2	Typical Meteorological Year
Vmp	Voltage at Peak Power
Voc	Voltage at Open Circuit
XPS	X-ray Photoelectron Spectroscopy

Appendix A– Navigant Consulting Manufacturing and System Cost and Volume Report for Boeing

Executive summary

This report discusses the progress of Boeing toward its Levelized Cost of Energy (LCOE) goals as reviewed for Stage-Gate 2. For Stage-Gate 2, Navigant Consulting Inc. (NCI) reviewed Boeing's Direct Manufacturing Cost, Annual Manufacturing Capacity, and LCOE Key Performance Parameters. NCI also reviewed Boeing's commercialization plan.

Table 1 below displays Boeing's current Solar Advisory Model (SAM) inputs, along with its revised projected SAM inputs in 2010 and 2015. Boeing has made significant progress with regards to further development of its system design, including major cost reductions and establishment of high volume manufacturability of its prototype designs, with clear "proof of design"(POD), "proof of manufacture"(POM), and "high volume" design pathways. Initial prototype modules have been created, with design modifications beginning to be incorporated in these POD, POM, and production designs. Boeing also has installed test modules at NREL for additional performance validation. It has continued refinement of its Monte Carlo simulation cost studies, interacting with hundreds of vendors, continuing to increase its confidence in the Stage Gate 2 figures presented, which are valid for 2010.

Boeing is implementing both a 100 kW POD and a 1 MW POM facility, in preparation for 20 MW of production by 2010. The design is largely frozen, allowing these manufacturing developments to take place. In keeping with its design for cost methodology, preliminary 2015 figures shown are design-to-cost targets. Commercialization partners under negotiation are interested in significantly expanding production to >100 MW annually.

Table 1: Boeing's SAM Inputs

Category	Units	Stage Gate 1 2010 Projected (43% conf)	Stage Gate 2 2010 Projected (90% conf)	Stage Gate 2 2015 Projected
System Power	Wdc	21,766,464	24,400,418	22,998,528
Array (Module) Price	$/Field	$37,997,568	$45,476,352	$18,570,240
Inverter Price	$/Field	$4,838,400	$5,184,000	$3,360,000
Total BOS Price	$/Field	$8,500,000	$9,900,000	$4,000,000
Installation Price	$/Field	$11,000,000	$7,500,000	$5,500,000
Contingency	$/Field	$9,350,395	$10,209,053	$4,714,536
Miscellaneous	$/Field	$11,039,700	$7,983,479	$3,433,754
Total	$/Field	$82,726,063	$86,252,884	$39,578,530

	$/Wpdc	$3.39	$3.53	$1.72
Average Annual O&M	$/kW-Yr	$55	$55	$33
Annual O&M Escalation	%	0%	0%	0%

As shown in Table 1, Boeing's stage gate 1 figures were at a 43% confidence level; current stage gate 2 figures are at a 90% confidence level, a significant improvement despite ~ 5% higher costs overall. In developing the estimates, Boeing developed bottoms up or quoted "system assembler" price estimates for each component of system cost, including indirect costs, and applied a 1.25 markup for profit, overhead, and contingency. In keeping with the SAM input format, a 15% contingency was applied to direct costs; the contingency for indirect ("misc") line items is therefore in the misc category. Miscellaneous now includes indirect costs of "Engineer, Procure, Construct" and "Project, Land, Miscellaneous". Some definitions of BOS, installation, and miscellaneous continue to be naturally mixed, with correct total costs. For instance, array foundations are normally part of balance of system, but are typically executed by a construction company, whose contract is under indirect "engineer, procure, construct"; while foundation costs were separated into the BOS category, some indirect construction profits associated with these foundation costs may appear in the BOS category.

Table 2 summarizes primary and secondary concerns raised by NCI during Boeing's Stage-Gate 2. Primary concerns are issues that can strongly impact a TPP's ability to meet LCOE objectives and should be tracked as the program progresses; secondary concerns are those that are either less likely to occur, or have a reduced impact.

Table 2: Summary of NCI Concerns Relative to Boeing SAI Stage Gate I

Primary Concerns		
Category	**Item**	**Comment**
Cost	Long term (2015) cost	While 2010 estimates are in alignment, NCI's 2015 estimates for the Boeing system are higher than the 2015 SG2 targets. Because many years of design freeze are needed to fully develop high volume manufacturing production lines, and to establish reliability, a few planned innovations should be placed into the current design freeze earlier if possible, through devotion of more resources as

		applicable. These design decisions include: Plastic vs. metal chassis Detailed provision for higher concentration, if proven out Aspect ratio vs. grid reflection tradeoffs and processes 4th generation heat sink Increase in module length by 1 cell, or 17% Once decided and refined, a Boeing high volume projection of 2015 cost could further focus cost reduction acceleration efforts. Acceleration could potentially reduce program development costs, as 2015 production process development could then be brought forward to 2010/2011/2012.
Capacity	CPV Market Development	Boeing anticipates using ~1/10th of Spectrolab's production capacity for its own needs, thereby assuming cell cost at 10X its projected volume; Spectrolab is putting into place 200-300 MW of capacity to address Boeing's needs. The CPV market to date has been centered in Spain, which cratered last year as a 500 MW incentive cap was put in place; PV markets as a whole have been down due to both this and to the credit crisis, and emerging CPV markets have been disproportionately affected, as this technology is less well established and bankable, and larger-scale utility scale applications typically have quite high initial capital costs that need to be financed; CPV is a modular technology, however, that may not suffer this disadvantage. Spectrolab's near-term cell prices have adjusted upward in response to this turmoil---Spectrolab's costs will be higher, as it spreads out high factory capacity costs over lower actual volumes. It will continue to be important to monitor Spectrolab's total installed production capacity and annual pro-

		duction volumes moving into 2011; we expect prices to decline as volumes ramp, but this ramp will be delayed, likely slightly longer than the general economic recession. On the positive side, the 30% ITC credit passed last year, removing a key market barrier, and further possible congressional action regarding carbon and/or RECs could ignite the market in the coming years.
Commercialization	Partner assumption of warranty risk	In the current risk-intolerant credit climate, large scale 20 MW field deployment may depend on a well-respected, long-lived and experienced entity taking on project warranty risk, especially for new technologies. Boeing does not want to shoulder this risk from a business perspective; partners may be willing, but are still being selected and can therefore not be evaluated yet. NCI recommends that Boeing explore government support options for this risk, whether though NREL, the DOE loan guarantee program, or some other conduit.
	Market absorption delay leading to near-term lower production volumes, and therefore higher cost	The sum of transmission access scheduling, development redesign cycles, reliability verification, credit crisis/recession, and normal project funding cycle times likely dictate a delay in U.S. market development compared to Boeing's projections by at about 1-3 years. In turn, this could mean lower near term production volumes, and therefore higher costs, than projected. Boeing continues to attempt to reduce fixed capital NRE (molds, dies, etc.), to lower cross-over production volume thresholds and reduce costs in general.
Secondary Concerns		
Cost	Interconnections, & Wire	Interconnections, wire, and electrical component costs continue to be high. Monitor the number and type of connectors required per MW, their performance (reliability), and total assembly time / MW. Monitor wire type and length. Boeing has a first cut design, and continues to optimize.

	Cell efficiency, cost	Spectrolab has accelerated its 6" wafer developments; the next year's yields and process optimizations will be critical to see if the metamorphic design, and 6" wafers, is feasible and cost effective.
	Customer Spectral Distributions	Spectral distribution is a key design input that GaAs CPV technology is highly sensitive to, with limited data available that takes a long time to gather. A widespread customer spectral distribution database should be gathered --- perhaps by NREL on a nationwide basis. Boeing is starting to gather data for key customer sites.
	O&M Costs	Component MTBF under field conditions are being assessed, as POD and POM systems are designed, built, and tested. Boeing has worked individual component reliability, but not necessarily conducted whole-system modeling to establish an O&M system wide reliability pareto. This should be tracked as full system prototypes are actualized, as it is a key uncertainty regarding O&M costs and market acceptance. From its space experience, Boeing's reliability record and capabilities are unparalleled.

Beyond the aforementioned primary concerns, NCI found Boeing to be on target to meet its 2010 SAI LCOE goals and Key Performance Parameter targets.

Throughout the process of this stage gate review, Boeing has shared detailed cost breakdown data, made its assumptions very clear, answered all questions, and been extremely helpful and forthright. For Stage Gate 3, further additional information that NCI would like to see include:

(1) A system level reliability report, incorporating individual component reliability information/updates, as well as whole-system reliability modeling and POD/POM status and

(2) A part count and DFMA design efficiency[1] for each subsystem, including progress in these parameters over the year.

Costs

Boeing has applied a "Design to Cost" methodology, which segments the design of the system into pieces, and applies costs targets for each piece. Cost targets are then compared to updated projections (vendor estimates, quotes, RS Means estimates, etc.), and large disparities between targets and projections are worked, in Pareto fashion.

Boeing's cost drivers are:

SAM Category	Driver Type	Cost Element
Module	Per Cell	GaAs Concentrator Cell
		Primary Optic Element
		Secondary Optic Element
		Cell Cooling
	Assembly	Panel Assembly
		GaAs Cell Assembly
	Electrical	Module Chassis
		Module Interconnect
Inverter		Inverter Cost
BOS	Tracker	Assembly
		Foundation Cost
	Project Cost	Construction Management
Installation		Utility HV Substation
		Permit / Site Development
		Transmission Capacity Upgrades

[1] "Product Design for Manufacture and Assembly", 2nd Ed, Boothroyd, Dewhurst, & Knight, 2002, CRC Press, p 8-15.

O & M		O & M
Overall		Cell & Optical Efficiency, Field Power Output

In the Boeing system, the "per cell" items above get multiplied by >900,000 units, for a 20 MW utility scale system; individual costs of these items are therefore magnified in importance. Similarly, assembly costs and electrical interconnections are functions of the number of cells / field. This, in turn, is driven by overall cell, optical, and DC to AC conversion efficiency –-- as total field power increases, fewer cells are needed for a particular system size. A key advantage of the system is the use of high efficiency multi-junction GaAs cells.

Boeing is addressing these cost drivers through the following roadmap:

Cost Element	**Roadmap / Action**	**NCI Comment**	**Key Metric**
GaAs Concentrator Cell, Cell Assembly	*Automate cell testing '07* *Automate cell welding '07* *Automate die handling '08* ***Domestic Ge Supplier '08*** **Next Gen reactor '08** **Improved Sectioning '09** **6" Wafer Fab '10**	Current year work is relatively std engineering Reduces FX risk, and competition/volume Samples being qualified High Uncertainty Efforts accelerated; samples under test	Cycle Time, Downtime, Yield, # Suppliers, Supplier size; Make vs. Buy Cycle Time, Batch Size, Machine Cost, MOPVE Material Utilization Kerf Loss Large Area Uniformity Labor Cost (% of total)
Primary Optic Element	*Multiple sources*	**Coating cost vs. durability uncertain and under test; moisture control solution will improve durability.**	# Suppliers, Coating Reliability / Type

	All-plastic chassis design	Profits traditionally are relatively high for proprietary coatings – consider developing in-house, and/or reverse engineering—especially to guide reliability efforts. Exposure to sulfur or H_2S (albeit poisonous) may be an effective accelerated test for the silver coating. **Will reduce number of parts/handling**	
Secondary Optic Element	*Multiple sources* **2X improvement in concentration**	Likely to hit target if concentration improvement works, as # of parts will be reduced by 50%	# Suppliers, concentration level
Cell Cooling	*All Cu, to Heat Sink, to Heat Pipe (Al); Base Fitting Cu to Al; part count reduction. Pulling HX manufacture in-house* ***A high level of cooling improves cell efficiency***	Further progress made, hitting 2010 goals; 2015 costs are still high. Potential further explorations: expanding tube to attach fins per A/C industry practice (eliminating solder/brazing/adhesives), bring COTS mfgr in-house, or a wrapped flat heat pipe chassis.	Cooling Capability vs. Material Weight, % Cu vs. Al usage, Part Count
Panel Assembly	*Automate; rect to T to Round light-weighting; DFMA*	*448 to 280 lbs reduction achieved.* 70% over target; welding is a low volume proc-	Part Count, Total Weight

		ess—switch to a single plastic connector like McMaster Carr part # 2339T36, with two hefty back to back snap fits to connect torque tube to cross-beams—this will eliminate welding and ease assembly (with appropriate fixture automation)	
Module Chassis	*Prototype A to B to C*	Automated Assy; *Press Brake Sheet Metal parts*	Part Count, Total Weight
	Plastic Chassis for 2015	Technically challenging: (1) At edge of process capabilities: planned injection molding process is generally not economical for these part sizes due to too high die pressures, requiring large dies and press sizes; conversely, lower cost vacuum molding may not meet tolerance requirements (2) glass window plastic mismatch means module window substitution must succeed for a plastic chassis to be feasible (see below) (3) locational tolerances of CCA to mirror are critical, and cross a parting line (4) longitudinal warpage/twist due to residual stress may be	Process mold cost, tolerance capability

		an issue Potential approaches: structural foam molding may be a more appropriate process (large shapes, higher accuracy, low tooling cost); fill w/glass fiber or beads to add stiffness	
Module Window	Substitute (likely oxide) coated acrylic for iron free glass	Cost savings may be up to ~30-40%, in high volumes, but high coating capex points to high cross-over volumes (not evaluated). Technical issues are challenging: Acrylic/coating combination may absorb more spectral energy than iron-free glass, reducing efficiency and increasing system cost; more porous to water/gasses; reliability of scratch resistant coating under sandstorm conditions is likely limited; less structurally stiff, requiring more plastic to maintain critical and tight tolerance POE/SOE/cell positional tolerances under wind loading	
Module Interconnect	Flex Ribbon	Durability for outside use uncertain vs. cost, currently $$; consider	Wt/Unit Length, Type

		aluminum foil + UV-stabilized polyolefin insulation ? or standard wire w/ automatically soldered connections ? Consider focusing light laterally with POE to allow 3 double CCAs/module, to reduce # of interconnections needed	
Inverter Cost	*Closely held, Supported Supplier* Refurbish rather than replace	Price is 20% below market; higher reliability will cost ~ 20% more (improved components) While potentially lower cost, inverters are more likely to be replaced rather than refurbished, as inverter technology will change enough over ten years to make replacement attractive (reduced cost, increased efficiency, etc.).	Inverter Price
Tracker Assembly	***Designed own unit:*** ❖ ***reducing overdesign (wind loads, light-weighting to reduce inertia, SOE allows low tracking tolerances, etc.)*** ❖ ***pulling in vendor profit***	Impressive, and feasible, reduction in costs. 30 year reliability still needs to be established (PWM motors, controller boards, extreme / non-normal conditions, etc.) Consider use of Non-PWM motors to reduce cost (albeit with	Tracker weight, motor type, control scheme

	❖ ***eliminating NRE (controls design, etc.)*** ❖ ***Eliminating sensors through using cell power data as inputs*** Custom-designed drives Shuffle drive invention University Research – independent benchmarking analysis **Add 1 cell/module, slightly increasing tracker structural costs**	a likely higher parasitic power penalty and/or lower brush reliability) Further cost reductions may be muted, as piggy-backing off of motor suppliers higher volumes is not possible with a custom drive. Reduces # of arrays required, reducing array dependent system costs	Machining cost, material weight per drive
	Compact Sun-orbit Tracker	Lightweight, less expensive tracker may reduce overall cost – but with more parts, and higher #s of connectors, wires, motors, etc. Not enough data to evaluate	
Foundation Cost	Optimize (CPV specific instead of std construction)	Optimization should close target gap	CY concrete, lbs steel
	Steel micropile screw foundations	Innovative use of commercial micropiles – eliminates concrete, reduces installation time/cost	

		dramatically.	
Electrical Wire, Equipment	Multiple Bids, sources Battery powered DC tracker power circuit	Connection boxes, wireless control, AC/DC wiring, MV transformers & disconnects, grounding & lightning rods are all well known Avoids AC->DC conversion, improves reliability Electrical costs are high relative to targets.	Cu wt / system, part costs
Utility HV Substation	Multiple Bids Single bus substation, with simple radial feeder system	Utility may require use of own personnel, at high profit—but this is highly utility and site dependent	HV substation costs
Permit / Site Development	Multiple Bids	Site dependent and quite variable; CA relatively high	Permitting, Environmental Assessment, and Site Topography costs
Transmission Capacity Upgrades	Pass to Consumer	Interest costs on loan over 5-year payback to consumers will accrue; highly location dependent (CA high, TX low)	Transmission Capacity available for Renewables by State/Network
O & M	Reliability engineering & test prototypes to reduce uncertainty	Inverter replacement underestimated by 25%; reliability unknown	System reliability (unanticipated breakdown frequency), Inverter lifetime, water usage, parasitic electricity %
Cell Efficiency	***Improved Front Contact*** ***(1) Improved Gridline***	*Ht:Width from .5:1 to 1:1 (C1MJ to C2MJ+) improved cell efficiency from 37% to*	Aspect Ratio (Ht:Width) of front grid. Modeling of cell efficiency vs. aspect ratio showing efficiency de-

	process	*37.5%*	pendence.
	Enables higher concentration levels (allowing elimination of SOE parts)	Processes implemented to date appear highly conservative, compared to 20:1-10:1 aspect ratios found in MEMS research arenas; optimal triangular shape may be possible to etch back from current trapezoidal shape:  Much higher aspect ratios may be available through a combination of electroplating, etchback, pulse plating, FIBRotools, etc.	
	(2) Grooved SOE	Tradeoffs are unclear due to time constraints, and may be technically difficult: (1) a move to fewer, larger cross-section gridlines increases lateral resistance losses, in opposition to concentrator cell development trends; (2) thicker ITO to compensate introduces conductivity vs. transparency tradeoffs; (3) uneven flatness/gaps at SOE /	

		wafer interface may degrade electrical contact intimacy (heat to diffusion bond may be an issue; ultrasonic bond may damage cell, etc.) (4) manufacturability of SOE grooves is unclear It is important to separate front grid resistance losses from "non-orthogonal to the cell" light reflection losses engendered by the SOE, a recent discovery. (1) above, and possibly (2), improves the former, but worsens the latter, as taller grid lines shade lateral light.	
Cell Efficiency	**Optimize MOVPE process** **Improve current matched designs (metamorphic)** **Spectral Cell Tuning**	Likely, given Spectrolab expertise and continued demonstrated gains to date Technically difficult—dislocations, uniformity, reproducibility, reliability, and yields must be proven. Pollution, seasonal, and cloud spectral absorption varies, potentially limiting gains to ~1.5% absolute; but relatively easy to execute at the cell level	Subcell Band-gaps vs. optimum, Efficiency distribution width Spectral input variations vs. design type – layer thicknesses / band gaps Seasonal, daily, locational spectral variations

	Cell Matching	Already tight distributions may limit gains to .5%-1%, but this standard technique used in crystalline silicon technology is easily worth the automation equipment needed to execute, despite higher POM factory costs. Should be executed at module, array, and inverter string levels.	Cell matching losses
	Enhanced Multi-junction Cells	Wide and narrow gap candidates are harder to process, dope, and manufacture. Seasonal and daily spectral fluctuations may also severely limit efficiency gains of 4+ sub-cells—these, and cost(added layers, complexity) vs. efficiency tradeoffs, should be explicitly modeled as part of this R&D pathway.	Cell efficiency (modeled and/or measured)
	Advanced Concepts (exotic cell concepts – quantum wells, nanostructures, etc)	Current extraction, and manufacturability/cost, can severely limit nano-scale architectures.	
Optical Effi-	***On-Axis to Off-***	Improved shading,	--

ciency	***Axis Design***	reliability	
	Increase concentration by 2X	Current cell efficiency vs. concentration curves show degradation at higher concentration levels – this improvement is wholly dependent on improving the front contact	Concentration level, cell efficiency
	Open Architecture	POE reliability, exposed to environment, is likely to decrease.	
System Level	Increase Maximum Power Point Tracker Functionality	Has potential to eliminate diodes (~.5 $$MM/system), but is complex to model—modeling and experiments to follow.	
	Active Cooling	Will improve efficiency, depending on additional parasitic, but likely decrease in reliability (leakage); potential higher water usage in deserts may also an issue.	
	Increase system voltage to 1000V from current 600V	Reduces i^2r losses, improving efficiency ~ 1%. May be U.S. code, or US electrical practice, limited. EU practice is 1000V, so this approach is safe and a matter of engineering and more stringent reliability conditions. Throughout program, test products at higher voltage regimes to enable this pathway.	

Items that are *italicized* are items that are substantially complete. Bold items are key drivers

Cost drivers below are in order of importance.

System Efficiency

A primary cost driver of CPV systems is overall system efficiency, including cell, optical, and power transformation losses. Spectrolab has a well defined roadmap and plan to improve efficiency, as is discussed elsewhere in the stage-gate. The recent discovery of lateral reflection losses shows aspect ratio vs. lateral reflection tradeoffs that may delay progress as solutions are found. Note, also, that these tradeoffs were only recently discovered, and solutions are still under development.

Improved optical efficiency in shifting from an On-Axis to an Off-Axis design eliminates center pole shading, and allows a sheet of glass to be used to exclude dust and water from the system. Inverter efficiency improvements are covered elsewhere.

For 2010, Boeing is using an 86.2% DC to AC de-rate factor in its LCOE calculations, based on a detailed analysis of all losses for a CPV system, and more accurate loss modeling via comparing the model to current prototypes—and is a significant shift from the 95.3% target used in Stage Gate 1. This is natural at this stage of development. For 2015, Boeing is using a target 95.3% DC to AC de-rate factor in its LCOE calculations, which appears high, despite plans to improve mismatch, eliminate blocking diodes, and improve soiling via washing (which should be included in 2010 estimates). NCI's rule of thumb tends toward 91%; recently, a technical committee has been formed to address uniformity of assumptions across TPP projects—see the LCOE cost report.

GaAs Cell Cost

For GaAs cell cost reduction, Spectrolab/Boeing is appropriately focused on increasing the capacity of its production line, and on their cost pareto. Currently, terrestrial cells are sold in relatively small volumes, and have been manually assembled (derived from space lines). Spectrolab has added to its automated cell testing and welding, with a fully automated production line with larger, 150mm capability. The larger machines are being used with 100mm wafers to improve costs for their current production, as 150mm sizes are debugged and qualified. As is natural with a high level of automation, this will take some time.

Aside from automation, three key cost drivers are being addressed to commercialize terrestrial cells on a large scale: 1) Ge wafer cost, 2) MOVPE process speed / material utilization, and 3) Process scrap (kerf loss & yield).

Germanium, while not currently supply constrained, is a very expensive base material due both to material scarcity, and the purity levels required. Due to the extremely low volumes in use today, the number of suppliers is limited, limiting competition as well. Use of non-U.S. suppliers to date has also exposed Spectrolab to exchange rate risk and recent cost increases. Spectrolab has found a domestic supplier, qualified them, and is introducing competition as volumes increase.

The 2nd concern has been addressed by accelerating 6" wafer implementation, as described above. Uniformity issues/yields are being worked, addressing the 3rd key cost driver.

Per cell costs

The primary optical element is made of coated polycarbonate, with the coating cost vs. durability still under test. The recent shift to off-axis optics will increase the mirror longevity, as the coating will not be exposed directly to the environment, although condensation, expansion/contraction, aging, etc. will be long term factors. Condensation, found to be a reliability issue due to 600V sparking, is being addressed through three approaches: (1) purge approach, for prototypes only, for comparison/control; (2) well sealed module, with dessicant in module + vent; and (3) well sealed module, with dessicant, and bladder that expands/contracts to allow for internal gas diurnal expansion/contraction pressure changes. In addition to dessicant, NCI recommends use of a sulfur scavenger, as sulfur is known to degrade silver (i.e. as seen in tarnishing of flatware). Polycarbonate is a plastic derived from oil, so future fluctuations in crude prices indicate that the cost target for this item may be difficult to reach; further weight decreases may obviate this trend. For 2015, NCI assumes that integration of the POE into the chassis will succeed (either via plastic chassis integration, or multi-stage stamping of POE shape into current metal chassis), significantly reducing part count. Coating costs, in particular, may be high (not just silver, but oxide protection overcoat); by 2015, NCI expects that Boeing will bring coating manufacture in-house to reduce costs.

The secondary optical element, made of glass, appears likely to hit its cost targets, if doubling of concentration succeeds.

Boeing has dramatically reduced the cost of cell cooling from its initial "all copper" design, to an Al heat sink, to an Al fin heat pipe. In its current design state, it still appears

to be 25% over target. Further DFMA [casting tubes as half-clamshells w/base, reducing fin part count, use of tube expansion to lock fins in place instead of adhesive, etc.] may be able to close the gap. Adhesive bonding of fins may also be of questionable reliability (creep, etc.). Boeing also plans to bring heat fin assembly in-house; a further extension of this strategy would be to bring COTS in-house.

Module interconnects are flexible copper ribbon, with possible strain relief loops; these are still relatively expensive (3X target), potentially due to tolerance requirements and copper cost. Further work is needed and planned – aluminum substitution, if welding/soldering to CCA's are feasible, could potentially reduce material costs and increase long term reliability (oxidation resistance).

Per array (144 cells) costs

The module chassis has been redesigned from prototype A to B to C, to allow for automation, and uses press-brake bent sheet metal. DFMA has also been used to reduce part count and weight. Welding endcaps is used to seal the module, but is a relatively low volume process. Stamping flat sheets with shape cutouts at ends, bending up to form endcaps, and seaming (per gutter practice), may be lower cost than current approach. Further part count reduction (bundling 2 parts each vertically, or 3 across horizontally), mimicry of gutter processing, and/or shifting to roll forming if suitable, may also allow cost targets to be firmly met. Boeing is also working on an all-plastic chassis, which faces a number of technical hurdles as outlined in the table above. NCI recommends continuing to work on both metal/glass and plastic/acrylic approaches in parallel to reduce risk.

Panel assembly costs are relatively high due to the number of total parts. Redesigns from Prototype A to B to C have reduced assembly part count and weight dramatically, and there is potential for further part count reduction, design for automatic assembly, snap-in fastening, and automation. Automation, in particular, is proceeding apace; however, use of more snap-in fastening to eliminate fasteners and welding (a low volume process) would be useful.

Tracker costs

Boeing's in-house tracker development is an impressive cost reduction relative to current industry practice, and use of steel micropile screw foundations is highly innovative. Reliability, however, still needs to be proved out, especially against extreme conditions (snow loads in AZ once/decade, high winds, flooding, earthquakes, etc.), and stringent 30-year lifetimes. In particular, due to low duty cycles, accelerated testing of motors/controllers/control boards can be completed relatively quickly.

Tracker development over the years has seen the development of larger and larger arrays, to reduce the total number of motors/controllers/field wiring, etc.; the Compact Sun-orbit Tracker idea for 2015 runs counter to this trend. It is unclear whether the reduced cost tracker includes system level impacts, including likely poorer reliability due to much higher total system part count.

Site/Construction costs

Electrical support costs -- connection boxes, wireless control, AC/DC wiring, MV transformers & disconnects, grounding, & lightning rods – continue to be higher than target costs. Boeing continues to examine a variety of configurations and components to control and optimize these costs, and to obtain a variety of quotes/sources for these components. The screw micropile array masts will do double duty as grounding rods. Boeing is pursuing DC battery power for powering the tracker, charged during on-sun hours, to avoid unnecessary DC->AC->DC conversions. For some components—such as wire – Boeing already purchases wire in very large volumes and is applying its sourcing resources to obtain high volume discounts. Due to the many design options and optimizations available, there is still potential to reduce these costs. For example, there are tradeoffs between MV substation size and location, and the wiring cost to reach those locations. Nevertheless, many of these component costs are well known and at commercial scale, with more-limited cost reduction potential for innovation.

In general, automatic assembly of all wiring (intra-module, panel, and system) is a cost driver, as floppy wiring is in general more difficult to handle automatically. The difficultly is increased because connections/ interconnects are cost elements themselves, and each connection presents reliability & efficiency issues (as oxides form over time, resistance can increase). A balance between assemble-ability (either automatic or manual), reliability, and cost must be struck. Potential solutions may include “paint on” wiring (modules), modularizing wire harnesses with off-shore assembly, and modularizing system wiring as well, with use of quick connects on site and in-factory. Boeing continues to search for reasonable solutions, amongst a large array of options.

“Off” site costs

It is likely for California, Boeing’s initial target market, that the relevant utilities will require use of their own personnel to design and build the high voltage substation that will connect the plant to the grid, at higher cost than one might build it oneself for. Nationwide, utility interconnection and HV substation costs vary widely.

Similarly, permitting, environmental assessment, and topology site survey costs appear to be underestimated – and vary widely by location.

In the Mohave desert, there is ~ 1/3 less transmission grid capacity than needed to support the current crop of PV and wind projects attempting to connect. Typically, utility or state ratepayers will be charged for transmission upgrade costs over 5 years. Project developers, however, must provide the cash for these very large costs (>50-100 million $$). There are therefore interest costs incurred to support this loan (if Boeing internal corporate fronts this money, they also would expect an internal IRR)

Table 3: Summary of Boeing's Cost Secondary Concerns

Item	Comment
Primary Concerns	
Long term cost	While 2010 estimates are in alignment, NCI's 2015 estimates for the Boeing system are higher than the 2015 SG2 targets. Because many years of design freeze are needed to fully develop high volume manufacturing production lines, and to establish reliability, a few planned innovations should be placed into the current design freeze earlier if possible, through devotion of more resources as applicable. These design decisions include: Plastic vs. metal chassis Detailed provision for higher concentration, if proven out Aspect ratio vs. grid reflection tradeoffs and processes 4^{th} generation heat sink Increase in module length by 1 cell, or 17% Once decided and refined, a Boeing high volume projection of 2015 cost could further focus cost reduction acceleration efforts. Acceleration could potentially reduce program development costs, as 2015 production process development could then be brought forward to 2010/2011/2012.
Secondary Concerns	
Interconnections, & Wire	See above. Monitor the number and type of connectors required per MW, their performance (reliability), and total assembly time / MW. Monitor wire type and length.

	Boeing has a first cut design, and continues to optimize.
Cell efficiency, cost	Spectrolab has accelerated its 6" wafer developments; the next year's yields and process optimizations will be critical to see if the metamorphic design, and 6" wafers, is feasible.
Customer Spectral Distributions	Spectral distribution is a key design input that GaAs CPV technology is highly sensitive to, with limited data that takes a long time to gather. A widespread customer spectral distribution database should be gathered --- perhaps by NREL on a nationwide basis. Boeing is starting to gather data for key customer sites.
O&M Costs	Component MTBF under field conditions are being assessed, as POD and POM systems are designed, built, and tested. Boeing has worked individual component reliability, but not necessarily conducted whole-system modeling to establish an O&M system wide reliability pareto. This should be tracked, as it is a key uncertainty regarding O&M costs.

Capacity

Table 4: Boeing's Scale Up Plan

Category	**Current Stage Gate**	**2010 Projected**	**2015 Projected**
SAI Proposal	0	20	150
Revised Production Capacity [MW]	.1-1	20	100
Revised Installations [MW]	.1-1	1	100

As shown in Table 4, Boeing's scale up plan above has remained essentially unchanged, as 2015 scale-up plan can be adapted to market demand once the first 20 MW plant has been installed and debugged (in 2010-2012) The large difference in 2010 between installations and capacity is also appropriate and realistic for technologies at this stage of development. A number of Boeing's investors and potential partners have indicated that a 20MW facility is not of interest, and want to jump directly to >50 MW or 100 MW in scale.

Boeing is implementing factory automation of cell assemblies (at Spectrolab), and continues to refine its designs of both product and factory for both POD and POM. Technical scale-up hurdles [covered in previous section] include:

(1) Transition from 4" to 6" wafer size
(2) Difficulty in assembly and handling of fragile Ge wafers
(3) Automatic assembly of wiring and parts (intra-module, panel, and system)

Boeing clearly has the expertise and capability to create the first 20 MW factory, and work through the above issues, and is progressing well, as explicated in sections 4 thru 6 of the Continuation Report, where proof of design (POD), and manufacturing (POM) plans and progress are shown.

Boeing is assuming that the Germanium supply production chain will grow with Spectrolab's needs. Volumes are extremely small at this time, and direct analogues exist with silicon and semiconductor production technologies, so technical risk is low. NCI does, however, potentially expect supply hiccups to occur – as illustrated by the recent silicon shortage; we did not have time to thoroughly examine this issue, however.

Table 5: Summary of Boeing's Capacity Concerns

Primary Concerns	
Item	**Comment**
CPV Market Development	Boeing anticipates using ~1/10th of Spectrolab's production capacity for its own needs, thereby assuming cell cost at 10X its projected volume; Spectrolab has put into place higher capacity to address Boeing's needs. The CPV market to date has been centered in Spain, which cratered last year as a 500 MW incentive cap was put in place; PV markets as a whole have been down due to both this and to the credit crisis, and emerging CPV markets have been disproportionately affected, as this technology is less well established and bankable, and larger-scale utility scale applications typically have quite high initial capital costs that need to be financed. Spectrolab's near-term cell prices have adjusted upward in response to this turmoil, as Spectrolab's costs will be higher, as it spreads out high factory capacity costs over lower actual volumes. It will continue to be important to monitor Spectrolab's total installed production capacity and annual production volumes moving into 2011; we expect prices to de-

	cline as volumes ramp, but this ramp will be delayed, likely slightly longer than the general economic recession. On the positive side, the 30% ITC credit passes last year, removing a key market barrier, and further possible congressional action regarding carbon and/or RECs could ignite the market in the coming years.

Commercialization Plans

Key aspects of Boeing's business plan to support the planned installation capacity were reviewed:

Revenue

The CPV market is currently <.5% of the total PV market, and barriers to further growth exist. These include:

- Performance
  - Tracking uses direct sunlight, reducing available captured light by 20%; reduced dawn/dusk losses more than compensate for these losses, but this is not widely known.
  - Shading from nearby trackers increases land area necessary.
- Cost
  - Concentrator cells use tiny grids, with high tolerances; GaAs cell processing costs are very high (using extremely slow processes), and Si concentrator cells have limited efficiency. This combination means that concentrator cells are very expensive, even at high concentration ratios.
  - Tracking and lens cost expenses are added compared to flat plate; large trackers are necessary to resist wind forces. There is a chicken and egg phenomenon: high volumes are needed to produce a low cost product; and low costs are needed to sell high volumes.
- Reliability
  - 25 year warranties are standard, with module lifetimes sometimes in excess of 30 years. Tracking devices, with moving parts, have not been proven to last this long and add to O&M costs
- Markets
  - Larger size installations point toward wide-area land based utility markets, where competing wholesale power is less expensive than retail; this may not apply to modular CPV.

- Customers have been reluctant to use a new technology that is not significantly less expensive; and more maintenance than flat plate PV is likely to be required.
- Access to transmission lines at high direct solar insolation sites can be limited.

The reliability issue, above, in particular, has been an Achilles heel, especially for large scale plants which cost greater than $50 million. Reliability must be proven for >20 years, and the economics of financing are severely impacted if failures occur early. While accelerated testing and reliability modeling can provide some comfort, multi- year field testing is highly desired by the financial community. To date, therefore, demonstration volumes have been reached, to prove reliability, but wide-scale deployment has lagged.

Nevertheless, with the advent of RPS, climate change, tight oil supplies, higher natural gas prices, coal emissions, and nuclear NIMBY issues, there has been significant interest in utility ownership or purchase of renewable energy generation, and solar's characteristics can match loads more effectively than wind.

Boeing has shown market projections of 200 MW by 2010, and 800 MW by 2015 in the United States, and anticipates obtaining 10% market share in these time-frames. Due to the market turmoil cited in the last section, NCI's near term 2010 projections are ~50% of Boeing's; nevertheless, it is feasible that 1 MW out of 100 MW will be sold in 2010, as Boeing plans. NCI's 2015 market projections are higher than Boeing's, fully supporting Boeing's later year ramp-up expectations.

If cost, reliability, and credit-crisis concerns are addressed, Boeing's projections can apply—although the sum of transmission access scheduling, development redesign cycles, reliability verification, credit crisis/recession, and normal project funding cycle times likely dictate a delay in U.S. market development compared to Boeing's projections by at about 1-3 years.

Cost

See other sections.

Reliability

See individual line item reliability reports for current status.

Financing

To address the above challenges, Boeing is participating in the SAI program to both reduce cost, and improve reliability. Boeing's SAI team has obtained expanded internal funding within Boeing, and for financial support to build the next-step 20MW POM assembly plant. In general, Boeing plans to finance its own development, which is a huge strength compared to smaller and less financially solvent entities; we expect a number of startups to fail in the current environment.

Partnering

Boeing core competencies include technology development and manufacturing of airplanes, space, solar cell, and defense products; it is not a construction company, automation supplier, or PV site developer. Accordingly, it is engaged in detailed discussions with a number of entities to provide these services for the project, under an ownership structure to be negotiated (JV, subsidiary, arms-length, etc.); in particular, it seeks an entity willing to invest in the technology and assist in the product's commercialization, potentially including factory buildout and rampup. Boeing's cost estimates have included partner markups as appropriate for the purposes of costing. In addition to capital, partnering will bring needed knowledge and experience toward commercialization of the product, and is a distinct strength of the Boeing TPP team. As partner(s) are selected, their business plans and competencies may need to be assessed as part of Stage Gate 3, depending on how agreements are structured.

A key aspect of the partnering agreement that will affect market acceptance is assumption of warranty liability, which Boeing does not want to shoulder from a business perspective. A well respected, long-lived partner willing to assume project warranty liability risk could be critical for 20 MW field project financing to occur, especially in the current risk-intolerant credit climate. As a new key barrier to new technology development and deployment, NCI believes that the US government could play a role in shouldering this particular risk, as a project insurer of last resort in some manner, or as a project financier (aka the DOE loan guarantee program).

In the flat plate marketplace, IEC certification is becoming a customer requirement, especially by the financiers and insurers of solar installations. While the IEC standard is in flux for concentrating systems, NCI expects a similar market focus on IEC certification will exist once the above barriers are overcome. On the flat plate side, IEC certification is a minimum requirement, with many companies doing extensive reliability testing beyond, to ensure that warranty periods can be met. For CPV, NCI expects this to be doubly true, given higher move part complexity and market perception of CPV.

Table 6: Summary of Boeing's Commercialization Concerns

Primary Concerns	
Partner assumption of warranty risk	In the current risk-intolerant credit climate, large scale 20 MW field deployment may depend on a well-respected, long-lived and experienced entity taking on project warranty risk, especially for new technologies. Boeing does not want to shoulder this risk from a business perspective; partners may be willing, but are still being selected and can therefore not be evaluated yet. NCI recommends that Boeing explore government support options for this risk, whether though NREL, the DOE loan guarantee program, or some other conduit.
Market absorption delay leading to near-term lower production volumes, and therefore higher cost	The sum of transmission access scheduling, development redesign cycles, reliability verification, credit crisis/recession, and normal project funding cycle times likely dictate a delay in U.S. market development compared to Boeing's projections by at about 1-3 years. In turn, this could mean lower near term production volumes, and therefore higher costs, than projected. Boeing continues to attempt to reduce fixed capital NRE (molds, dies, etc.), to lower cross-over production volume thresholds and reduce costs in general.
Secondary Concerns	
IEC Certification	Once POD and POM designs pass internal reliability testing, IEC certification should be pursued.

SAM Inputs

Table 6 holds Boeing's SAM inputs as submitted to NCI.

Table 7: Boeing's SAM Inputs

Category	Units	Stage Gate 1 2010 Projected	Stage Gate 2 2010 Projected	Stage Gate 2 2015 Projected
System Power	Wdc	21,766,464	24,400,418	22,998,528
Array (Module) Price	$/Field	$37,997,568	$45,476,352	$18,570,240
Inverter Price	$/Field	$4,838,400	$5,184,000	$3,360,000
Total BOS Price	$/Field	$8,500,000	$9,900,000	$4,000,000
Installation Price	$/Field	$11,000,000	$7,500,000	$5,500,000
Contingency	$/Field	$9,350,395	$10,209,053	$4,714,536
Miscellaneous	$/Field	$11,039,700	$7,983,479	$3,433,754
Total	$/Field	$82,726,063	$86,252,884	$39,578,530
	$/Wpdc	$3.39	$3.53	$1.72
Average Annual O&M	$/kW-Yr	$55	$55	$33
Annual O&M Escalation	%	0%	0%	0%

Boeing shifted “Other, Direct Cost, and Profit” costs from the Miscellaneous category into the relevant first four price categories, as its understanding of the SAM model improved. Miscellaneous now includes indirect costs of “Engineer, Procure, Construct” and “Project, Land, Miscellaneous”.

Category	Units	NCI (Min) (-2σ)	NCI (Most Likely) (2010)	NCI (Max) (+2σ)	NCI (Min) (-2σ)	NCI (Most Likely) (2015)	NCI (Max) (+2σ)
System Size	Wdc	24400418	24400418	24400418	21058248	21058248	21058248
Array (Module) Price	$/Field	$41,989,470	$45,231,841	$48,474,212	$27,460,042	$29,448,492	$31,436,941
Inverter Price	$/Field	$5,400,453	$5,750,391	$6,100,329	$4,797,141	$5,105,936	$5,414,731
Total BOS Price	$/Field	$9,781,694	$11,655,706	$13,529,717	$6,994,007	$8,305,069	$9,616,131
Installation Price	$/Field	$6,270,695	$7,410,195	$8,549,695	$3,994,869	$4,549,304	$5,103,738
Contingency	$/Field	$9,516,347	$10,507,220	$11,498,093	$6,486,909	$7,111,320	$7,735,731
Miscellaneous	$/Field	$8,283,639	$11,719,631	$15,155,623	$5,410,832	$7,237,740	$9,064,648

Total Cost	$/Field	$81,242,297	$92,274,984	$103,307,670	$55,143,801	$61,757,861	$68,371,920
	$/Wpdc	$3.33	$3.78	$4.23	$2.62	$2.93	$3.25
Average Annual O&M	$/kW-Yr	$50	$57	$63	$34	$41	$47

NCI's Most Likely case is ~7% higher than Boeing's 90% confidence Stage Gate 2 case, in good agreement, and is based on an analysis of POM at 20 MW. It does not consider future cost innovations that are likely to be applicable, only the innovations presented during this stage gate and planned for future SAI work (the above roadmap). The NCI Min and Max cases indicate our estimate of variability in the cost estimate (i.e. material price variations, knowledge of variations in site-dependent variables, etc.). They do not fully consider all potential design configuration changes, or process changes.

Boeing's Stage Gate 2 2010 figures are based on 90% confidence Monte Carlo simulations, for a particular design freeze of a design which is constantly changing and being improved. Given the current state of the design, and further cost reduction opportunities (delineated above), NCI believes that the ~ 6% cost reduction (.159 $/kWh to .15 $/kWh) that is needed through further innovation to hit the 2010 cost goals will naturally follow as Boeing continues to redesign the system and reduces its need for contingency. This level of improvement, despite downward performance revisions due to higher accuracy, was exhibited over the past year.

One key difference in the estimate of O&M cost is NCI assumes that inverters will be replaced rather than re-furbished, as inverter technology will change enough over ten years to make replacement attractive (reduced cost, increased efficiency, etc.). Key drivers of LCOE costs are (1) reliability ratio (i.e. percent of total system cost spent on unexpected maintenance annually), and (2) inverter lifetime. See the individual item reliability reports and performance reports for information on these two factors.

Regarding 2015 cost targets, Boeing has supplied updated target figures, with too many unknowns present for the rigor associated with their 2010 updated projections (and a focus on the current design iteration). NCI has projected 2015 costs at 20MW volumes that incorporate the design innovations shown at the stage gate, and the results are ~70% higher than the Boeing 2015 cost targets. If 100MW or higher production volumes are attained, another 10-20% reduction could ensue; these projected costs, if achieved, are quite competitive commercially. However, to attain the aggressive 2015 cost goals, further innovation will be needed to close the gap. Boeing has a long history of delivering such innovation.

Appendix B – Remote Site Testing

U.S. Department of Energy
Solar Energy Technology Program
Technology Pathway Partnership

SG2 Remote Test Modules Report

SAI_EDX100171_Rev_NEW

Award No. DE-FC36-07G017052:
High Efficiency Concentrating Photovoltaic Power System
15 June 2009

Submitted to:
United States Department of Energy
Golden Field Office
Golden, Colorado

By:
Boeing Research and Technology, The Boeing Company

Program Manager:
Robert Burns
Mail Station 110-SK86
2201 Seal Beach Boulevard
Seal Beach, CA
Phone: 562-797-2436
email: **robert.a.burns2@boeing.com**

Contract Administrator:
Carol Farmer
Mail Code S306-4150
P.O. Box 516
St. Louis, MO
Phone: 314-232-7319
email: **carol.j.farmer@boeing.com**

Document Control

Approvals

Action and Actor	Date	Signature
Prepare: Systems Engineering MTS lead Lee Bailey	2009-05-29	<signature on file>
Review & Approve Chief Engineer, Array: John Hall	2009-06-10	<signature on file>
Review & Approve Chief Engineer, Power Plant System: Doug Caldwell	2009-06-10	<signature on file>
Authorized for Release, Program Manager: Bob Burns	2009-06-10	<signature on file>

Change Log

-	2009-06-15	DMA	Formal Release

A			
B			

Table of Articles Under Test:

MTS Unit	**#1**	**#2**	**#3**	**#4**
POD Module S/N	045D	013D	023D	026D
Test Start Dates	06/09/09	04/01/09	05/27/09	04/30/09
SG2 Report Dates	06/12/09	06/11/09	06/10/09	06/10/09
Presentation Update	07/10/09	07/09/09	07/08/09	07/08/09
Exposure kWh/m^2	**4**	**327**	**26**	**273**
Spray Cleanings	**2**	**3**	**1**	**2**
Coordinates	33.8° N 118.1° W	34.2° N 118.5° W	34.1° N 117.7° W	34.9° N 116.9° W
Address	2201 Seal Beach Blvd Seal Beach, CA 90740	18111 Nordhoff St Northridge, CA 91330	265 N. East End Ave Pomona, CA 91767	37000 Santa Fe St Daggett, CA 92327
Insolation	middle to poor	middle	middle w/ smog	very good
Elevation	20 ft	900 ft	909 ft	1926 ft
Climate	coastal	inland valley	inland city	desert
Temp: ave hi/lo	64F 100/37	67F 111/32	67F 108/35	68F 113/25
Precip d/yr: fog + rain	17 + 36	0 + 75	13 + 36	0 + 31
Humidity%: ave hi/lo	68% 100/5	23% 90/7	53% 100/3	30% 100/4
Winds: ave	3 mph	3 mph	5 mph	11 mph
Gusts: max	38 mph	29 mph	75 mph	71 mph

Table of Contents:

3.3.2. Insolation:
3.3.3. IV Curves:

Table of Contents (cont'):

1. Scope:

1.1. Purpose:

top

This report provides status details of on-going testing using the Module Test System (MTS). The MTS is a stand-alone collection of systems designed to expose individual modules of a Concentrated Photovoltaic (CPV) system to real world operation. The MTS and CPV systems were developed by Boeing under the Department of Energy's Solar Energy Technology Program (SETP). The MTS is deployed in various environments to collect performance data on the "Proof of Design" (POD) module while exposed to weather and solar radiation.

1.2. SG2 Requirements:

top

- Accumulate* 430 kWhr/m^2 of Direct Normal Irradiance (DNI) on POD module design
- Secure placement of at least 4 locations capable of receiving > 600 W/m^2 DNI
- Demonstrate less than 1% power degradation
- Demonstrate no degradation of interior and no water visible inside module
- Wash modules using representative cleaning method
- Visually inspect and document with photos
- Provide notification to DOE/NREL of cleaning schedule and provide site access
- Provide documentation and report to DOE/NREL for review

*actual power generation and tracking is not required

1.3. Derived Requirements:

top

- Tracking is needed to fully exercise the module (thermally and electrically)
- Data recording (time) needed to show time in the field
- Data recording (I and V) needed to monitor the operation of the cells
- Data recording (temp) needed to corroborate expected solar insolation
- Data recording (humidity) needed to monitor module interior conditions
- Show by analysis that the required irradiance is achieved

2. Executive Summary:

2.1. Energy Targets:

top

At the time of this writing, each of the four deployed POD modules have been exposed to various amounts of solar DNI energy as determined by analysis of the actual power delivered to the load resistor of the MTS. The greatest exposure was determined to be for MTS2 at 327 kWh/m^2 since it was deployed on 04/01/09, and the least exposure was for MTS1 at 4 kWh/m^2 since it was deployed on 06/09/09. No measureable power degradation has been observed on any of the POD modules during this exposure time.

2.2. Washing:

top

Each of the POD modules under test were cleaned at least once using a 2000 psi pressure washer in a manner representative of full scale powerplant practice. Timing and flow of the test equipment were matched to provide the same .2 gal/m^2 of spray washing as recommended by full scale powerplant O&M analysis. This method of cleaning seems to be effective at removing loose debris. A less frequent “special cleaning” is required using contact and agitation to restore the cover glass to original cleanliness.

2.3. Visual Inspections:

top

Photo assays of the POD modules have been performed to document the visual inspection regimen. Modules were inspected at the start of testing to document the module condition, as well as after each cleaning to show no visible water inside module. Additional inspections and photo assays are performed on an on-going basis to provide status as contained in this report. No visual degradation of the POD optical pathway was observed during testing to date. No water was observed collecting inside any of the POD modules after cleaning. One POD module exhibited an adhesive de-bond discrepancy which allowed moisture to wick onto the inside of the cover glass. A field repair and subsequent washing showed no water inside this module.

3. Approach:

3.1. Site Selection Considerations:

top

The following considerations went into the selection sites for deployment of the MTS. While a mountainous site was highly sought after for its combination of elevation and cold temperatures with the possibility of exposure to wind as well, no such site could be secured within the SG2 time frame.

3.1.1. Insolation:

The minimum criteria is the site must be able to receive >600 DNI per the SG2 requirements. Any site in the South West part of the United States would meet this requirement, so number of cloudy days per year was also considered.

3.1.2. Temperature:

Temperature extremes were considered and a variety of climates were desirable from coastal marine influence to dry hot desert environs. Freezing conditions that would subject the module to snow and/or ice formation were of interest.

3.1.3. Humidity:

Humidity and precipitation were important to subject the modules to a range of moisture conditions from coastal salt fog, to urban pollution with rain, and on to dry arid conditions.

3.1.4. Elevation:

Elevations from near sea level to 5000 ft were considered to expose the module to differing solar spectra due to atmospheric filtering as well as combinations with temperature and wind extremes.

3.1.5. Wind:

A variety of wind conditions were desirable as wind can affect cleaning frequency and cooling capacity as well as subject the module to wind driven debris and rain.

3.1.6. Access and Security:

Of paramount concern was the ability of a site to afford the trucking and support equipment access needed to install and maintain the equipment. Site requirements and placement guidelines were prepared to ensure suitability of proposed sites. A secure

site behind perimeter fencing was required to ensure the unattended equipment was not subject to tampering or criminal acts.

3.2. Continuous Measurements:

top

Datalogger programming allows for periodic sampling at two different rates of record collection on a continuous basis. A sample rate of once every 5 min is the default speed. Between the hours of 9am and 6pm local time, the rate was increased to once every 1 min which still allows for up to 30 days of unattended data collection.

3.2.1. Module Load voltage:

This measures the voltage drop across the load bank resistors for each of the modules under test. Fixed resistance is a close tolerance set of 3 Ω resistors wired in parallel for a load of 1.5 Ω.

Module Temp/Humid:

This measures both the temperature and relative humidity of the air inside the module chassis. Positioning of the probe was carefully considered to avoid heating the probe directly with solar radiation and therefore skewing the readings provided by the sensor.

3.2.2. Ambient Temp/Humid:

This measures the ambient conditions using the same probe as was used with the module. Placement under the flat solar panel provided shade and some protection from the wind.

3.2.3. Black Body Temp:

A thermal couple mounted to the underside of a black painted Aluminum plate serves as a qualitative measure of DNI and provides corroboration of module radiation exposure.

3.2.4. MTS EQ Status:

Numerous other voltage and thermal sensors were employed to monitor the health status of the self contained MTS Equipment Stand which houses the systems needed to support tracking and data collection operations. The list of items recorded include: System voltage; Charge voltage (from the flat panels); Battery temperatures; and load resistor temperatures.

3.3. Intermittent Measurements:

top

Specialized instrumentation required to perform calibrated IV curve measurements and data collection was not sustainable on a continuous basis without the support of a much larger infrastructure than provided for by the MTS EQ Stand. Measurements using these instruments were supported by a mobile lab installed into the equipment van used to carry personnel and wash support equipment to and from the remote sites.

3.3.1. Tracking Verification:

Module tracking accuracy is verified by a spot check using the Module Alignment Tool which can measure accurately to within +/-0.5 deg using the module cover glass as the surface of significance.

3.3.2. Insolation:

Direct Normal Irradiance (DNI) is measured using a pyroheliometer and scanner combination. The instrument is securely mounted to a heavy base and pointed by hand for the 20 seconds it takes to record a full IV curve sweep.

3.3.3. IV Curves:

A programmable e-load and power supply are connected to monitor remotely current and voltage of the module under test according to the manufactures instructions. A lap-top running LabView is used to control the e-load via communication cables and also records the DNI measured by the scanner.

3.4. Visual Inspection:

top

A complete photo assay of the entire site and setup was done at the start and end of testing according to guidelines contained in the "Photo Assay Requirements v1.0" document. Intermediate photographs were taken to document before and after spray cleaning results. Start condition photos were printed and taken to the sites at each visit for comparison during the visual inspection. Any significant changes observed from the Start condition or other remarkable conditions were captured in these intermediate photos.

3.4.1. Site:

Overall pictures of the site showing the full installation and the sites view of the solar ecliptic were recorded to document conditions and provide for comparison should conditions change at the site.

3.4.2. Module Exterior:

A series of photos are used to capture module mounting and condition of the external features, such as heat pipe fins, seals and cover glass. These can be used to qualitatively document any visual degradation of the module under test.

3.4.3. Module Interior:

A series of photos are used to capture the condition of the optical elements such as mirror elements, secondary optics and optical adhesives. These can be used to qualitatively document any visual degradation of the module under test.

3.5. Cleaning:

top

3.5.1. Baseline Cleaning Study Assumptions:

The study titled "SAI_EDX100138_BOE_ArrayWashing" details the assumptions and methods intended to be cost effective for large scale powerplants. Based upon real world cleaning practice in the solar industry, key performance measures were identified to be carried forward as our basis of estimate for a CPV powerplant. The key performance measures important to the MTS study were water usage of 0.19 gal/m^2 per washing with washings expected to occur once every 18 days, or 20 washings per year.

3.5.2. Representative MTS cleaning:

Scaling from the full size array and washing assumptions contained in the study to an MTS installation of two modules (approx 1.1 m^2) as well as accounting for the 1.6

gal/sec flow rate of the MTS pressure washer, results in a 4 sec time allowance for each module. The MTS pressure washer is a 2000 psi unit, were the baseline calls for a 3000 psi wash. This higher pressure is expected to be need because of the 6 ft distance from a live circuit above 50 V called for in the baseline array washing and does not apply to the MTS washing as it operates at under 50 V.

3.5.3. Special Cleaning

This cleaning method, referred to as “special cleaning” in the baseline study, used de-ionized (DI) water with either lint free wipers or mop and squeegee to ensure all debris and deposits were removed from the cover glass.

4. Equipment:

4.1. POD Module:

top

The “Proof of Design” module is the baseline design for proceeding to the “Proof of Manufacturing” (POM) milestone (Fig. 1). It utilizes a single piece receiver wall which integrates critical hardware into a single assembly for improved reliability, easier assembly and meaningful quality testing prior to final assembly.

4.2. POC Module:

top

The “Proof of Concept” module was developed to prove out feasibly of the offset optical system which allows the modules to be packed closer together in the array with the heat sinks under the optics for improved cooling (Fig. 2). It uses a similar mirror element and secondary optic system as the POD, but there have been significant improvements on this design in materials and fabrication which have gone into the POD system to improve assembly and reliability. Other differences include the cover glass and Anti-Reflective (AR) coatings and adhesives used to mount the cover glass and seal the chassis interior.

Fig. 1: POD Modules as they array together for a close packing factor.

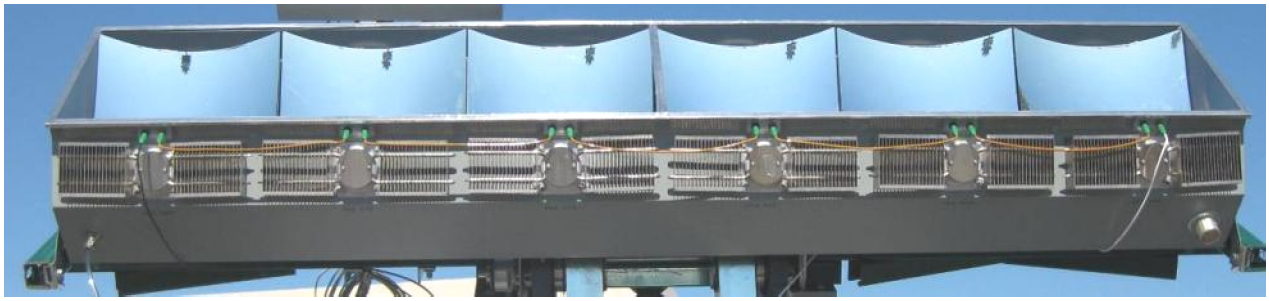

Fig. 2: POC Module with individually installed receivers and heat sinks.

4.3. Tracker:

top

The ATI-125, 2-axis tracking unit was used to provide tracking (Fig. 3). Two 24 volt motors operate the Elevation and Azimuth drives using a closed loop (sun sensor) control system to follow the sun position.

4.4. Base:

top

A portable 5000 lb cement base was developed for surface deployment without the need for earth moving or a permanent installation (Fig. 4). The base was designed to support a full size array of 24 modules. It serves as a pathfinder for trades in full size powerplant development. The base is made with reinforced concrete. A metal fitting of 6" SCH 40 pipe anchored into the top of the cement column with "L" bolts serves as an interface for the ATI 125 type tracker.

Fig. 3: ATI 125 Tracker (2-axis)

Fig. 4: Portable Cement Base (5000 lbs)

4.5. Datalogger and Sensors:

top

The Omega-320 datalogger and accessories were used with Vaisala HMP50YCC1B1X probes and TT-K-20S-TWSH-100 type K thermocouple wire to capture, record and archive the MTS datalogger data (Fig. 5-a,b,c).

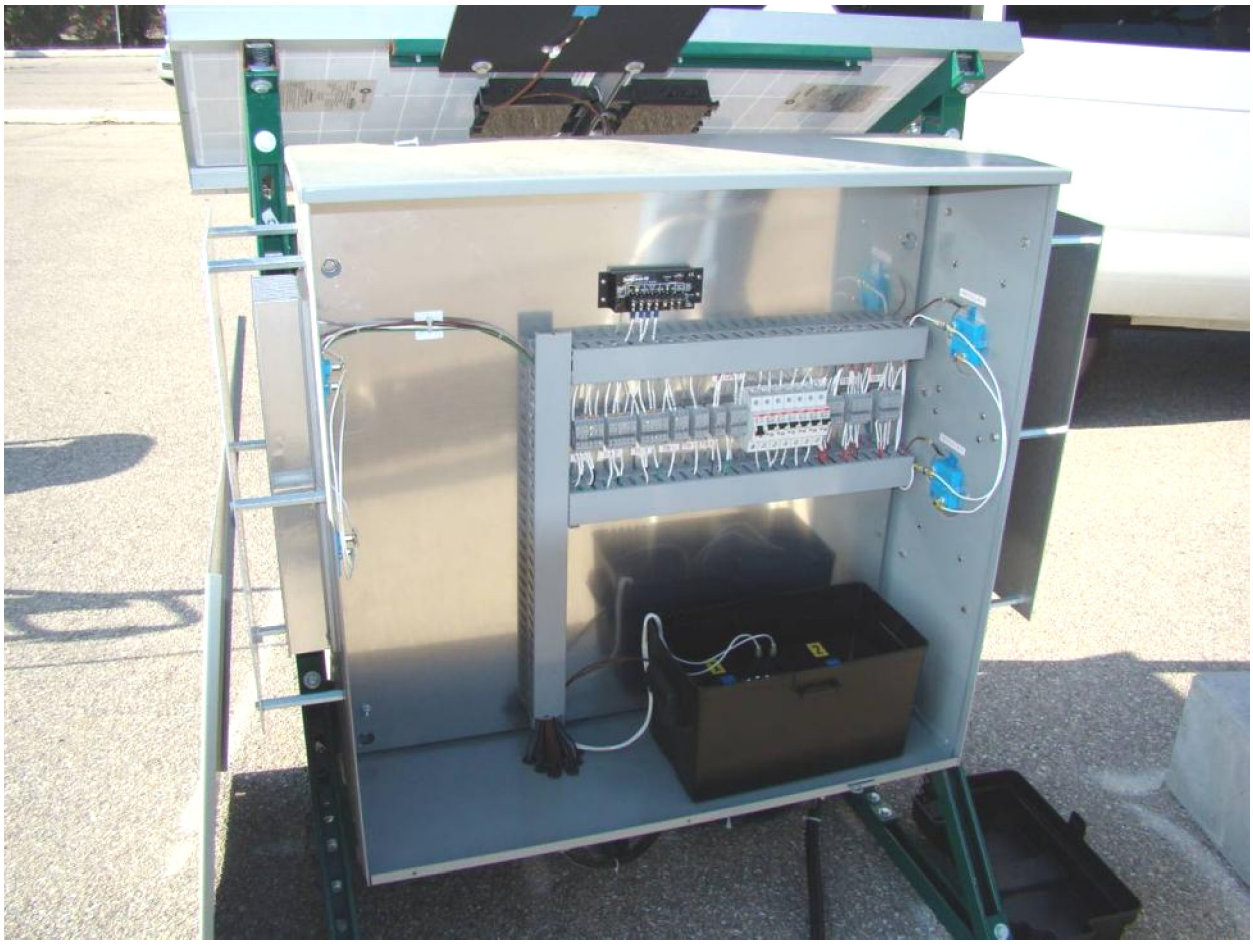

Fig. 5-a: Equipment stand cabinet interior showing batteries, load resistor banks and heat sinks.

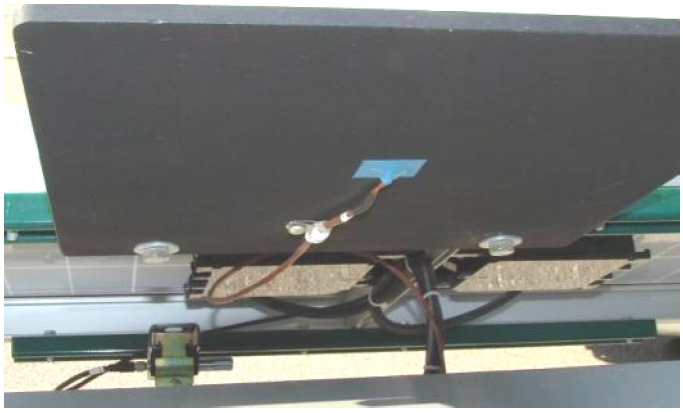

Fig. 5-b: Black Body and Ambient sensors.

Fig. 5-c: Omega Datalogger

4.6. Agilent setup (IV Curves):

top

The Agilent N3300A e-load and 34970A scanner were used with an HP DC Power Supply 6002A to provide the IV curve sweep. An Eppley Radiation Sensor and thermocouple were also connected to the scanner. Everything was networked to a PC laptop running LabView software which was used to control, capture and archive the MTS IV curve data (Fig. 6). A dedicated set of 4-wire leads was used for all IV curve data.

Fig. 6: Agilent IV Curve lab equipment supported by an AC inverter from the equipment van.

4.7. Purge system:

top

A 6 hp oil less shop compressor and RainBird sprinkler timer were used with a 10 – 100 CFH flow meter to provide and control the purge gas where AC power was available (Fig. 7). A stand alone DC system was underdevelopment for sites without AC power, but this effort was put on hold pending evaluation of the purge system vs. desiccant-only effectiveness. MTS units #1 and #2 have active purge, while remote units #3 and #4 are without.

Fig. 7: Purge compressor, timer and flow controls.

Washer system:

top

A portable gas powered high pressure washer (1.6 gal/sec @ 2000 psi) was used with a 15 gal pressure tank to feed DI water for cleaning (Fig. 8). The narrow spray nozzle was used to direct all the water normal to the module cover glass with minimal overspray.

4.8. Module Alignment Tool:

top

A simple pinhole site was designed and fabricated to close tolerance for measurement of the cover glass optical alignment with respect to Sun position (Fig. 9-a,b). The first ring indicates a 2° half angle and the dot size represents ½° alignment normal to Sun position.

Fig. 8: Pressure washer and DI water tank.

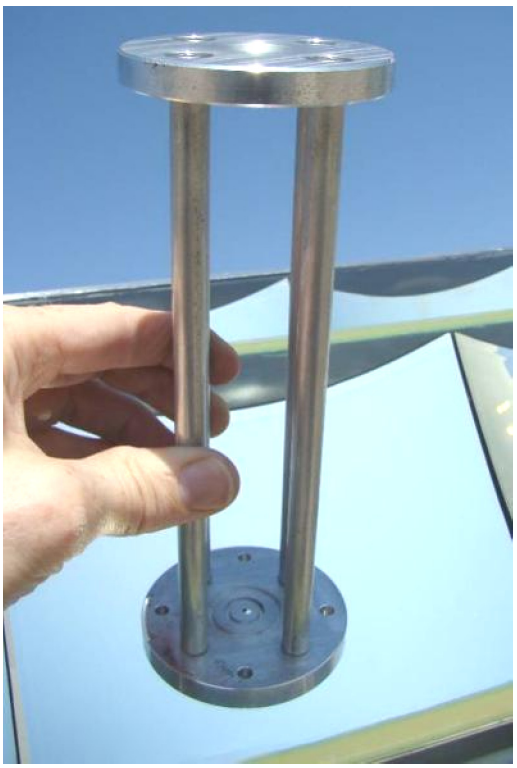

Fig. 9-a: Module Alignment Tool

Fig. 9-b: Module cover glass is within ½° of Sun position.

5. Sample Data:

5.1. Datalogger data:

top

This data was collected continuously by the data logger (Fig. 10) and archived at least every 30 days. The raw data format is processed thru the Omega Hyperware software to generate text files which are then imported into Excel for analysis.

Post Processing

DESCRIPTION: DETECTS TEMP ABOVE 8 0' F
UNIT ID: OM-320
UNIT NAME: OM-320
SESSION: #1 starting Wed Apr 01 1 3:37:37 20 9

Sample Time date/time	BATT VDC	BB Temp 'F	B01 Temp 'F	B02 Temp 'F	SP Volts VDC	A Humid VDC	PC Humid VDC	PC Temp VDC	PC Volts VDC	A Temp VDC	PD Humid VDC	PD Temp VDC	PD Volts VDC	PCR1 Tem 'F	PCR2 Tem 'F	PDR1 Tem 'F	PDR2 Tem 'F
4/1/2009 13:37	13.1899	109.338	72.043	73.2969	20.0508	30.0493	-0.23391	-40.5205	-0.02	80.6563	13.1636	92.2149	10.0498	78.8027	76.9219	86.8203	86.2051
4/1/2009 13:42	13.2324	106.742	73.0723	74.9531	20.1855	31.4507	-0.676956	-41.417	-0.234898	80.1582	14.8245	93.4121	10.0002	78.6231	77.3711	92.1406	92.1406
4/1/2009 13:47	13.2183	105.467	73.0293	74.9062	20.1719	32.1885	-0.344574	-40.6201	-0.02827	79.3594	18.9214	91.2188	9.85156	79.2051	77.9531	97.6387	95.1758
4/1/2009 13:52	13.2041	107.184	72.8496	74.7285	20.1689	32.5586	-0.233818	-40.5205	-0.02	78.7285	20.8706	91.0918	9.99756	79.6504	79.0274	101.773	96.2324
4/1/2009 13:57	13.1758	102.609	73.207	74.4609	20.2681	36.0283	-0.23391	-40.5205	-0.02	77.7305	21.2031	91.8906	10.0059	77.5039	77.5039	103.928	100.277

Fig. 10: Sample image of reduced data logger data file.

5.2. IV curve data:

top

This data was collected using the Agilent IV curve setup (Fig. 11) at the start and end of SG2 testing with intermediate times as available. The data includes both raw IV curve values as well as a normalized set of values for DNI of 1000 W/m^2. During post processing the normalized power and the maximum power point details are determined. This data also serves as a look up table for finding the fixed resistor current (Ir) based on the measured voltage (Vr) while under load.

Date / Time	4/16/2009	2:10 PM				
Air Temp 1(F)	69.809	DNI 1 (W/m^2)	948.60247	DNI 2 (W/m^2)	949.29849	DNI AVG (W/m^2) 948.95048
Voltage (Volts)	Current (Amps)	Normalized Current (Amps)	Power (Watts)	Normalized Power (Watts)		
2.02881	7.86336	8.286375	15.953263	16.811481	Max Normalized Power	116.74457
2.03192	7.86441	8.287482	15.979852	16.8395	Max Measured Power	110.78482
2.02985	7.86547	8.288599	15.965724	16.824613	Vmp	15.1033
2.02881	7.86336	8.286375	15.953263	16.811481	Imp	7.33514

Fig. 11: Sample image of reduced IV curve data file.

5.3. Photo Assay:

top

This data was collected using an 8MP Sony digital camera (Fig.12) with macro zoom function. A full photo assay of the module and site are done at the start and end of test with photo documentation of significant changes and cleaning results for intermediate visits.

Fig. 12: Sample photo assay compilation.

6. Results:

6.1. Visual Inspections:

top

6.1.1. Module Interior:

Interior conditions were inspected and photos taken at the start and periodically throughout the test period. Inspections and photos were done at each intermediate site visit as well as to document any changes and to show the effects of cleaning operations. The mirror elements and general module interior photos (Fig. 13-a,b,c) with close up views of each secondary optic, document interior conditions and the optical bond to the solar cell (Fig. 14-a,b).

Interiors were inspected for presence of water after each cleaning and the condition was documented with high resolution photos showing the mirror elements and the low points within the chassis where water would collect if present. No evidence of water collection inside any of the POD modules could be found during this testing. Water was observed to wick onto the inside surface of the cover glass in one case due to a discrepant bond between the cover glass and the chassis as detailed below. Photos were taken to document the extent of the water intrusion.

Fig. 12-a,b,c: Module mirror elements and chassis interior showing desiccant bags.

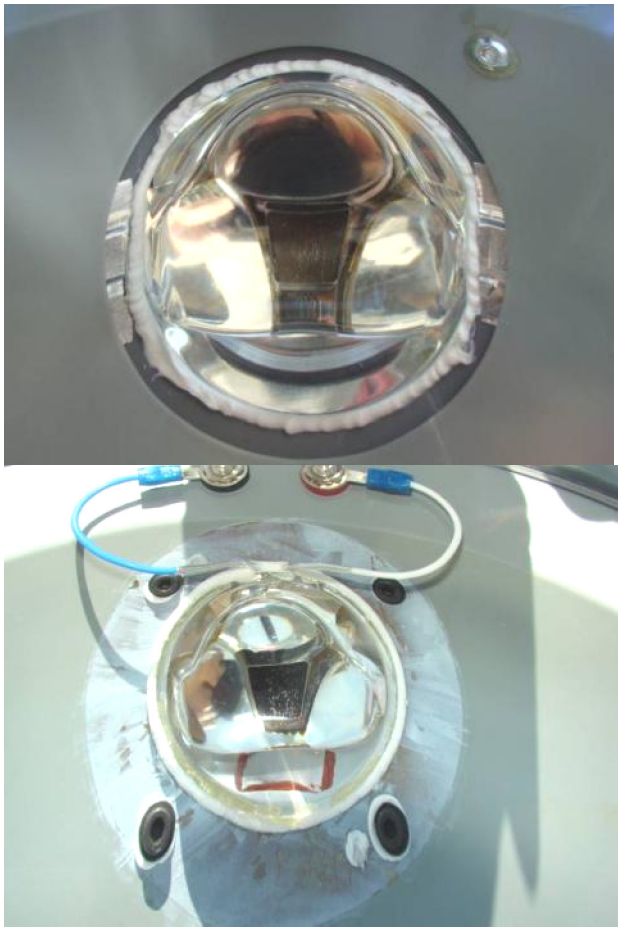

Fig. 13-a,b: Secondary optics and optical adhesive bond to solar cell (POD and POC types).

6.1.2. Module Exterior:

Visual inspections of the module exteriors were documented with a photo assay of the cover glass, chassis, heat sinks, receiver wall and other penetration seals (Fig. 15-a,b).

Fig. 15-a: Chassis.

Fig. 15-b: Heat sinks and receiver wall penetrations.

6.1.3. Cleaning effectiveness:

For modules deployed to remote sites which are subject to dirt accumulation over time, before and after photos (Fig. 16-a,b,c) were taken of the module cover glass at each cleaning to document the effectiveness of a single pass with the pressure washer. Each module under test was subjected to this method of cleaning as documented in the table at the top this report. While some harder to remove debris remain, the vast majority of loose debris is rinsed away using this method.

Fig. 16-a,b,c: Cover glass cleanliness before and after the 4 sec pressure spray wash shown.

6.2. Performance Evaluation:

top

6.2.1. Load Resistor Power:

Power delivered by the POD module to the fixed resistance was calculated from direct measurement of MTS components. The voltage drop across the POD load resistor bank was recorded by the datalogger as “PD Volts”. The instantaneous power delivered by the POD module can be determined in a straightforward manner from the known relationships I = V/R and P = I*V by using the measured voltage and the actual fixed resistance value (Fig. 17). The time interval between records was used to calculate instantaneous energy in watt-hours which can then be accumulated over the entire datalogger record (Fig. 29). Assigning a Vr cutoff value limits the energy accumulation to those times where the DNI was above the 600 W/m^2 threshold. The relationship between Vr and DNI, and details of how the IV curve data was correlated with the datalogger data will be explained in the next section.

It should be noted that the energy dissipated (Er) is less than true the POD module performance because a fixed resistor is not operating at the maximum power point. Actual delivered energy would be higher if maximum power point tracking were employed.

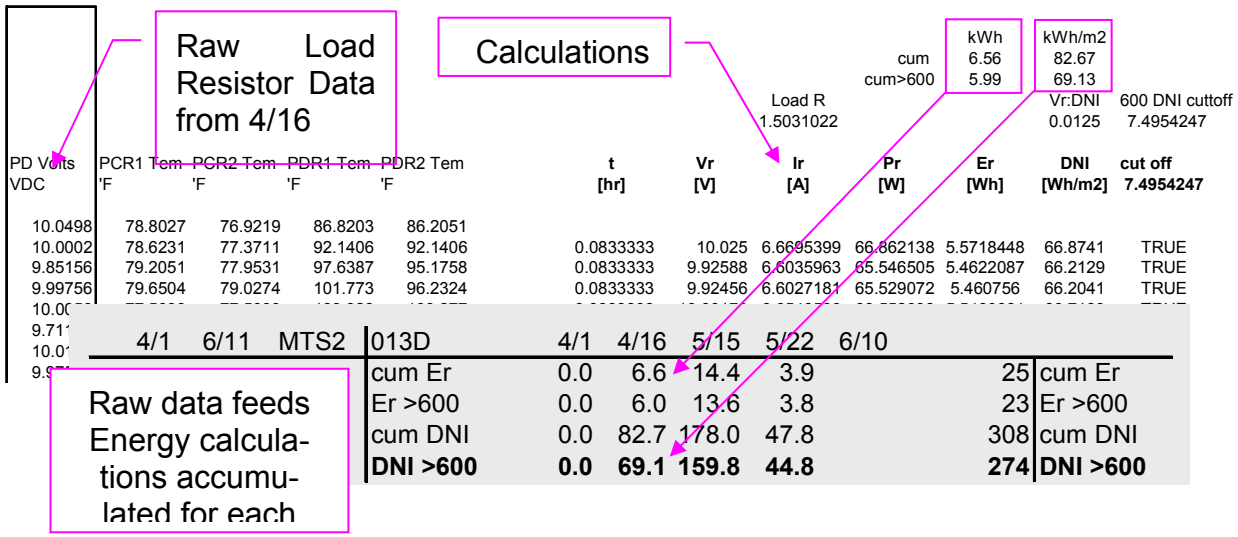

Fig. 17: Data flow from Load voltage (Vr) to DNI exposure totals

The resistance value for the MTS was selected to intersect a typical CPV module IV curve to the left of the maximum power point (Fig. 18) so that changes in current due to DNI variations throughout the day could be reliably monitored using the load voltage data alone. Since there exists a linear relationship between DNI and current (Fig. 19),

and the current variations operate along the linear resistance curve, the load voltage can be said to be a reliable indication of DNI level once the proper calibrations are determined.

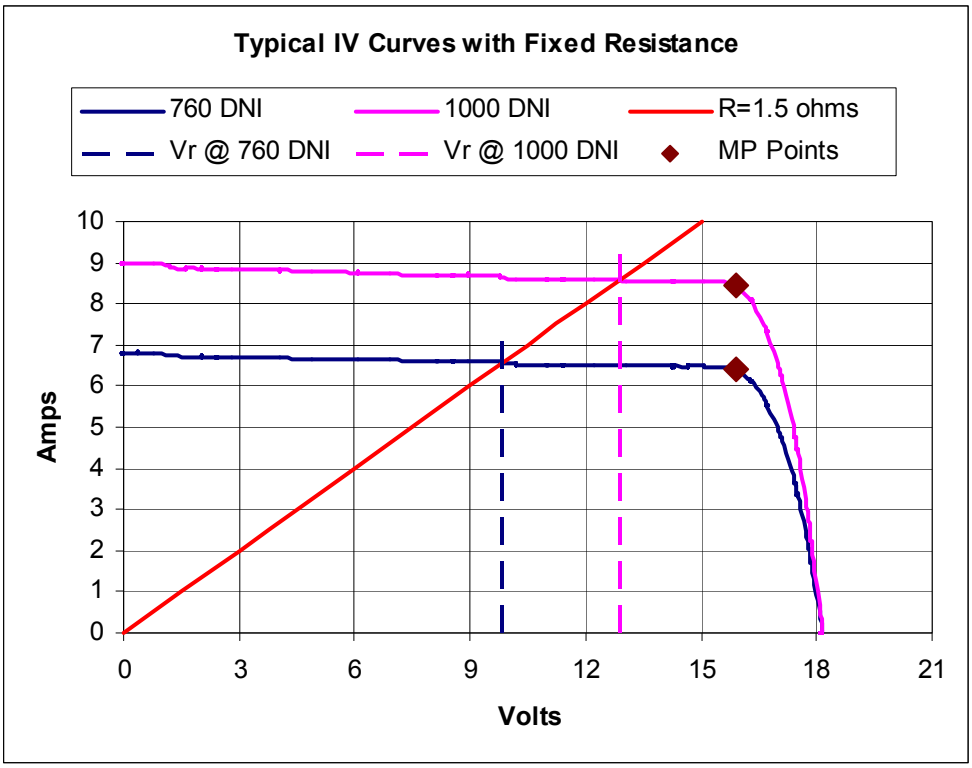

Fig. 18: Load voltage (Vr) is a linear function of module current.

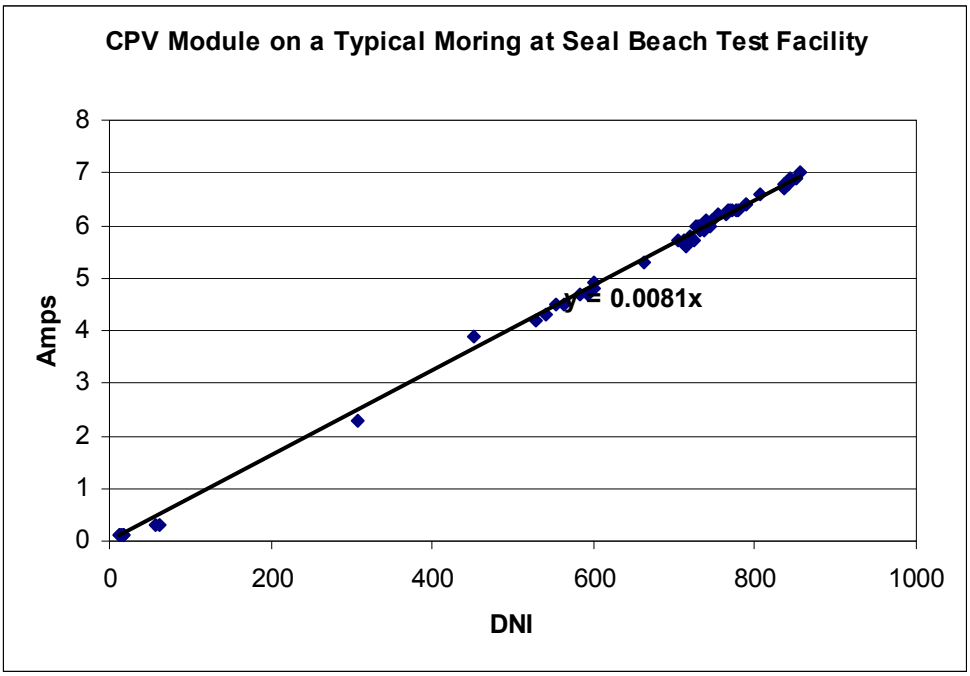

Fig. 19: CPV module current rises proportionally to DNI.

6.2.2. Radiation Exposure:

The DNI exposure of the POD modules is calculated by properly calibrating direct measurements of MTS components with periodic IV curve measurements taken of the POD module where DNI is also recorded. These separate measurements are time synchronized in later analysis to develop a strong correlation between the datasets (Fig. 20-a,b). A properly calibrated linear relationship (with y-intercept = 0) between the recorded DNI data and the load resistance voltage (Vr) was established as the Vr:DNI ratio. Validation of the 1.5 ohm resistance value was also done.

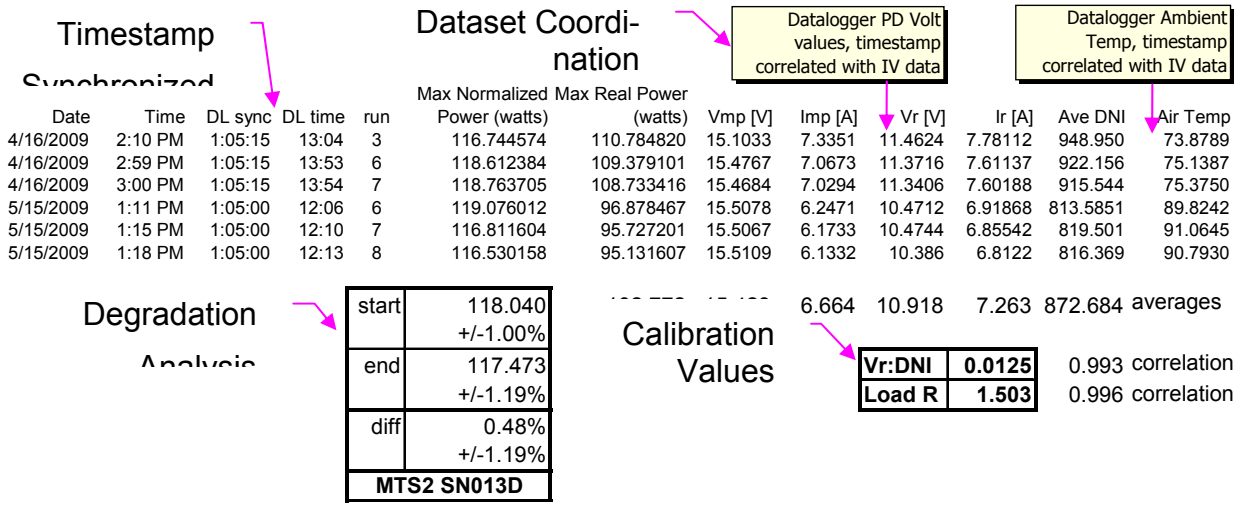

Date	Time	DL sync	DL time	run	Max Normalized Power (watts)	Max Real Power (watts)	Vmp [V]	Imp [A]	Vr [V]	Ir [A]	Ave DNI	Air Temp
4/16/2009	2:10 PM	1:05:15	13:04	3	116.744574	110.784820	15.1033	7.3351	11.4624	7.78112	948.950	73.8789
4/16/2009	2:59 PM	1:05:15	13:53	6	118.612384	109.379101	15.4767	7.0673	11.3716	7.61137	922.156	75.1387
4/16/2009	3:00 PM	1:05:15	13:54	7	118.763705	108.733416	15.4684	7.0294	11.3406	7.60188	915.544	75.3750
5/15/2009	1:11 PM	1:05:00	12:06	6	119.076012	96.878467	15.5078	6.2471	10.4712	6.91868	813.5851	89.8242
5/15/2009	1:15 PM	1:05:00	12:10	7	116.811604	95.727201	15.5067	6.1733	10.4744	6.85542	819.501	91.0645
5/15/2009	1:18 PM	1:05:00	12:13	8	116.530158	95.131607	15.5109	6.1332	10.386	6.8122	816.369	90.7930
								6.664	10.918	7.263	872.684	averages

start	118.040 +/-1.00%
end	117.473 +/-1.19%
diff	0.48% +/-1.19%
MTS2 SN013D	

Vr:DNI	**0.0125**	0.993 correlation
Load R	**1.503**	0.996 correlation

Fig. 20-a: Module Performance determined by combining the datalogger and IV curve datasets.

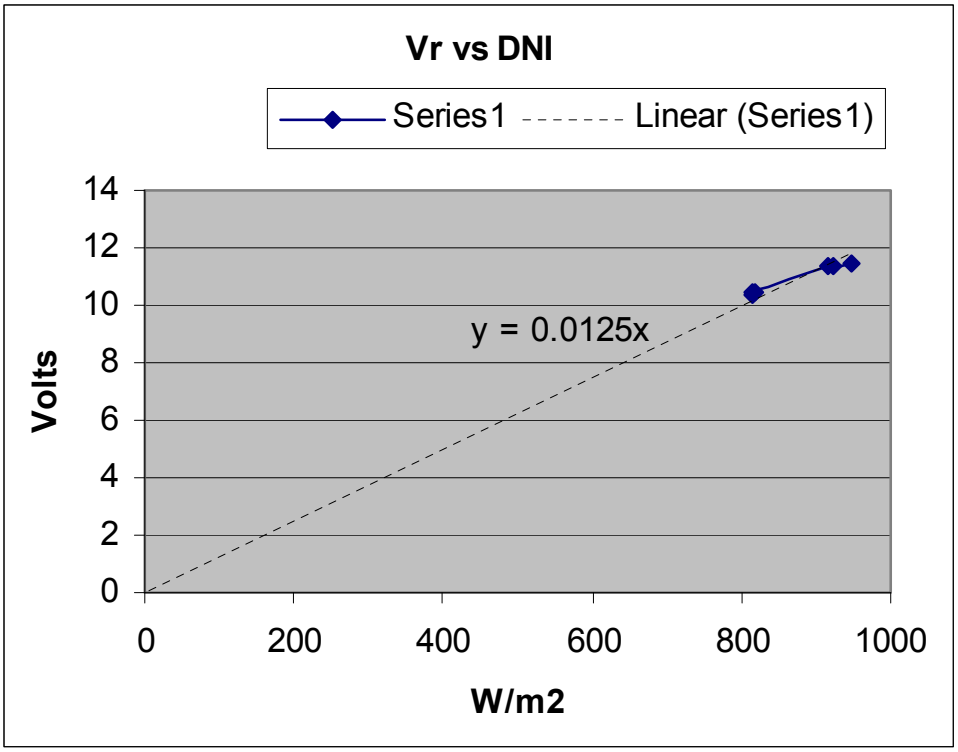

Fig. 20-b: Calibrated relationship between Load voltage (Vr) and DNI.

The instantaneous DNI exposure in kWh/m^2 can now be calculated by DNI = Vr*t/(Vr:DNI) where t is the time interval between load voltage records. The 600 DNI cutoff value for Vr used to filter the energy summation was determined by reversing this calculation assuming DNI = 600. This flow can be seen in the data flow diagram from the previous section.

The instantaneous DNI data was accumulated over time to arrive at the exposure level for each POD module under test (Fig. 29). The results for exposure are also shown in the table at the top of this report. While the target exposure of 430 Wh/m^2 for DNI above the 600 W/m^2 threshold was not achieved at the time of this writing, it is projected that at least two of the test articles will reach their goal within the next few days or weeks. Each module was of course exposed to DNI below the threshold value, which tends to be about 10% of the total, and prior to being deployed with the MTS, each of these POD modules were exposed to DNI during checkout at the Seal Beach Test Facility starting as early as 3/27/09. This additional exposure is not counted toward the accumulation totals reported here.

6.3. Determination of Degradation:

top

6.3.1. Optical:

Visual inspections and comparison of photo assays from the start of testing were examined for signs of optical degradation (Fig. 21-a,b,c,d). Signs of degradation would include: Pitting or cracking of the cover glass; Yellowing of the mirror element's silver surface; Burning or cracking of the secondary optical elements; Changes in appearance of the secondary optic to solar cell adhesive interface.

The inspection of each POD module under test shows no visual degradation of the optical systems for the exposure times documented in this report. Results shown here are typical.

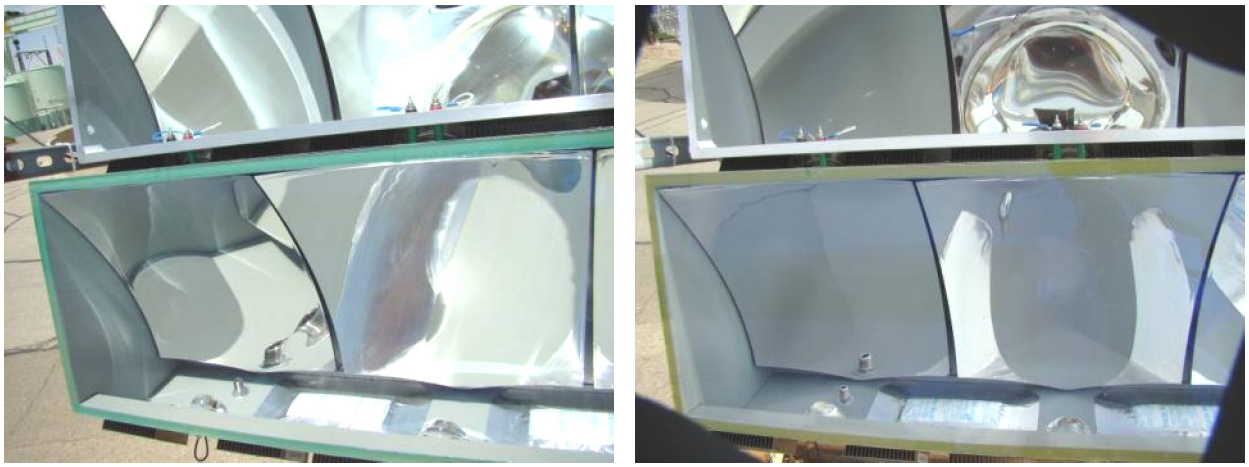

Fig. 21-a: SN026D mirror elements on 4/30/09. Fig. 21-b: Same mirrors on 6/10/09

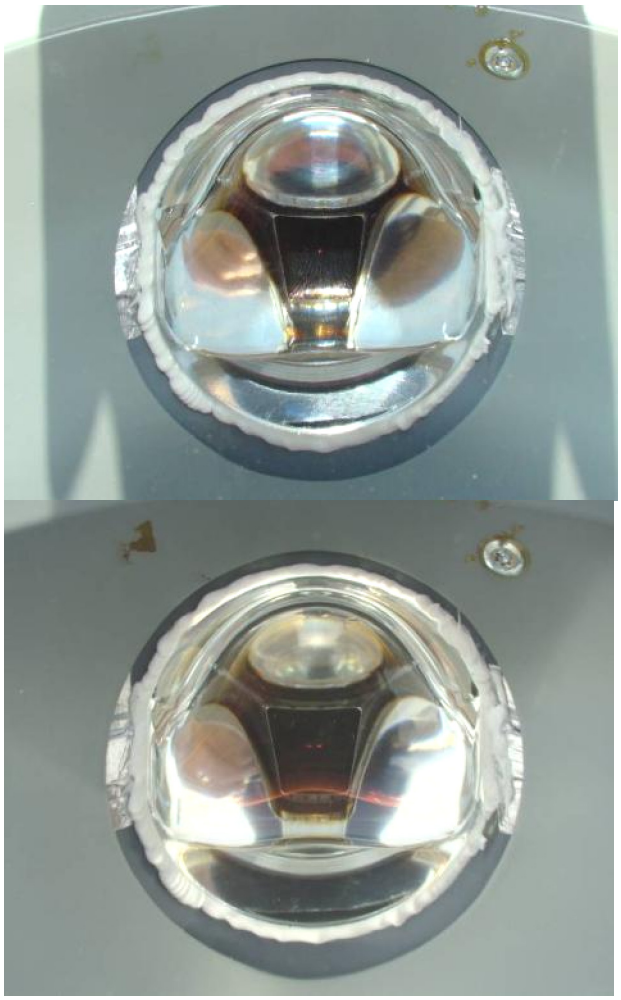

Fig. 21-c: SN026D secondary #5 on 4/30/06. Fig. 21-d: Same optic on 6/10/09.

As of this writing, the POC module mirrors have been observed to exhibit the appearance of yellowing to various degrees at the various sites. One POC module in particular stands out in comparison to newer modules mounted nearby (Fig. 22). This POC module had been under sun and tracking since January of 2009 (before the start of official testing as at MTS1).

MTS data including relative humidity of the interior has been collected nearly continuously on this module since 02/01/09. However, as of this writing the data has not been reviewed for overall DNI or moisture exposure. Recently installed SN049 is also a POC type module but uses the cover glass of the POD units. Continued observations of this unit will help to differentiate visual effects due to differences in AR coatings over time.

Fig. 22: Older POC mirrors show a slightly yellow cast compared to newer modules.

The secondary optic of a POC module at MTS4 has shown evidence of cracking since the start of testing (Fig. 23-a,b). The POC uses a different mechanical mounting for the secondary optic that involves more contact between the glass and the metal structure which can allow greater heating of the optic due to off-pointing events. In addition, the optical adhesive used for POC has been problematic for de-bonding which can further raise glass temperatures of the optic (Fig. 24-a,b). No cracking of the optic or de-bonding of the optical adhesive has been observed in the POD modules which have been subject to same period of off-pointing since the start of testing.

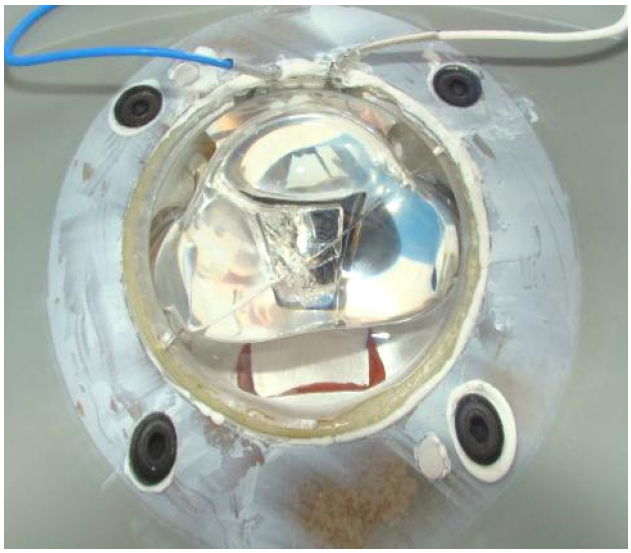

Fig. 23-a,b: SN047B secondary optic #6 on 4/30/09 and again on 6/10/09 showing crack.

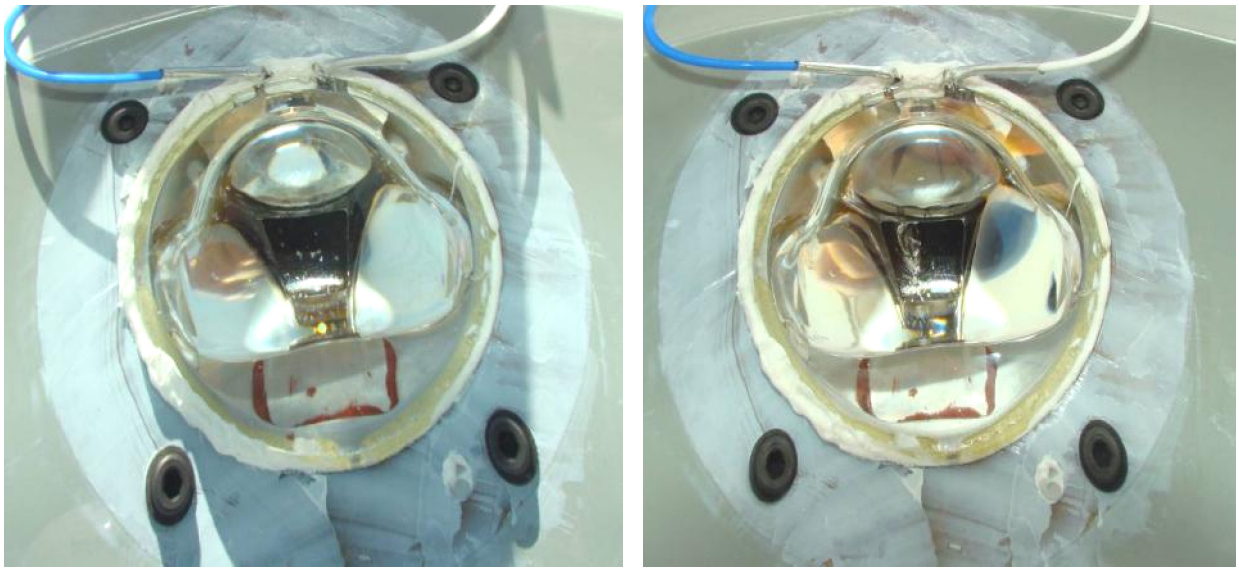

Fig. 24-a,b: SN047B secondary optic #5 on 4/30/09 and gain on 6/10/09 showing de-bonding.

Boeing is evaluating the various material differences between POC & POD articles under test and possible causes for the observed optical degradation noted to date. Boeing will continue to closely monitor all modules undergoing outdoor exposure testing to assess any impacts on the design and material choices for the production of the POM hardware.

6.3.2. Electrical:

Comparison of the IV curve data taken using the Agilent setup from the start of testing was done to characterize the module performance degradation (Fig. 25). The Normalized peak comparisons were used for this report to compensate for variations in DNI. While this is the most straightforward measure of degradation, compensating for DNI alone ignores other effects on measured performance such as cell temperature, variations in pointing accuracy and optical degradation not visible to the naked eye. These influences are more difficult to account for, however. Efforts to compensate for thermal effects are discussed in a latter section.

As a result there is considerable scatter in the data. A statistical approach is used to examine the magnitude of the uncertainty. The standard deviation values of the small sample size tend to overwhelm the measured difference between evaluations and in some cases exceed the <1% degradation criteria established for SG2. Improving on this uncertainty will require greater sampling rates over longer time periods.

Within the capability of the instrumentation to measure POD module performance, no significant degradation could be determined. The evaluation of MTS4 is the only comparison based on IV curved taken after a special cleaning and it reports a negative degradation (improved performance). A second evaluation point for the other sites could not be obtained for this status report due to poor weather conditions in those locations. MTS2 does show a comparison between start with clean cover glass and a latter time with only spray washed glass, but again the results are inconclusive due to the uncertainty.

start pt	111.108 +/-2.13%	start pt	118.040 +/-1.00%	start pt	115.127 +/-0.73%	start pt	113.210 +/-1.48%
eval pt	111.108 +/-2.13%	eval pt	117.355 +/-1.19%	eval pt	115.127 +/-0.73%	eval pt	117.764 +/-1.42%
% degr	0.00% +/-2.13%	% degr	0.58% +/-1.19%	% degr	0.00% +/-0.73%	% degr	-4.02% +/-1.48%
MTS1 SN045D		**MTS2 SN013D**		**MTS3 SN023D**		**MTS4 SN026D**	

Fig. 25: SG2 Power Performance Degradation Calculations with Statistical Uncertainties.

6.3.3. Mechanical:

Visual inspections and comparison of photo assays from the start of testing were examined for signs of mechanical degradation. Signs would include: Corrosion; De-bonding of adhesives and sealants; Loose or missing hardware.

One POD module exhibited an adhesive de-bond between the cover glass and chassis that allowed water to wick onto the interior of the cover glass (Fig. 26). This has been identified as a discrepancy in the bonding process due to a deviation from the surface preparation requirements. The module was repaired in the field by application of metal tape to seal off the upper edge to allow further washings. Subsequent washings showed no new signs of water inside the module.

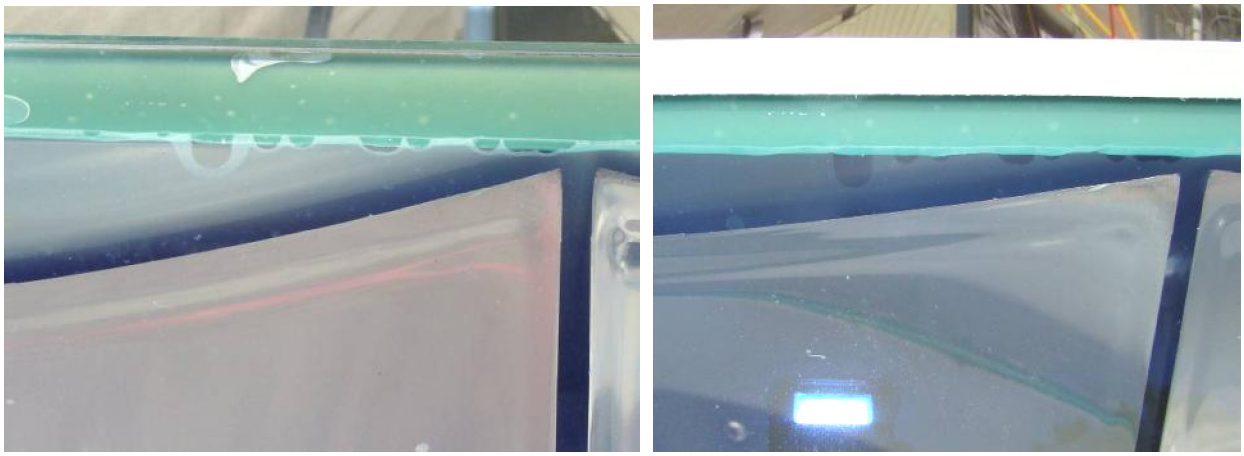

Fig. 26-a,b: Adhesive de-bond with water inside and field repair after pressure spray wash.

Minor corrosion was observed on the heat sinks nickel plated aluminum cooling fins and the older POC module chassis (Fig. 27-a,b). Under the sheet metal attachment between the chassis and the mounting frame were signs of rust developing. The nickel plating thickness and/or pitting in the plating process is suspected in the case of the heat sinks. Access for paint to get under the sheet metal clip is limited in the case of the chassis.


Fig. 27-a,b: Observed minor corrosion on heat sinks and POC chassis.

All other chassis seals and penetrations for purge and power appeared unchanged. No missing or damaged hardware was observed during the testing.

The bonding adhesive used between the cover glass and chassis was observed to change color on the POD modules (Fig. 28-a,b). The color changed from a blue green to a more brownish tone, However, bond integrity appears uncompromised by the color change.


Fig. 28-a: Cover glass adhesive 4/1/09 (green) Fig. 28-b: Adhesive on 6/11/09 (brown)

6.4. Purge Effectiveness:

top

6.4.1. Comparison of Purge and Non-Purge data:

Relative humidity data was collected at all MTS sites for both ambient conditions and module interiors throughout the testing. Active purge systems were employed on only two of the four sites (MTS1 and MTS2). All four sites utilized a passive desiccant system inside the POD module chassis (Note: POC modules do not have desiccant). Reduction of the humidity data was not completed at the time of this writing. The active

purge parameters used for MTS testing are: 13 CFH flow rate; 40 min per day in the afternoon; 7 days per week; tank pressure 105-130 psi. This results in a throughput of approximately 263 CF of dried air per month. This compares to about 60% of the 433 CF per month used on the POD modules mounted to the POD array in Seal Beach.

6.5. Discussion of Uncertainty:

top

6.5.1. Data Collection Methodology:

In and effort to minimize uncertainty, the start and end of test IV curve data was collected from modules with completely clean cover glass (see: Special Cleaning). Intermediate IV curves were taken after baseline spray cleaning and are not directly comparable due to some deposits remaining on the cover glass. Modules were always allowed to air dry before IV curves were taken. At least three “good” curves were taken over a brief period to acquire a statistically meaningful sample. To qualify as a “good” curve, the spread between DNI readings taken during the IV curve process was controlled to be less than 5 W/m^2 so as to introduce less than 1% uncertainty into the data due changing conditions during the sweep.

6.5.2. Power Extraction Effects:

The IV curve measure of performance for a CPV module is affected by the extent of electrical power extracted from the solar cell just prior to the sweep. With no power extraction, all the energy delivered by the optics to the solar cell has to be dissipated thru the heat sink and therefore cell temperature rises rapidly under sun when power extraction is stopped. To minimize this effect the MTS load resistor is used to extract some power (not at maximum power point) from the module prior to taking IV curves, and every effort was made to switch connections from the MTS to the IV curve setup as quickly as possible given that it is a manual operation. Also, to minimize the time delay between datalogger recording (writing to memory) and the IV curve sweep, a coordination procedure was used where the datalogger was observed and the IV sweep was timed to be taken immediately after a new record was logged.

6.5.3. Thermal Effects:

In addition to DNI, another significant influencing factor on moment to moment module performance is cell temperature. Cell temperature can be affected by level of power extraction as discussed, but also by ambient temperature and wind conditions as well. These latter influences are difficult to control for in the real world data being collected without more modeling and instrumentation. Measuring temperature close to the cell as possible helps cull wind and air temp effects to some extent, but this can become impractical if significant design changes and/or costs are involved.

An attempt was made to compensate for thermal changes using a simple cell temperature adjustment factor Nt determined from the equation Nt = (1-dT)*Ct, where dT is the cell temperature difference in degrees centigrade from the ideal cell temperature of 25° C, and Ct is the thermal coefficient inherent to the multi-junction cell technology used in the module. The dT value had to be estimated as an offset from ambient temperature since no direct measurement was made of the solar cell. This adjustment factor could then be used in conjunction with the DNI normalization factor Nd to arrive at an ideal module output Pi under the ideal conditions of DNI = 1000 W/m^2 and Cell Temperature = 25° C.

Pi = Pm*Nd*Nt, where Pm is the measured power under actual conditions.

This method, while sound, proved insufficient to establish a consistent idealized power value for a given module. More work in this area is needed.

6.5.4. Pyroheliometer Tolerance:

The Eppley instrument is used to measure local DNI at the time of the IV curve sweep so that the IV data can later be normalized for a predicted DNI of 1000 W/m^2. A dedicated instrument was assigned to all MTS recordings so as to minimize confusion over calibration factors and to avoid inconsistencies that have been observed in side by side comparisons of apparently identical instruments.

7. **Conclusions:**

top

A portable stand alone system for meaningful but inexpensive monitoring of the Boeing CPV modules was successfully developed and deployed in four locations. The systems were deployed to a variety of environments with two generations of module design attached. Calibration of the monitoring data was achieved by correlation with periodic more detailed measurements using calibrated laboratory level equipment in the field. Analysis of the collected data was able to demonstrate exposure levels and to a certain extent quantify power degradation (or lack thereof) within the statistical error of the methods used.

Visual observations were documented with photos and comparisons were made to show the POD module's optical design does not degrade with exposure to real world conditions and can be cost effectively maintained using the washing method planed for full scale powerplants.

Accumulation Breakdown

Test Dates start	Test Dates SG2	MTS#	SN#	Accumulation Dates					Cum Values
6/9	6/12	**MTS1**	045D	6/8	6/9	6/12			
		0.0111	cum Er		0.2	0.2			0
		1.4683	Er >600		0.2	0.1			0
			cum DNI		1.7	5.1			7
			DNI >600		**1.6**	**2.5**			**4**
			Cleanings	**1**	**1**				**2**
4/1	6/11	**MTS2**	013D	4/1	4/16	5/15	5/22	6/11	
		0.0125	cum Er	0.0	6.6	14.41	3.9	4.7	30
		1.4999	Er >600	0.0	6.0	13.59	3.8	4.5	28
			cum DNI	0.0	82.6	177.7	47.7	59.0	367
			DNI >600	**0.0**	**68.9**	**159.4**	**44.7**	**53.76**	**327**
			Cleanings			**1**	**1**	**1**	**3**
5/27	6/10	**MTS3**	023D	5/27	6/10				
		0.0117	cum Er	0.1	2.2				2
		1.4174	Er >600	0.1	1.9				2
			cum DNI	0.8	33.8				35
			DNI >600	**0.7**	**25.8**				**26**
			Cleanings		**1**				**1**
4/30	6/10	**MTS4**	026D	4/30	5/20	6/10			
		0.0124	cum Er	0.1	13.2	12.2			25
		1.4825	Er >600	0.1	12.6	11.6			24
			cum DNI	1.1	154.6	144.2			300
			DNI >600	**0.9**	**140.8**	**131.2**			**273**
			Cleanings		**1**	**1**			**2**

Fig. 29: Accumulation summary of MTS activity.

8. **References:**

top

8.1. Photo Assay Requirements v1.0
8.2. SAI_EDX100138_BOE_ArrayWashing
8.3.

